Rotational Spectroscopic and *Ab initio* Studies on the Weakly Bound Complexes Containing O-H•••π and S-H•••π Interactions

A Thesis

Submitted for the Degree of

Doctor of Philosophy

in the Faculty of Science

by

Mausumi Goswami

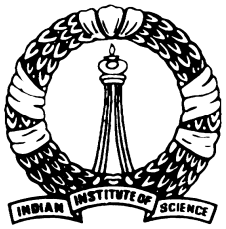

Department of Inorganic and Physical Chemistry

INDIAN INSTITUTE OF SCIENCE

Bangalore – 560012, India

July, 2009

Dedicated to my dear parents
&
Bani

DECLARATION

I hereby declare that the work presented in this thesis entitled "**Rotational Spectroscopic and *Ab initio* Studies on the Weakly Bound Complexes containing O-H•••π and S-H•••π Interactions**" has been carried out by me at the Department of Inorganic and Physical Chemistry, Indian Institute of Science, Bangalore, India under the supervision of Professor E. Arunan.

Date: Mausumi Goswami

CERTIFICATE

I hereby certify that the work presented in this thesis entitled "**Rotational Spectroscopic and *Ab initio* Studies on the Weakly Bound Complexes containing O-H•••π and S-H•••π Interactions**" has been carried out by Ms. Mausumi Goswami at the Department of Inorganic and Physical Chemistry, Indian Institute of Science, Bangalore, India under my supervision.

Date:

Professor E. Arunan

(Research Supervisor)

Acknowledgements

First of all, I would like to thank my thesis supervisor ***Prof. E. Arunan*** *for his valuable guidance and moral support during the entire course of my work which has made working in IISc an immensely enjoyable and memorable experience. His enthusiasm for science has always been a source of inspiration and motivation especially during tough times. I greatly appreciate that despite a busy schedule, he has always found time for discussions whenever it was needed and I have been greatly benefited from those discussions. I sincerely thank him for his encouragement and for the tremendous positive influence he has had in my life.*

I would like to thank Prof. P. C. Mathias (NMR Research Center, IISc) for his involvement and timely help regarding the electronics of the spectrometer.

I would also like to thank Mr. A. P. Tiwari for his help and discussions during the course of the LabView programming.

I take this opportunity to thank my past and present labmates for their co-operation during the course of my work. I thank Mr. Anandraj, Dr. Pankaj Kanti Mandal, Dharmedar J. Ramadass, Janardan, Dr. Raghavendra, Aiswarya, Prasanta, Harish and Devendra for their help and support. My sincere thanks to Dr. Pankaj Kanti Mandal and Dharmendar for teaching me how to do experiments and the details about the spectrometer. I have had a great time with them in this lab. It was my pleasure to have labmates like them. I would like to thank Sanjeev, Narasimhan, Manju and Lavanya for helping in many aspects of the lab. I thank Lavanya for her caring and friendly gestures. My special thanks go to Narasimhan for his help during the setting up of the stepper motor driver connections. I would also like to express my thanks to Manju for taking care of all the matters of the lab and also for his help during the experiments. I thank all the short-term workers who visited our lab during my stay here. My special thanks to Lakshmi for being so friendly and nice to me. I would also like to thank Ankit, Atisha,

Arghya, Saajesh, Aparna and Seshagiri Rao, Manikkavalli for the nice time I have had in their company.

I would like to thank Prof. P. K. Das and Prof. K. L. Sebastian for their encouragement during my stay here. I would like to thank them for the valuable lessons I have learnt from them through the Chemical Dynamics Group meetings. My special thanks to Prof. K. L. Sebastian for giving a wonderful course in Quantum Chemistry which has been very beneficial to me.

I take this opportunity to thank all the Chemical Dynamics Group members for contributing to my knowledge and growth through the seminars and discussions.

I would like to thank the past and the present chairmen of the department of Inorganic and Physical Chemistry for providing me the infrastructure and support to carry out the research work here. I thank all the faculties and staff of the department for their help whenever I needed them. Working in this department has been a very pleasant experience for me. I take this opportunity to thank all my friends and colleagues in this department whose timely help and suggestions have helped a lot in my progress.

It is my immense pleasure to thank all my friends and well-wishers here. I would like to thank Praveen, Manabendra, Animesh, Srinidhi, Bhaskar, Dibyendu, Debashis, Sounik, Sampa, Vikrant, Mily, Brojo for the nice time I have had with them. My special thanks to Bhaskar, Dibyendu and Sounik for their many helps which made the life in IISc better. I would also like to thank Akshay, Sangita, Oindrila, Swati, Debojyoti, Pijush, Sampa, Susmita, Usha for their suggestions and help. I would like to take this opportunity to thank my friends Banishree, Rumki, Rosy, Rohini, Geetha for making the hostel life here livelier.

My sincere thanks to all my IITG friends Ballav, Angshuman, Ankur, Lokman and Sumana for the cherishable time I have had with them.

I specially thank Pankajda, Trips, Arindamda and Udayanda and their family for being so nice to me always. With them, I have always felt like being at home. Special thanks to Paramita for many special moments she has brought into my life. I am grateful to Debangshuda for his valuable advice in the time of need.

I thank Dr, Rangarajan and his family for being so kind and nice to me during my Ohio conference trip.

I thank CSIR for the research fellowship. I thank DST and IISc for the travel funds for the Ohio conference trip.

I thank IISc for providing the facility, infrastructure and SERC for the computational facility.

Words would not be enough to thank my parents. I am grateful to them for the confidence they have in me. I am grateful to them for their encouragement, support which has helped me to become whatever I am today. I specially thank my father Mr. Nirmalendu Goswami for teaching me many great lessons in life and also for teaching me the values. I sincerely thank my mother Mrs. Anupama Goswami for her constant encouragement and also for teaching me the value of perseverance. At this moment, I would like to thank my grandfather whose memories will always be a treasure. I specially thank my sister Poulami for many fun-filled moments we had together and also for sharing the ups and downs in life.

At last, I thank my husband Dr. Bani Kanta Sarma for filling my life with love, care and inspiration. In fact, joining for a Ph.D in IISc would not have happened without his moral support. The influence that he has in my life is beyond words and his love is felt everyday.

Mausumi Goswami

Contents

Preface

FTMW (Fourier Transform Microwave) spectroscopy in the supersonic beam provides accurate structural information about the 'near-equilibrium' geometry of small dimers and trimers in isolation. Spectroscopy in this isolated condition is the stepping stone towards a molecular level understanding of the intermolecular interaction. The data from high-resolution spectroscopy are useful when one wants to testify the accuracy of a model intermolecular potential energy hyper-surface. The spectroscopy of weakly bound complexes of H_2O and H_2S are of fundamental interest as one can gain insight about the nature of intermolecular interaction present in them from these studies. The work in this thesis mainly comprises of a) rebuilding the complete software for the PNFTMW (Pulsed Nozzle Fourier Transform Microwave) spectrometer in Labview 7.1 and b) rotational spectroscopic studies of the structure and dynamics of few weakly bound complexes of H_2O and H_2S with π systems like ethylene and phenylacetylene. The home-built Pulsed Nozzle Fourier Transform Microwave Spectrometer, having a spectral range of 2-26.5 GHz, built in our laboratory has been used to record the microwave spectrum of these complexes. The spectrometer consists of a Fabry-Perot cavity which is the interaction zone of the molecules and the radiation, the electronic circuit for the detection and the polarization of the signal, the mechanical and diffusion pumps which are used to maintain the vacuum inside the cavity. The gas molecules of interest are then mixed with a carrier gas and pulsed supersonically inside the cavity through a nozzle of 0.8 mm diameter. The emission from the complexes formed during the expansion is detected by super-heterodyne detection technique and then Fourier transformed.

The first chapter of the thesis gives a brief introduction to intermolecular interaction and hydrogen bonding. It also gives a brief introduction to the weakly bound complexes of aromatic/aliphatic π systems with H_2O and H_2S. The chapter also includes a brief introduction to rotational spectroscopy.

The second chapter of the thesis discusses the experimental and theoretical methods. It also includes a detailed discussion of the software. The earlier version of the software which was being used in the laboratory was built in CVI Labwindows

environment. The complete software has been rebuilt in Labview 7.1. This software includes 1) GPIB interfacing of the frequency synthesizer and the two delay generators which control the delay and width of the gas pulse and microwave pulses 2) software control of the stepper motor driver for moving the mirror 3) programming the NI-scope digitizer card for the data acquisition using its multiple acquisition capabilities 4) Transferring the FIDs (Free Induction Decay) from the card to the computer and saving and displaying the time domain and the frequency domain data for the user. Further, the scanning mode of the spectrometer is also fully automated as it used to be in the earlier version.

The third chapter of the thesis discusses the rotational spectroscopy of weakly bound complex C_2H_4•••H_2S and its isotopologues. In this complex, H_2S has been found to act as hydrogen bond donor to the π system of ethylene. The spectra reveal the complex to be a nearly prolate asymmetric top with κ= -0.9912. Though, the structure of the complex is very similar to its H_2O counterpart, the floppier potential in case of H_2S complex is directly reflected in the observed microwave spectrum. Each of the transitions for C_2H_4•••H_2S, C_2H_4•••D_2S, C_2H_4•••$H_2{}^{34}S$, C_2D_4•••H_2S, C_2D_4•••D_2S and $^{13}CCH_4$•••H_2S is split into four components, whereas C_2H_4•••HDS and C_2D_4•••HDS show only doubling of each transition. The smaller splitting is 0.14 MHz and the higher splitting is 1.67 MHz in (B+C)/2 for the parent isotopologue. The splitting observed in the spectra indicates the degree of floppiness of the complex. Each series has been fitted separately using Watson's S-reduction Hamiltonian. The splitting pattern of the parent and all the isotopologues indicate that the smaller splitting is arising due to the rotation of ethylene about its C-C bond axis along with the contraction of S-H bond whereas the larger motion arises due to the interchange of equivalent hydrogens of H_2S in the complex. Molecular symmetry group analysis for this complex and all the mentioned isotopologues has been performed and it shows a good agreement with the intensity pattern observed for all the states. Geometry optimizations with various basis sets were performed for the complex at MP2(full) level of theory and the intermolecular interaction energies have been obtained. CCSD(T) single point calculations have also been done for some of the basis sets. The potential energy curves for different motions of C_2H_4 and H_2S in the complex have been calculated at MP2(full)/aug-cc-pVDZ and MP2(full)/aug-

cc-pVTZ level and the *ab initio* barrier heights for these one dimensional motions have been obtained. The details of the experimental and theoretical results are discussed in this chapter.

The fourth chapter contains the microwave spectroscopic studies of phenylacetylene•••H_2O and their isotopologues. Phenylacetylene is an interesting system having different potential sites, which can participate in hydrogen-bond formation. Hence, it is not straightforward to conclude about the orientation of the monomers in the complex formed by phenylacetylene with a second molecule like H_2O. The spectra of the parent complex C_6H_5CCH•••H_2O resembles an asymmetric top with κ = -0.73. Both *a* and *b* dipole transitions have been observed. The rotational spectra of C_6H_5CCH•••HOD, C_6H_5CCH•••D_2O, C_6H_5CCH •••$H_2{}^{18}O$ and C_6H_5CCD•••H_2O have also been measured. The rotational spectra reveal that H_2O is bound to phenylacetylene by forming a C-H•••O bond (ortho C-H group of phenylacetylene donating hydrogen to the oxygen of H_2O) and O-H•••π bond (π cloud of acetylene moiety acting as hydrogen bond acceptor). All the transitions of the parent complex and C_6H_5CCH•••D_2O, C_6H_5CCH •••$H_2{}^{18}O$ and C_6H_5CCD•••H_2O complexes are split into two resulting from a possible internal rotation of H_2O whereas C_6H_5CCH•••HOD shows no doubling of the transitions. The details of the structure of the complex determined by microwave spectroscopy are discussed in this chapter.

The fifth chapter of the thesis comprises of the rotational spectroscopic studies of phenylacetylene•••H_2S complex and its isotopologues. The rotational spectra of C_6H_5CCH•••H_2S, C_6H_5CCH•••$H_2{}^{34}S$ and C_6H_5CCH•••HDS, C_6H_5CCH•••D_2S and C_6H_5CCD•••H_2S complexes have been obtained. The spectra of the parent complex is that of an asymmetric top with κ = 0.69. The rotational spectra indicate that H_2S is located on the top of the phenyl ring. H_2S is shifted from the phenyl ring center towards the acetylenic group. Further, each of the transition frequencies for all the isotopes except C_6H_5CCH•••HDS/D_2S are split into two resulting from the interchange of equivalent hydrogens of H_2S. *Ab initio* calculations have been performed for all the possible orientations of phenylacetylene•••H_2S complex at the MP2/aug-cc-pVDZ level of theory to find out the structure of the global minima. The *ab initio* calculations show

the experimentally observed structure to be the global minima. The details of the experimental results and the theoretical calculations are discussed in this chapter.

The sixth chapter of the thesis proposes a criterion for calling a complex to be hydrogen bonded based on the dynamic structure rather than the static structure of the complex. The question asked is if the anisotropy of the interaction is strong enough to hold the 'hydrogen bond' when one takes dynamics into account. The proposed criterion is that the zero point energy of the motion which takes the hydrogen away from the acceptor should be much less than the barrier height of the respective motion supporting at least one bound level below the barrier. The complexes Ar_2•••H_2O, Ar_2•••H_2S, C_2H_4•••H_2O and C_2H_4•••H_2S have been taken as model systems to test and emphasize this criterion. *Ab initio* calculations at MP2(full)/aug-cc-pVTZ level have been done to generate the potential energy curves for different motions of H_2O and H_2S in these complexes. The barrier heights of these motions have been compared to the zero point energy of the respective modes. This test shows that Ar_2•••H_2O and Ar_2•••H_2S are not hydrogen bonded even at zero Kelvin whereas C_2H_4•••H_2O and C_2H_4•••H_2S are hydrogen bonded. These results support the experimental findings on these complexes and also the recent findings on H_2S crystal and Ar•••H_2O/ H_2S scattering experiments. The details of these results are discussed in this chapter.

List of Abbreviations

AIM	Atoms in Molcecules
BCP	Bond Critical Points
BSSE	Basis Set Superposition Error
c.m.	Center of mass
CVI	C for virtual Instruments
DIB	Diffuse Interstellar Bands
FID	Free Induction Decay
Freq.	Frequency
HBCP	Hydrogen Bond Critical Point
H-bond	Hydrogen bond
MO	Master Oscillator
MS group	Molecular Symmetry group
PAH	Polycyclic Aromatic Hydrocarbons
PI	Permutation Inversion
PNFTMW	Pulsed Nozzle Fourier Transform Microwave
Res.	Residue
RF	Radio Frequency
SCCM	Standard Cubic Centimeter per minute
SLM	Standard Litre per Minute
SPDT	Single Pole Double Throw
SSBM	Single Side Band Mixer
UIR	Unidentified Infrared Bands

List of Tables

List of Figures

Chapter I

Introduction

I.A. Intermolecular Interactions

Nature, as we know of it exists because of intermolecular interaction. The vast importance of intermolecular interaction has brought about a wide research activity in this field.[1-3] Intermolecular interaction plays an essential role in every form of matter be it solid, liquid or gas. Strength of the intermolecular interaction determines the state of matter under ambient conditions. Water, the essential component for all forms of life on the earth has intermolecular hydrogen bonds (one of the several types of intermolecular interactions). In ice, each water molecule is hydrogen bonded to four other water molecules in a tetrahedral arrangement.[4] At room temperature, H_2O is a liquid whereas H_2S is a gas. This is because the hydrogen bonds are stronger in H_2O than in H_2S. The physical properties both at the molecular and bulk level are enormously influenced by these interactions. Even in the biological systems, non-covalent bonds play crucial roles. The complex molecule DNA which is the very basic of life, holds up it double stranded structure with the help of π-π stacking and intermolecular hydrogen bonds formed between the Adenine-Thymine(AT) and Guanine-Cytosine (GC) base pair. Interaction of nearby C=O and N-H groups in the polypeptides facilitates the twisting into α helixes.[5] The three dimensional structure of protein which governs its function is influenced by intermolecular interactions. The biological specificity which is at the heart of the functioning of life depends on the specificity of the intermolecular interaction.[6-8] The recognition of a given antigen with its relevant antibody is the result of many local interactions.[6] These highlighted examples are just a glimpse of the importance of the intermolecular interaction. The existence of intermolecular interaction was proposed by Clapeyron in 1834.[9] The first realization that molecules attract each other goes back to 1867[10] when van der Waals proposed the equation of state given below:

$$\left(P + \frac{a}{n^2V^2}\right)(V - nb) = nRT \qquad (1)$$

P, V, T and n are pressure, volume, temperature and number of moles of a gas and R is the gas constant. The constant '*a*' depends on the intermolecular interaction. This equation tells us that the actual pressure exerted by the gas molecules on the container would be less than what would be predicted if the gases were ideal. However, this equation does not shed light on the nature of intermolecular interaction. The nature of

interaction among different molecules is still not well understood yet. A correct description of the forces between two molecules is necessary to develop exact potential energy function.[11,12] The total intermolecular interaction energy can be decomposed into four terms as given below:

$$E^{total} = E^{ele} + E^{ind} + E^{ere} + E^{disp} \quad (2)$$

E^{ele} is the electrostatic energy, E^{ind} is the induction energy, E^{ere} is the exchange-repulsion energy and E^{disp} is the dispersion energy contribution to intermolecular interaction energy. The subtle balance of the different interaction energy components vary depending on the interacting partners. An understanding of the relative role of these interactions in the molecular complexes is the ultimate goal of research on intermolecular interaction. Electrostatic forces result from the interaction of permanent electric multipole moments of the monomers. The electrostatics plays a major role in determining the structure of complexes like FH•••FH. Induction plays a dominant role in case of complexes such as the Ar•••HF. Here it can be thought of as the dipole-induced dipole interaction. In general, the interaction of the permanent electric multipole moments of one monomer with induced multipole moment in the other monomer is known as induction. The dispersion can be thought of as the interaction which arises due to the instantaneous fluctuation of the electron density of the molecule. Dispersion is the dominating force in the complexes where two rare gas atoms interact with each other such as in Ar•••Ar. The interaction can be called as instantaneous dipole-induced dipole interaction and result from the mutual polarization of the two interacting monomers. The exchange energy is a repulsive term and arises due to Pauli Exclusion Principle which prevents the electrons from one monomer from penetrating the space of the other monomer. Understanding the relative contributions of different components need highly accurate potential energy surfaces and the high resolution spectroscopic and scattering data are inevitable tools in this field of research.

I.B. The Hydrogen Bonding

'Hydrogen-bonding' is the interaction where two atoms which are not bound by a conventional chemical covalent bond are linked by a H atom forming a X-H•••Y type of

bond. The hydrogen bonding can be of two types: intermolecular and intramolecular hydrogen bonds. Although, the hydrogen bonding is known for long now, the precise definition of hydrogen bonding is not yet available.[13] In past, the concept of hydrogen bonding was limited and it was thought that only electronegative atoms like F, O and N participate in hydrogen bond formation. However, there are many examples in the literature now, where less electronegative atoms like C and S atoms act as hydrogen bond acceptor[14,15]. Moreover, even the lone pair, π pair, unpaired electron, sigma bonding electrons, hydride ions and in principle any electron-rich region in the molecule can accept as hydrogen bond acceptor.[16-19] Similarly, apart from the conventional donors such as O-H and F-H groups, C-H, S-H and N-H can also act as hydrogen bond donors.[20-22] Thus, the concept of 'hydrogen bonding' is evolving and it is still a growing field.[14, 23-25]

In general the intermolecular interactions are usually classified as the van der Waals and hydrogen bonding interactions. However, the nature of physical forces are same in both the cases and in a broader perspective, hydrogen bonding is more specific case of the van der Waals interaction. Is there anything that sets apart the hydrogen bonding from other interaction? Umayema and Morokuma[26] in their paper showed that the decomposed energy components for FH•••FCl and HF•••ClF are similar. As Jeffrey points out in his book, the term 'hydrogen bond' refers to a wide range of interaction and understanding the nature of the hydrogen bond appears to be elusive.[23] Very strong hydrogen bonds resemble covalent bonds whereas a very weak hydrogen bond resembles van der Waals interaction. This is the reason for having a wide range of hydrogen bond energy. The typical energy range of hydrogen-bonding is 3-40 kcal/mol, whereas typical chemical bond energy is in the range 50-100 kcal/mol. The vast range of interaction makes defining the hydrogen bond comparatively difficult as the contribution of different forces may be different as we go to different hydrogen-bonding systems. A complete knowledge of the nature of hydrogen bonding interaction would help us to predict how the nature of the interaction changes when we change the interacting partner. However, it is difficult to extract information about the nature of interaction from the condensed phase data because of many body effects. The spectroscopy in the isolated condition in the gas phase provides information about the structure and dynamics of the molecular pairs in isolation. This thesis employs the tool of Fourier Transform Microwave

Spectroscopy (FTMW) to study hydrogen bonded dimers in supersonic beam and the focus is on the interaction of hydrogen bonded complexes of H_2O and H_2S with π system. The next section gives a very brief introduction to the molecular clusters of π system and it also touches on the interaction of H_2O and H_2S with the aromatic and aliphatic π electron density.

I.C. Molecular clusters of π system

Molecular clusters of π systems find their applications in many diverse fields. These are encountered in many chemical systems and chemical reactions.[27] They occur in many biological systems, in aerosols[28] etc. Many binding motif such as cation-π[29], amino-aromatic[30] and polar-π interactions[31] are crucial in molecular recognition and conformational folding dynamics etc. The fundamental questions of interests are a) which components of the interaction energy are most dominating in these complexes? b) How does the nature of the substituents vary the interaction energy components? c) Is there any difference between the aliphatic and aromatic π cloud as a hydrogen bond acceptor? The nature of the interaction varies depending on the interacting partner. Thus, the major component of the interaction energy in case of the complexes where a nonpolar molecule interacts with the π cloud is dispersive. In case of the complexes of Ar with benzene system, the Symmetry Adapted Perturbation Theory (SAPT) calculations of the angular dependence of the interaction energy term showed that the exchange repulsion is the smallest at the center of the ring where the dispersion effect is larger over the carbon sites.[27] In fact the geometry of Ar•••C_6H_6 indicates that argon sits just on top of the ring center.[31,32] Thus though the main stabilizing component of the complex is dispersion and induction, the repulsive exchange repulsion term directs the argon towards the center of the ring. In case of the fluorobenzene•••Ar and di-fluorobenzene•••Ar dimers, the argon atom is located on the top of the ring.[33] It has been found that that dispersion is maximized on the top of the ring and it is the dominating force in the interaction energy. Thus, the interplay of dispersion and the exchange repulsion determines the geometry of the complexes of the rare gas with the aromatic π clouds. On the other hand, the geometry of ethylene•••Ar systems is the one where the

Ar atom is in the plane of ethylene and is was concluded by these authors that the rare gas atoms favor to go to the sites of the lowest electron density in the molecule.[34]

Kim, Tarakeshwar and Lee suggests that, Dewar was the first to suggest that π complexes can act as a proton acceptor in 1946.[27] However, Jatkar and co-workers presented the evidence of hydrogen bonding in benzene in 1943.[35] The earliest theoretical calculation involving a 'π hydrogen bond' in water-formaldehyde system was carried out by Morokuma.[36] It is to be noted that in case of the molecules which have polar π-cloud, the interaction often happens through the lone pair electrons whereas the molecules which have nonpolar π cloud like ethylene and benzene, the interaction of the hydrogen happens through the π cloud. Dispersion also plays a major role in case of the complexes of benzene with methane which possesses C-H•••π hydrogen bond.[27,37] Benzene forms a similar π hydrogen bonded complex with polar molecule like HF, however there is a substantial increase in the electrostatic contribution and there is a decrease in the dispersive contribution.[27,38] This variation of the nature of the dominating forces is essential to the understanding of the structure and binding a priori.

The interaction of H_2O with the π system can act as a model of hydrophobic interaction. The binding with H_2O can be more complex when the substituents on the benzene ring are changed. The role of water may be as a donor in some cases and it may act as an acceptor in some cases. A simple example is that benzene forms a π hydrogen bonded complex with H_2O.[39,40] However the hexafluorobenzene forms a complex where the oxygen atom is facing the π cloud in benzene.[41,42] Investigation on the water complexes of fluorobenzene and difluorobenzene showed that water resides in the plane donating its hydrogen atom to the fluorine atom.[43,44] A number of complexes of water with aromatic systems have been studied such as benzene•••H_2O,[39,.40] phenol•••H_2O[45,46], catechol•••H_2O[47], benzylalcohol•••H_2O[48], benzonitrile•••H_2O[49-51], pyridine•••H_2O[52], fluorobenzene•••H_2O[44], difluorobenzene•••H_2O[44], aniline•••H_2O[53], anisole•••H_2O[54,55], indole•••H_2O[56] etc. and very recently the Infrared-UV double resonance studies on phenylacetylene•••H_2O[57] and fluorophenylacetylene•••H_2O[58] complexes. Most of them have been subjected to the microwave investigations and their structures are known without any ambiguity.[39,40,44,45, 46,49-51,53,55,56] The interactions of the H_2O molecules with these π systems are diverse as indicated by these studies. Substituted benzene rings

provide many possibilities to the incoming water molecule. An important question to ask is whether the H_2O binds to the phenyl π cloud or the interaction is through the substituent. In most of the cited complexes above, the interaction is through the substituents except benzylalcohol•••H_2O (the microwave spectroscopic studies are not yet known). Among the complexes of aliphatic π cloud with H_2O, C_2H_4•••H_2O [59,60] and HCCH•••H_2O[61,62] are known and have been subjected to microwave investigation.[59,60,61] In case of C_2H_4•••H_2O, water forms π bond with ethylene whereas in HCCH•••H_2O, water acts as a hydrogen bond acceptor. These investigations on the water complexes with π system help to understand the interaction of water with the organic compound and hence, the phenomenon of hydrophobic interaction which is essential to the understanding of many biological phenomena that take place in water.

Compared to the water complexes of π system, the complexes of H_2S with π system are scarce. The only microwave investigation where H_2S has been known to interact with π electron system is benzene•••H_2S.[63] Its structure is similar to the benzene•••H_2O complex. However, there is no experimental data available on the interaction of the H_2S with aliphatic π cloud. The complexes of H_2S with the π cloud can be interesting as here in case of the second row hydrides, the dispersion may come into play whereas in case of H_2O complexes, the electrostatics play the main role. Some recent theoretical studies have probed into this.[64,65] Thus the change from H_2O to H_2S may change the type of interaction leading to different structure and dynamics. Hence, a detailed structural and dynamical probing of these complexes by experimental means is a prerequisite to the understanding of the forces acting in these complexes.

I.D. Microwave Spectroscopy

Microwave Spectroscopy can give enormous wealth of information about the molecular structures. The rotational constants which have inverse dependent on the moment of inertia can be determined with very high accuracy with this technique. The moments of inertia depend on the mass and the distance of each of the atom from the axes of rotation. Thus by extracting highly accurate rotational constants one can get highly accurate structure. The pattern of the observed spectrum is different depending on the symmetry of the moment of inertia ellipsoid for that molecule. Depending on the symmetry of the

moment of inertia the molecules are divided into four classes: 1) Linear 2) Symmetric Top 3) Asymmetric Top and 4) Spherical Top. In general, rotational spectra can be seen only for the first three types as the spherical top does not have a permanent dipole moment. The detailed theory of the rotational spectra for these different classes is not discussed here and can be found elsewhere.[66,67] This section gives a very brief summary of the information that we can gain from the microwave spectra.

Very accurate structural information can be extracted from the microwave spectra if a large set of isotopic data are available. The accuracy of the extracted parameters may be limited due to the vibrational effects. There are several procedures to fit the structural parameters to the moment of inertia of all the isotopes. All of these procedures give different structural parameters. Thus, the equilibrium bond lengths (r_e) may be deduced by the correction for the effects of vibrations including the zero point vibrations. The effective bond lengths (r_o) can be calculated from fitting the vibrationally averaged rotational constants to an effective structure. The substitution bond lengths (r_s) can be derived from isotopic substitution method. The mass dependent bond lengths (r_m) can be derived from a large number of isotopic species by a first-order treatment of isotopic effects. When a large set of isotopic data are available, the iterative least-squares fit of the inertial moments is the preferred method.

The substitution method would be a preferred one when only limited set of isotopic data are available. By the help of the Kraitchman's equations,[68] one can calculate the position of the substituted atom from the center of mass. For a linear molecule and for a symmetric top molecule with a substitution on the symmetry axis, the distance of the particular atom from the center of mass is given by:

$$|z| = \left[\frac{1}{\mu}\left(I_x' - I_x\right)\right]^{1/2} = \left[\frac{1}{\mu}(I_y' - I_y\right]^{1/2} \qquad (3)$$

Here, I_x' and I_x are the moment of inertia of the substituted species and the parent species respectively. μ is the reduced mass of the molecule and $|Z|$ is the distance of the substituted atom from the center of mass of the molecular system in question.

For a symmetric top molecule, an off axis substitution converts the molecule to an asymmetric top. Let Z be the symmetry axis and the atom is in the YZ plane. The

Kraitchman equations to find out the co-ordinates for the substituted atom from the center of mass are given by:

$$|y| = \left[\left[\frac{\Delta I_z}{\mu}\right]\left(1+\frac{\Delta I_y}{I_y - I_z}\right)\right]^{1/2} \tag{4}$$

$$|z| = \left[\left[\frac{\Delta I_y}{\mu}\right]\left(1+\frac{\Delta I_z}{I_z - I_y}\right)\right]^{1/2} \tag{5}$$

Here, ΔI_x, ΔI_y and ΔI_z are the changes in moment of inertia after substitution, μ is the reduced mass for the isotopic substitution.

For a planar asymmetric top molecule, the co-ordinates for the substituted atoms from the center of mass can be found by

$$|x| = \left[\left[\frac{\Delta I_y}{\mu}\right]\left(1+\frac{\Delta I_x}{I_x - I_y}\right)\right]^{1/2} \tag{6}$$

$$|y| = \left[\left[\frac{\Delta I_x}{\mu}\right]\left(1+\frac{\Delta I_y}{I_y - I_x}\right)\right]^{1/2} \tag{7}$$

$$|z| = 0 \tag{8}$$

For a general asymmetric rotor, it is convenient to use the planar moments of inertia rather than the moments of inertia. The planar moments of inertia and the moments of inertia are related to each other by the following relation:

$$P_x = \frac{1}{2}\left(-I_x + I_y + I_z\right) \tag{9}$$

and so on. The co-ordinates of the substituted atom from the center of mass is given by:

$$|x| = \left[\frac{\Delta P_x}{\mu}\left(1+\frac{\Delta P_y}{I_x - I_y}\right)\left(1+\frac{\Delta P_z}{I_x - I_z}\right)\right]^{1/2} \tag{10}$$

$$|y| = \left[\frac{\Delta P_y}{\mu} \left(1 + \frac{\Delta P_z}{I_y - I_z} \right) \left(1 + \frac{\Delta P_x}{I_y - I_x} \right) \right]^{1/2} \quad (11)$$

$$|z| = \left[\frac{\Delta P_z}{\mu} \left(1 + \frac{\Delta P_x}{I_z - I_x} \right) \left(1 + \frac{\Delta P_y}{I_z - I_y} \right) \right]^{1/2} \quad (12)$$

Here, $\Delta P_x = \frac{1}{2}(-\Delta I_x + \Delta I_y + \Delta I_z)$ and $\Delta I_x = I_x' - I_x$ is the change in the principal moment of inertia due to isotopic substitution. Distance of the substituted atom from the center of mass is given by:

$$|r| = \left[\left(\frac{1}{2\mu} \right) (\Delta I_x + \Delta I_y + \Delta I_z) \right]^{1/2} \quad (13)$$

For the substitution of an atom on a symmetry plane which is a principal inertial plane (may be taken as the *xy* plane), $\Delta P_z = (\Delta I_x + \Delta I_y - \Delta I_z)/2 = 0$ and

$$|x| = \left[\frac{\Delta P_x}{\mu} \left(1 + \frac{\Delta P_y}{P_y - P_x} \right) \right]^{1/2} \quad (14)$$

$$|y| = \left[\frac{\Delta P_y}{\mu} \left(1 + \frac{\Delta P_x}{P_x - P_y} \right) \right]^{1/2} \quad (15)$$

Nuclear hyperfine coupling such as quadrupole coupling produced by D, Cl and N nuclei and spin-spin coupling produced by H, F *etc.* provide the information regarding the orientation of two monomers with respect to each other in the complexes.

If one or more number of nuclei in the molecule have nuclear spin, $I \geq 1$ nuclear hyperfine structure is observed in the rotational spectrum. The non-spherical distribution of nuclear charge gives rise to nuclear quadrupole moment. The non-spherical distribution of electronic charge about the nucleus gives rise to an electric field gradient at the nucleus. The quadrupole moment of the nucleus interacts with the electric field gradient at the nucleus. No such interaction will be observed if either the nuclear charge distribution or the electric field distribution around the nucleus is spherical. The

quadrupole coupling produced by D, ^{35}Cl, ^{37}Cl and N nuclei provide the information regarding the orientation of two monomers with respect to the principal inertial axes system of the complex. There can be other kinds of coupling between the spins such as the coupling of spins of H and F (both have I =1/2). This kind of coupling is known as spin-spin coupling and gives rise to splitting in the spectra.

Apart from the highly accurate rotational constants, distortion constants can also be extracted from the spectra. The distortion constant D_J can give information about the binding strength in these complexes. The Stark effect measurement can give accurate dipole moments of these complexes. The information obtained from the rotational spectroscopy is not only limited to structure. The information about the ground state dynamics can also be gained from the spectrum. The molecules often exhibit large amplitude motions such as in ethane (H_3C-CH_3), one CH_3 group rotates with respect to the other about the C-C bond. This kind of motion typically converts one configuration to other energetically equivalent minima. The presence of such kind of motion can cause splitting in the spectra. In case of weakly bound complexes which have floppy potentials, there are large amplitude motions which can cause splitting. The barrier heights for these motions can be extracted from the spectra if the direction of the dipole moment changes during the motion. However, if the direction of the dipole moment does not change during the motion, barrier height cannot be extracted directly from the spectra. Further, the intensities of the observed transitions can differ depending on which rotational-torsional state it arises from. This depends on the nuclear spin statistical weights of that particular level. Molecular Symmetry Group analysis for different motions can be performed to match experimental intensity pattern with the calculated statistical weights.[69,70] These dynamical informations help to understand the shape of the bottom of the potential energy surface.

I.E. Pulsed Nozzle Fourier Transform Microwave Spectrometer

It has been emphasized in last sections that the accurate structural determination of the van der Waals and hydrogen bonded complexes are essential to the understanding of the fundamentals of the intermolecular forces. The technique of microwave spectroscopy in the supersonic beam is the best in terms of an unambiguous structural determination of

these complexes. Balle and Flygare were the first to make these studies feasible by combining the technique of Fourier Transform Microwave Spectroscopy with the supersonic molecular beam technique.[71] The supersonic expansion helped in the formation and stabilization of these weakly bound complexes. Further, it also helped to avoid the spectral congestion as in general only the ground vibrational state and lower rotational states are occupied in the expansion. Both sensitivity and resolution are attained by the combination of Fourier Transform Microwave Spectroscopy with the supersonic beam technique. The very first weakly bound complex that was observed by this technique was Ar•••HCl, which had previously been studied by Molecular beam Electric Resonance technique.[72] Since then, this technique has found wide applications to study the structure and dynamics of many interesting classes of molecules. In our laboratory, a Pulsed Nozzle Fourier Transform Microwave Spectrometer has been fabricated and has been used to record the spectra of the complexes described in this thesis.[73] The technique is described in detail in Chapter II.

I.F. Present Investigations

In this thesis, the rotational spectra of three weakly bound complexes C_2H_4•••H_2S, phenylacetylene•••H_2O and phenylacetylene•••H_2S and their isotopologues have been recorded using the Pulsed Nozzle Fourier Transform Microwave Spectrometer (PNFTMW). The observed rotational spectra have been assigned. The structural and dynamical information on these complexes have been analysed in detail. Supportive *ab initio* calculations have been done on these complexes to corroborate the experimental data. Chapter II briefly discusses the experimental and theoretical techniques. Chapter III discusses the rotational spectra, structure, dynamics of eight isotopologues of C_2H_4•••H_2S complex. The rotational spectra and structure of phenylacetylene•••H_2O complex have been discussed in chapter IV. Chapter V of this thesis discusses the rotational spectra and structure of phenylacetylene•••H_2S complex. Apart from these, a dynamical criterion to call a weakly bound complex as 'hydrogen bonded' has been proposed based on the calculations for four model systems Ar_2•••H_2O, Ar_2•••H_2S, C_2H_4•••H_2O and C_2H_4•••H_2S. This criterion has been discussed in chapter VI of this thesis.

I. G. References:

1. van der Waals molecules I, special issue, *Chem. Rev.* **1988**, 88(6).
2. van der Waals molecules II, special issue, *Chem. Rev.* **1994,** 94(7).
3. van der Waals molecules III, special issue, *Chem. Rev.* **2000**, 100(11).
4. L. Pauling, *The Nature of Chemical bonding*, Cornell Univeristy Press, Ithaka, **1960**.
5. R. R. Hudgins, M. F. Jarrold, *J. Am Chem. Soc.* **1999**, 121, 3494.
6. W. Kauzman, *Rev. Mod. Phys.* **1959,** 31, 549.
7. P. D. Schnier, J. S. Klassen, E. F. Strittmatter, E. R. Williams, *J. Am. Chem. Soc.* **1998,** 120, 9605.
8. F. Pichierri, M. Aida, M. M. Gromiha, A. Sarai, *J. Am. Chem. Soc.* **1999,** 121, 6152.
9. Source: Wikipedia http://en.wikipedia.org/wiki/Ideal_gas_law.
10. J. D. van der Waals, *Ph. D. Thesis*, Univ. Leiden, **1873** and J. D. Van der Waals, *Physical Memoirs*, Physical Society of London, vol I, Longmans Green, London **1890.**
11. A. J. Stone, *Science*, **2008**, 321, 787.
12. O. Enkvist, P. Åstrand, G. Karlström, *Chem. Rev.* **2000,** 100, 4087.
13. E. Arunan, *Chemistry International*, **2007**, 29, 16. See also the website: http://ipc.iisc.ernet.in/iupac/ for more details.
14. G. R. Desiraju, T. Steiner, *The Weak Hydrogen Bond: In Structural Chemistry and Biology,* Oxford University Press, Oxford, **1999.**
15. B. Raghavendra, E. Arunan, *Chem. Phys. Lett.* **2008**, 467, 37.
16. I. Alkorta, I. Roza, J. Ekguero, *Chem. Soc. Rev.* **1998**, 27, 163.
17. J. J.Sczymczak, S. J. Grabowski,. S. Roszak, J. Leszczynski, *Chem. Phys Lett.* **2004**, 393, 81.
18. T. F. Koetzle, O. Eisenstein, A. L. Rheingold, R. H. Crabtree, *Angew. Chem., Int. Ed. Engl.* **1995**, 34, 2507.
19. B. Raghavendra, E. Arunan, *J. Phys. Chem.A* **2007,** 111, 9699.
20. T. Steiner, G. R. Desiraju, *Chem. Comm.* **1998,** 891.
21. E. Arunan, T. Emilsson, H. S. Gutowsky, G. T. Fraser, G de Oliveria, C. E Dykstra, *J. Chem. Phys.* **2002**, 117, 9766.

22. D. A. Rodham, S. Suzuki, R. D. Suenram, F. J. Lovas, S. Dasgupta, W. A. Goddard III, G. A. Blake, *Nature*, **1993**, 362, 735.
23. G. A. Jeffrey, W. Saenger, *Hydrogen Bonding in Biological Structures,* Springer Verlag, Berlin, **1991.**
24. S. Scheiner, *Hydrogen Bonding: A theoretical perspective,* Oxford University Press, Oxford, **1997.**
25. S. J. Grabowski (Ed.), *Hydrogen Bonding: New Insights*, Springer, Dordrecht, The Netherlands, **2006.**
26. H. Umeyama, K. Morokuma, *J. Am. Chem. Soc.* **1977**, 99, 1316.
27. K. S. Kim, P. Tarakeshwar, J. Y. Lee*, Chem. Rev.* **2000**, 100, 3891. and references therein.
28. J. H. Steinfield, *Science*, **1991**, 243, 745.
29. J. C. Dougherty, *Chem. Rev.* **1997**, 97, 1303.
30. S. K. Burley, G. A. Petesko, *FEBS Lett.* **1986,** 203, 139.
31. Th. Weber, A. von Bargen, E. Reidle, H. J. Neusser, *J. Chem. Phys.* **1990**, 92, 90.
32. Th. Brupbacher, A. Bauder, *Chem. Phys. Lett.* **1990,** 173, 435.
33. R. J. Wilson, S. A. Peebles, S. Antolínez, M. E. Sanz, R. L. Kuczkowski, *J. Phys. Chem. A* **1998**, 102, 10630.
34. Y. Lu, W. Jäger, *J. Chem. Phys.* **2003**, 109, 8448.
35. N. S. Rao, S. K. K. Jatkar, *Quart. J. Indian Inst. Sci.* **1943,** 6, 1.
36. K. Morokuma, *J. Chem. Phys.* **1971**, 55, 1236.
37. P. Hobza, Z. Havlas, *Chem. Rev.* **2000**, 100, 4253
38. F. A. Baiocchi, J. H. Williams, W. Klemperer, *J. Phys. Chem*, **1983**, 87, 2079.
39. S. Suzuki, P. G. Green, R. E. Bumgarner, S. Dasgupta, W. A. Goddard III, G. A. Blake, *Science*, **1992**, 257, 942.
40. H. S. Gutowski, T. Emilsoon, E. Arunan, *J. Chem. Phys.* **1993**, 99, 4883.
41. Y. Danten, T. Tassaing, M. Besnard, *J. Phys. Chem. A* **1999**, 103, 3530.
42. J. P. Gallivan, D. A. Dougherty, *Org. Lett.* **1999**, 1, 103.
43. P. Tarakeshwar, K. S. Kim, B. J. Brutschy, *J. Chem. Phys*. **1999**, 110, 8501.
44. Jäger and co-workers, *International Symposium on Molecular Spectroscopy*, Columbus, Ohio, **2002.**

45. M. Gerhards, M. Schmitt, K. Kleinermanns, W. Stahl, *J. Chem. Phys.* **1996**, 104, 967.
46. S. Melandri, A. Maris, P. G. Favero, W. Caminati, *Chem. Phys.* **2002**, 283, 185.
47. M. Gerhards, W. Perl, S. Schumm, U. Henrichs, C. Jacoby, K. Kleinermanns, *J. Chem. Phys.* **1996**, 104, 9362.
48. N. Guchhait, T. Ebata, N. Mikami, *J. Chem. Phys.* **1999**, 111, 8438.
49. V. Storm, D. Consalvo, H. Dreizler, *Z. Naturforsch. A*, **1997**, 52, 293.
50. R. M. Helm, H-P Vogel, H. J Nuesser, V. Storm, D. Consalvo, H. Dreizler, *Z. Naturforsch*, **1997**, 52, 655.
51. S. Melandri, D. Consalvo, W. Caminati, P. G. Favero, *J. Chem. Phys.* **1999**, 111, 3874.
52. S. Schlücker, R. K. Singh, B. P. Asthana, J. Popp, W. Kiefer, *J. Phys. Chem. A.* **2001**, 105, 9983.
53. U. Spoerel, W. Stahl, *J. Mol. Spetrosc.* **1998**, 190, 278.
54. M. Pasquini, N. Schiccheri, G. Piani, G. Pietraperzia, M. Becucci, M. Biczysko, M. Pavone, V. Barone, *J. Phys. Chem .A* **2007**, 111, 12363.
55. B. M. Giuliano, W. Caminati, *Angew. Chem., Int. Ed.* **2005**, 44, 603.
56. S. Blanco, J. C. Lopez, J. L. Alonso, P. Ottaviani, W. Caminati, *J. Chem. Phys*. **2003,** 119, 880.
57. P. C. Singh, B. Bandyopadhyay, G. Naresh patwari, *J. Phys. Chem. A* **2008**, 112, 3360.
58. S. Maity , G. Naresh Patwari *J. Phys. Chem. A* **2009**, 113, 1760.
59. K. I. Peterson, W. Klemperer, *J. Chem. Phys*. **1986**, 85, 725.
60. A. M. Andrews, R. L. Kuczkowski, *J. Chem. Phys.* **1993**, 98, 791.
61. K. I. Peterson, W. Klemperer, *J. Chem. Phys.* **1984**, 81, 3842.
62. P. A. Block, M. D. Marshall, L. G. Pederson, R. E. Miller, *J. Chem. Phys.* **1992**, 96, 7321.
63. E. Arunan, T. Emilsson, H. S. Gutowski, G. T. Fraser, G. de Oliveria, C. E. Dykstra, *J. Chem. Phys.* **2002***,* 117, 9766.
64. E. M. Cabaleiro-Lago, J. A. Carrazana-García, Jesús Rodríguez, *J. Chem. Phys.* **2009**, 130, 234307.

65. E. M. Cabaleiro-Lago, J. Rodríguez-Otero, A. Peña-Gallego, *J. Phys. Chem. A* **2008,** 112, 6344.

66. Walter Gordy, Robert L. Cook, *Microwave Molecular Spectra*, Wiley, New York, **1984.**

67. C. H. Townes, A. L. Schawlow, *Microwave Spectroscopy*, Dover Publications, INC. New York, **1975**.

68. J. Kraitchman. *Am. J. Phys.* **1953**, 21, 17.

69. H. C. Longuet-Higgins, *Mol. Phys.* **1963**, 6, 445.

70. P. R. Bunker, P. Jensen, *Molecular Symmetry and Spectroscopy*, NRC Research Press, Ottawa, **1998.**

71. T. J. Balle, W. H. Flygare, *Rev. Sci. Instrum.* **1981,** 52, 33.

72. S. E. Novick, K. C. Janda, S. L. Holmgren, M. Waldmen, W. Klemperer, *J. Chem. Phys.* **1976**, 65, 1114.

73. E. Arunan, A. P. Tiwari, P. K. Mandal, P. C. Mathias, *Curr. Sci.* **2002**, 82, 533.

Chapter II

Experimental and Theoretical Methods

II. A. Introduction

Pulsed Nozzle Fourier Transform Microwave Spectroscopic (PNFTMW) technique was developed by Flygare and co-workers in 1979.[1] Traditionally, the spectroscopy in the Microwave region is inherently less sensitive compared to other regions such as Infrared or UV-visible. This is because the population difference between the ground and excited state is very small. However, invention of PNFTMW technique enhanced the sensitivity and resolution both[2] which made the detection of the complexes having very low dipole moment such as Ar•••Ne possible.[3] With time, there are many modifications which have been introduced into the technique which has increased the range of the molecular systems which can be studied by this technique.[3,4] In our laboratory, a Balle-Flygare type spectrometer has been set up and its details and performance can be found elsewhere.[5,6] However, some description of the components has been given in this chapter.

II. B. Design of PNFTMW Spectrometer

II. B.1. Mechanical design

The mechanical design of the Fourier Transform Microwave spectrometer is shown in Figure II.1. The spectrometer consists of a Fabry-Perot cavity which is housed by a vacuum chamber. This vacuum chamber is cylindrical in shape and made of stainless steel, SS 304. The length of the vacuum chamber is 1000 mm long whereas the diameter is 850 mm. The chamber is directly seated on top of the 20" diffusion pump (Vacuum Techniques, Bangalore, India). The pumping speed of the diffusion pump is 10,000 l s^{-1} and it is backed by a roots blower (Boc Edward, EH 250) and a belt-less rotary mechanical pump (Boc Edward, E2M80). The combined pumping speed of the backing pumping system is ~4000 l min^{-1}. The chamber can be evacuated to 10^{-6} Torr. The diffusion pump is water-cooled and a closed circuit water circulation facility includes a water circulation pump, a cooling tower cum water reservoir to keep the water at room temperature. Inside the chamber, two spherical Aluminium mirrors are mounted co-axially on 3 SS guide rods. The mirrors were made from 65 mm thick Aluminium disks with a diameter of 500 mm. The radius of curvature of both the mirrors is 800 mm and the surface roughness and the radius were good to 1 micron. The distance between the

mirrors could be varied in steps of microns between 630 and 730 mm. The low frequency cut-off for the spectrometer is about 3.8 GHz which is determined by the radius of the mirror (a) and its radius of curvature (R). The low frequency limit of the spectrometer is the one at which the Fresnel number is unity:[7]

$$a^2/R\lambda = 1 \qquad (1)$$

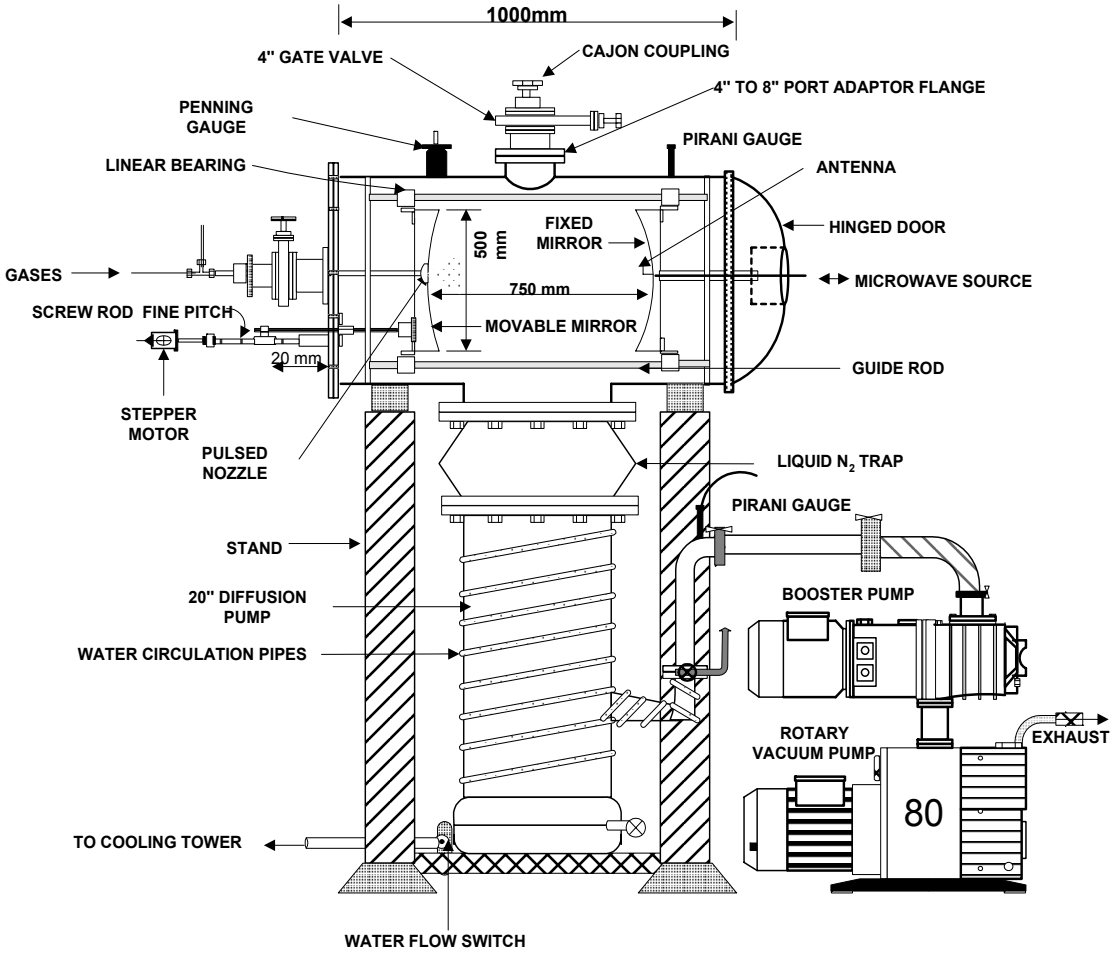

Figure II.1. Mechanical design of the PNFTMW spectrometer

However the spectrometer operates well within the range 2-26 GHz and the spectrum of $Ar_2 \bullet\bullet\bullet H_2S$[6] complex has been collected at 2447.8427 MHz in our laboratory. The movable mirror is fixed with a micrometer controlled fine pitch screw rod and it is driven

by a synchronized stepper motor (103H8221-5041, Sanyo Denki, Japan). The linear screw rod has a pitch of 5 mm i.e. the linear distance covered by the mirror for a 360° rotation is 5 mm. The stepper motor, in high-resolution mode, takes 4000 steps for a complete rotation and thus the mirror moves in steps of 1.25 μm. The original design used the stepper motor driver (PMM-BA-4803). However, during this thesis work, we used a stepper motor driver from MicroLogix, embedded systems Ltd (MSB-403) for some part of the work.

The movable mirror has a 10 mm hole at the center. A pulsed nozzle (General Valve, USA, Series 9) of 0.8 mm diameter is connected with a stainless steel tube of ¼ inch OD and is placed at the movable mirror. The trigger to open and close the nozzle is fed through a pin connector, which is sealed with a 'O' ring and a clamp. A coaxial cable runs through the supporting tube with an SMA female connector at the mirror end. This cable has a hermetically sealed SMA connector at the other end so that the microwave power can be coupled in and out of the cavity at vacuum. The SMA connector goes through a small hole at the center of the mirror and an antenna (L-shaped bent wire made from the central wire of the coaxial cable) can be placed at the connector. Antennas of different lengths are used for different frequency range. The length (L) of the antenna and the wavelength (λ) of the radiation are related as

$$L \approx \lambda/4 \qquad (2)$$

This is a good enough approximation to make antenna for a particular frequency region having the range extended by few GHz on both side of central frequency corresponding to λ. Using 3-4 antennas of different lengths one could cover the entire range of the spectrometer, 2-26.5 GHz.

II. B.2. Electrical design

The electrical design of the spectrometer which is used for the polarization and detection of molecular signal is shown in Figure II.2. The microwave source is a frequency synthesizer (#1 in Figure II.2, HP 83630L, 13 dBm power), which can generate any frequency between 10 MHz and 26.5 GHz to 1 Hz accuracy. The output from the synthesizer (at ν) is routed to a single pole double throw (SPDT) switch (#7, Sierra Microwave Technology, SFD0526-001, Isolation 60 dB), from which the output either

goes through a single side band generator (#5 Miteq, SM-0226-LC1A) or an image rejection mixer (#11 Miteq, IR-0226-LC1A). The SSBM mixes the synthesizer output at ν with a synchronous 30 MHz signal (Stanford Research Systems DS345) and generates ν+30 MHz signal. This signal is amplified by a medium power amplifier (#6, Miteq, JS3-02002600-5-7A) with a gain of 24 dB. The amplified signal goes through another SPDT switch (similar to #7). Both switches work synchronously connecting the polarization and detection parts (top and bottom of the SPDT switches in the Figure II.2), alternatively. During the polarisation, the SPDT output goes through a directional coupler (#8, Narda, 4227-16) and a DC block (#18, HP 11742 A) to the antenna inside the chamber. The antenna couples radiation inside the cavity. The microwave pulse has a bandwidth associated with it (typically 1 MHz for 1 μs pulse). If there is any molecular transition within this bandwidth, the molecules will absorb this frequency and will emit ν+30±Δ. The same antenna couples the molecular signal out of the cavity to the detection circuit. The molecular signal is detected by double super heterodyne detection scheme. This signal is amplified by a low noise amplifier (#10, Miteq JS4-02002600-3-5P, noise 2.8 dB, gain 28 dB) and mixed with the synthesizer signal at ν in an image rejection mixer (#11, Miteq, IRO-0226-LC1A). The IRM gives only the 30±Δ signal, which passes through a band pass filter (#12, Minicircuits BBP 30) and a low noise amplifier (#13, Minicircuits, ZFL-500LN). The 30±Δ signal is down converted to Δ by the RF mixer (#14, Minicircuits ZAD-1) and a low pass filter (#15, Minicircuits, BLP-5). This signal (Δ), generally in kHz range, is amplified and digitized by the virtual scope card (National Instrument, PCI 5112) and transferred to the computer for further processing. Thus digitising the <1 MHz signal is much easier as it does not need a high speed digitiser and does not need storage of large amount of data. The typical sampling speed that we use is 5MHz.

During the polarization pulse, if the Fabry-Perot cavity is not tuned to the particular frequency ν+30 MHz, most of the mw power is reflected. The directional coupler routes 2.5 % of this reflected signal to the oscilloscope (#27, Tektronix, TDS 2022) via a diode detector (#9, Narda, 4507). The moving mirror is moved in steps of

micron until the reflected power shows a dip in the scope. The resonant frequencies,ν, of Fabry-Perot resonator for the TEM_{mnq} modes are:[3]

$$\nu = c/2d\,[(q+1) + (1/\pi)(m+n+1)\cos^{-1}(d/R)] \qquad (3)$$

Here, d is the distance between the mirrors and R is the radius of curvature; m, n and q are the number of nodes in the three perpendicular axes. Thus, within the maximum variation of the distance between the mirrors (100 mm), several resonances can be observed for a given frequency. As the mirror moves the reflected signal is monitored in the oscilloscope. It is preferable to do the experiment with the cavity tuned to the TEM_{00q} mode at a particular frequency. All the components in our spectrometer are ultra wide-band and the experiment can be performed from 2 GHz to 26.5 GHz without changing any component. The signals from the spectrometer appear as a doublet due to Doppler splitting. As the radiation travels back and forth, the molecular beam faces two relative velocities of the radiation which causes this Doppler splitting of the transitions. The typical resolution of the spectrometer is in sub kHz.

II. B. 3. Time sequence of the pulses

At the beginning of each cycle, a MW pulse of 0.3-3 μs is sent to polarize the gas pulse. The microwave pulse forms a standing wave inside the cavity and the decay time for this pulse is typically a few microseconds. There are instances where this delay can go to 40 μs as well. The molecular emission lasts for hundred of microseconds. A delay called 'record delay' is introduced before the digitizing process starts so that the polarizing pulse dies down. The peak to peak amplitude of the standing wave formed by the microwave pulse is 6-8 V and to digitize a mV amplitude signal in presence of such a high background is not feasible. This is the reason to introduce the delay. After the digitization process is over, the data is stored as noise. Then, the gas pulse of typically 1 ms duration is pulsed within the cavity. The microwave pulse of typically 0.3-3 μs follows this. There is typically a delay of few microseconds before we send the microwave pulse so that the gas molecule comes within the interaction zone of the cavity. However, this delay is taken care of by the processing time of the programme. After sending the microwave pulse, the process of digitization starts again. However, the gas

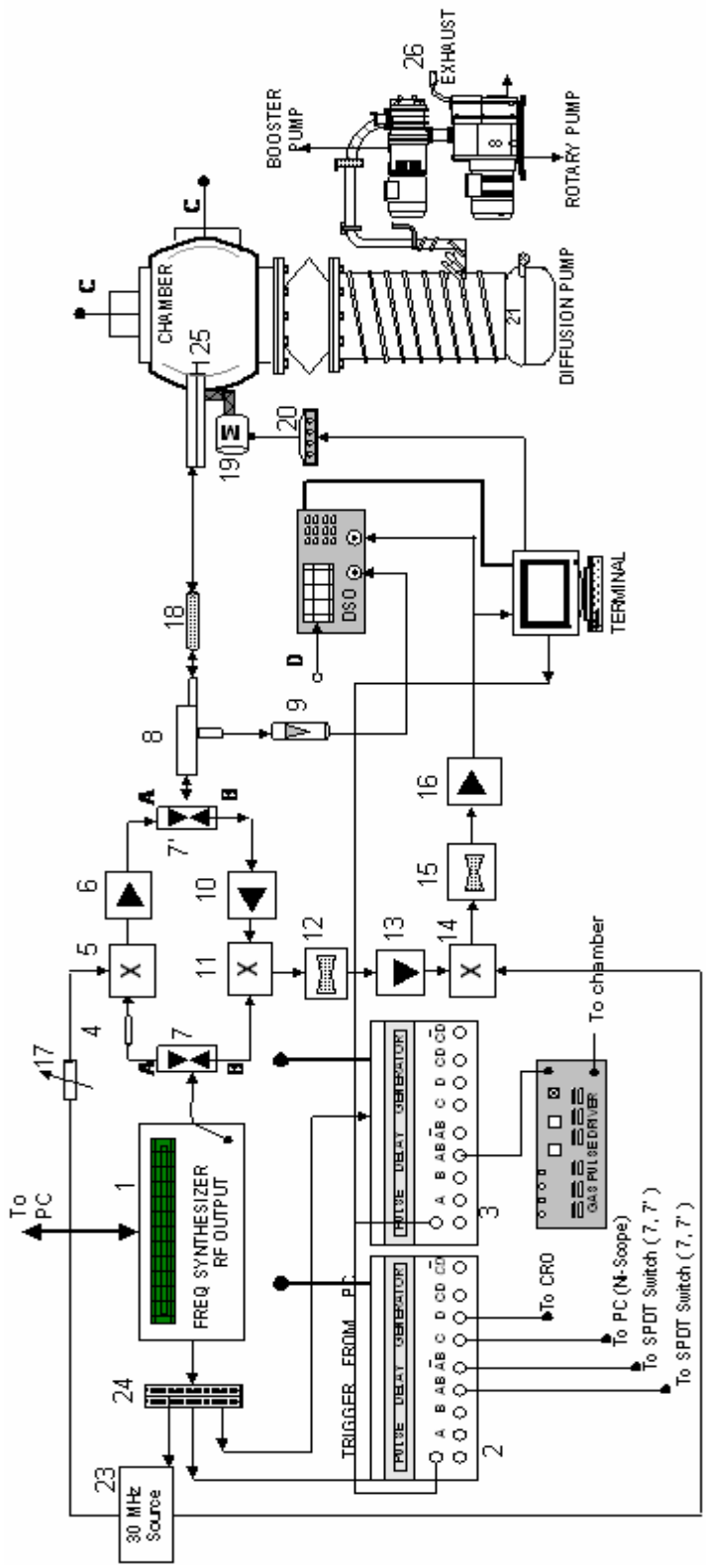

Figure II.2. Electrical design of the spectrometer. [(1) Frequency Synthesizer (Hewlett Packard, HP83630L); (2) & (3) Delay generator; (4) Microwave Attenuator (HP, 8493C, 3dB); (5) SSB Mixer (Miteq, SMO-226LC1A); (6) Medium Power Amplifier (Miteq, JS3-02002600-5-7A); (7) MW SPDT Switch (Sierra MW, 0.5-26.5 SFD0526-000); (8)Direction Coupler (Narda, 1.7-26.5-4227-16); (9) Diode Ditector (Narda, 0.01-26.5-4507); (10) Low noise Amplifier (Miteq, JS4-02002600-3-5P); (11) Image Rejection Mixer (Miteq, IRO-0226LC1A); (12) Band Pass Filter (Mini Circuits, BBP-30); (13) RF Amplifier (Mini Circuits, ZFL-500LN); (14) RF Mixer (Mini Circuits, ZAD-1); (15) Low Pass Filter (Mini Circuits, BLP-5); (16) RF Amplifier (HD Communications Corp., HD 17153BB); (17) Attenuator (Mini Circuits, ZAFT-51020); (18) Blocking Capacitor (HP, 11742A); (19) Stepper motor; (20) Motor Driver; (21) Diffusion Pump, (22) Rotory Pump, (23) 30 MHz Function Generator (Stanford Research System. DS345). (24) Distribution Amplifier (Stanford Research System. FS710): (25) Antenna: (26) Exhaust.

pulse resides within the cavity for 2 ms, whereas typical time of acquisition is 100 μs. Hence, multiple radiation pulses can be sent for a single gas pulse. This process can be repeated for the desired number of times. Each record collected before sending the gas pulse is subtracted from the corresponding record after sending the gas pulse and is called signal and this signal is stored for further processing.

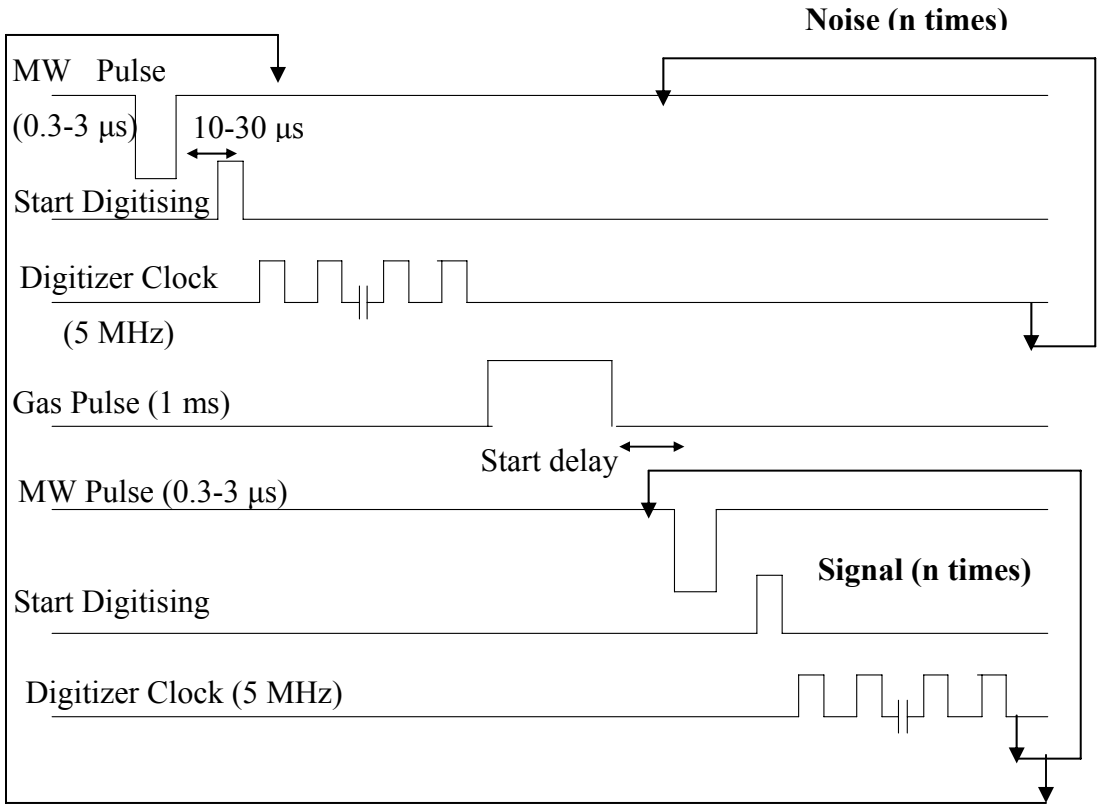

Figure II.3. The MW pulse and gas pulse sequences of PNFTMW spectrometer

II.C. Software for the PNFTMW Spectrometer

Earlier the PNFTMW spectrometer in our laboratory was using a code which was based on CVI Lab Windows platform from National Instruments. This code is not compatible with the latest versions of Windows. Hence, an up-gradation of the code was an obvious need to keep up-to-date with the recent developments of the hard-wares which were

incompatible with the previous version of the windows. We chose Lab View 7.1 from National Instruments considering its user friendly environment. The new code which is being used in our laboratory has been fully developed using Lab view 7.1. The main functionalities of the codes are: A. GPIB control of two SRS delay generators and the frequency synthesiser B. Controlling the stepper motor driver via the parallel port of the PC to automate the mirror movement. C. Programming the NI PCI-5112 card for multiple record acquisition and D. Processing and presenting the data for the user. Each of these will be discussed in the next section after a brief introduction of the Labview

Labview is a graphical development programme provided by the National Instruments. It provides built-in functions which can be used to create different applications depending on the needs. Labview programs are called virtual instruments (VIs). The VI has three main parts 1. Front Panel 2. Block diagram and 3.Connectors. The design of Front panel determines how the user interacts with the VI. Front panel displays the inputs and outputs. Through Front Panel, the user can provide inputs to the programmes. The terminology for the inputs and outputs in Labview are 'controls' and 'indicators' respectively. Every control and indicator has a corresponding terminal in the Block Diagram. Block Diagram contains the graphical source code that controls the programme. The synonym of the subroutine in Labview is SubVI. When a VI is run, the values from controls flow through the Block Diagram. These values are used by the functions and the results are passed onto other functions or indicators. The Block diagram contains different nodes e.g. control and indicator terminals, functions, SubVIs, structures etc. Data flow through the wires, which connect these nodes in the Block Diagram and determines the direction of data flow. The nodes will execute when data is available to all the input terminals and it supplies data to the outputs when done. The details of the Labview development software can be found at the National Instruments website and the help manual which comes with the package.

II.C.1. Parts of the programme

The software which is in current use for the PNFTMW spectrometer has been named as FTMW_final.vi. The front panel of this programme is shown in Figure II.4. The

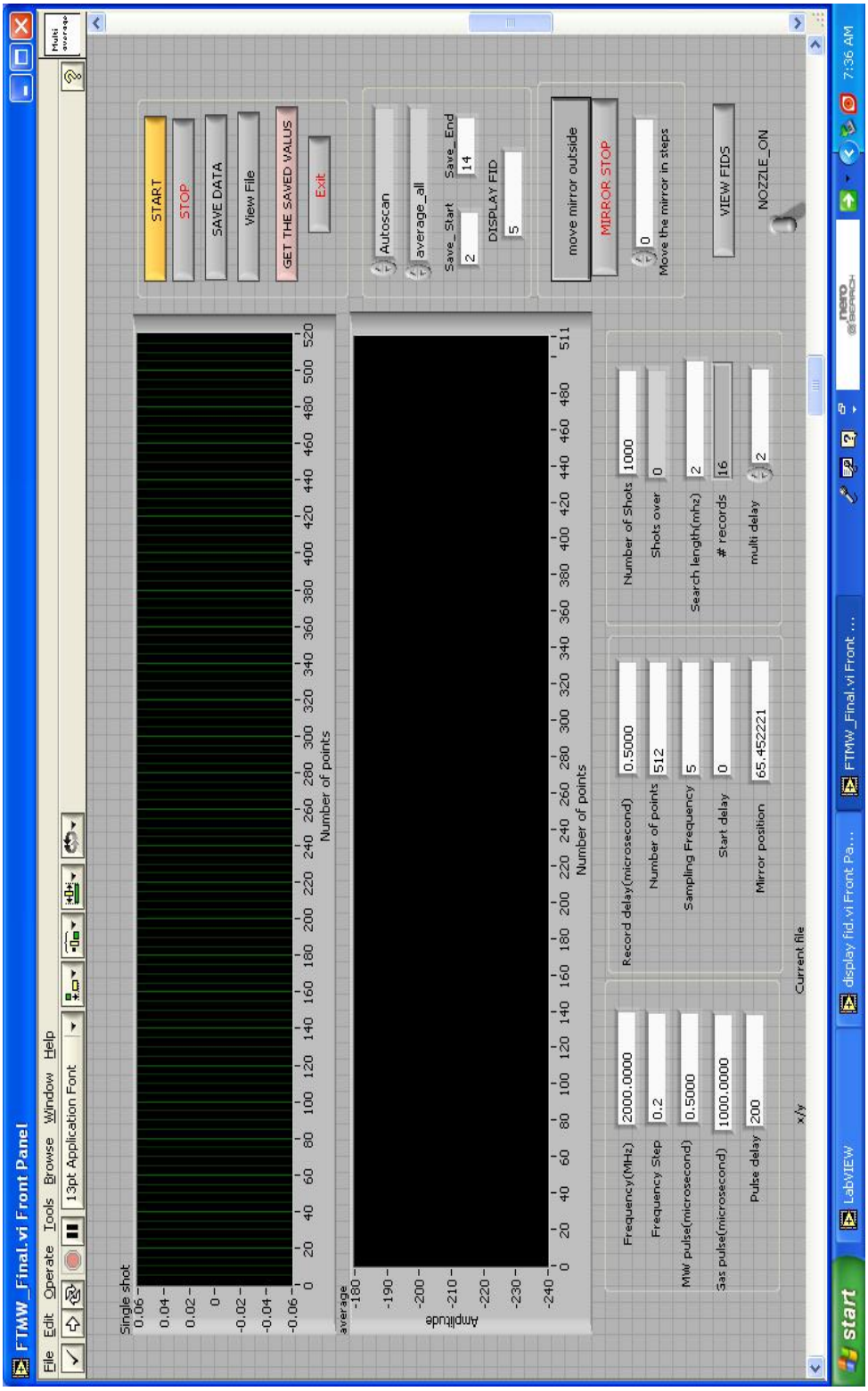

Figure II.3. Design of the front panel

programme mainly uses five other subVIs apart from the Lab view inbuilt VIs. The flat sequence structure of the Labview has been used in the main programme and in all the subVIs. This sequence structure ensures that the sub-diagrams execute sequentially. These subVIs perform several tasks. Functioning of each of the subVI is discussed below.

II.C.1.a. frequencygpib.vi

This VI is used to write the value to the frequency synthesiser. The frequency synthesiser (HP 83630L) is interfaced via GPIB (General Purpose Interface Bus). The block diagram has two frames in sequence. The function 'GPIB Write' provided by the Lab view is used to write the value to the synthesiser. This function has five input terminals. Four of the inputs are wired. The specified inputs are -1) timeout in milliseconds for the write, 2) the GPIB address which is '1' for this device, 3) the data to be written to the device and 4) the mode of ending the GPIB write. The data to be written is sent as a string. The input value for the frequency is appended to "FREQ " and the data is fed to the 'GPIB write' function. After the execution of the first frame of the sequence, the 'EnableLocal' function placed in the second frame is executed. This function takes the synthesiser back into the 'local' mode from the 'remote' mode which enables the user to enter data from the keys if needed.

II.C.1.b. mwpulsegpib.vi

This VI is used to communicate with the delay generator which is used to send the radiation pulse. The communication is via GPIB. This delay generator can generate nine outputs T_0, A, B, C, D, AB, -AB, CD and –CD, five delays and four pulses. T_0 defines the start of the timing cycle. The delay generator can be triggered internally or externally. Once triggered, the timing cycle starts according to the delays set in different channels. AB and -AB are two pulses of opposite polarity and are generated as specified by the intervals between delays of two channels A and B. Similarly, the delays set for C and D define the pulse duration of CD. The outputs AB and AB- from the delay generator is connected to two SPDT switches which open for the specified amount of time to allow the signal to pass into the polarising circuit or the detection circuit. This VI sets the delay value for the channel A to the desired value. The same function 'GPIB write' is again

used with its four inputs wired as described for the previous VI. The address for this delay-generator is '3'. The value to be written is sent as a string in the form of command DT i{,j,t}. This command sets the delay of channel i to t seconds relative to channel j. The value assigned to all the channels can be found in the manual for the delay generator. This VI sets the delay of channel A with respect to T_0. The delay of channel B is preset as "zero" with respect to T_0. Thus the delay set to the channel A defines the duration of the microwave pulse. After the execution of the 'GPIB Write' function, the 'EnableLocal' function takes the delay generator back to the local mode.

II.C.1.c. record-delaygpib.vi

This VI is used to set the delay of channel C of the first delay generator with respect to the channel A via GPIB communication. The same command DT i{,j,t} is used to introduce the delay thorough 'GPIB write' function. This delay is called record delay. The output C from the delay-generator is used to trigger the digitizer card. The digitisation starts only after the card receives the trigger from the channel C. Output D triggers the oscilloscope to monitor the reflected signal. This external trigger occurs via the parallel port of the computer and is done by the software. The values for the delays can be set from the Front Panel.

II.C.1.d. gaspulsegpib.vi

This VI is used to communicate with the delay generator which is used to send the gas pulse. The GPIB address of the device is '4'. The output AB from the second delay generator goes to the pulse driver which drives the nozzle. The VI writes the value of the delays of channels A with respect to T_0. B is preset as 'zero' with respect to T_0. This VI is similar to mwpulsegpib.vi.

II.C.1.e. freqdom.vi

This subVI is used to open an existing data file. It displays the existing time-domain plot and performs Fourier Transform to read and display the frequency domain information. It also displays the frequency at which the spectrum was collected, duration of gas pulse and microwave pulse, record delay, start delay, number of shots averaged, number of

points and the sampling rate of the acquisition in their respective text boxes. When the VI is run, the first frame executes first. The 'File Dialog' function executes and it opens a dialog box where we can specify the path to a file or directory. The file path information selected by the user flows to the next function 'Open datalog', which enables the user to open an existing file. The reference number information of the opened file is passed onto the next function 'Read datalog' which reads the records. The output from this function is returned as a cluster and then split into different elements. These elements have all the information about the frequency, gas pulse, microwave pulse etc. and the values are fed into the text box indicators to display for the user. It also returns the points collected during the acquisition which goes as an input to the 'Power Spectrum.vi' and the averaged auto power spectrum is returned. The magnitude of the auto power spectrum is plotted along the y-axis. The frequency scale is plotted along the x-axis. For the x-axis, the start frequency f_0 is 'zero' and the resolution of the spectrum (df) is in kHz, which can be calculated based on the number of points and the sampling frequency. These informations are plotted and displayed for the user. The time-domain points are also fed into the 'Plot Waveform.vi' and the FID is plotted as such. Then the second frame starts executing. This frame has an event structure inside a while loop. The event is specified as the release of the mouse on the button labelled as 'OPEN FILE'. When the event loop is executed a similar sequence as described in the first frame is executed and the loop continues and the programme again waits for the event to occur. This VI can be stopped by pressing the 'abort execution' button directly.

II.C.2. Main programme: FTMW_final.vi

The main body of the current programme FTMW_final.vi uses all the five sub VI s described above. Apart from these, it also has different subparts which can execute in parallel. These subparts involve the programming which controls the mirror movements, data acquisition by NI scope digitizer card (PCI 5112). All of these parts use several subVIs provided by the Lab View. These different parts are described one by one. Each of different sub parts are kept within a while loop and can be executed multiple times in a single session without restarting the programme.

II.C.2.a. Mirror Movement Control

The mirror distance can be varied from 63 to 73 cm in order to tune the cavity for a particular frequency. The movement of the mirror is controlled by the stepper motor driver. The stepper motor driver is controlled by the software through the parallel port. The whole programme is within a while loop structure. The while loop structure has two sequential frame structures inside. The first frame has an event structure. The event structure executes whenever the user changes the value of the Boolean control 'move mirror outside/inside'. If the value of the boolean control is changed from false to true, the mirror moves inside whereas if the value of the control is changed from true to false, the mirror moves outside. The event has a case structure within it. If the value of the boolean control is read as 'true' after the user click, the programme checks if the value read at the "mirror position" control is less than 63.5 cm. If this is true, the programme does not execute. If this is false, a while loop structure executes which uses the outport.vi to send write bytes to the parallel port. The bytes written to the parallel port for moving the mirror inside (Sanyo driver, PMM-BA-4803) is 00001000. After writing this value, the function rewrites 00000000 again. This completes one trigger event. At each trigger, the distance between the mirrors deceases by 0.00125 cm. At each step, the "mirror position" controls is updated by the programme. The rate of writing bytes to parallel port has been kept as 10 ms in the programme. At the beginning of each step, the programme checks if the value of the boolean control "move mirror" is changed to true or if the "Mirror Stop" button has been clicked by the user. If either of this is true, the execution stops. On the other hand, if the value of the boolean control "Move mirror" is read false after the user click, the mirror moves outside and for moving mirror outside, the bytes written are 00000100. After writing this value, the function rewrites 00000000 again and thus completes one trigger event. Here, the mirror will not move if the distance between the mirror is more than 72.5 cm. The algorithms for moving mirror in both directions are the same. There is a provision in the software where we can move the mirror in steps. When the user presses the up and down cursor keys, the mirror moves inside or outside step by step. This is helpful to move the mirror slowly near the resonance.

The bytes written to the parallel port are different for MSB-403 stepper motor driver as the pin configuration is very different than the Sanyo driver. The bytes written to the parallel port for moving the mirror inside are 00001100 and 00001000 sequentially. For moving the mirror outside, the values 000001000 and 00000000 are written sequentially.

II.C.2.b. Data acquisition

The programme can acquire data in two modes 1) average and 2) autoscan. In average mode, the programme is used to average the FID at a particular frequency. In the 'autoscan' mode, the frequencies are scanned over a range. Thus, the entire data acquisition part is within a case structure. When the user clicks on the START button, the event structure executes. Now depending on whether the selected mode is autoscan or average, either of the case (Case 0 for autoscan or Case 1 for average) gets executed.

1. Average: At first, the 'niScope Initialize.vi' opens a new session to the digitiser and returns an instrument handle. This handle is specific to the digitiser card. The next function 'niScope Configure Acquisition.vi' defines the type of acquisition for the digitiser whether normal or flexible. Parameters such as number of points, number of records, maximum sampling rate, reference point (the position of the reference event as a percentage of the acquired waveform) are configured via 'niScope Configure Horizontal Timing.vi'. The function 'niScope Configure Chan characteristics' configures the channel and the electric properties of the signal such as 'input impedance' and maximum input frequency etc. 'niScope configure vertical' function chooses whether the coupling is AC, DC or ground. The function 'niScope Configure Trigger Digital.vi' sets the trigger source and the trigger slope etc. Then the programme enters the main while loop (may be called as the data acquisition loop) structure for the acquisition which continues till the user specified 'number of shots' are exhausted or until the user clicks the Boolean button labelled as 'STOP'. This main 'while loop' structure contains 'flat sequence' structure, where the frames are executed sequentially. The first frame executes 'niScope Initiate Acquistion.vi' which makes the digitiser ready to receive the trigger. The second frame does the job of sending triggers to the first delay generator. This frame basically

does the job of multiple-acquisition. This frame contains a loop structure which executes as many number of times as specified by the number of records. What it does basically is triggering the delay generator for MW pulse multiple times. Each time the delay generator is triggered, its timing cycle is executed and the digitiser receives a trigger. Triggering the delay generator is done via the parallel port. The function 'outport.vi' does this job. This function writes bytes to the pin which is connected to the first delay generator. Here, the value to be written is '00000001'. The next step for this function is to clear all the values. Then the programme waits for some time. An artificial delay is created before the loop starts again. The purpose is to wait for the acquisition by the card to be completed. The problem is that the delay functions provided by the Labview cannot create delay < 1 ms. This is of no use to us as this will negate the usefulness of the multiple -acquisition for a single gas pulse as the gas pulse would escape the cavity by 2 ms. This creation of the artificial delay basically involves a while loop. This delay depends on the sampling frequency and the number of points for the acquisition. Suppose, we are using 5 MHz sampling rate and 512 points for the acquisition, then this loop should create a delay which should be more the 102.4 μs. Different delay-time can be created entering different values to textbox control specified as 'multidelay'. This is basically related to the number of times the while loop executes. In a test with a 1.8GHz Pentium IV PC, it was noted that this value is 1 for 256 points and 5 MHz sampling rate, 2 for 512 points and 5 MHz sampling rate, 4 for 1024 points and 5MHz sampling rate. This value will change as we move to a faster processor and should be confirmed by the user before running the experiment. As the required number of records are acquired the function executes the while loop where the function 'niScope Acquisition Status.vi' is placed. This function returns a value of 1 if the acquisition is complete and the programme leaves the loop and goes to the third frame.

It is to be noted that if the value of 'multi delay' entered by the user creates a delay time which is less than the required time of acquisition, this function 'niScope Acquisition Status.vi' returns a value of zero and the loop keeps on running infinitely and the programmes does not proceed further. Once, the acquisition status returns a value of '1', the programme leaves this loop and the data is fetched to the computer. Fetching the data is done by 'niScope Fetch.vi'. This function returns a 2-dimesional array of binary

voltages, where the records are indexed at 0,1,....n-1. The 'wfm info' output from this function is wired into a 'for' loop and the auto-indexing is enabled. The 'wfm info' returns an array of cluster. Each element of the array is a cluster of eight elements which give information about different parameters of the waveform. The auto-indexing allows processing of each element (here, the elements are clusters) of the array individually. Thus, the parameters for a single record are passed into the loop at a time. These data is converted into scaled voltages using the formula scaled voltage = (binary data*gain) + offset. This operation is done for each record and the array of scaled voltages is returned as an output from the loop. This set of data is stored and called 'noise'. Next frame in sequence executes 'niScope Initiate Acquistion.vi' and makes the digitiser ready for the next acquisition. Next, the 'outport.vi' function writes data to the 2^{nd} pin of the parallel port, which is connected to the second delay generator. After receiving the trigger it executes its delay cycle and the AB pulse output from the generator goes to the pulse driver which drives the nozzle. Next frame in the sequence structure executes the while loop for the multiple radiation pulse as was described previously. The same sequence of events as was described during the collection of the noise executes and the data is fetched and stored as an array of scaled voltages as signal. The array of noise is subtracted from the array of signal and is stored. This stored data is fed into the 'Index array' function, This function takes an n-dimensional array and then returns an element or subarray depending on the 'index' input which takes value from 0 to n-1. Here, the 'Index array' function takes the 2-dimensional waveform and returns a record as indicated by the user on the textbox labelled 'DISPLAY FID', which is basically indicating the index of the desired subarray. The returned waveform is displayed in the graph labelled 'Single shot'. The next frame in sequence has a case structure. The case structure has two sub-diagrams. Either of them executes at a given time depending on the value wired to the selector terminal is true or false. The value read at the terminator is false if the execution is going on for the first shot and it returns a true value if the value indicated in the textbox labelled 'number of shots over' is more than one. If the selector reads true value, the waveform arrays acquired during the current shot is added to the waveform arrays acquired during the earlier ones and the averaging is performed and the averaged waveform is saved as a two-dimensional array of scaled voltages. This saved waveform

is fed into a 'while loop' in the next sequence. This loop contains a flat sequence structure. First, the 'Index array' function executes. It takes two inputs-1) the averaged waveform array returned from the previous frame and 2) is from the 'shift register'. This 'shift register' is initialised with a value indicated by the user on the textbox control labelled 'Save_start'. The value of this control indicates the index of the subarray returned by the function 'Index Array'. A 'shift register' passes value from iteration to the next iteration. A shift register appears as a pair of terminals, one on the left hand side as a down arrow and the other on the right hand side as an up arrow. After the completion of iteration, the data is stored on the terminal on the right hand side. Labview transfers the data from the right hand terminal to the terminal on the left hand side. The loop then uses the data from the left terminal as the initial values for the next iteration. Thus, here the value of the index keeps on changing from one iteration to the next iteration and the values differ by one unit as the left terminal and the right terminal is wired via an 'Increment' function. During each iteration, the next frame in the sequence structure of this loop adds the current sub-array to the sub-array returned during the previous iteration. Thus finally, the sum of all the FIDs starting from the number indicated in the text box 'Save_start' to the number indicated in the text box control 'Save_end' is performed. This loop stops when the addition of all the FIDs indicated by the user is complete. The sum is saved as a one-dimensional array of voltages. The next frame in the sequence structure of while loop is related to the display options of the graph labelled as 'average'. This frame has a case structure. The selector terminal is connected to a ring control which either reads 0 or 1. Either of two sub-diagrams is executed depending on whether the value read at the selector is 0 or 1. This value is controlled by the user. The user can select either of these two options: 1. the average for all the FIDs which can be selected by choosing 'average_all' option. This is assigned to a value of '0' for the ring control. This option lets the user view the saved one dimensional array obtained by averaging all the FIDs returned from the previous frame 2. The user can view the average for the nth FIDs of all the gas pulses. n is the selected record acquired for a gas pulse. This option is selected by entering the option 'average_gas' in the ring control. This has been assigned a value of '1'. If user selects the 'average_gas' option the graph displays four waveforms for record number n to n+4 averaged over the gas

pulses. The two-dimensional array of scaled voltages is passed onto a while loop as input to the "index array" function. The input "DISPLAY FID" is entered by the user depending on which FID the user would like the programme to display and this value is fed into while loop through the 'shift register'. This is the 2nd input to the "Index Array" function. The "Index array" function returns the selected FID and saves it as "array 1". This while loop gets executed a total of four times. At each step the value of the "DISPLAY FID" is increased by one unit and so the next arrays will be saved as "array 2", "array 3" and "array 4". Further, the records averaged over the gas pulses can also been seen afterwards if one wishes to. This can be done by clicking on 'VIEW FIDS' button. This executes a subVI which does the function as has been described just now. In the next frame, the "Build array" function appends this four arrays and displays in the 'average' graph as one array. Thus, four consecutive arrays for the gas pulses can be seen in one screen and at times it helps to choose the user to save the FIDs which contain signals and the rest may not be saved. Thus accordingly, the values can be entered in 'Save_start' and 'Save_end' boxes. The next part of the programme saves the two dimensional array of voltages (averaged for the gas pulses) in a new file so that any FID can be viewed later if desired by the user. After the acquisition is over, the delay function 'Time delay' introduces a delay before staring the while loop all over again. This while loop stops if the 'number of shots' are over. After the acquisition is over, the programme displays a dialogue box which prompts the user to create a new file to save the FIDs. As the required number of shots gets over, the programme leaves this loop and the niScope.vi function executes which closes this session for this digitiser. Once, the session is over, all the parameters of the experiment are assembled as a cluster and saved as new file for future reference. This file has been named as 'ram'. The user then saves the data by clicking 'save data' in a new file. This data contains frequency, start delay, MW pulse, gas pulse, record delay, sampling frequency, number of shots, number of points and the 1-D array of saved averages which can later be read and processed by the freqdom.vi.

2. Autoscan: The algorithm of the data acquisition is the same as the 'average mode'. However, there are added features. The other desired inputs the programme would look

for are "frequency step" and the "search length" which is not required during the 'average' mode. As soon as the user clicks on the start button, the information about the previous acquisition is read back in their respective text boxes. The information are frequency, start delay, MW pulse, gas pulse, record delay, number of points and number of shots etc. Next, the programme prompts the user to provide the path for a new file where the data will be saved. The path of the first file is entered by the user. Then the programme enters into a while loop structure which stops when the search length is over. The number of times this loop is executed depends on the search length and the stepsize. The other added features are autosaving of the data and then auto-tuning of the cavity by moving mirror at each step. After entering the main while loop structure, the increment or decrement in the mirror position is calculated by the formula

$$\Delta d = -\left(\frac{d}{\nu_0}\right)\Delta\nu \qquad (4)$$

where d is the current mirror position, ν_0 is the current frequency, $\Delta\nu$ is the step frequency. Thus the required number of triggers to move the mirror is calculated and the programme sends the triggers to the stepper motor driver. If the mirror distance is less than 63.5 cm or 72.5 cm, this part does not execute. Then, in the loop a new file is created in the location as indicted by the user. As the frequency is changed depending on the step frequency, the file name also changes. Basically the file name has been linked to the index of the while loop. The functions which have been used to give a filename are 'Path to String' function, 'Concatenate string' and 'string to path functions. Thus, the 'path to string' function converts the pathname given by the user to string format. The index of the while loop is also written as a string. Then both of these are combined into one string by the 'Concatenate string' function and then converted back to the path information by the 'string to path' function. At each step of this loop, a new file name is saved as the index of the while loop changes. Then, the programme enters into the 'data acquisition' loop which stops when the number of shots gets over. At each frequency, the data containing all the informations are saved in the new file which has been crated previously. After the search length is over, the information from the last file is saved in a

file which can be read back later whenever the user clicks the 'START' button keeping the mode as 'autoscan'.

II.D. Sample preparation

The typical carrier gases used in the experiment are argon or helium. Typically 1-3% of the monomers are mixed with the carrier gas. The ratio would vary depending on the size of cluster. To maintain the flow of the gases, four mass flow controllers (MKS, 1179A) are used. The unit to measure the flow rate is Standard Cubic Centimeter per Minute (SCCM) or Standard Litter per Minute (SLM). Two numbers of 2 channel mass flow meters are used for setting and reading the input flow rate. The samples are mixed with argon or helium in a four-way junction and are expanded from a pressure 0.5-1 bar to 10^{-6} mbar through the nozzle of 0.8 mm diameter to undergo supersonic expansion. Before the expansion, the gas may be described as having a Maxwellian velocity distribution. After the expansion, there is a highly directional mass flow. During the expansion, in the nozzle, lots of binary and ternary collisions take place which cools the internal degrees of freedom of the seeded molecules. As a result of these collisions, the translational, rotational and vibrational degrees of freedom of the molecules get cooled. The translational energy equilibrates at a faster rate than do the rotational and the vibrational energies. Thus, the typical translational temperature attained during this expansion is 0.02-0.03 K whereas the rotational and the vibrational temperatures are 2-3 K and 50-100 K respectively. The random translational energy of the molecules are converted to directional mass flow, which means the velocity distribution narrows and the central peak of the distribution moves towards right. Thus, when the molecules emerge from the nozzle, they are effectively in the collisionless expansion and the weakly bound complexes which are formed during the expansion stabilise in that condition and can be studied. Typically to study samples which are liquids, argon or helium is flown over the sample to carry the gas molecules through the nozzle.

II.E. *Ab initio* calculations

Ab initio[8-11]calculations have been done for the complexes studied by PNFTMW spectrometer. These calculations were done to get the optimized geometries, frequencies,

rotational constants and the interaction energies. The relative stability of different minimum on the potential energy surfaces can also be estimated which helped a lot in the search. Most of the calculations have been done using MP2 method while some of the calculations involved CCSD methods as well. The potential energy surface calculations have been done to explore the dynamics on the potential energy surfaces wherever necessary. All the calculations have been done using Gaussian 98[12] and Gaussian 03[13] suites of programmes.

The intermolecular energies for the complexes have been calculated using supermolecular[14] approach. In this approach, the interaction energy is given by

$$\Delta E_c = E_c - \sum (E_M) \quad (5)$$

Here, E_c is the absolute energy of the complex and E_M are the constituent monomers energies in the complex. However the interaction energy calculated in this manner can have contaminations from the Basis Set Superposition Error (BSSE).[15-17] The BSSE corrections were done by using the 'counterpoise = n' key words of the Gaussian. Here n indicates the number of monomer constituents in the complex. This uses the counterpoise method of Boys and Bernardi.[18,19] Using this keyword also takes care of the monomer distortion in the complex. Thus, the BSSE for a complex where A•••B can be evaluated from the following equation:

$$BSSE = [E_A^{*\{A\}} - E_A^{*\{AB\}}] + [E_B^{*\{B\}} - E_B^{*\{AB\}}], \quad (6)$$

A, B are the constituent monomers of the complex. $E_A^{*\{A\}}$, $E_B^{*\{B\}}$ denote the energy of the distorted monomer calculated in the monomer basis set whereas $E_A^{*\{AB\}}$, $E_B^{*\{AB\}}$ denote the energy of the distorted monomer in the complex basis set. The CP corrected interaction energy is calculated by:

$$\Delta E_{AB}^{CP} = \Delta E_{AB} + BSSE \quad (7)$$

II.E. Atoms in Molecules calculations

AIM[20] theoretical calculations have been done on the complexes to characterise the bond critical points and to find out the electron density at the bond critical points (BCP) and the Laplacian of the electron densities at the BCP. Based on AIM theory, Koch and Popelier have given eight criteria to detect hydrogen bonds which were used to

characterise the C-H•••O contacts.[21] The first two of these criteria are about the electron density at BCP and the Laplacian of the electron density at BCP. According to Koch and Popelier, The ρ value at BCP should lie within the range [0.002, 0.035] au and the Laplacian of the electron density at BCP should lie within the range [0.024, 0.139] au for the hydrogen bonding interaction. Both of these criteria have been used for the complexes studied in this thesis.

II.E. References

1. T. J. Balle, and W. H.Flygare, *Rev. Sci. Instrum.* **1981**, 52, 33.
2. J. S. Muenter, in *Structure and Dynamics of Weakly Bound Complexes* (Ed. Weber, A.), Reidel, Dordrecht, 3 ,**1987.**
3. Yunjie Xu, Jennifer van Wijngaarden, Wolfgang Jäger, *Int. Rev. Phys. Chem.* **2005***,* 24, 301.
4. E. Arunan, S. Dev and P. K. Mandal, *Appl. Spec. Rev.* **2004**, 39, 131.
5. E. Arunan, A. P. Tiwari, P. K. Mandal, P. C. Mathias, *Curr. Sci.* **2002**, 82, 533.
6. P. K. Mandal, *Rotational Spectra of Weakly Bound H_2S complexes and 'Hydrogen Bond Radius',* Ph.D. Dissertation,Indian Institute of Science, Bangalore, India, **2009**.
7. J-U. Grabow, W. Stahl, H. Dreizler, *Rev. Sci. Instrum.* **1996***,* 67, 4072.
8. Szabo, N. S. Ostlund, *"Modern Quantum Chemistry: Introduction to Advanced Electronic Structure Theory*", Dover Publications Inc., Mineola, **1996**.
9. D. R. Yarkony (ed.), "*ModernElectronic Structure Theory*", Part I & II, World Scientific, Singapore. **1995**.
10. F. Jensen, "*Introduction to Computational Chemistry*", John Wiley & Sons, New York **1999.**
11. M. Springborg, "*Methods of Electronic Structure Calculations*" John Wiley & Sons, New York, **2000**.
12. M. J. Frisch, G. W. Trucks, H. B. Schlegel, G. E. Scuseria, M. A. Robb, J. R. Cheeseman, V. G. Zakrzewski, J. A. Montgomery, Jr., R. E. Stratmann, J. C. Burant, S. Dapprich, J. M. Millam, A. D. Daniels, K. N. Kudin, M. C. Strain, O. Farkas, J. Tomasi, V. Barone, M. Cossi, R. Cammi, B. Mennucci, C. Pomelli, C. Adamo, S.

Clifford, J. Ochterski, G. A. Petersson, P. Y. Ayala, Q. Cui, K. Morokuma, N. Rega, P. Salvador, J. J. Dannenberg, D. K. Malick, A. D. Rabuck, K. Raghavachari, J. B. Foresman, J. Cioslowski, J. V. Ortiz, A. G. Baboul, B. B. Stefanov, G. Liu, A. Liashenko, P. Piskorz, I. Komaromi, R. Gomperts, R. L. Martin, D. J. Fox, T. Keith, M. A. Al-Laham, C. Y. Peng, A. Nanayakkara, M. Challacombe, P. M. W. Gill, B. Johnson, W. Chen, M. W. Wong, J. L. Andres, C. Gonzalez, M. Head-Gordon, E. S. Replogle, and J. A. Pople, *Gaussian 98*, Revision A.11.3, Gaussian, Inc., Pittsburgh PA, **2002.**

13. M. J Frisch, G. W. Trucks, H. B Schlegel, G. E. Scuseria, M. A.Robb, J. R.Cheeseman, J. A. Montgomery Jr., T. Vreven, K. N. Kudin, J. C. Burant, J. M. Millam, S. S. Iyengar, J. Tomasi, V. Barone, B. Mennucci, M. Cossi, G. Scalmani, N. Rega, G. A Petersson, H. Nakatsuji, M. Hada, M. Ehara, K. Toyota, R. Fukuda, J. Hasegawa, M. Ishida, T. Nakajima, Y. Honda, O. Kitao, H. Nakai, M. Klene, X. Li, J. E. Knox, H. P. Hratchian, J. B.Cross, C. Adamo, J. Jaramillo, R. Gomperts, R. E. Stratmann, O. Yazyev, A. J. Austin, R. Cammi, C. Pomelli, J. W. Ochterski, P. Y. Ayala, K. Morokuma, G. A. Voth, P. Salvador, J. J. Dannenberg, V. G. Zakrzewski, S. Dapprich, A. D. Daniels, M. C. Strain, O. Farkas, D. K. Malick, A. D. Rabuck, K. Raghavachari, J. B. Foresman, J. V. Ortiz, Q. Cui, A. G. Baboul, S. Clifford, J. Cioslowski, B. B. Stefanov, G. Liu, A. Liashenko, P. Piskorz, I. Komaromi, R. L. Martin, D. J. Fox, T. M. Keith, A. Al-Laham, C. Y. Peng, A. Nanayakkara, M. Challacombe, P. M. W. Gill, B. Johnson, W. Chen, M. W. Wong, C. Gonzalez, J. A. Pople, *Gaussian 03*, Revision C-02; Gaussian, Inc. Wallingford CT, **2004.**
14. F. B. van Duijneveltd, J. G. C. M. van Duijneveltd-van de Rijdt, J. H. van Lenthe, *Chem. Rev*. **1994**, 94, 1873.
15. B. Liu , A. D. McLean, *J. Chem. Phys*. **1973**, 59, 4557
16. M. N. Szczesniak, S. Scheiner, *J. Chem. Phys.* **1986**, 84, 6328.
17. M. Gutowski, G. Chalasinski, *J. Chem. Phys*. **1993**, 98, 5540.
18. S. F. Boys, F. Bernardi, *Mol. Phys.* **1970**, 19, 553.
19. S. Simon, M. Duran, J. J. Dannenberg, *J. Chem. Phys.* **1996**, 105, 11024.
20. R. W. F. Bader, *Atoms in Molecules: A Quantum Theory,* Clarendon Press: Oxford, **1990.**

21. U. Koch, P. L. A. Popelier, *J. Phys. Chem.* **1995,** 99, 9747.

Chapter III

Structure and Dynamics of $C_2H_4 \cdots H_2S$ Complex

(Preliminary results from this work have been published as a communication in
Chem. Phys. Lett, 2004, 393, 22)

III.A. Introduction

It has been recognized for long that different physical properties of H_2O and H_2S under ambient conditions are a result of their very different 'hydrogen-bonding' capabilities.[1] H_2S has always been regarded as a weaker donor and acceptor of hydrogen bonds compared to H_2O. In order to know these differences, one has to have a microscopic understanding of the origin of these differences. Thus, there are studies which seek to understand these differences via theoretical and experimental means.[2,3] Of course, one needs to obtain a large set of experimental data which explores different regions of the potential energy surfaces of these complexes to understand them better. Microwave spectroscopic studies can give valuable information about the near-equilibrium structure as well as the dynamics of these H_2S complexes in the supersonic beam. Further, it provides a ground for the direct comparison of the H_2S complexes with their H_2O counterpart in an isolated environment and establishes the first step to know and understand the differences or similarities between them. For example, microwave spectroscopic study of Ar•••H_2S[4] and Ne•••H_2S[5] complexes exhibit an unusual isotopic effect due to the effect of large amplitude motions. This is because Ar•••H_2S is floppier compared to Ar•••H_2O[6]. The microwave spectrum of Ne•••H_2O has not been assigned yet and hence, is not available for a direct comparion.[5]

However, relative to the weakly bound complexes of H_2O, the data on H_2S complexes are rare. The data on the weakly bound complexes where H_2S acts as a hydrogen bond donor is further scarce. As far as our knowledge goes, C_6H_6•••H_2S is the only example to have the H_2S act as a hydrogen-bond donor.[7] Experimental data on these complexes are also essential for the semi-empirical evaluation of the 'hydrogen bond radii' for H_2S, which has been determined for other HX (X = F, Cl, Br, OH), for which extensive data are available.[8,9] The microwave investigation of C_2H_4•••H_2S could be important in this aspect if it has a S-H•••π bonded geometry. Moreover, S-H group as hydrogen-bond donor is important in amino acid cysteine and its derivatives.[10]

There exists an earlier theoretical report of C_2H_4•••H_2S complex which talked about the C-H•••S interaction but did not mention anything about the existence of the S-H•••π bonded geometry.[11] Several complexes of C_2H_4 with the first row and second row hydrides such as H_2O, HF, HCl have been studied in literature.[12-15] All of them have a π-

bonded geometry with one of the hydrogen bonded to the ethylene π cloud. C_6H_6•••H_2S has a π-bonded geometry similar to C_6H_6•••H_2O.[16,17] However, depending on the geometries of these first row hydride complexes, it is not straightforward to draw any conclusions regarding the geometry of C_2H_4•••H_2S complex. The first reason being the ethylene π cloud is electron poor than the benzene π cloud and the second reason is that the proton donating abilities of the first row and second row hydrides go as HF>HCl and H_2O>H_2S. Thus, one would wonder if C_2H_4•••H_2S would have S-H•••π or C-H•••S geometry. Moreover, the weakly bound complexes of ethylene have also been interesting from a dynamical point of view as the potential energy surfaces are quite shallow. Almost all the complexes of C_2H_4 except the C_2H_4•••HF and C_2H_4•••HCl complexes show the splitting in their spectra due to some internal rotation of one of the subunit. To mention a few among them, Ne•••C_2H_4[18] and Ar•••C_2H_4[18] exhibit internal rotations of C_2H_4 subunits, whereas C_2H_4•••H_2O[12] exhibits internal rotation of the H_2O sub-unit in the complex and complexes like C_2H_4•••CO_2 [19] are double rotors. The potential energy surfaces of H_2S complexes are expected to be floppier than their H_2O counterpart and it is of interest to see the effects of these dynamics in the spectra. These splitting patterns of course tell us a lot of about the strength of the interaction between the two monomers. Here, in this part of the work, rotational spectra for C_2H_4•••H_2S and its isotopologues have been studied. The structure and dynamics obtained from the experiments and *ab initio* theory have been presented and discussed.

III.B. Experimental details

All the spectra were recorded with the PNFTMW Spectrometer built here in IISc and is described in detail in chapter II and references therein. 1-2 % of C_2H_4 and H_2S were seeded into argon and the mixture was expanded from a backing pressure of 0.5 bar to undergo supersonic expansion. The sample was polarized using a microwave pulse of 0.5 μs duration. The signals could be observed in a single shot. The signals were checked for the component dependence by running the experiments in the absence of C_2H_4 and H_2S and the signals didn't appear in absence of either. Further, the signal could be observed by using helium as a carrier gas. Higher back pressure (~1 bar) was needed

to see the signal in helium. HDS/D_2S signals were observed by passing H_2S through HDO/D_2O. The identity of the D_2S signals were confirmed by passing H_2S through a mixture of 50% H_2O/D_2O, which diminished the C_2H_4•••D_2S/C_2D_4•••D_2S signals significantly because of the relative higher concentration of HDS in the expansion. The relative increase in HDS concentration was confirmed by monitoring the Ar•••HDS and Ar•••D_2S signals. The samples e.g. Ar (99.999%), C_2H_4 (99.9%) and H_2S (99.5%) were obtained from Bhuruka Gases Ltd. and were used without any further purification. The spectra for $^{13}CCH_4$•••H_2S and C_2H_4•••$H_2{}^{34}S$ were observed in natural abundances. Isotopically enriched samples were used for C_2D_4 (99 atom% D, Aldrich) and D_2O (99.95 atom% D, Aldrich).

III.C. Results and Discussion

III.C.1. Search and assignment

A π-bonded structure very similar to that of other hydride complexes such as C_2H_4•••HF,[14] C_2H_4•••HCl[15] and C_2H_4•••H_2O[12,13], was assumed for C_2H_4•••H_2S. A preliminary *ab initio* geometry optimization at MP2/6-31G* predicted a geometry having S-H•••π interaction. The details of the calculations are discussed later. The initial search for the transitions of the complex was based on the comparison of the rotational constants for several B•••HCl and B•••H_2S (where B = Ar, C_6H_6 and C_2H_4) complexes. The rotational constants have inverse dependence on the intermolecular distances and the masses. HF and H_2O have similar masses. Thus, for the complexes of HF and H_2O with the same acceptor, the rotational constants will be a function of the intermolecular distances, which indeed depends on the strength of the interaction. The benzene π cloud being a strong acceptor of hydrogen bonds binds with equal strength to both HF and H_2O. Hence, both C_6H_6•••HF[20,21] and C_6H_6•••H_2O[16,17] have very similar values for the rotational constants. The rotational constant of C_6H_6-HF is 2048.5 MHz and that of C_6H_6•••H_2O is 1994.8 MHz. Both HCl and H_2S have similar masses and the same is the situation with C_6H_6•••HCl[22,23] and C_6H_6•••H_2S[2] complexes. The *B* rotational constants for C_6H_6•••HCl and C_6H_6•••H_2S are 1237.7 MHz and 1168.5 MHz respectively. On the other hand, argon being a weaker acceptor of hydrogen bonds cannot distinguish the

better hydrogen bond donors such as HF/HCl than H_2O/H_2S and exhibit similar intermolecular distances. Thus, the *B* rotational constant of Ar•••HCl[24] and Ar•••H_2S[25] are 1678.5 MHz and 1681.4 MHz respectively. C_2H_4 seems to be the intermediate of these two extreme cases. C_2H_4•••HF has higher values of the rotational constants than C_2H_4•••H_2O. The rotational constants for C_2H_4•••HF[14] are *A* = 24122 MHz, *B* = 4368.0 MHZ, *C* = 3898.7MHz whereas the rotational constants for C_2H_4•••H_2O[12,13] are *A* = 25960 MHz, *B* = 3823.6 MHz and *C* = 3452.1 MHz. Based on these observations, it was expected that for C_2H_4•••H_2S, the rotational constants would be close to those of C_2H_4•••HCl but on the lower side. The higher value of the *A* rotational constant for the rigid structure excluded the possibility of seeing the *b* and *c* dipole transitions in our spectrometer range. A search for $1_{01}\rightarrow2_{02}$ transition was started at 8950 MHz as the same transition for C_2H_4•••HCl occurs at 8951.366 MHz. The first transitions for C_2H_4•••H_2S were observed as a doublet at 7788.9219 MHz and 7788.0750 MHz. One more doublet was located at 7780.7434 MHz and 7779.9832 MHz. These four transitions were assigned to be the $1_{10}\rightarrow2_{11}$ quartet later. An immediate search near 100 MHz down these frequencies located one more quartet which was tentatively assigned as the $1_{01}\rightarrow2_{02}$ quartet (very close to $1_{01}\rightarrow2_{02}$ transition for C_2H_4•••Ar[18] at 7655.7 MHz). Having this in mind, search was performed for $1_{11}\rightarrow2_{12}$ transitions at 100 MHz down the $1_{01}\rightarrow2_{02}$ quartet. The quartet could be located immediately. After having these sets of transitions, other transitions could be located within 1-2 MHz of the predictions as the spectrum turned out to be that of a nearly prolate asymmetric top. Each of the rotational transitions is split into four lines –two sets of doublets separated by several MHz which is designated as L-U splitting. The smaller splitting is less than 1 MHz and denoted by L1-L2/U1-U2 splitting. A schematic of the four line pattern observed for C_2H_4•••H_2S is shown in Figure III.1. A total of 68 transitions were measured. The transitions are listed in Table III.1. The lines were fitted into *a* dipole transitions in four independent series using Watson's S-reduction Hamiltonian. The fitted parameters are shown in Table III.9. Four of the distortion constants were varied during the fitting. Inclusion of D_K worsens the fitting and this behaviour is consistent for all the isotopes. Some more transitions which are dependent on C_2H_4 and H_2S but could not be assigned are listed in the appendix at the end of this chapter. These transitions may arise from some other

structure of C_2H_4•••H_2S. The rotational constants for C_2H_4•••$H_2{}^{34}S$, C_2H_4•••HDS, C_2H_4•••D_2S, C_2D_4•••H_2S, C_2D_4•••HDS, C_2D_4•••D_2S, $^{13}CCH_4$•••H_2S were predicted from the rotational constants of C_2H_4•••H_2S. The lines could be observed readily. The transitions are listed from Table III.2-III.8. The $2_{02}\rightarrow3_{03}$ transitions for C_2H_4•••H_2S are shown in Figure III.2

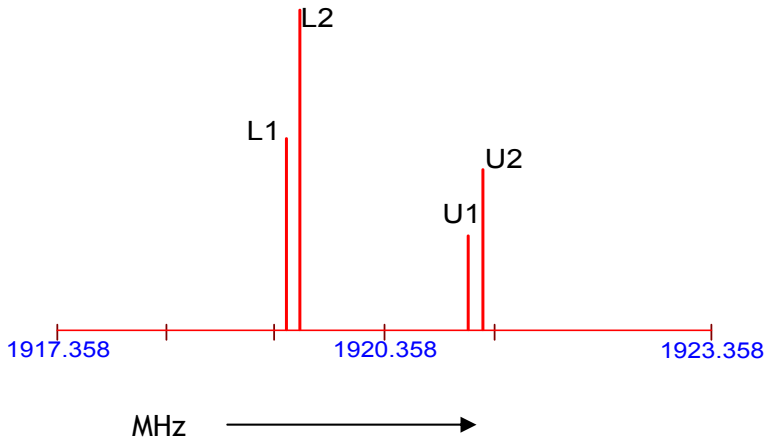

Figure III. 1. A schematic of the four line pattern observed for C_2H_4•••H_2S complex. (B+C)/2 for each series is plotted in the diagram.

Like the parent isotopologue, all the lines were split into four for C_2H_4•••$H_2{}^{34}S$, C_2H_4•••D_2S. The lines appeared as a doublet for C_2H_4•••HDS. In case of C_2D_4•••H_2S, C_2D_4•••HDS, C_2D_4•••D_2S complexes, all the transitions could not be resolved at the lower J s as the splitting was very small. At higher J, the transitions could be resolved and as it can be seen from the tables that the lines are split into four for C_2D_4•••H_2S and C_2D_4•••D_2S whereas the lines are observed as doublets for C_2D_4•••HDS. For $^{13}CCH_4$•••H_2S, all the transitions could not be observed. The strongest $2_{02}\rightarrow3_{03}$ transition for $^{13}CCH_4$•••H_2S is shown in Figure III.3. The intensities of the K=1 lines were less compared to the K=0 lines. Hence, the K = 1 transitions needed averaging of 10000-15000 gas pulses in our spectrometer to achieve a good S/N ratio. The transitions for $^{13}CCH_4$•••H_2S are listed in Table III.5. In Table III.5., some of the transitions have been measured at the University of Virginia. The residues and the standard deviations of the

fittings are quite high and it is mainly because of the inclusion of the lines from the broad-band measurements which have a resolution of 100 kHz. For $^{13}CCH_4$•••H_2S, the value of *A* was fixed at the calculated value of *C* rotational constant for $^{13}CCH_4$ during the fitting of both the series. The fitted parameters for the isotopes of C_2H_4•••H_2S are listed in Table III.10-Table III.16. For C_2H_4•••$H_2{}^{34}S$, C_2H_4•••HDS and C_2H_4•••D_2S and C_2D_4•••HDS only three distortion constants D_J, D_{JK}, d_1 were fitted. For C_2D_4•••H_2S and C_2D_4•••D_2S, values of d_1 and d_2 constants were fixed at the values for the parent isotopologues and only D_J and D_{JK} were varied. The hyperfine structure arising due to the quadrupole coupling of the deuterium nucleus was resolved for the J=0→J=1 transitions of C_2H_4•••HDS complex and are shown in Figure III.4. Each of the doublets is split into three hyperfine components. The fitting of the hyperfine structures for both the series is shown in Table III.17. However, no hyperfine structures could be observed and resolved for the C_2D_4 complexes.

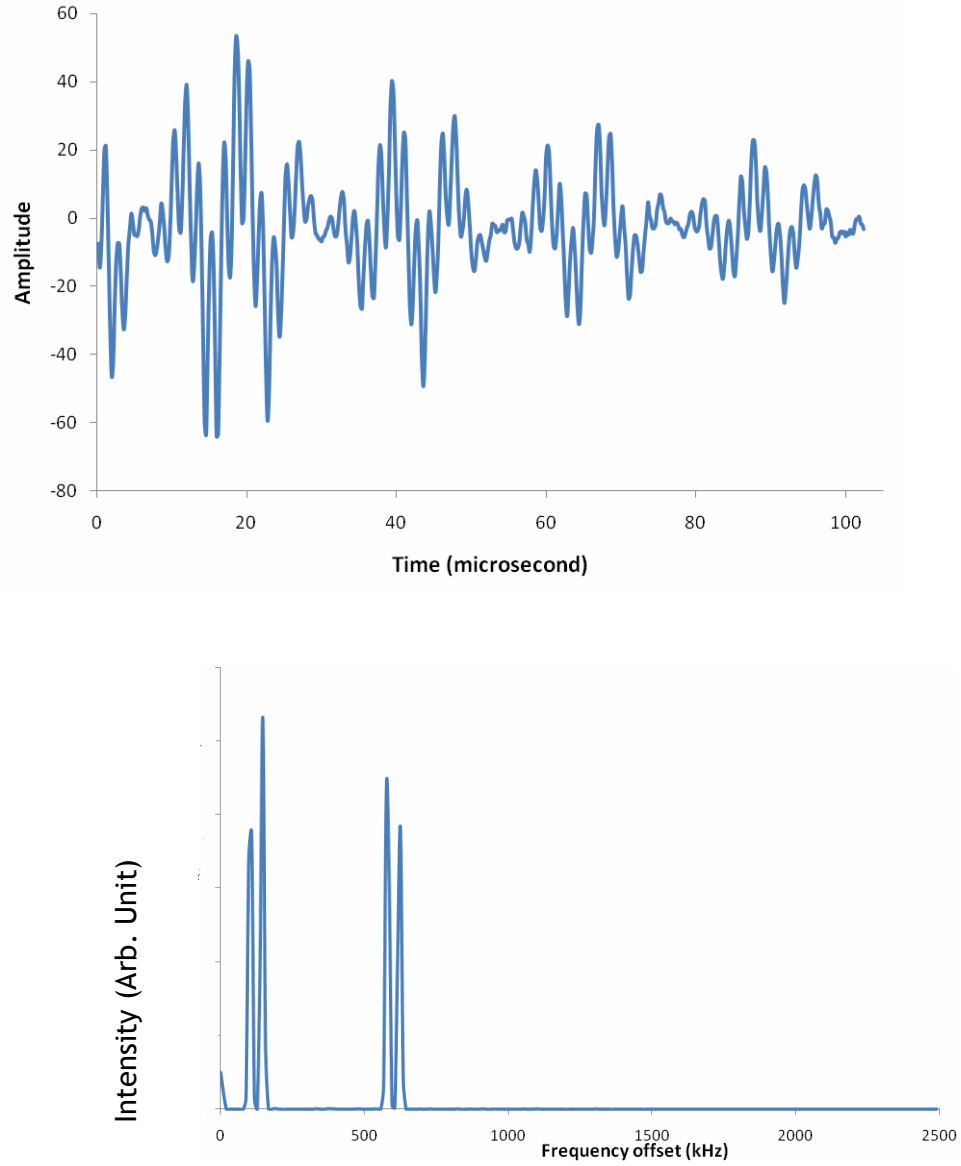

Figure III.2. Time domain and corresponding frequency domain spectrum of $2_{02}\rightarrow 3_{03}$ transition of $C_2H_4\bullet\bullet\bullet H_2S$ complex at 11515.0758 and 11515.8051 MHz. The MO frequency was 11515.2 MHz. 200 gas pulses (13 FIDs for each gas pulse) have been averaged for this signal.

Table III.1. Experimentally observed rotational transitions, assignments and their residues for C_2H_4•••H_2S complex.

Transitions[a]	L1		L2		U1		U2	
	Freq/MHz	Res./ kHz	Freq/MHz	Res./ kHz	Freq /MHz	Res./ kHz	Freq/MHz	Res./ kHz
0_{00}-1_{01}	3839.2887	6.6	3839.5289	3.3	3842.5789	9.1	3842.8441	3.9
1_{11}-2_{12}	7567.9895	2.0	7568.2071	-5.6	7573.8046	-5.1	7574.0447	-4.7
1_{01}-2_{02}	7677.8746	4.2	7678.3620	6.5	7684.4786	12.1	7685.0082	3.1
1_{10}-2_{11}	7779.9832	-1.5	7780.7434	0.8	7788.0750	-5.5	7788.9219	-5.1
2_{12}-3_{13}	11350.9490	-3.6	11351.2883	-1.5	11359.7351	-6.7	11360.0947	-5.6
2_{21}-3_{22}	11491.0770	-7.6	11491.8364	-7.1	11503.1952	-6.8	11504.0171	-10.2
2_{20}-3_{21}	11492.4402	-5.8	11493.2019	-8.2	11504.5662	-9.1	11505.4004	-8.0
2_{02}-3_{03}	11515.0758	4.4	11515.8051	10.9	11525.0275	10.1	11525.8346	15.0
2_{11}-3_{12}	11668.8501	-1.7	11669.9797	-6.2	11681.0539	-5.2	11682.3206	-4.6
3_{13}-4_{14}	15132.6796	-4.8	15133.1301	-2.6	15144.5033	-4.3	15144.9772	-6.4
3_{22}-4_{23}	15319.6033	7.2	15320.6143	7.9	15335.8775	8.9	15336.9759	10.9
3_{21}-4_{22}	15323.0052	6.4	15324.0305	8.4	15339.3111	9.8	15340.4269	10.0
3_{03}-4_{04}	15350.1954	3.5	15351.1487	1.8	15363.5568	6.8	15364.6246	15.6
3_{12}-4_{13}	15556.3646	-3.1	15557.8716	-3.5	15572.7576	-5.4	15574.4373	-6.9
4_{14}-5_{15}	18912.7730	-0.5	18913.3293	-2.5	18927.7185	-1.5	18928.3108	-1.1
4_{04}-5_{05}	19182.5398	0.1	19183.7196	0.2	19199.3912	-1.7	19200.6394	-6.2
4_{13}-5_{14}	19442.0792	-1.6	19443.9559	-1.4	19462.7645	-1.3	19464.8552	-1.2

[a] *Transitions are listed as $J''_{Ka''Kc''}$-$J'_{Ka'Kc'}$*

Table III.2. Experimentally observed rotational transitions, assignments and their residues for C_2H_4•••$H_2{}^{34}S$ complex.

Transitions[a]	L1		L2		U1		U2	
	Freq. (MHz)	Res. (kHz)	Freq. (MHz)	Res. (kHz)	Freq. (MHz)	Res. (kHz)	Freq. (MHz)	Res. (kHz)
1_{11}-2_{12}	7384.5013	0.4	7384.7179	0.8	7389.1277	0.3	7389.3592	0.2
1_{01}-2_{02}	7489.0897	-0.3	7489.5513	-0.2	7494.4374	-1.0	-	-
1_{10}-2_{11}	7586.2239	0.4	7586.9425	1.0	7592.9745	1.9	7593.7722	0.5
2_{12}-3_{13}	11075.7750	-0.4	11076.0982	-1.0	11082.7733	-0.3	11083.1158	-0.2
2_{02}-3_{03}	11232.0186	0.3	11232.7072	0.2	11240.0919	1.2	11240.8492	0.0
2_{11}-3_{12}	11378.2675	-0.4	11379.3426	-1.1	11388.4563	-2.2	11389.6529	-0.6
3_{13}-4_{14}	14765.8778	0.1	14766.3108	0.3	14775.3199	0.1	14775.7672	0.07
3_{03}-4_{04}	14973.0072	-0.1	14973.9187	-0.1	14983.8630	-0.4	14984.8636	0.0
3_{12}-4_{13}	15169.0329	0.1	15170.4634	0.4	15182.7437	0.7	15184.3299	0.2

[a] *Transitions are listed as $J''_{Ka''Kc''}$-$J'_{Ka'Kc'}$*

Table III.3. Experimentally observed rotational transitions, assignments and their residues for C_2H_4•••D_2S complex.

Transitions[a]	L1		L2		U1		U2	
	Freq(MHz)	Res. / kHz	Freq(MHz)	Res. /(kHz)	Freq(MHz)	Res. /(kHz)	Freq(MHz)	Res. /kHz
0_{00}-1_{01}	–		–		–		–	
1_{11}-2_{12}	7414.4024	6.0	7414.4349	-4.9	7425.2728	5.3	7425.3197	-1.5
1_{01}-2_{02}	7515.1408	-1.1	7515.2731	-1.3	7527.5600	-2.6	7527.7034	-2.1
1_{10}-2_{11}	7609.0975	7.0	7609.3036	-2.0	7623.2463	4.4	7623.4775	1.9
2_{12}-3_{13}	11120.7259	-3.6	11120.8037	4.2	11137.0203	-3.9	11137.1130	2.3
2_{02}-3_{03}	11271.2567	2.4	11271.4535	1.6	11289.8530	2.4	11290.0654	1.4
2_{11}-3_{12}	11412.6988	-5.1	11413.0257	-0.1	11433.9095	-2.7	11434.2546	-2.8
3_{13}-4_{14}	14826.0215	-2.2	14826.1240	0.0	14847.7288	-1.0	14847.8497	-1.4
3_{03}-4_{04}	15025.6148	-1.9	15025.8773	-0.7	15050.3471	-0.2	15050.6304	0.6
3_{12}-4_{13}	15215.1990	-1.4	15215.6323	2.4	15243.4388	-1.5	15243.8974	1.5
4_{14}-5_{15}	18529.9327	1.5	18530.0625	-0.6	18557.0376	1.0	18557.1868	0.3
4_{04}-5_{05}	18777.6469	0.5	18777.9694	0.07	18808.4560	-2.6	18808.8058	-0.5
4_{13}-5_{14}	19016.2105	1.4	19016.7501	-1.1	19051.4442	1.1	19052.0163	-0.3

[a] *Transitions are listed as $J''_{Ka''Kc''}$-$J'_{Ka'Kc'}$*

Table III.4. Experimentally observed rotational transitions, assignments and their residues for C_2H_4•••HDS complex.

Transitions[a]	L1		L2	
	Freq(MHz)	Res. (kHz)	Freq(MHz)	Res. (kHz)
0_{00}-1_{01}	3824.0561	2.0	3824.1348	0.2
1_{11}-2_{12}	11307.8889	-2.2	11307.9794	-1.3
1_{01}-2_{02}	11469.7124	-1.4	11469.9463	-0.7
1_{10}-2_{11}	11623.2862	-1.2	11623.6691	-1.4
2_{12}-3_{13}	15075.6076	2.9	15075.7267	1.7
2_{02}-3_{03}	15290.0909	1.7	15290.3977	0.8
2_{11}-3_{12}	15495.9988	1.6	15496.5075	1.8
3_{13}-4_{14}	18841.9624	-1.0	18842.1144	-0.6
3_{03}-4_{04}	19108.0116	-0.6	19108.3915	-0.2
3_{12}-4_{13}	19367.2306	-0.6	19367.8625	-0.6

[a] *Transitions are listed as $J''_{Ka''Kc''}$-$J'_{Ka'Kc'}$*

Table III.5. Experimentally observed rotational transitions, assignments and their residues for $^{13}CCH_4\bullet\bullet\bullet H_2S$ complex. The fitting was not performed for the U1 and U2 series as the number of lines observed were not enough for fitting three rotational constants.

Transitions[a]	L1		L2		U1	U2
	Freq(MHz)	Res. (kHz)	Freq(MHz)	Res. (kHz)	Freq(MHz)	Freq(MHz)
1_{01}-2_{02}	7535.2388	-139.0	7535.5622	-198.0	-	7541.4822
1_{10}-2_{11}	7637.92[b]	34.4	7638.72[b]	238.0	-	-
2_{12}-3_{13}	11138.7560	-0.0	11139.0810	-0.0	11146.9192	11146.5721
2_{02}-3_{03}	11301.6351	158.0	11302.3314	224.4	11310.5567	11311.3354
2_{11}-3_{12}	11455.26[b]	-38.1	11456.44[b]	-25.3	11466.94[b]	11468.04[b]
3_{03}-4_{04}	15065.6428	-48.8	15066.5730	-69.2	15077.6346	15078.6548
3_{12}-4_{13}	15270.8905	11.3	15272.3525	7.1		15287.3703

[a] *Transitions are listed as $J''_{Ka''Kc''}$-$J'_{Ka'Kc'}$*

[b] *These transitions were observed at the broadband MW spectrometer at the University of Virginia at Brooks Pate's laboratory. The resolution of the spectrometer is 100 kHz.*

Table III. 6. Experimentally observed rotational transitions, assignments and their residues for $C_2D_4\bullet\bullet\bullet H_2S$ complex

Transitions[a]	L1		L2		U1		U2	
	Freq(MHz)	Res. /kHz	Freq(MHz)	Res. /kHz	Freq(MHz)	Res. (kHz)	Freq(MHz)	Res. (kHz)
1_{11}-2_{12}	6964.9014	-14.2	6964.9622	2.7	6966.0674	-12.0	6966.1397	8.2
1_{01}-2_{02}	7075.1265	2.1	7075.1852	-0.9	7076.6290	-3.5	7076.7149	-2.1
1_{10}-2_{11}	7177.1473	-0.2	7177.2496	-11.3	7180.2634	3.3	7180.4022	-2.5
2_{12}-3_{13}	10446.3604	7.7	10446.4181	7.0	10448.1661	7.5	10448.2290	-3.8
2_{02}-3_{03}	10610.6054	-2.5	10610.7029	1.0	10612.9260	4.0	10613.0525	2.4
2_{11}-3_{12}	10764.6117	8.8	10764.7662	2.8	10769.3418	2.5	10769.5471	-2.7
3_{13}-4_{14}	13926.5682	1.3	13926.6245	-6.6	13929.0878	0.4	13929.1776	-1.2
3_{03}-4_{04}	14143.5976	0.8	14143.7247	-0.4	14146.7785	-1.2	14146.9518	-0.8
3_{12}-4_{13}	14350.7076	-6.4	14350.9134	3.5	14357.1515	-3.6	14357.4272	3.3

[a] *Transitions are listed as $J''_{Ka''Kc''}$-$J'_{Ka'Kc'}$*

Table III. 7. Experimentally observed rotational transitions, assignments and their residues for C_2D_4•••D_2S complex.

Transitions[a]	L1		L2		U1		U2	
	Freq(MHz)	Res. (kHz)	Freq(MHz)	Res. (kHz)	Freq(MHz)	Res. (kHz)	Freq(MHz)	Res. (kHz)
1_{11}-2_{12}	6819.7157	15.9	6819.7157	20.6	6826.8591	-6.5	6826.8591	-3.7
1_{01}-2_{02}	6921.0702	-1.3	6921.0702	1.6	6929.2683	-7.2	6929.2683	-3.8
1_{10}-2_{11}	7015.1638	8.0	7015.1638	-6.6	7024.8113	5.4	7024.8113	-0.0
2_{12}-3_{13}	10228.6835	-5.6	10228.6835	-2.9	10239.4417	6.2	10239.4417	-4.6
2_{02}-3_{03}	10379.8404	1.5	10379.8404	-1.7	10392.1300	8.2	10392.1300	4.3
2_{11}-3_{12}	10521.7540	-21.9	10521.7866	-13.2	10536.2510	-4.9	10536.2856	8.9
3_{13}-4_{14}	13636.6438	-3.8	13636.6438	-8.1	13650.9701	-1.4	13651.0196	5.3
3_{03}-4_{04}	13836.4842	-0.5	13836.5034	0.5	13852.8163	-2.6	13852.8393	-1.3
3_{12}-4_{13}	14027.2575	12.4	14027.2936	12.0	14046.5613	1.0	14046.6052	-6.6

[a] *Transitions are listed as $J''_{Ka''Kc''}$-$J'_{Ka'Kc'}$*

Table III. 8. Experimentally observed rotational transitions, assignments and their residues for C_2D_4•••HDS complex.

Transitions[a]	*L1*		*L2*	
	Observed freq. (MHz)	Res. (kHz)	Observed freq. (MHz)	Res. (kHz)
1_{11}-2_{12}	6932.7465	0.1	6932.7465	0.2
1_{01}-2_{02}	7040.9638	4.8	7040.9638	9.7
1_{10}-2_{11}	7143.1787	4.5	7143.1787	10.2
2_{12}-3_{13}	10398.2692	-0.1	10398.2692	-0.1
2_{02}-3_{03}	10559.5620	-5.5	10559.5620	-11.1
2_{11}-3_{12}	10713.8302	-5.2	10713.8302	-11.8
3_{03}-4_{04}	14075.9326	1.7	14075.9656	3.5
3_{12}-4_{13}	14283.3848	1.6	14283.4239	3.7

[a]*Transitions are listed as $J''_{Ka''Kc''}$-$J'_{Ka'Kc'}$*

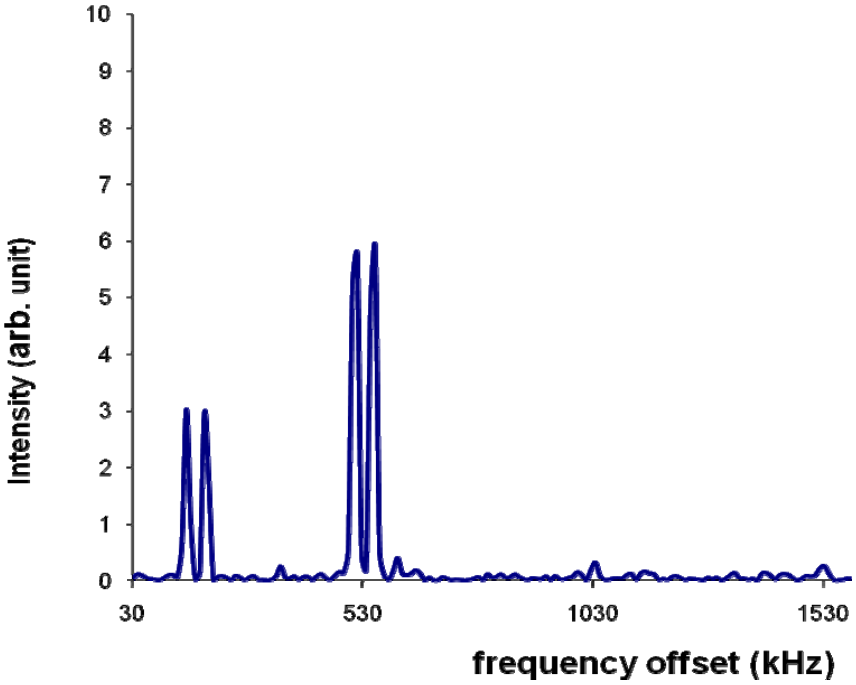

Figure III.3. The $2_{02} \rightarrow 3_{03}$ transition of $^{13}CCH_4$•••H_2S collected in 1% natural abundance. The molecular frequencies are 11301.6351 MHz and 11302.3311 MHz. These signals were averaged for 400 gas pulses. A total of thirteen FIDs were collected for each single gas pulse. Collection time was around 1 minute 20 seconds.

Table III.9. Fitted rotational constants, centrifugal distortion constants and standard deviation of the fits for all the four series of C_2H_4•••H_2S complex.

Parameters	L1	L2	U1	U2
A (MHz)	25961(34)	25968(42)	26189(55)	26204(61)
B (MHz)	1972.682(2)	1972.937(2)	1974.891(3)	1975.178(3)
C (MHz)	1866.658(2)	1866.646(2)	1867.732(3)	1867.715(3)
d_1(kHz)	-0.80(2)	-0.82(2)	-0.74(3)	-0.76(4)
d_2(kHz)	-0.21(2)	-0.22(2)	-0.24(3)	-0.24(3)
D_J (kHz)	14.30(2)	14.31(2)	13.26(3)	13.28(3)
D_{JK} (MHz)	1.0587(2)	1.0575(3)	0.9691(4)	0.9684(4)
Sd (kHz)	4.4	5.6	7.1	8.1

Table III. 10. Fitted rotational constants, centrifugal distortion constants and standard deviation of the fits for all the four series of C_2H_4•••$H_2{}^{34}S$ complex

Parameters	L1	L2	U1	U2
A (MHz)	25920(19)	25924(36)	25907(58)	25907[a]
B (MHz)	1922.905(6)	1923.146(5)	1924.764(9)	1925.0341(5)
C (MHz)	1822.019(6)	1822.009(5)	1822.819(9)	1822.8062(5)
d_1(kHz)	-0.77(2)	-0.76(2)	-0.69(1)	-0.674(8)
D_J (kHz)	13.722(7)	13.72(1)	12.60(2)	12.652(7)
D_{JK} (MHz)	1.0112(2)	1.0102(4)	0.9282(6)	0.9277(1)
Sd (kHz)	0.3	0.6	1.1	0.6

[a]*The A rotational constant has been fixed at the value obtained from the fitting of the U1 series.*

Table III.11. Fitted rotational constants, centrifugal distortion constants and standard deviation of the fits for all the four series of C_2H_4•••D_2S complex.

Parameters	L1	L2	U1	U2
A (MHz)	25674(74)	25580(54)	25671(54)	25653(48)
B (MHz)	1927.636(2)	1927.712(1)	1931.568(1)	1931.647(1)
C (MHz)	1830.274(2)	1830.264(1)	1832.560(1)	1832.524(1)
d_1(kHz)	-0.52	-0.54(1)	-0.62(1)	-0.63(1)
D_J (kHz)	11.86(2)	11.81(2)	12.01(2)	11.99(2)
D_{JK} (MHz)	0.924(1)	0.925(8)	0.904(9)	0.904(8)
Sd (kHz)	3.6	2.6	2.7	2.3

Table III. 12. Fitted rotational constants, centrifugal distortion constants and standard deviation of the fits for two series for C_2H_4•••HDS complex

Parameters	L1	L2
A (MHz)	25877(36)	25872(25)
B (MHz)	1964.638(9)	1964.726(7)
C (MHz)	1859.463(9)	1859.453(7)
d_1(kHz)	-0.592(9)	-0.606(7)
D_J (kHz)	11.14(1)	11.138(9)
D_{JK} (MHz)	0.8821(6)	0.8820(5)
Sd (kHz)	1.5	1.1

Table III. 13. Fitted rotational constants, centrifugal distortion constants and standard deviation of the fits for the two series (stronger set) for $^{13}CCH_4$•••H_2S complex

Parameters	L1	L2
A (MHz)	24287	24287
B (MHz)	1937.16(8)	1937.5(1)
C (MHz)	1830.9(1)	1830.8(2)
d_1(kHz)	-11(2)	-12(3)
D_J (kHz)	11(1)	9(2)
D_{JK} (MHz)	0.95(2)	0.93(3)
Sd (kHz)	84	117.0

Table III.14. Fitted rotational constants, centrifugal distortion constants and standard deviation of the fits for all the four series for C_2D_4•••H_2S complex

Parameters	L1	L2	U1	U2
A (MHz)	17470(12)	17638(95)	17572(94)	17685(64)
B (MHz)	1822.084(3)	1822.118(2)	1822.940(2)	1822.985(2)
C (MHz)	1715.943(3)	1715.941(2)	1715.826(2)	1715.824(1)
d_1(kHz)	-0.80	-0.82	-0.74	-0.76
d_2(kHz)	-0.21	-0.22	-0.24	-0.24
D_J (kHz)	12.2(1)	12.42(8)	11.09(8)	11.21(6)
D_{JK} (MHz)	11.578(3)	1.152(3)	1.002(3)	0.998(2)
Sd (kHz)	4.6	5.3	5.3	3.6

Table III. 15. Fitted rotational constants, centrifugal distortion constants and standard deviation of the fits for all the four series of C_2D_4•••D_2S complex.

Parameters	L1	L2	U1	U2
A (GHz)	17.3(2)	17.5(2)	17.3(1)	17.2(1)
B (MHz)	1779.342(4)	1779.345(4)	1782.015(2)	1782.016(1)
C (MHz)	1681.589(4)	1681.583(4)	1683.022(1)	1683.017(2)
d_1(kHz)	-0.80	-0.82	-0.74	-0.76
d_2(kHz)	-0.21	-0.22	-0.24	-0.24
D_J (kHz)	10.4(2)	10.4(1)	10.2(8)	9.96(8)
D_{JK} (MHz)	1.025(5)	1.023(5)	0.978(3)	0.977(2)
Sd (kHz)	10.5	9.2	5.3	4.9

Table III. 16. Fitted rotational constants, centrifugal distortion constants and standard deviation of the fits for all the two series of C_2D_4•••HDS complex.

Parameters	L1	L2
A (GHz)	17.6(1)	17.7(2)
B (MHz)	1813.062(4)	1813.056(9)
C (MHz)	1707.829(4)	1707.83(1)
d_2(kHz)	0.6(1)	0.4(2)
D_J (kHz)	9.3(2)	9.2(3)
D_{JK} (MHz)	0.881(3)	0.879(6)
Sd (kHz)	3.6	7.8

Figure III.4. J=0→1 spectrum of C_2H_4•••HDS showing D quadrupole coupling and the tunnelling doublets. Each component of the doublet is split into three hyperfine components. The spectrum was collected for 2000 gas pulses. Single FID was collected for each gas pulse. Total of 2048 points were collected at a sampling frequency of 5 MHz.

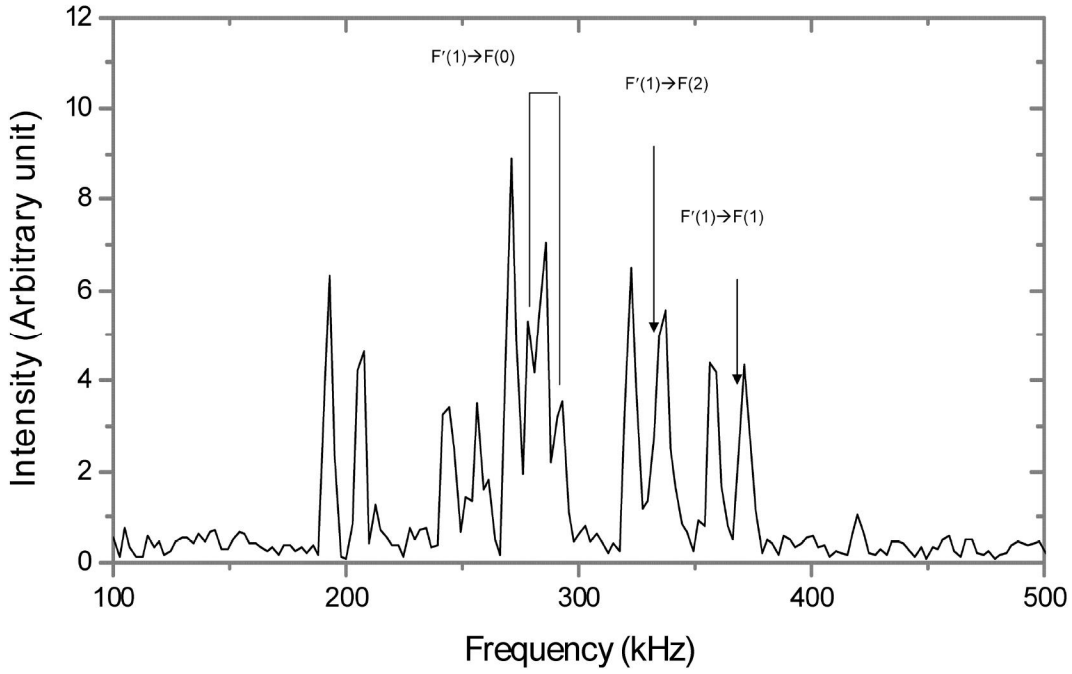

Table III.17. Fitted hyperfine components of J=0→J=1 transition of C_2H_4•••HDS

F′	F	Observed (MHz)	Res.(kHz)	Observed(MHz)	Res. (kHz)
1	0	3824.0851	0.4	3824.1640	0.3
1	2	3824.0497	-0.7	3824.1286	-0.5
1	1	3823.9993	0.3	3824.0773	0.2

III.C.2. Structural analysis

Table III.9. lists the rotational constants for $C_2H_4\bullet\bullet\bullet H_2S$ complex. The differences in *B* and *C* rotational constants of the four states are very small. Though, the error in the *A* rotational constant is quite large, these constants were used to get an approximate zero point energy averaged structure of $C_2H_4\bullet\bullet\bullet H_2S$. The *B* and C rotational constants of the ethylene monomer were determined to be 29990 MHz and 24860 MHz from an Infrared study.[26] From Table III.9., it is apparent that the *A* rotational constant of the complex is close to the *C* rotational constant of ethylene (*c*-axis of the ethylene monomer is perpendicular to the molecular plane of C_2H_4) which indicates that H_2S is lying on an axis perpendicular to the plane of C_2H_4 (the *c* principal axis of ethylene is perpendicular to it) and does not contribute much to the moment of inertia about this axis. Further, the differences in the *A* rotational constants of H_2S and $H_2{}^{34}S$ isotopologues are less than the uncertainties for all the four states, which indicates that the S atom is located on the dimer *a* principal axis.

The distance of the substituted atoms from the center of mass is given by Kraitchman's equation:

$$|r| = \left[\left(\frac{1}{2\mu}\right)(\Delta I_x + \Delta I_y + \Delta I_z)\right]^{1/2} \qquad (1)$$

Here, μ is the reduced mass of the substitution and ΔI is the change in moment of inertia upon substitution. From the rotational constants of $C_2H_4\bullet\bullet\bullet H_2S$, $C_2H_4\bullet\bullet\bullet H_2{}^{34}S$, $C_2H_4\bullet\bullet\bullet HDS$ and $C_2H_4\bullet\bullet\bullet D_2S$ and $^{13}CCH_4\bullet\bullet\bullet H_2S$, the distances of the substituted atoms from the center of mass were calculated by using the above equation. The distance of the S from the center of mass was found to be 1.852 Å and the distances of the two H atoms from the center of mass is 1.034 Å and 2.163 Å. The unequal distances of the two hydrogen atoms from the center of mass indicate that only one H is bonded to the π center of ethylene. Using the rotational constants of $C_2H_4\cdots H_2S$ and $^{13}CCH_4\cdots H_2S$, the distance of the carbon atom from the center of mass of the complex has been calculated to be 2.395 Å. Using the planar moments of inertia relations,

$$|x| = \left[\frac{\Delta P_x}{\mu} \left(1 + \frac{\Delta P_y}{I_x - I_y} \right) \left(1 + \frac{\Delta P_z}{I_x - I_z} \right) \right]^{1/2}$$ and so on, the x, y and z c-ordinates of the carbon atom can be found as $|a|$ = 2.086 Å, $|b|$ = 0.993 Å, $|c|$ = 0.634 Å. The $|c|$ co-ordinate is close to the $|a|$ co-ordinate of the free ethylene monomer which is 0.6685 Å (the C-C bond length determined in reference 26 is 1.337 Å). The *a* co-ordinate for the substituted carbon is also reasonable and closer to the *ab initio* optimized value of 2.088 Å and 2.083 Å. However, the value of the *b* co-ordinate derived from these equations is rather surprising. From the derived value of the $|a|$ and $|c|$ co-ordinates, if one assumes that the *ac* inertial plane is passing through the C-C bond of ethylene, the |b| co-ordinate should be close to zero. However, this inconsistency may arise due to the poorly determined values of the rotational constants of $^{13}CCH_4 \bullet\bullet\bullet H_2S$ complex. As was mentioned previously, the fit used a fixed value for the *A* rotational constant of the complex. The value of the *A* rotational constant was put equal to the *C* rotational constant of the ^{13}C ethylene monomer while fitting. Further, the situations may be more complex, as a nearly free rotation of the non-bonded hydrogen in the complex will result in the interchange of the *b* and *c* principal axes of the complex, which can result in the poorly determined values of the *b* and *c* co-ordinate of the carbon atoms.

In order to calculate the intermolecular distance, it was assumed that both the hydrogens are symmetrically bonded to ethylene π cloud. The moment of inertia about the *b* and *c* principal axes of the complex can be written as:

$$I_b(\text{complex}) = I_a(C_2H_4) + I_a(H_2S) + \mu R^2 \quad (2)$$

$$I_c(\text{complex}) = I_b(C_2H_4) + I_c(H_2S) + \mu R^2 \quad (3)$$

The rotational constants of the strongest series of $C_2H_4\cdots H_2S$ were used to find out the c.m.-c.m distance. The intermolecular distance (c.m-c.m separation) was determined by using the equations 2 and 3. The c.m-c.m. separation determined from the equations are 4.041(1) and 4.037(1) Å respectively. An assumption of H_2S to be spherical changed the c.m-c.m separation only by 0.01Å. Hence, the orientation of H_2S has very little effect on the moment of inertia of the complex. The assumption of H_2S being symmetrically bonded is not a very gross approximation here.

The hyperfine structure arising due to the quadrupole coupling of the deuterium nucleus was analysed to find out the average angle θ of the S-D bond with the dimer *a* axis. For free HDS, the diagonal components of the D quadrupole interaction are 153.7 kHz, -65.3 kHz and -88.4 kHz for χ_{xx}, χ_{yy} and χ_{zz} respectively. The three hyperfine transitions were fitted to a line-center to find out χ_{aa}(D), which is the projection of the D quadrupole interaction tensor on the dimer's inetial *a* axis. The fit gives χ_{aa}(D) to be -114(2) kHz for the stronger series and -115(1) kHz for the weaker series. Hence, they are identical within the error limit. The average angle θ can be found from the relation:

$$\chi_{aa} = \frac{\chi_{xx}}{2}\left\langle 3Cos^2\theta - 1\right\rangle \qquad (4)$$

By using equation 4, the θ value is calculated to be 24.8° for the stronger series and 24.2° for the weaker state. A very similar value of θ for the two states of C_2H_4•••HDS indicates that the orientation of H_2S is very similar for both the states, which is expected as these states arise due to the internal rotation of ethylene. The value of θ is very close to the C_6H_6•••HDS complex, which also possesses a π-bonded structure. The value is 26° for C_6H_6•••HDS. No hyperfine transitions have been reported for C_2H_4•••H_2O complex. However, the value of θ is 34° for the C_6H_6•••HOD complex.

III.C.3. Internal rotation and the splitting

As mentioned in the previous section, each of the transition is split into four for the parent isotopologue. This splitting essentially indicates the presence of large amplitude motions in the complex. The fact that we have been able to fit each of this series independently using the semi-rigid rotor Hamiltonian indicates that the transitions occur among the individual tunnelling states and not across them. This is not surprising as all of the observed transitions are *a* dipole and none of the internal motions involving C_2H_4 or H_2S reverse the *a* dipole component in the complex. This limits the determination of the tunnelling splitting directly from the spectrum. However, the difference between the rotational constants of the individual tunnelling states could indirectly be related to the tunnelling splitting. Splitting in (B+C)/2 for all the isotopologues are listed in Table III.18. The dependence of the splitting pattern on the isotopic substitution provides important clue about the mechanism of internal motions in the complex.

TableIII.18. Experimental splitting in (B+C)/2 observed for C_2H_4•••H_2S isotopologues

	1-2 (MHz)[a]	L-U (MHz)[b]
C_2H_4•••H_2S	0.1215	1.6483
C_2H_4•••$H_2{}^{34}S$	0.1155	1.3363
C_2H_4•••HDS	0.0390	-
C_2H_4•••D_2S	0.0330	3.1033
C_2D_4•••H_2S	0.0160	0.3723
C_2D_4•••HDS	0.003	-
C_2D_4•••D_2S	0.002	2.0528
$^{13}CCH_4$•••H_2S	0.1161[c]	1.4938[c]

[a] *The reported values have been calculated using the constants of L1-L2 series.*
[b] *The splitting in (B+C)/2 has been reported as the difference of the line centers of L1-L2 and U1-U2 series.*
[c] *Calculated by dividing the $2_{02}\rightarrow 3_{03}$ transition frequencies by 2(J+1) as the uncertainty in the fitted rotational constants are high compared to other isotopes.*

Let us consider the smaller splitting (L1-L2/U1-U2) first. This splitting decreases by a very small magnitude (only 5%) in C_2H_4•••$H_2{}^{34}S$. The small reduction in the splitting is indicative of the fact that the sulphur atom undergoes minimal movement during the motion which causes this splitting. The splitting decreases by three times in C_2H_4•••HDS. In general the single deuterium substitution always happens at the bonded hydrogen as the zero point energy effect makes this isomer more stable than the other where a non-bonded hydrogen is deuterated. The smaller splitting decreases by only 15% in C_2H_4•••D_2S compared to C_2H_4•••HDS. Thus, replacing the non-bonded hydrogen does not affect the smaller splitting in C_2H_4•••D_2S. This indicates that the hydrogen of H_2S which is bonded to the ethylene π cloud is involved in the dynamics, whereas the non-bonded hydrogen has very little contribution to the dynamics. A drastic decrease of seven times in the smaller splitting was observed in C_2D_4•••H_2S. Thus, the four hydrogens of ethylene play a significant role in the dynamics causing the splitting. Hence, the motion is a coupled motion which involves both the monomer units. The

smaller splitting shows a decrease of five times in C_2D_4•••HDS compared to C_2D_4•••H_2S. As we go from C_2D_4•••HDS to C_2D_4•••D_2S, the magnitude of the splitting is affected very little. The decrease is only ~33%, much less compared to the effect observed after the bonded deuterium substitution. These facts when put together indicate that the dynamics causing the smaller splitting involves the motion of ethylene along with the movement of the S-H bond. The mechanism by which ethylene undergoes internal rotation could be one of these three: 1. rotation of ethylene about C-C bond axis (rotation about its *a* principal axis) 2. in -plane rotation of ethylene (rotation about its *c* principal axis) and 3. end-over-end rotation of ethylene (rotation of ethylene about its *b* principal axis). The first motion does not interchange the two carbons whereas the last two motions would involve the interchange of two equivalent carbon atoms in the complex. Hence, the splitting pattern for $^{13}CCH_4$•••H_2S can tell us if the motion involves the interchange of the two carbon atoms or not. If any mechanism interchanges the two carbon atoms we would expect the smaller splitting to vanish for singly substituted ^{13}C-isotopologue. Observation of all the four states in case of $^{13}CCH_4$•••H_2S clearly tells us that the rotation of ethylene about the C-C bond axis is the pathway for the motion causing the smaller splitting. However, as we note from Table III.18., there is a very minute change in the smaller splitting (~5% reduction) upon the ^{13}C substitution. This small change may be the result of the coupling of the radial co-ordinate to the ethylene rotation about the C-C bond axis.

Like the smaller splitting, the larger splitting also shows little dependence on sulphur substitution. Vanishing of this splitting in C_2H_4•••HDS indicates that it arises because of some internal rotation/tunnelling which interchanges the equivalent hydrogens of H_2S. The splitting increases by two times as we go from C_2H_4•••H_2S to C_2H_4•••D_2S. This increase in the magnitude indicates that the splitting arises because of some nearly free rotation of the hydrogen sulphide moiety. A similar situation was observed in case of C_6H_6•••H_2O and C_6H_6•••D_2O. Splitting in C_6H_6•••D_2O increases twice compared to C_6H_6•••H_2O. If this motion is solely because of the H_2S moiety, the larger splitting in C_2D_4•••H_2S should be same as that of C_2H_4•••H_2S. It is intriguing to see that the larger splitting also decreased almost by four times, as we go from C_2H_4•••H_2S to C_2D_4•••H_2S. Thus, we conclude that the larger splitting has contribution from the ethylene hydrogens

as well. Even in C_2H_4•••H_2O, the motion which interchanges the equivalent hydrogens of H_2O had some degree of coupling with the ethylene hydrogens. In case of C_2H_4•••H_2O, this dependence on the ethylene hydrogens was manifested via the complex dependence of the splitting magnitude on the ethylene hydrogen substitutions. Coming back to C_2H_4•••H_2S, the larger splitting vanishes in C_2D_4•••HDS as can be expected. For the C_2D_4 complexes, substituting H_2S with D_2S causes a further increase in the larger splitting like C_2H_4•••H_2S/C_2H_4•••D_2S complexes. The magnitude of the increase is more pronounced in case of C_2D_4 complexes. The splitting increases by six times when we go from C_2D_4•••H_2S to C_2D_4•••D_2S. Thus, the magnitude of the increase is much exaggerated compared to C_2H_4•••H_2S/C_2H_4•••D_2S. The exact reason for this is beyond the scope of this study. The larger splitting remains almost unaffected (~10%) as we substitute the ^{12}C by ^{13}C as can be seen from the Table III.18. This indicates that the motion of H_2S is coupled to the movement of ethylene hydrogens but there is a minimum involvement of the carbon atoms of C_2H_4. From these observations, it can be concluded that the larger splitting involves the interchange of two equivalent hydrogens of H_2S and the motion is coupled to the movement of ethylene hydrogens.

III.C.4 *Ab initio* calculations

All the calculations were performed using Gaussian 98[27] or Gaussian 03[28] suite of programme. Calculations were done at different levels of theory to determine the optimized geometries, binding energies, vibrational frequencies of C_2H_4•••H_2S which are discussed in the following subsections. The binding energies were corrected for BSSE and the zero point energy effects wherever possible. Details of the BSSE correction are described in chapter II. In addition to that, potential energy curves were calculated for different internal motions of C_2H_4 and H_2S to know the barrier heights. The curves were calculated at MP2(full)/aug-cc-pVDZ and MP2(full)/aug-cc-pVTZ level. For the potential energy surface calculations, BSSE corrections were done at each point of the curve using the previously mentioned method. To find out the adequacy of the level of calculations, potential energy curve for the rotation of ethylene about the C-C bond axis (the *a* principal axis of C_2H_4 monomer), has been calculated at CCSD(T)/aug-cc-pVTZ and was compared to the barrier height at MP2(full)/aug-cc-pVTZ level. The barrier

height for this motion changes by 69 cm^{-1} between the MP2(full) and CCSD(T) level. The barrier height is 344 cm^{-1} at CCSD(T)/aug-cc-pVTZ level and 413 cm^{-1} at MP2(full)/aug-cc-pVTZ level. Further, the position of the minima and the maxima of the curve is same at both the level of calculations. However, performing the CCSD(T) calculation along with the counterpoise calculations turned out to be really time-consuming and were not done for all other motions. Hence, all the potential energy curves reported here, were calculated at MP2(full) level.

III.C.4.a. Optimized geometries and the binding energies

At the very first step of the geometry optimization, the monomers were optimized at the same level of theory. The optimized geometries of the monomers were used in the input specifications during the geometry optimization of the complex structure. Different initial geometries were chosen but given a chance to relax, the geometries converged to a minimum having S-H•••π interaction. The optimised geometry at MP2(full)/aug-cc-pVTZ level is shown in Figure III.5. The geometry optimisations have been performed at both BSSE corrected and the uncorrected surfaces for most of the basis sets. Frequency calculations were done to ensure that the obtained stationary points were true minima. The binding energies of the π-bonded complex at different basis sets are shown in Table III.19. and Table III.20. In general, one would expect that a better basis sets will lead to smaller Basis set superposition error. However, from Table III.19 and Table III.20, one can see that the magnitude of BSSE does not show a consistent decrease as the basis set size increases. It is rather oscillating. This behaviour has been previously observed in literature.[29,30] The complex is bound at all level of calculations except the counter-poise uncorrected optimization at MP2(full)/6-311++G** level. It is worth noting that the optimization of C_2H_4•••H_2S on the counterpoise corrected surface at MP2(full)/6-311++G** level yields a bound geometry. The optimized structural parameters of the π-bonded geometry of C_2H_4•••H_2S have been listed in the appendix at the end of this chapter. The geometry of C_2H_4•••H_2S obtained via the optimization on the counter-poise corrected surface is different than the one obtained on the counterpoise uncorrected surface. This shift in the minimum position on the curve is mainly caused by the fact that the BSSE increases as the two fragments get closer to each other because the basis set

extension increases at a smaller distance. Thus, the minimum in the energy is shifted to a higher intermolecular distance upon the optimization on the BSSE corrected surface. Consequently, all of the optimized parameters would also change. Further, the shape of the interaction potential may also change. It has been pointed out in literature that the magnitude of the interaction energy obtained after the optimization on the uncorrected surface followed by counterpoise correction is always less then the interaction energy obtained via the optimization on the counterpoise corrected surface.[31] The same has been observed for C_2H_4•••H_2S complex for all basis sets employed at MP2(full) level.

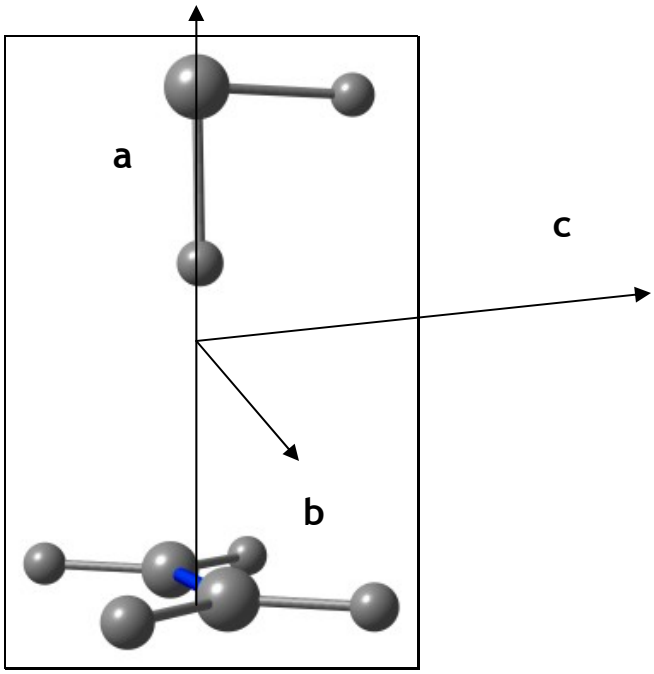

Figure III.5. Optimized geometry of C_2H_4•••H_2S at MP2(full)/aug-cc-pVTZ level of theory. The optimized structure has C_1 symmetry. The principal axes system of C_2H_4•••H_2S is shown.

Apart from the S-H•••π bonded structure shown in Figure III.5., few other stationary points could be located. Another minimum having C-H•••S interaction could be located and the geometry is shown in Figure III.A.1 as Structure F in the appendix at

the end of this chapter. Some more geometries were optimized as transition state or saddle point of order two. Their geometries, interaction energies and the vibrational frequencies are listed in the appendix at the end of this chapter.

Table III.19. Binding energies (in cm^{-1}) of the optimized geometries of the π bonded complex of C_2H_4•••H_2S using different basis sets at MP2 (full) level. All the reported binding energies have been corrected for BSSE and ZPE effect. The optimizations have been done at counterpoise uncorrected surface.

Basis set	6-31G*	6-311++G**	6-311++G(3df, 2p)	6-311++G(3df, pd)	6-311++G(3df, 3pd)	aug-cc-pVDZ	aug-cc-pVTZ	aug-cc-PVQZ
ΔE	-31	60	-262	-239	-221	-197	-220	-214[a]
BSSE	325	443	206	214	284	438	425	150

[a]*The ZPE correction at this level has been done by adding the zero point energy of the complex calculated at MP2(full)/aug-cc-pVTZ level*

Table III.20. Binding energies (in cm^{-1}) of the optimized geometries of the π bonded complex of C_2H_4•••H_2S using different basis sets at MP2(full) level. All the reported binding energies have been corrected for BSSE and ZPE effect. The optimizations have been done at counterpoise corrected surface.

Basis set	6-31G*	6-311++G**	6-311++G(3df, 2p)	6-311++G(3df, pd)	6-311++G(3df, 3pd)	aug-cc-pVDZ	aug-cc-pVTZ
ΔE	-99	-176	-320	-306	-558	-316	-367
BSSE	256	321	165	189	236	361	347

III.C.4.b. AIM calculations

AIM[32] calculations have been performed for the S-H•••π bonded structure of C_2H_4•••H_2S to locate the bond critical points (BCP) between the atoms and the bond paths connecting them. These calculations have been performed using the MP2(full)/aug-cc-pVTZ and MP2(full)/6-311++G** wave functions. The critical points and the bond paths are shown in Figure III.6. At MP2(full)/aug-cc-pVTZ level, the bond critical point connects the hydrogen of H_2S to the carbon atom of ethylene instead of the center of π bond. At MP2(full)/6-311++G** level, the bond critical point has been found between the hydrogen and the center of π bond of ethylene. The electron density (ρ) and the Laplacian of the electron density at the bond critical point are shown along with the figures. These values are well within the range for hydrogen bonds as was suggested by Popelier. [33]

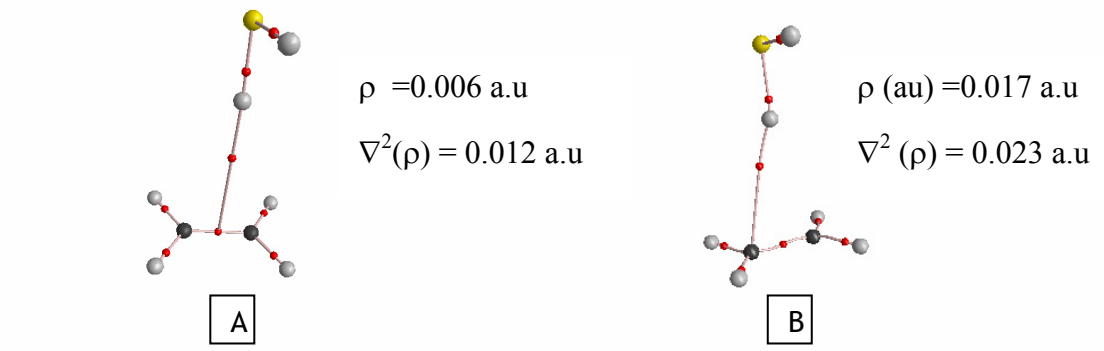

*Figure III.6. The bond critical points and the bond paths for C_2H_4•••H_2S calculated using A. 6-311++G** basis set B. aug-cc-pVTZ basis set*

III.C.4.c. Potential energy curves, barrier heights and the dynamics

From the experimental spectrum, it was clear that two large amplitude motions led to observable splitting. In order to identify these motions, it was decided to calculate the barriers for several possible internal motions within the complex. For the potential energy surface scan, a C_s symmetric structure having S-H•••π interaction was chosen as the reference geometry. The geometry is shown in Figure III.9. The geometry was chosen

such that the plane of H_2S bisects the C-C bond of ethylene. The structural parameters of the monomers were frozen at their optimized values obtained at the same level of theory. The intermolecular separation, R, is defined as the distance between the sulphur and the mid point of C-C bond. For the MP2(full)/aug-cc-pVDZ calculations, R is fixed at a value obtained from the optimized geometry of the complex at this basis set. R was fixed at 4.192 Å for all the potential energy scans at MP2(full)/aug-cc-pVDZ level. For the MP2(full)/aug-cc-pVTZ level calculations, R was varied from 3.5 to 14 Å. The minimum of the interaction energy was located at R = 4.0 Å. The potential energy curve obtained by varying R at MP2(full)/aug-cc-pVTZ level is shown in Figure III.8. Having these sets of parameters fixed, potential energy curves were calculated for different motions of C_2H_4 and H_2S. The approximate location of the principal axes system of the two monomers is shown in Figure III.7.

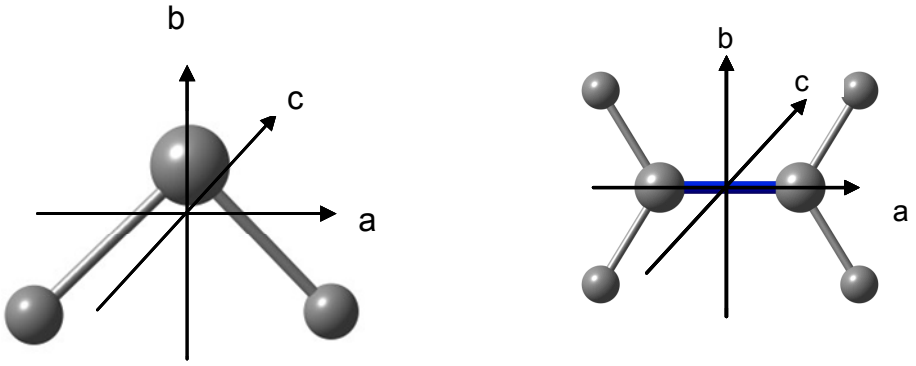

Figure III.7. The principal axes system of H_2S and C_2H_4 monomer

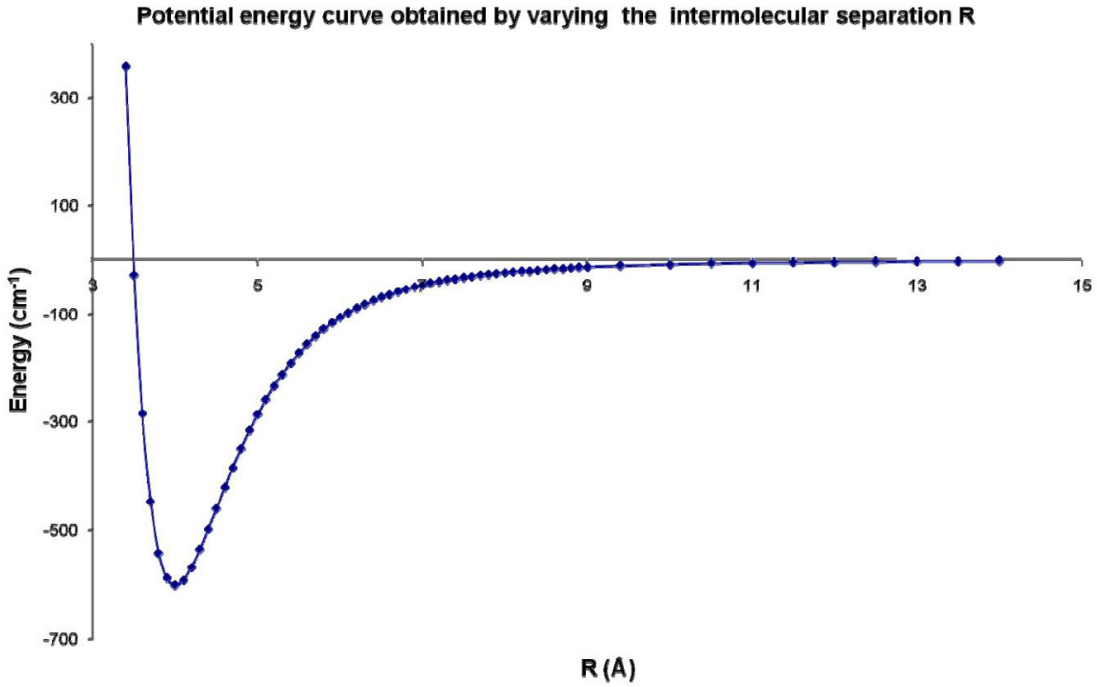

Figure III.8. Variation of energy along the stretching co-ordinate for C_2H_4•••H_2S complex

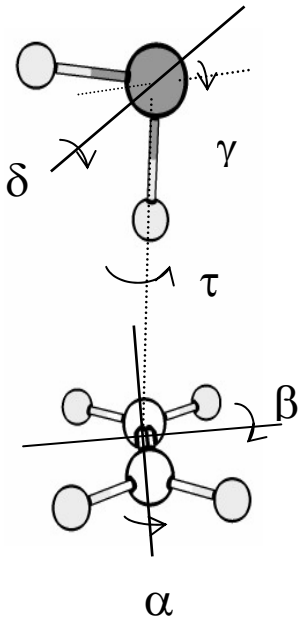

Figure III.9. The reference geometry (α =0°, β=0°, γ=0°, τ=90°, δ=0°) of C_2H_4•••H_2S complex chosen for the potential energy scans. The structural parameters varied during the scans are shown in the figure.

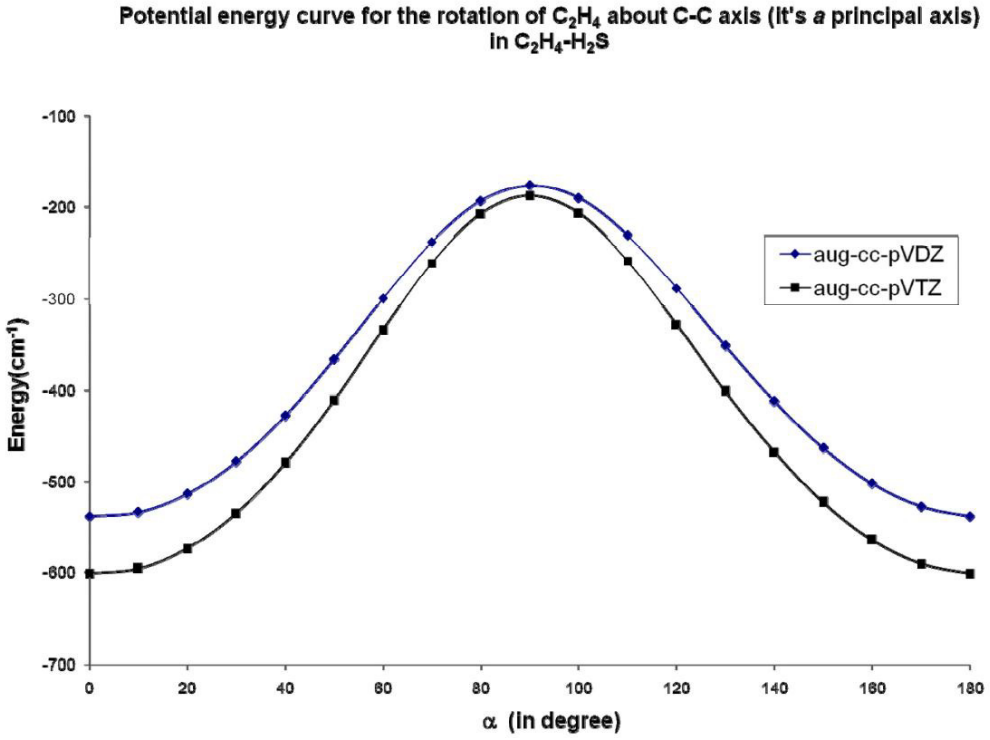

Figure III.10. Variation of potential energy due to the rotation of C_2H_4 about its 'a' principal axis (C-C bond axis) in C_2H_4•••H_2S complex.

Potential energy curve for the rotation of C_2H_4 about its *a* axis i.e. along the α co-ordinate is shown in Figure III.10. The vale of α at the reference geometry is 0° (the S-H bond is perpendicular to the plane of the ethylene monomer). The barrier for this motion lies at α = 90°, where the S-H bond is in the plane of ethylene C_2H_4 monomer. The potential energy barrier for this rotation is 413 cm^{-1} with aug-cc-pVTZ basis set whereas it is 362 cm^{-1} with aug-cc-pVDZ basis set.

Variation of energy along the β co-ordinate i.e. the rotation of C_2H_4 about its *b* axis in the complex is shown in Figure III.11. The angle β is 0° for the reference geometry. The barrier for this motion lies at β = 90°. Using aug-cc-pVDZ basis set, the barrier for this motion was found to be 675 cm^{-1}. The calculated barrier is much higher at aug-cc-pVTZ level and it is 1443 cm^{-1}.

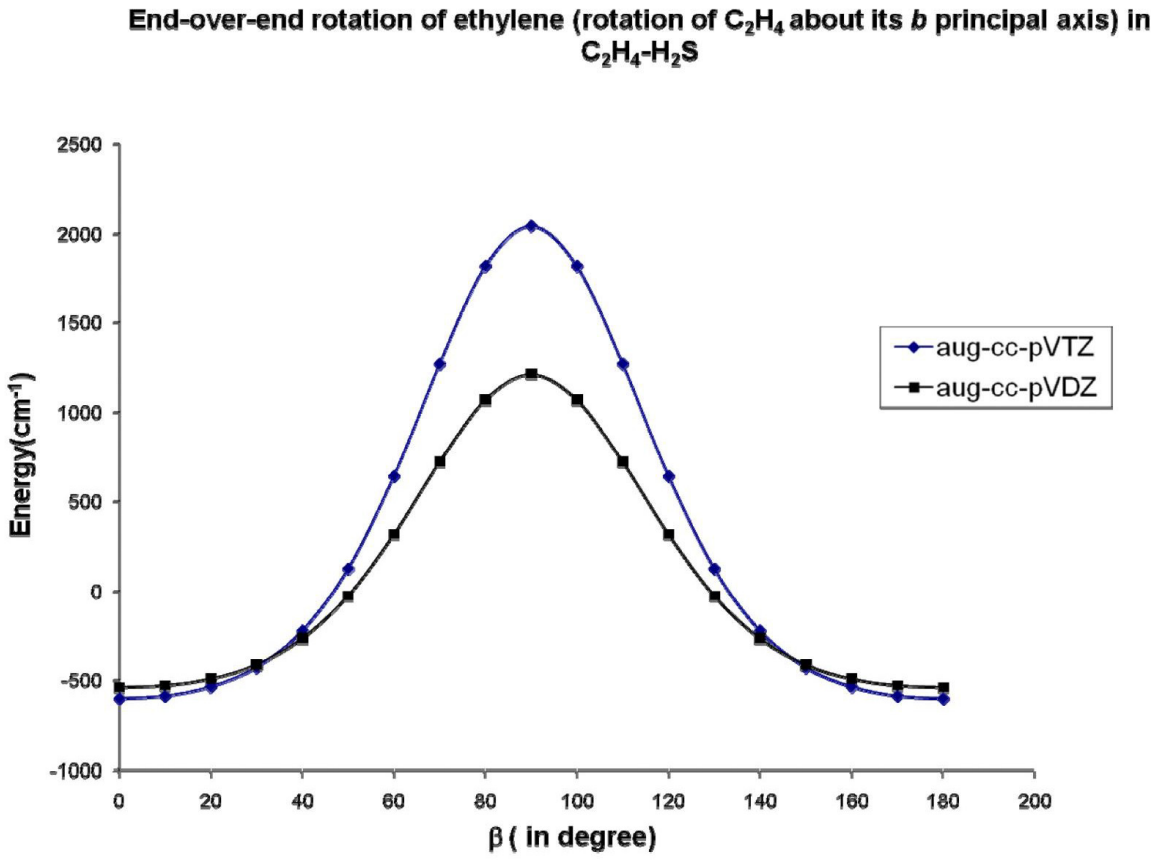

Figure III.11. Variation of potential energy due to the rotation of C_2H_4 about its 'b' principal axis in C_2H_4•••H_2S complex.

Figure III.12. shows the variation of energy along the τ co-ordinate i.e. the rotation of H_2S about the hydrogen bond. The barrier calculated for this motion was found to be ~10 cm^{-1} using both aug-cc-pvDZ and aug-cc-pVTZ basis sets. The value of τ in the reference geometry is 90°. The barrier lies at τ = 0° which corresponds to a configuration where the non-bonded hydrogen of H_2S is lying along the C-C bond axis.

Figure III.13. shows the variation of energy along the δ co-ordinate i.e. the rotation of H_2S about its C_2 symmetric axis (*b* principal axis of the H_2S monomer). The value of δ is 0° for the reference geometry. The barrier for this motion lies at δ = 90° and corresponds to a geometry where the sulphur is facing the ethylene π cloud. Calculation using aug-cc-pVDZ basis set yields a barrier of 404 cm^{-1} whereas the calculation using aug-cc-pVTZ basis set gives a barrier of 422 cm^{-1}.

Figure III.14. shows the variation of energy along the γ co-ordinate i.e. the rotation of H_2S about its *c* principal axis. This motion faces two barriers. The smaller barrier is for a doubly hydrogen bonded geometry (γ = 50°) and the larger barrier is for the S-down (S atom facing the π-cloud of ethylene) configuration i.e γ = 270° . The smaller barrier is 148 cm^{-1} at aug- cc-pVDZ basis set and 155 cm^{-1} at aug-cc-pVTZ basis set. The larger barrier is 448 cm^{-1} at aug-cc-pVDZ and 469 cm^{-1} aug-cc-pVTZ.

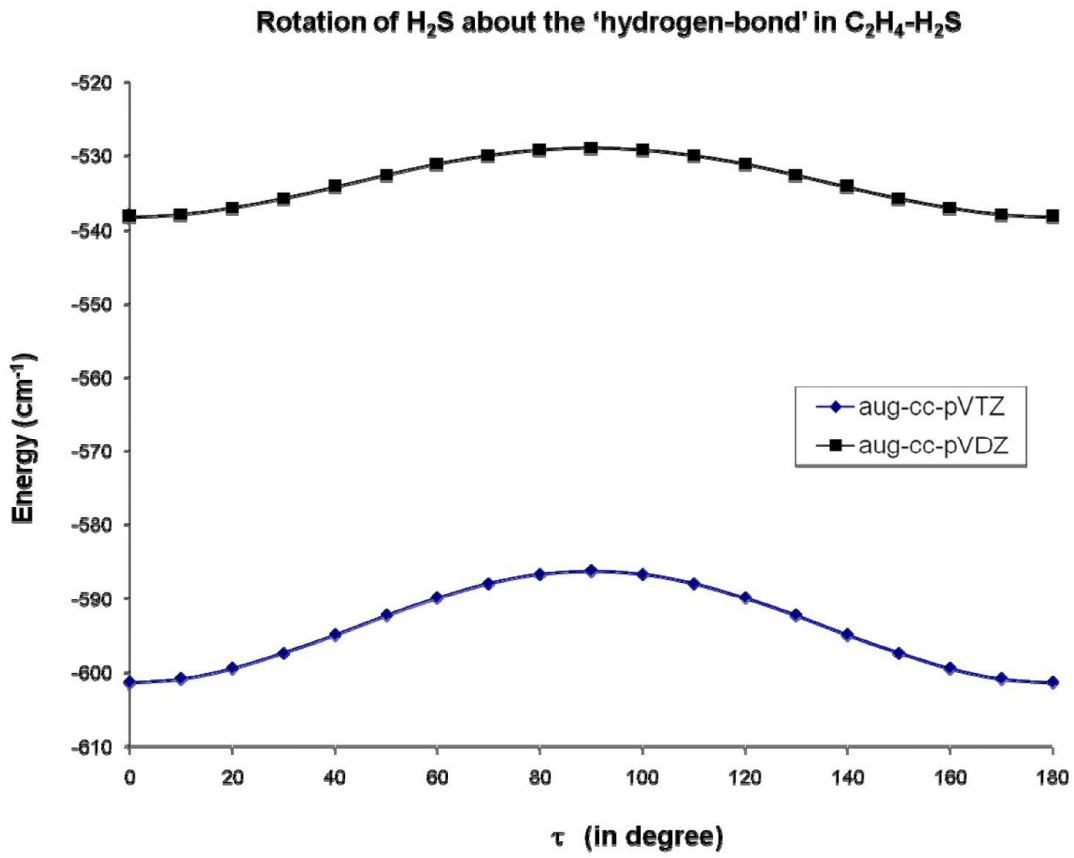

Figure III.12. Variation of potential energy due to the rotation of H_2S about the hydrogen bond in C_2H_4•••H_2S complex.

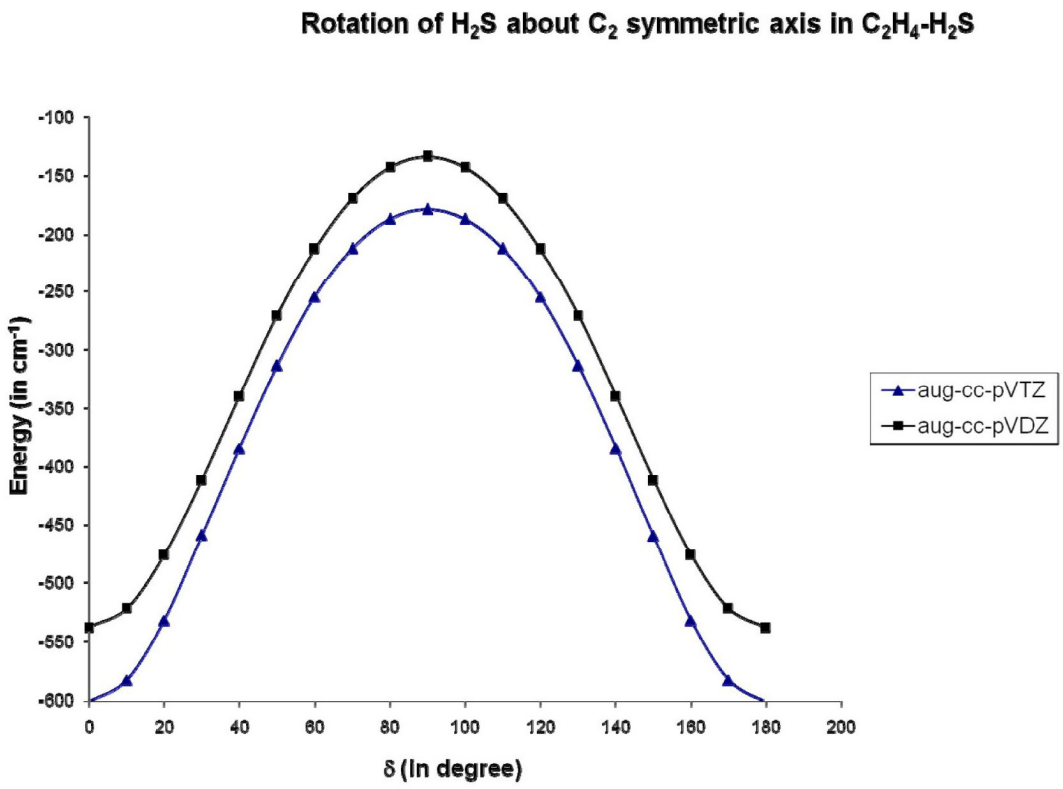

Figure III.13. Variation of potential energy due to the rotation of H_2S about its C_2 symmetric ('b' principal axis) axis in C_2H_4•••H_2S complex.

A comparison of the barrier heights for all the motions discussed above sheds some light on the dynamics observed in the C_2H_4•••H_2S complex. An inspection of the barrier heights makes it clear that the barrier for the end-over-end rotation of C_2H_4 moiety (rotation of C_2H_4 about its *b* principal axis) is too high and can be excluded from any further consideration. The in-plane rotation of ethylene can be best thought of as the rotation of the H_2S about the hydrogen-bond as the reduced mass for the former would be too high. An extremely low value for this motion makes it highly probable to be present in the complex. However, the present experimental data do not show any evidence in support of this particular motion. The reason may be the splitting is too large to detect in our spectrometer range or the higher internal rotation levels may not be populated enough in the expansion. Thus, all the evidences points to a mechanism indicate mechanism by which the ethylene unit rotates about it's *a* principal axis.

Figure III.14. Variation of potential energy due to the rotation of H_2S about its 'c' principal axis in C_2H_4•••H_2S complex.

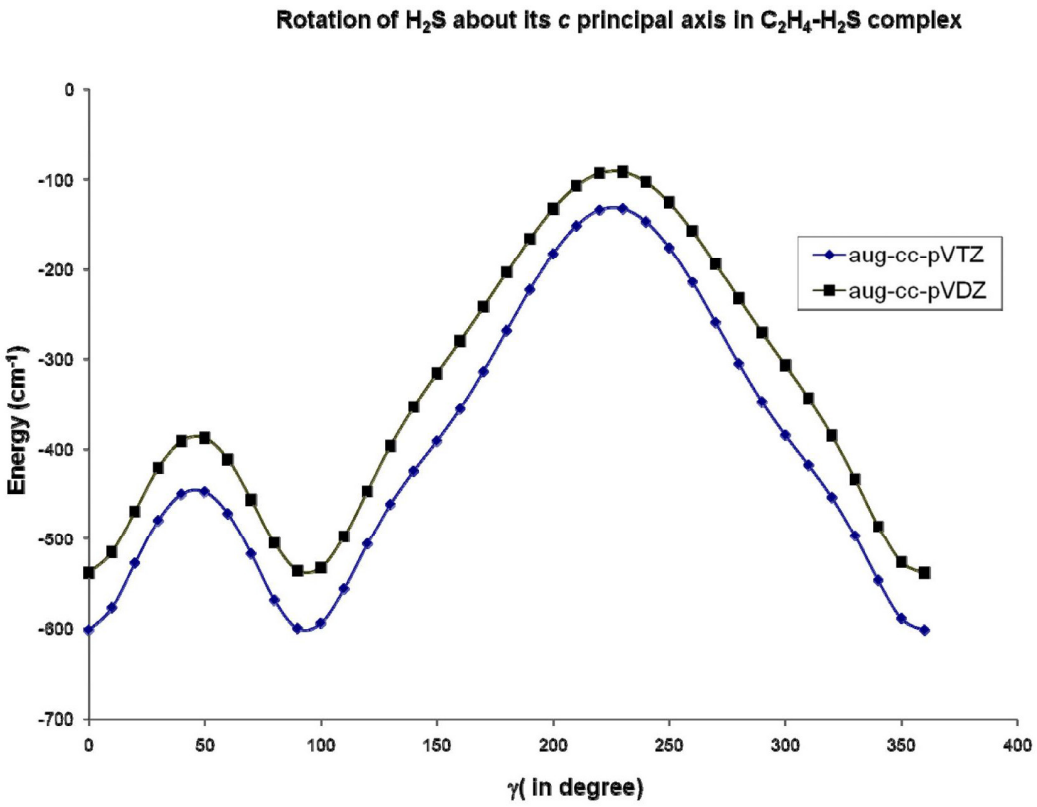

Let us consider the larger splitting. From the experimental data, it is clear that the larger splitting arises from the interchange of two equivalent hydrogens of H_2S. The first mechanism that comes in mind is the rotation of H_2S about its C_2 symmetry axis. The barrier for this motion is reasonable and the magnitude is comparable to the barrier height of the ethylene rotation about its C-C bond axis. The other mechanism which may cause the splitting is the rotation of H_2S about its *c* principal axis coupled with the rotation of H_2S about the hydrogen bond. The second motion was believed to play a role in case of C_2H_4-•••H_2O complex. In case of C_2H_4•••H_2O, there was an indirect evidence of this motion from the Stark effect measurements. First of all, the Stark effect measurements for C_2H_4•••H_2O revealed a very low value for μ_c as the component of the dipole moment in the *c* axis was averaged out by the rotation of H_2O about the 'hydrogen bond'. Further, a higher value of the dipole moment for the symmetric tunneling states of

C_2H_4•••H_2O suggested the presence of a pathway which maximises the *a* dipole component at the top of the barrier. This indicated towards a 'doubly hydrogen bonded' transition state and the pathway for the motion being the rotation of H_2O about its *c* principal axis. However, this conclusion was not very certain as the experimental difference in the *a* dipole moment of the two states were marginal in comparison to the experimental uncertainties. With this knowledge, let us have a look at the *ab initio* barrier heights for these motions in C_2H_4•••H_2S complex. From the potential energy surface calculations it can be seen that a 360° rotation about the *c* principal axis is not likely as the barrier for placing the sulphur towards the π cloud of ethylene is really high. However, a 90° rotation about this axis is still favourable as it passes through a doubly H-bonded structure. The barrier for this motion is 2-3 times less than the rotation of H_2S about its C_2 symmetry axis and is likelier to happen. Though the Stark effect measurement is not possible in our instrument, the pulse dependence of the L and U states can give some clue regarding the dipole moment of the two states which arise from the H_2S internal rotation. The optimum microwave pulses for these states are same. Hence, one can say that these states arise from the rotation of H_2S about its C_2 symmetry axis. However, from the experimental dataset, it is difficult to draw a definite conclusion about the mechanism as all we have is the rotational constant differences of the two states. These differences in the rotational constants depend upon the barrier heights of the motions, the reduced mass of the motions causing the splitting and the anharmonicity of the respective potentials. Further, all these motions which cause the splitting involve both C_2H_4 and H_2S subunits and are actually coupled. Hence, these one-dimensional *ab initio* calculations serve as only a qualitative guidance to decipher the dynamics.

In Ne•••C_2H_4,[18] it was observed that there is some degree of coupling between the radial motion and the rotation of ethylene about C-C bond axis. To have some idea of the degree of coupling of these intermolecular motions with the radial co-ordinate in C_2H_4•••H_2S, the intermolecular distances were varied from 3.5-4.5 Å, at a step of 0.1 Å, keeping a fixed value for the α, β, γ and δ co-ordinate. These calculations are repeated for several values of each of the angle co-ordinates. All the calculations were performed at MP2(full)/aug-cc-pVTZ level. The barriers along the minimum energy path and the changes in the radial co-ordinates are listed in Table III.21.

Table III.21. Barrier for different internal motions of C_2H_4•••H_2S obtained by optimizing R (intermolecular separation) at each of the angle. All the calculations have been performed at MP2(full)/aug-cc-pVTZ level.

Motions	Barriers (cm^{-1})	Change in R along the minimum energy path (Å)
Rotation of ethylene about C-C bond axis	361	0.2
End-over-end rotation of ethylene	476	1.0
Rotation of H_2S about the C_2 symmetry axis	424	0.2
Rotation of H_2S about its *c* principal axis	468,155[a]	-

[a] *There are two saddle points along this co-ordinate*

Thus, the barrier for the rotation of ethylene about C-C bond axis (about the *a* principal axis of the ethylene monomer) decreases by 52 cm^{-1} as we vary the intermolecular distance. The intermolecular distance changes by 0.2 Å during this motion. This supports the observation that while the ethylene rotates about its C-C bond axis, the intermolecular distance changes and as a consequence, there is a change in the S-H bond length (π bonded S-H group) as well. The barrier for the end-over-end rotation of ethylene decreases by three times at a cost of 1 Å movement along the radial co-ordinate. Such a large degree of change in the radial co-ordinate in order to adapt the minimum energy path makes this motion utterly impossible to happen. The rotation of H_2S about the C_2 symmetry axis requires a change of 0.2 Å along the minimum energy path. The intermolecular distance does not show any significant change if the H_2S is rotated by 90° about its *c* principal axis from the reference geometry. However a 360° rotation about this axis shows a strange oscillation in R, though the barrier to bring the sulphur closer to ethylene π cloud remains the same. Though, the shape of the potential energy curve is still the same, the minimum energy path is no longer smooth. The intermolecular distance decreases to its minimum value of 3.5 Å at 170°. The rotation of H_2S about the

hydrogen bond axis is unlikely to have any dependence on R and is not calculated for that reason.

III.C.4.d. Low frequency vibrations of $C_2H_4\cdots H_2S$

Vibrational frequency calculations have been done at all levels of theory to find the nature of the stationary points. The frequencies of the intermolecular modes for S-H•••π bonded structure of C_2H_4•••H_2S calculated at MP2(full)/aug-cc-pVTZ level are

Table III.22. Low frequency modes for C_2H_4•••H_2S calculated at MP2(full)/aug-cc-pVTZ level. The calculations were done on both counterpoise corrected and the uncorrected geometries.

Intermolecular motions	Vibrational frequencies (cm^{-1}) Counterpoise uncorrected	Vibrational frequencies (cm^{-1}) Counterpoise corrected
Rotation of H_2S about hydrogen bond coupled with the rotation of ethylene about its *b* principal axis	39	25
Rotation of ethylene about its b principal axis coupled with the rotation of H_2S about its *b* principal axis	50	33
Rotation of ethylene about the C-C bond axis coupled with the rotation of H_2S about its *c* principal axis	78	46
Intermolecular stretching	89	69
Rotation of H_2S about its *c* principal axis coupled with the rotation of ethylene about its *a* principal axis	176	123
sweeping of the bonded hydrogen of H_2S over the π cloud of ethylene coupled with the rotation of ethylene about its *b* principal axis	279	211

shown in Table III.22. A glance at Table III.22 makes one realise that the barriers calculated for all the motions are quite high comparable to the zero point energies along the normal modes except the rotation of H_2S about the hydrogen bond. Thus, all the motions which break the 'hydrogen-bond' are hindered. Further, it is worth noting that all the vibrational frequencies have some contribution from both C_2H_4 and H_2S monomers. There is not a single normal mode vibration where the motion is localized on one of the monomer. Thus, it is to be expected that the intermolecular motions which give rise to the splitting will have contributions from both the monomers. Further, the presence of six low frequency modes, especially the frequencies of the lowest four modes are quite close and the coupling of one normal mode to the other is also possible. However, a more accurate description of the mechanism of the motion which causes the splitting is beyond the scope of this study.

In order to have more insights over the mechanism of motions, Infrared-Microwave double resonance studies of the four tunnelling states have been performed by Prof. Brooks H. Pate's group at the University of Virginia.[34] The experiments were performed at both C-H and S-H stretch regions. Different band origins for the four tunnelling states (L1, L2, U1 and U2) have been observed in these regions. The S-H frequency shifts for $C_2H_4\bullet\bullet\bullet H_2S$ calculated at different levels of theory are listed in the appendix at the end of this chapter. Experimentally, a shift of ~-2.5 cm^{-1} has been observed for the asymmetric stretch whereas the symmetric stretch shows a shift of ~-6 cm^{-1}. These studies indicate that the motion which causes larger splitting in the rotational spectrum undergoes a change in the barrier upon excitation of the symmetric/asymmetric stretch of H_2S in the complex. For both symmetric and asymmetric stretches of H_2S, the 1-2 pairs showed the same band-origin which essentially means that these tunnelling states do not arise due to any internal rotation/tunnelling motions involving H_2S. In addition to this, two fundamental C-H stretch vibrations of ethylene monomer have been observed at 2987 cm^{-1} and 3103 cm^{-1}. Interestingly, the vibrational displacement vectors of the higher frequency band of the ethylene C-H stretch changes its sign while ethylene rotates about its C-C bond axis and hence, the vibrational transitions connect the 1 and 2 states. Thus, a shift of 0.1 cm^{-1} in the band origin was measured for the higher frequency tunnelling pair (U1-U2). Hence, these studies provide indirect evidence that the smaller

splitting involves the motion of ethylene whereas the larger splitting involves the motion of H_2S subunit in the complex and corroborate the microwave finding

III.C.5. Molecular Symmetry Group analysis and the relative Intensity pattern:

From Figure III.1., it is clear that the intensities of four lines differ. The intensities are proportional to the spin statistical weights of the corresponding levels. Molecular symmetry group analyses have been done to obtain the nuclear spin statistical weights of the rotational-torsional levels. For the analysis, the equilibrium geometry of the complex was assumed to be of C_s symmetry. The geometry is such that the plane of hydrogen sulphide moiety is passing through the C-C bond of ethylene. It is to be noted that the assumed orientation of the non-bonded hydrogen of H_2S does not alter the results obtained through this analysis. Further, the barrier for the rotation about the hydrogen bond is so low that locating this hydrogen in the equilibrium geometry is impossible from the present set of experimental data. The molecular symmetry group analysis was performed for different motions of ethylene which exchanges different pairs of equivalent hydrogens in the complex.

Considering the rotation of ethylene about its *a* axis, the feasible motions which can lead to the observed splitting patterns are 1. Rotation of C_2H_4 about C-C bond axis 2. Internal rotation of H_2S which interchanges its equivalent hydrogens 3. Both 1 and 2 together. Hence, the molecular symmetry group consists of eight feasible operations: E, (13)(24), (56), (13)(24)(56), E*, (13)(24)*, (56)*, (13)(24(56)*. This group is isomorphic with D_{2h} point group and is named G_8. The G_8 character table is shown in Table III.23. Effect of each of these operations on the equilibrium geometry of the complex is shown in Figure III.15. The conformations resulting from the inversion operation are shown on the right hand side of the Figure III.15. A careful examination of the figure reveals that the rotation of the complex by 180° about its *c* principal axis transforms each of the configurations on the right to one of those in the left. Hence, the numbers of non-superimposable distinguishable minima reduce to four for $C_2H_4\bullet\bullet\bullet H_2S$. Thus, the rotation-torsion wave function is expected to have four-fold degeneracy and

explains the four line splitting pattern observed in the spectrum. The characters of the reducible representation generated by the rotation-torsion wave function of the four distinct configurations can be found out easily. These are shown in Table III.24. The operations (13)(24), (56), E*, (13)(24)(56), (56)*, (13)(24)(56)* transform each configuration into another and thus have zero character. Only operations those contribute

Table III.23.G_8 character table

G_8	E	(13)(24)	(56)	(13)(24)(56)	E^*	$(13)(24)^*$	$(56)^*$	(13)(24)(56)*
A_1'	1	1	1	1	1	1	1	1
A_1''	1	1	1	1	-1	-1	-1	-1
A_2'	1	1	-1	-1	1	1	-1	-1
A_2''	1	1	-1	-1	-1	-1	1	1
B_1'	1	-1	-1	1	1	-1	-1	1
B_1''	1	-1	-1	1	-1	1	1	-1
B_2'	1	-1	1	-1	1	-1	1	-1
B_2''	1	-1	1	-1	-1	1	-1	1

Table III.24. The reducible representation generated by the rotation-torsion wave functions of C_2H_4•••H_2S

	E	**(13)(24)**	**(56)**	**(13)(24)(56)**	**E***	**(13)(24)***	**(56)***	**(13)(24)(56)***
Γ_A'	4	0	0	0	0	4	0	0
Γ_A''	4	0	0	0	0	-4	0	0

Figure III.15. Effect of each PI operation (considering the rotation of ethylene about the C-C bond axis) on C_2H_4•••H_2S complex. The equilibrium geometry was assumed to have C_s symmetry. The configurations linked by arrows are convertible to one another by a rotation of the complex about its c principal axis.

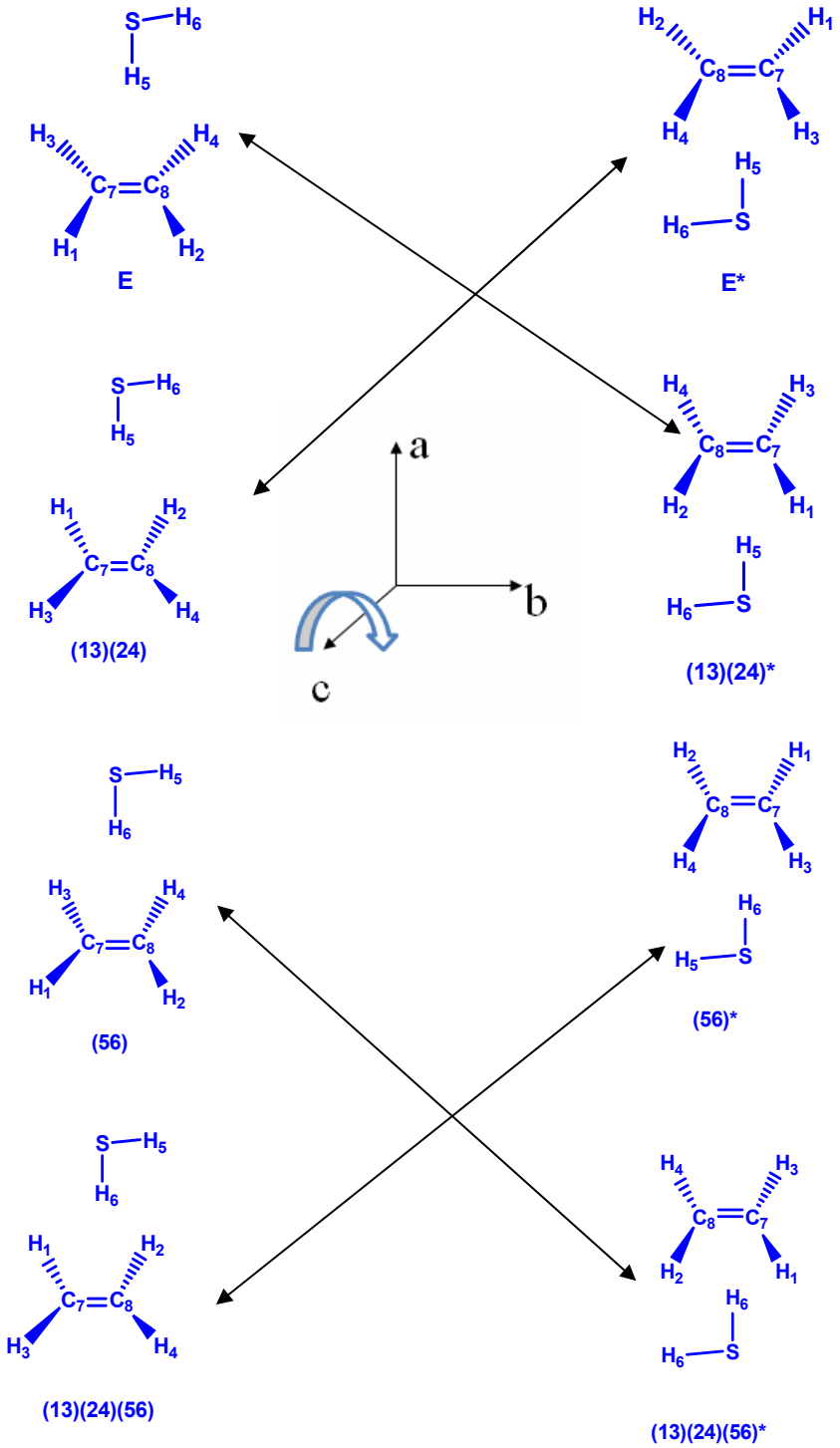

to the character are E and (13)(24)*. In case of $(H_2O)_2$, it was pointed out by Dyke[37] that for a prolate slightly asymmetric top, the rotational wave function transforms like A′ for J_{even} and A″ for J_{odd} for K=0. Thus, for K≠ 0, the upper half of the K doublet transforms like A′ for J_{even} and A″ for J_{odd}. For K≠ 0, the lower part of the K doublet transforms like A″ for J_{even} and A′ for J_{odd}. $C_2H_4\bullet\bullet\bullet H_2S$ is a nearly prolate asymmetric top with κ = -0.9912 and these conclusions are valid for $C_2H_4\bullet\bullet\bullet H_2S$ as well. Thus the energy level of $C_2H_4\bullet\bullet\bullet H_2S$ in the ground torsional state and with J =0 will split into the following sublevels:

$$\Gamma_A' = A_1' + A_2' + B_1'' + B_2'' \qquad (5)$$

Similarly the energy level of $C_2H_4\bullet\bullet\bullet H_2S$ in the ground torsional state and with J=1 (K=0) will split into following sub-levels:

$$\Gamma_A^{//} = A_1'' + A_2'' + B_1' + B_2' \qquad (6)$$

The total wave function for $C_2H_4\bullet\bullet\bullet H_2S$ is antisymmetric for odd permutation of the hydrogens and symmetric for the even permutation for the hydrogens. The effect of the inversion operation on the symmetry of the total wave function can be either of these. Thus from the character table one can find out the symmetry of the total wave function to be either A_2'or A_2''. The character of the reducible representation (Γ_{NS}**)** formed by the nuclear spin functions of six hydrogen atoms can be found out using the formula

$$\chi_p = \prod_i (2I_i + 1) \qquad (7)$$

and are shown in Table III.25.

Table III.25. The characters of the reducible representation formed by the nuclear spin functions of the six hydrogen atoms of $C_2H_4\bullet\bullet\bullet H_2S$.

	E	(13)(24)	(56)	(13)(24)(56)	E*	(13)(24)*	(56)*	(13)(24)(56)*
Γ_{NS}	64	16	32	8	64	16	32	8

The symmetry of the nuclear spin functions and their degeneracy can be found by reducing Γ_{NS}

$$\Gamma_{NS} = 30A_1' + 10A_2' + 18B_1' + 6B_2' \quad (8)$$

The statistical weight for the rotation-torsion state is given by the number of nuclear spin functions that can combine with that particular state such that the total wave function has symmetry A_2' or A_2''. The result for $C_2H_4\bullet\bullet\bullet H_2S$ is shown in Table III.26.

The allowed rotational-torsional states and their spin statistical weights could also be calculated in a simpler way by the formula given below:

$$\Gamma_{rvE}^{SW}(P) = 2\prod_{\alpha}\left(2I_{\alpha}+1\right)\left(-1\right)^{\left(\left(2I_{\alpha}\right)\left(n_{\alpha}-1\right)\right)} \quad (9)$$

Here the product contains one factor for each set of n_α nuclei having spin I_α, permuted by the permutation operation P. The characters in the Γ_{rve}^{SW} are zero for all the permutation operations in the MS group. The reducible representation obtained by this formula can be reduced to get the allowed rotational-torsional states and the co-efficients give us the spin statistical weights which is quite straightforward. Considering the rotation of ethylene about C-C axis, the weights for $C_2H_4\bullet\bullet\bullet D_2S$, $C_2D_4\bullet\bullet\bullet H_2S$ and $C_2D_4\bullet\bullet\bullet D_2S$ have been calculated using this formula. The weights are listed in Table III.27.

The calculated weights compare reasonably well with the intensity ratios obtained from the experiment. For $C_2H_4\bullet\bullet\bullet H_2S$, the calculated weight for the A_1' state is one-third of the weight of A_2' state. Similar is the case with B_2'' and B_1'' states. In case of $C_2H_4\bullet\bullet\bullet D_2S$, the calculated weights show a ratio of 2:1, the trend being reverse. The experimental intensity ratios of $C_2H_4\bullet\bullet\bullet H_2S$ and $C_2H_4\bullet\bullet\bullet D_2S$ are plotted in Figure III.16. and Figure III.17. Experiments show reversal of intensity pattern for the lower and upper states for $C_2H_4\bullet\bullet\bullet H_2S$ and $C_2H_4\bullet\bullet\bullet D_2S$ as expected from the statistical weights. Total intensity ratio of the lower and upper doublet is 2.2:1(compared to the calculated ratio of 3:1) for $C_2H_4\cdots H_2S$ and 1:1.5(compared to the calculated ratio of 1:2) for $C_2H_4\cdots D_2S$. It should be noted that experimental intensity ratios are not accurate match to the statistical weights due to the variation of sensitivity of the spectrometer over the frequency range.

Intensity pattern and ratios comparable to 3:1 and 1:2 for the H_2S and D_2S isotopologues agree with the fact that the larger splitting is due to internal rotation of H_2S, which interchanges the two equivalent hydrogens. The experimental intensity ratios of the 1-2 doublet is close to 3:5 for C_2H_4•••H_2S and C_2H_4•••D_2S as is expected from the calculated statistical weights. The spectra for C_2D_4•••H_2S and C_2D_4•••D_2S are shown in Figure III.18. and III.19. For C_2D_4•••H_2S and C_2D_4•••D_2S, the lower and upper sets show the reversal of the intensity pattern as was observed for C_2H_4•••H_2S and C_2H_4•••D_2S. For the smaller splitting, L1-L2/U1-U2 show almost same intensity. This is expected as the calculated statistical weights for these states have the ratio of 5:4.

Table III.26. Symmetry of the rotational-torsional states, symmetry of nuclear spin function and the symmetry of the total wave function along with the calculated statistical weights of the levels.

Rotational-torsional sublevel symmetry	Nuclear spin function symmetry	Total wave function symmetry	Spin statistical weights
A_1'	A_2'	A_2'	10
A_2'	A_1'	A_2'	30
B_1''	B_2'	A_2''	18
B_2''	B_1'	A_2''	6
A_1''	A_2'	A_2''	10
A_2''	A_1'	A_2''	30
B_1'	B_2'	A_2'	18
B_2'	B_1'	A_2'	6

Table III.27. Level symmetry of the rotational-torsioanl states and the spin statistical weights for the isotopes of C_2H_4•••H_2S.

Level symmetry	C_2H_4-D_2S	C_2D_4-H_2S	C_2D_4-D_2S
A_1'	60	45	270
A_2'	30	135	135
B_1''	36	36	216
B_2''	18	108	108
A_1''	60	45	270
A_2''	30	135	135
B_1'	36	36	216
B_2'	18	108	108

Figure III.16. Stick diagram showing the correlation of the calculated statistical weights with the experimental intensities for J =1→2 (K_a=0) transitions for C_2H_4•••H_2S

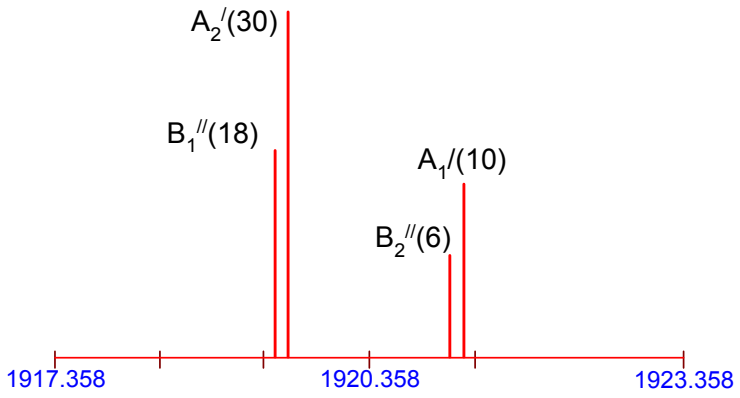

Figure III.17. Stick diagram showing the correlation of the calculated statistical weights with the experimental intensities for J =1→2 (K_a=0) transitions for C_2H_4•••D_2S

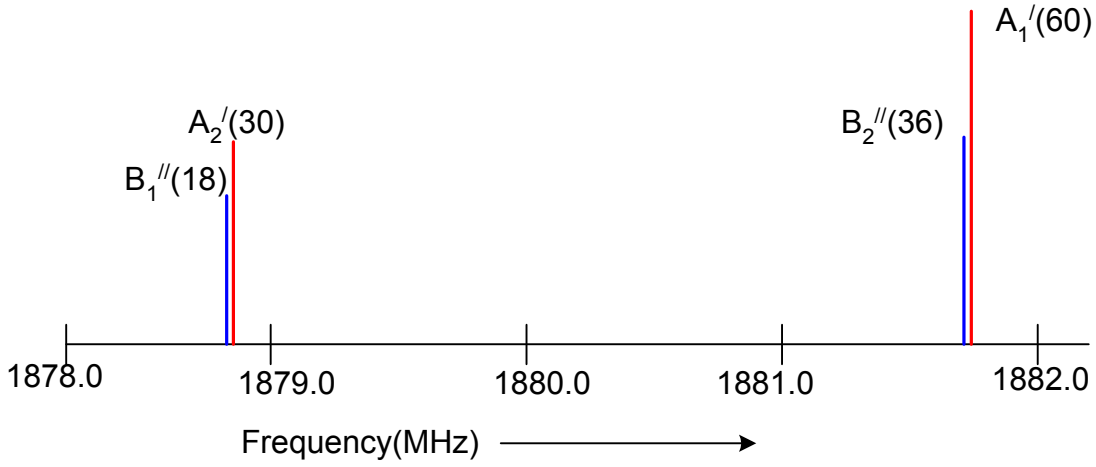

Figure III.18. $J = 2_{02} \rightarrow 3_{03}$ transitions for $C_2D_4\bullet\bullet\bullet H_2S$. From the intensity scale it is evident that the lower state doublets are almost thrice as intense as the upper state doublets.

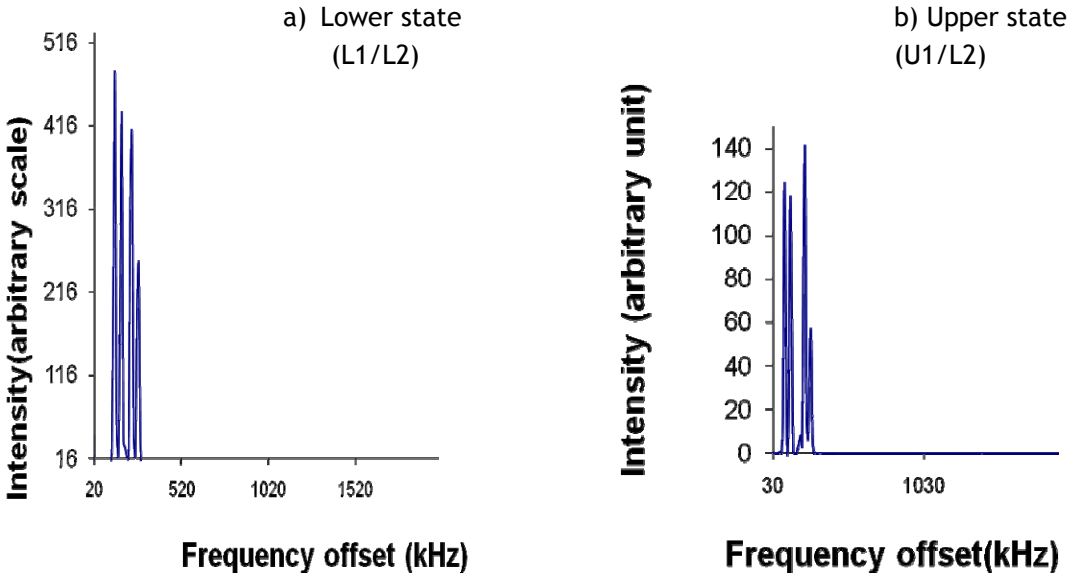

Figure III.19. $J = 3_{03} \rightarrow 4_{04}$ transitions of $C_2D_4\bullet\bullet\bullet D_2S$. From the intensity scale it is evident that the upper state doublets are almost twice as intense as the lower state doublets.

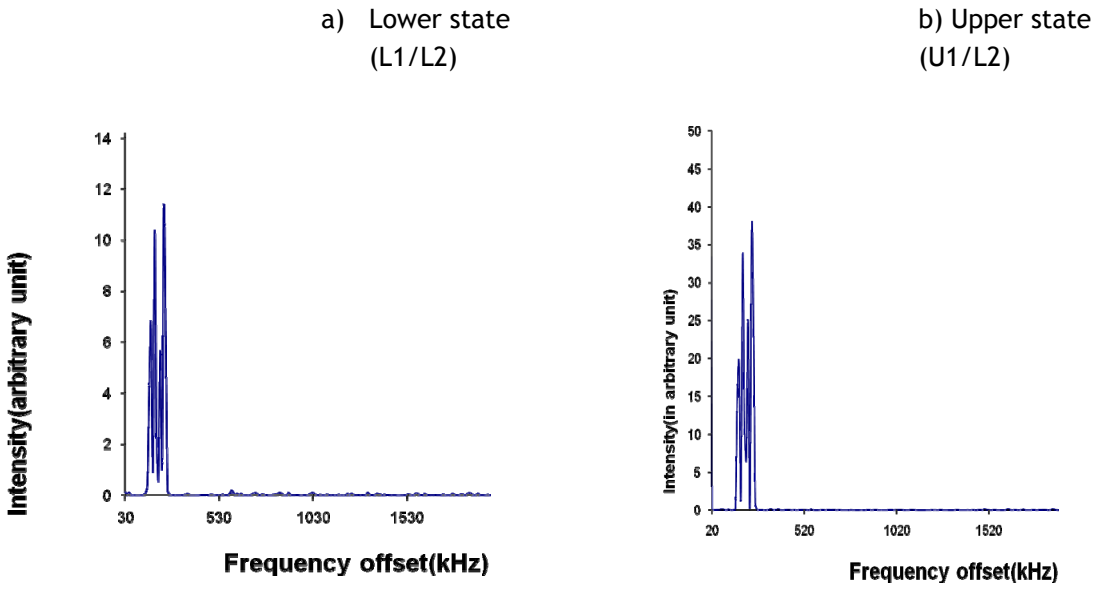

Of course there is enough evidence from the experiments to conclude that the dynamics of ethylene motion involves its rotation about C-C bond axis. However, independent analyses were performed considering the end-over-end rotation of ethylene and the in plane rotation of ethylene. Considering the in-plane rotation of ethylene, the feasible operations are: E, (14)(23)(78),(56), (14)(23)(56)(78), E*, (14)(23)(78)*, (56)* and (14)(23)(56)(78)*. All the operations are shown in Figure III.20. A careful examination of Figure III.20. reveals that none of the structure is superimposable on one another. Hence, the rotational-torsional wave functions will be eight fold degenerate. Considering the end-over-end rotation of ethylene monomer, the feasible operations are: E, (13)(24)(56), (56), (13)(24)(56)(78), E*, (13)(24)(56)*, (56)*, (13)(24)(56)(78)* and here, in this case also, the number of distinguishable minima are eight. None of the motions can transform one configuration to other. Thus, in both of these cases, the rotational-torsional states will be eight fold degenerate. Hence, the obtained statistical weights are same as were obtained for the rotation of ethylene about the C-C bond axis. Hence, the calculated weights cannot distinguish these three motions of ethylene of course. However, the total number of observed states in the spectrum is four, whereas any other rotation of ethylene except the rotation of ethylene about the C-C bond axis does not reproduce the observed four line pattern in the spectrum making our conclusions even more definite.

III. D. Is $C_2H_4\cdots H_2S$ hydrogen bonded?

The weakly bound $C_2H_4\bullet\bullet\bullet H_2S$ complex has a structure very similar to the other hydrides such as $C_2H_4\bullet\bullet\bullet HF$, $C_2H_4\bullet\bullet\bullet HCl$ and $C_2H_4\bullet\bullet\bullet H_2O$ complexes. However, one would wonder if this complex is to be called 'hydrogen-bonded'. The smaller frequency shift of 2.5 cm^{-1} observed in Infrared-Microwave Double resonance experiments can strengthen this doubt. However, a crude estimate of the position of the hydrogen from the present study showed that the average structure of the complex has the hydrogen closer to the ethylene π-cloud, which is an obvious indication of it to be 'hydrogen-bonded'. The AIM calculations reported in section III.C.4.b shows the complex to be 'hydrogen bonded' as it follows the criterion given by Popelier for the electron density (ρ) at the BCP and the Laplacian of the electron density at the BCP ($\nabla^2\rho$). Further, the

Figure III.20. Effect of each PI operation (considering the in-plane rotation of ethylene) on C_2H_4•••H_2S complex. The equilibrium geometry was assumed to have Cs symmetry. None of the configuration is convertible to another by rotation.

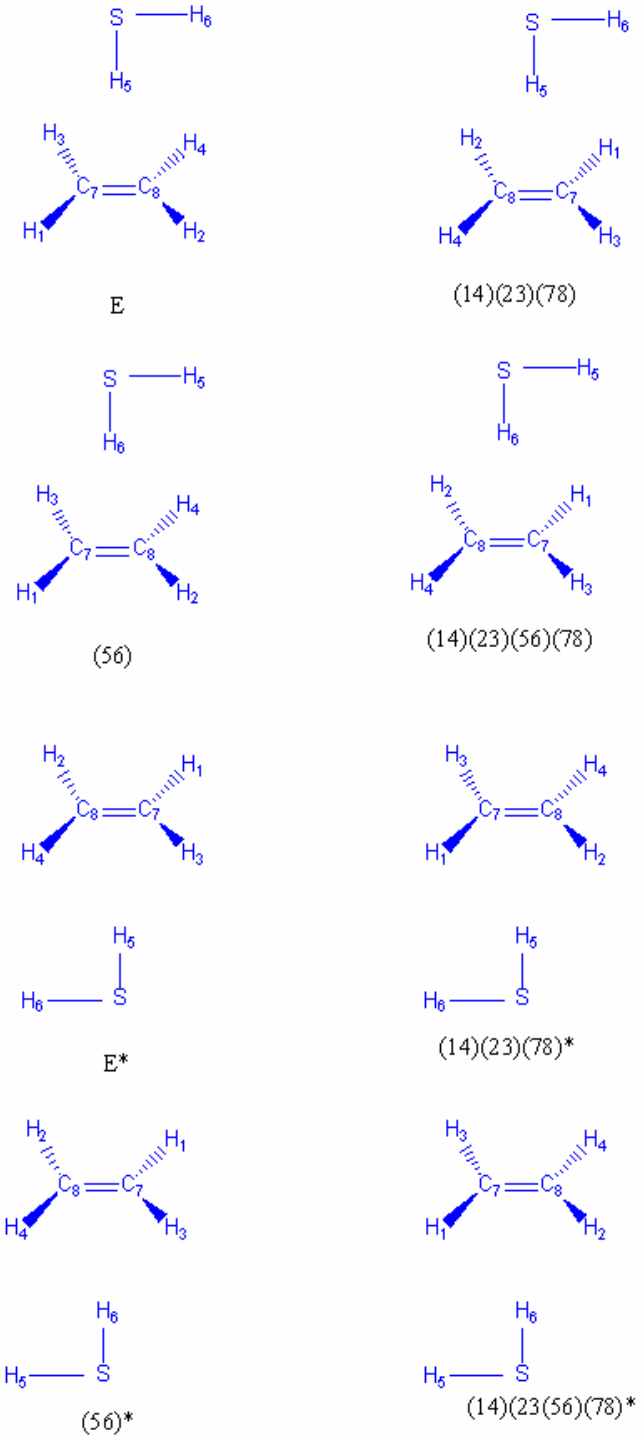

calculated zero point energies of all the large amplitude vibrations are significantly lower than the barrier heights calculated for these motions, which is a necessary and sufficient criterion to call this complex as hydrogen-bonded. A more in-depth discussion on this criterion is given in chapter VI. Further, the nature of the large amplitude motion and the splitting in the spectrum can shed some light on the strength of the interaction. Thus, larger is the splitting, floppier is the potential. Here, C_2H_4•••H_2S seems to be residing in the border of C_2H_4•••Ar and C_2H_4•••H_2O. The former complex is not 'hydrogen-bonded' and falls among the more general class of van der Waals complexes, whereas the later is 'hydrogen-bonded (proved by the FTMW experiments and the details are included in chapter VI). A stick diagram of the splitting patterns observed for these complexes is shown in Figure III.21. A splitting of 6 MHz in (B+C)/2 has been observed in C_2H_4•••Ar complex which arises because of the internal rotation of C_2H_4 about its C-C bond axis in the complex. On the other hand, C_2H_4•••H_2O has a splitting less than 1 MHz in (B+C)/2, which arises because of the internal rotation of H_2O moiety in the complex. The internal rotation of the ethylene moiety is quenched in the C_2H_4•••H_2O complex which is a strong indication of the strength of the 'hydrogen-bonding' present in it. In case of C_2H_4•••H_2S, we have both C_2H_4 and H_2S exerting internal rotation with respect to each other. It is more interesting to look at the splitting magnitude. The rotation of C_2H_4 about its C-C bond axis gives rise to a splitting of few hundred kHz which was 6 MHz in Ar•••C_2H_4 and whereas the interchange of the equivalent hydrogens of H_2S in the complex gives rise to the larger splitting which is almost 2 MHz in (B+C)/2 compared to the 1 MHz splitting observed in C_2H_4•••H_2O Thus, C_2H_4•••H_2S can be called as a bridge between the 'hydrogen bonding' and the other more general van der Waals interaction.

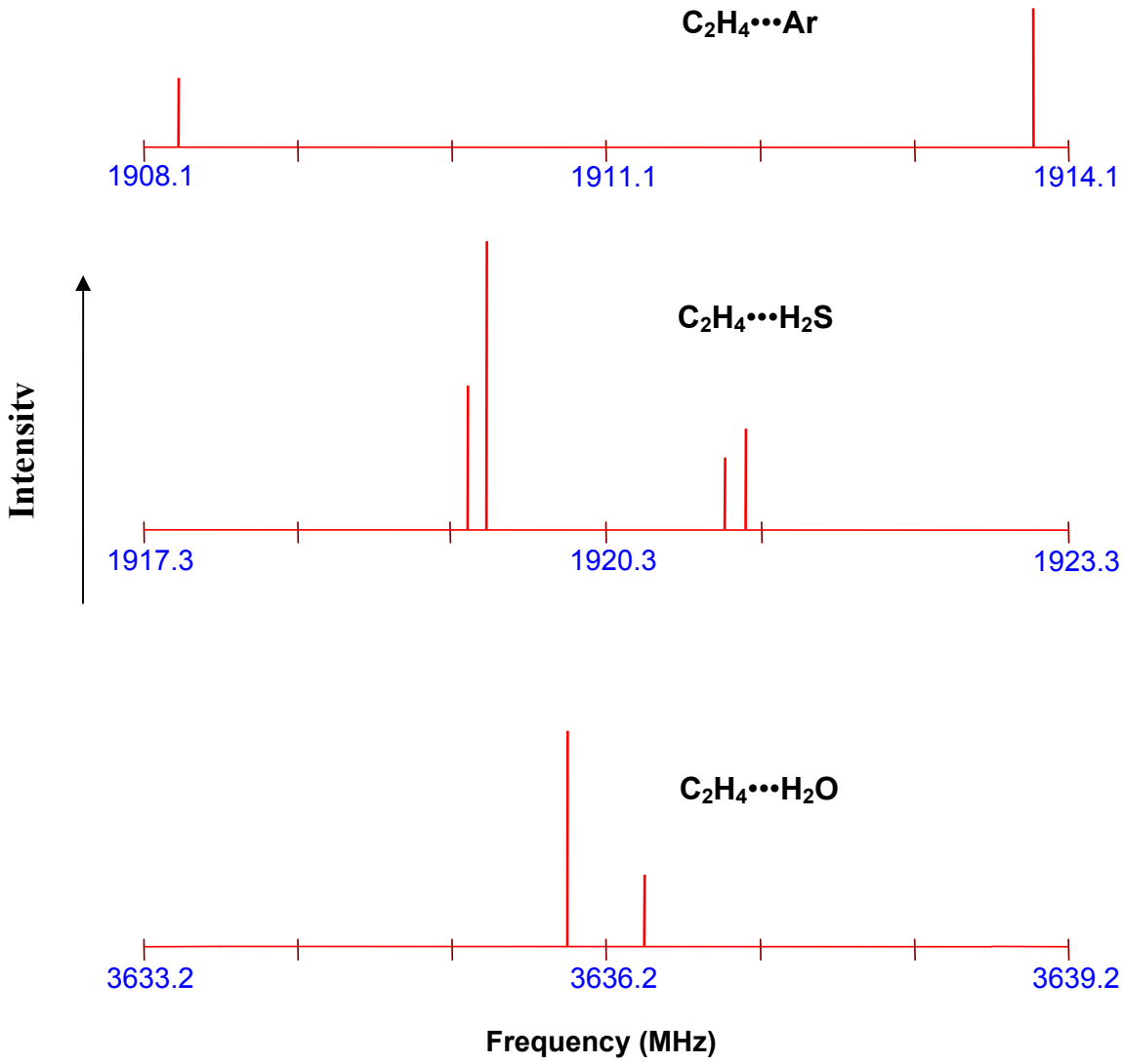

Figure III.21. Stick diagram of J= 1→2, K =0 transition frequencies for C_2H_4•••Ar, C_2H_4•••H_2S and C_2H_4•••H_2O. The transitions frequencies have been divided by 2(J+1) in order to plot with the same scale.

III.E. Conclusions

Rotational spectra of weakly bound complex C_2H_4•••H_2S and its isotopologues have been observed. In this complex, H_2S has been found to act as hydrogen bond donor to the π system of ethylene. The spectrum reveals the complex to be a nearly prolate asymmetric top with κ= -0.9912. Each of the transitions for C_2H_4•••H_2S, C_2H_4•••D_2S, C_2H_4•••$H_2{}^{34}S$,

C_2D_4•••H_2S, C_2D_4•••D_2S and $^{13}CCH_4$•••H_2S is split into four whereas C_2H_4•••HDS and C_2D_4•••HDS shows only doubling of each transition. The smaller splitting is 0.14 MHz and the higher splitting is 1.67 MHz in (B+C)/2 for the parent isotopologue. Each series has been fitted separately using Watson's S-reduction Hamiltonian. The splitting pattern of the parent and all the isotopologues indicate that the smaller splitting arises due to the rotation of ethylene about its C-C bond axis along with the movement of S-H bond whereas the larger motion arises due to the interchange of equivalent hydrogens of H_2S in the complex. These studies also indicate that both the motions evidenced by the microwave spectroscopy have contributions from both ethylene and H_2S subunits. Molecular symmetry group analysis has been performed for this complex and it shows a good agreement with the experimental intensity pattern. Intensity pattern and ratios comparable to 3:1 and 1:2 for L-U doublets of the C_2H_4•••H_2S and C_2H_4•••D_2S isotopologues agree to the fact that the larger splitting arises because of the internal rotation of H_2S. The intensity ratios of the 1-2 doublets is close to 6:10 for the parent isotopologue and agrees to the spin statistical weights calculated from the analysis. The π bonded structure for C_2H_4•••H_2S has been optimized at various levels of theory and the interaction energy has been reported. The binding energy of the π bonded structure is -214 cm^{-1} at MP2(full)/aug-cc-pVQZ level with counterpoise correction. Potential energy curves for different motions of C_2H_4 and H_2S in the complex have been calculated to know the relative barrier heights. These barrier heights support the fact the rotation of C_2H_4 about its C-C bond axis is the likeliest to cause the smaller splitting whereas the larger splitting may be arising from the rotation of H_2S about its C_2 symmetric axis or the rotation of H_2S about its *c* principal axis coupled with the rotation of H_2S about the hydrogen bond. The calculated barrier heights would indicate the later motion to be more preferable. However, the pulse dependence of the states arising due to the internal rotation of H_2S indicates that the rotation of H_2S about C_2 symmetry axis is the one which causes the splitting. These studies indicate that the potential energy surface of the C_2H_4•••H_2S complex is significantly floppier than C_2H_4•••H_2O to allow the internal rotation of both the subunits in the complex.

III.F. References

1. L. Pauling, *Nature of the Chemical Bond*, Cornell University Press, Ithaca, New York, **1960.**
2. E. Arunan, T. Emilsson, H. S. Gutowsky, G. T. Fraser, G. de. Oliveria, C. E. Dykstra, *J. Chem. Phys.* **2002**, *117*, 9766.
3. E. M. Cabeleiro-Lage, J. Rodriguez-Otero, A. Pena-Gallego, *J. Phys. Chem. A*. **2008**, 112, 6344.
4. H.S. Gutowsky, T. Emilsson, E. Arunan, *J. Chem. Phys.* **1997**, 106, 5309.
5. Y. Liu, W. Jäger, *Mol. Phys.* **2002**,100, 611.
6. G.T. Fraser, F.J. Lovas, R.D. Suenram, K. Matsumura, *J. Mol. Spetrosc.* **1990**, 144, 97.
7. E. Arunan, T. Emilsson, H. S. Gutowsky, G. T. Fraser, G de Oliveria, C. E Dykstra, *J. Chem. Phys.* **2002**, 117, 9766.
8. P. K. Mandal, E. Arunan, *J. Chem. Phys.* **2001**, 114, 3880.
9. B. Raghavendra, P. K. Mandal, E. Arunan, *Phys. Chem. Chem. Phys.* **2006,** 8, 5276.
10. C.H. Görbitz, B. Dalhus. *Acta Crystallogr. C.* **1996,** 52**,** 1756.
11. Michael Hartmann, Stacey D. Wetmore, Leo Radom, *J. Phys. Chem. A* **2005,** 105, 4470.
12. P. I. Peterson, Klemperer, W. *J. Chem. Phys.* **1986**, 85, 725.
13. A. M. Andrews, R.L. Kuczkowski, *J. Chem. Phys.* **1993**, 98, 791.
14. J. A. Shea, W. H. Flygare, *J. Chem. Phys.* **1982,** 76, 4857.
15. P. D. Aldrich, A. C. Legon, W. H. Flygare, *J. Chem. Phys.* **1981**, 75, 2126
16. S. Suzuki, P. G. Green, R. E. Bumgarner, R. D. Suenram, S. Dasgupta, W. A. Godderd III, G. A. Blake. *Science*, **1992**, 257, 942.
17. H. S. Gutowsky, T. Emilsson, E. Arunan, *J. Chem. Phys.* **1993,** 99, 4883.
18. Yaqian Liu, Wolfgang Jager, *J. Chem. Phys.* **2003**, 119, 8449
19. R. J. Blemish, P. A. Block, L. G. Pedersen, R. E. Miller, *J. Chem. Phys.* **1995**, 103, 7788.
20. L. W. Buxton, P. D. Aldrich, J. A. Shea, A. C. Legon, W. H. Flygare, *J. Chem. Phys.* **1981**, 75, 2681.
21. F. A. Baiocchi, J. H. Williams, W. Klemperer, *J. Phys. Chem*. **1983**, 87, 2079.

22. W. G. Read, E. J. Campbell, G. Henderson, W. H. Flygare, *J. Chem. Phys.* **1981**, 103, 7670.
23. W. G. Read, E. J. Campbell, G. Henderson, *J. Am. Chem. Soc.* **1983**, 78, 3501
24. S. E. Novick, P. Davies, S. J. Harris, W. Klemperer, *J. Chem. Phys.* **1973**, 59, 2273
25. H. S. Gutowsky, T. Emilsson, E. Arunan, *J. Chem. Phys.* **1997**, 106, 5309.
26. H. C. Allen, E. K. Plyler, *J. Am. Chem. Soc.* **1958**, 80, 2673.
27. M. J. Frisch, G. W. Trucks, H. B. Schlegel, G. E. Scuseria, M. A. Robb, J. R. Cheeseman, V. G. Zakrzewski, Jr. J. A. Montgomery, R. E. Stratmann, J. C. Burant, S. Dapprich, J. M. Millam, A. D. Daniels, K. N. Kudin, M. C. Strain, O. Farkas, J.Tomasi, V. Barone, M. Cossi, R. Cammi, B. Mennucci, C. Pomelli, C. Adamo, S. Clifford, J. Ochterski, G. A. Petersson, P. Y. Ayala, Q. Cui, K. Morokuma, N. Rega, P. Salvador, J. J. Dannenberg, D. K. Malick, A. D. Rabuck, K. Raghavachari, J. B. Foresman, J. Cioslowski, J. V. Ortiz, A. G. Baboul, B. B. Stefanov, G. Liu, A. Liashenko, P. Piskorz, I. Komaromi, R. Gomperts, R. L. Martin, D. J. Fox, T. Keith, M. A. Al-Laham, Vreven, C. Y. Peng, A. Nanayakkara, M. Challacombe, P. M. W. Gill, B. Johnson, W. Chen, M. W. Wong, J.L. Andres, C. Gonzalez, M. Head-Gordon, E. S. Replogle, J. A. Pople, *Gaussian98*, Revision A.11.3 Gaussian, Inc., Pittsburgh PA, **2002.**
28. M. J. Frisch, G. W. Trucks, H. B. Schlegel, G. E. Scuseria, M. A. Robb, J. R. Cheeseman, Jr.J. A. Montgomery, T. Vreven, K. N. Kudin, J. C. Burant, J. M. Millam, S. S. Iyengar, J.Tomasi, V. Barone, B. Mennucci, M. Cossi, G. Scalmani, N. Rega, G. A. Petersson, H. Nakatsuji, M. Hada, M. Ehara, K. Toyota, R. Fukuda, J. Hasegawa, M. Ishida, T. Nakajima, Y. Honda, O. Kitao, H. Nakai, M. Klene, X. Li, J. E. Knox, H. P. Hratchian, J. B. Cross, C. Adamo, J. Jaramillo, R. Gomperts, R. E. Stratmann, O. Yazyev, A. J. Austin, R. Cammi, C. Pomelli, J.W. Ochterski, P. Y. Ayala, K. Morokuma, G. A. Voth, P. Salvador, J. J. Dannenberg, V. G. Zakrzewski, S. Dapprich, A. D. Daniels, M. C. Strain, O. Farkas, D. K. Malick, A. D. Rabuck, K. Raghavachari, J. B. Foresman, J. V. Ortiz, Q. Cui, A. G. Baboul, S. Clifford, J. Cioslowski, B. B. Stefanov, G. Liu, A. Liashenko, P. Piskorz, I. Komaromi, R. L. Martin, D. J. Fox, T. M. Keith, A. Al-Laham, C. Y. Peng, A. Nanayakkara, M. Challacombe, P. M. W. Gill, B. Johnson, W. Chen, M. W. Wong,

C. Gonzalez, J. A. Pople, *Gaussian03*, Revision C-02; Gaussian, Inc., Wallingford CT, **2004.**

29. F. M. Tao, Y. K. Pan, *J. Phys. Chem.* **1991**, 95, 3582.
30. F. M. Tao, W. Klemperer, *J. Chem. Phys.* **1992,** 97, 440.
31. P. S. sedano, *Implementation and Application of Basis Set Superposition Error-Correction Schemes To The Theoretical Modelling of Weak Intermolecular Interaction*, Ph.D. Dissertation, Department of chemistry and Institute of Computational Chemistry, Univeristy of Girona, GIRONA, **2001.**
32. R. W. F. Bader, *Atoms in Molecules: A quantum Theory*, Clarendon Press, Oxford, **1990.**
33. U. Koch, P. L. A. Popelier, *J. Phys. Chem.* **1995**, 99, 9747.
34. Matt T. Muckle, Justin L. Neill, Brooks H. Pate, *63rd International Symposium on Molecular Spectrosocpy,* Columbus, **2008**.
35. T. R. Dyke, *J. Chem. Phys.* **1977**, 66, 492.

Appendix

Table III.A.1. Unassigned transitions dependent on both C_2H_4 and H_2S. The optimum pulse is reported wherever is tested.

Transitions	Component1	Component2	Carrier gas	MW pulse duration (μs)
8632.5	H_2S	C_2H_4	Ar	0.5
8618.571	H_2S	C_2H_4	Ar	0.5
8615.69	H_2S	C_2H_4	Ar	0.5
8429.543	H_2S	C_2H_4	Ar	0.5
8421.452	H_2S	C_2H_4	Ar	0.5
8322.58	H_2S	C_2H_4	Ar	0.5
7986.97	H_2S	C_2H_4	Ar	0.5
11396.405	H_2S	C_2H_4	Ar	0.5
11397.5959	H_2S	C_2H_4	Ar	
11417.4705	H_2S	C_2H_4	Ar	
11418.68	H_2S	C_2H_4	Ar	
11421.5268	H_2S	C_2H_4	Ar	
11421.6316	H_2S	C_2H_4	Ar	
11422.7348	H_2S	C_2H_4	Ar	
11425.5998	H_2S	C_2H_4	Ar	
11426.7916	H_2S	C_2H_4	Ar	
11431.3215	H_2S	C_2H_4	Ar	
11533.6227	H_2S	C_2H_4	Ar	
11533.6	H_2S	C_2H_4	Ar	
11537.8537	H_2S	C_2H_4	Ar	
11537.836	H_2S	C_2H_4	Ar	

Table III.A.2. Structural parameters for C_2H_4•••H_2S optimized at MP2(full) level using different basis sets on the counterpoise uncorrected surface. The bond lengths are given in Ås and the angles and the dihedrals are given in degrees.

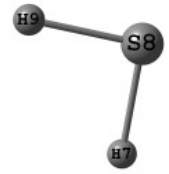

Structural parameters	6-31G*	6-311++G**	6-311++G(3df,2p)
C1-C2	1.336	1.339	1.331
C1-H3	1.084	1.085	1.079
C1-S8	4.103	4.071	4.027
S8-H7	1.341	1.334	1.335
S8-H9	1.339	1.335	1.332
∠H3-C1-C2	121.7	121.4	121.4
∠H4-C1-C2	121.7	121.5	121.4
∠H5-C2-C1	121.7	121.4	121.5
∠H6-C2-C1	121.7	121.5	121.4
∠S8-C1-C2	80.6	80.7	78.6
∠H7-S8-C2	9.8	11.7	10.3
∠H9-S8-H7	93.6	92.3	92.3
D(H4-C1-C2-H3)	-179.5	-179.7	-179.9
D(H5-C2-C1-H4)	-179.5	-179.7	-179.9
D(H6-C2-C1-H5)	179.5	179.7	179.8
D(S8-C1-C2-H6)	-97.4	-81.9	-91.8
D(H7-S8-C2-C1)	-16.6	-35.3	-12.9
D(H9-S8-H7-C2)	106.3	125.0	93.3

Table III.A.3. Structural parameters for C_2H_4•••H_2S optimized at MP2(full) level using different basis sets on the counterpoise uncorrected surface. The bond lengths are given in Å s and the angles and the dihedrals are in degrees.

Structural parameters	6-311++G(3df,pd)	6-311++G(3df,3pd)	aug-cc-pVDZ	aug-cc-pVTZ	aug-cc-pVQZ
C1-C2	1.330	1.331	1.350	1.330	1.328
C1-H3	1.082	1.080	1.092	1.078	1.078
C1-S8	4.022	3.980	3.983	3.902	3.975
S8-H7	1.334	1.333	1.351	1.335	1.335
S8-H9	1.332	1.330	1.348	1.333	1..332
∠H3-C1-C2	121.4	121.4	121.3	121.3	121.4
∠H4-C1-C2	121.4	121.4	121.3	121.3	121.4
∠H5-C2-C1	121.4	121.4	121.3	121.3	121.4
∠H6-C2-C1	121.4	121.4	121.3	121.3	121.4
∠S8-C1-C2	80.3	80.3	79.9	80.0	79.4
∠H7-S8-C2	10.3	9.8	10.3	10.0	10.7
∠H9-S8-H7	92.5	92.3	92.3	92.1	92.3
D(H4-C1-C2-H3)	-179.9	-179.9	-179.8	180.0	-180.0
D(H5-C2-C1-H4)	-179.9	-179.9	-179.8	180.0	-180.0
D(H6-C2-C1-H5)	179.9	179.889	179.8	180.0	180.0
D(S8-C1-C2-H6)	-93.5	-92.7	93.8	91.8	-93.
D(H7-S8-C2-C1)	-16.4	-11.5	-16.3	-6.7	-17.2
D(H9-S8-H7-C2)	106.6	100.9	104.4	96.6	108.3

Table III.A.4. Structural parameters for C_2H_4•••H_2S optimized at MP2(full) level using different basis sets on the counterpoise corrected surface. The bond lengths are given in Å s and the angles and the dihedrals are given in degrees.

Structural parameters	6-31G*	6-311++G**	6-311++G(3df,2p)	6-311++G(3df,pd)	6-311++G(3df,3pd)	aug-cc-pVDZ
C1-C2	1.336	1.339	1.331	1.330	1.331	1.349
C1-H3	1.085	1.085	1.080	1.082	1.082	1.092
C1-S8	4.298	4.295	4.089	4.142	4.143	4.149
S8-H7	1.340	1.334	1.334	1.334	1.333	1.350
S8-H9	1.339	1.333	1.332	1.331	1.330	1.348
∠H3-C1-C2	121.7	121.4	121.4	121.4	121.4	121.3
∠H4-C1-C2	121.7	121.4	121.4	121.4	121.4	121.4
∠H5-C2-C1	121.7	121.4	121.4	121.4	121.4	121.4
∠H6-C2-C1	121.7	121.4	121.4	121.4	121.4	121.3
∠S8-C1-C2	81.0	80.5	83.9	83.4	78.3	79.8
∠H7-S8-C2	9.5	10.8	14.5	13.4	10.2	11.5
∠H9-S8-H7	93.5	92.2	92.4	92.6	92.3	92.7
D(H4-C1-C2-H3)	-179.6	-179.6	-179.6	-179.8	-179.9	-179.8
D(H5-C2-C1-H4)	-179.6	-179.6	180.0	-179.9	-179.8	-179.8
D(H6-C2-C1-H5)	179.6	179.7	-179.6	180.0	179.6	179.8
D(S8-C1-C2-H6)	-97.5	-95.6	-99.5	-98.3	-92.1	-97.5
D(H7-S8-C2-C1)	-19.1	-18.4	-44.8	-40.1	-12.6	-30.8
D(H9-S8-H7-C2)	109.2	119.2	124.1	123.1	96.5	120.5

Table III.A.5. Rotational constants for C_2H_4•••H_2S calculated at MP2(full) level using different basis sets

Rotational constants (MHz)	6-31G*	6-311++G**	6-311++G(3df, 2p)	6-311++G(3df,pd)	6-311++G(3df, 3pd)	aug-cc-pVDZ	aug-cc-pVTZ	aug-cc-pVQZ
A(CP uncorrected)	22952	22984	23152	23125	23136	22551	23175	23229
B(CP uncorrected)	1986	2014	2087	2070	2114	2114	2203	2129
C(CP uncorrected)	1898	1923	1991	1977	2016	2017	2098	2031
A(CP corrected)	22973	22915	23029	23257	23171	22610	23205	-
B(CP corrected)	1809	1817	2018	1976	1976	1950	2029	-
C(CP corrected)	1736	1743	1904	1890	1890	1864	1939	-

Figure III.A.1. Several optimised geometries of C_2H_4•••H_2S are shown from A-H. Their interaction energies and the nature of the minima are quoted.

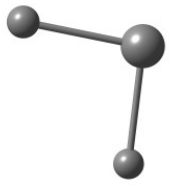

A

Structure A, Transition state, optimized at MP2(full)/6-311++G(3df,pd). The interaction energy is -255 cm^{-1} including the BSSE and ZPE correction

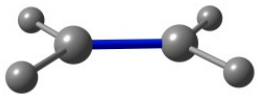

B

Transition state at MP2(full)/6-311++G**, Minima at MP2(full) /aug-cc-pVTZ level. The stabilisation energy is -372 cm^{-1} (with the counterpoise correction) at MP2(full)/aug-cc-pVTZ . With the zero pint correction at MP2(full)/aug-cc-pVTZ the binding energy becomes -44 cm^{-1}

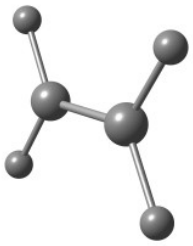

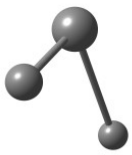

C

Saddle point of order 2, optimized at MP2(full)/aug-cc-pVTZ level. The interaction energy is -425 cm^{-1} (with the counterpoise correction) at this level of theory. The interaction energy is -258 cm^{-1} after the zero point correction.

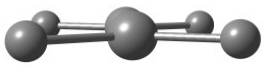

D

Saddle point of order 2, optimized at MP2(full)/aug-cc-pVTZ level. The interaction energy is -426 cm^{-1} (with the counterpoise correction) at this level of theory. The interaction energy is -299 cm^{-1} after the zero point correction.

E

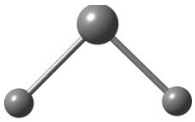

Saddle point of order 2, optimized at MP2(full)/aug-cc-pVTZ level. The interaction energy is -434 cm^{-1} (with the counterpoise correction) at this level of theory. The interaction energy is -302 cm^{-1} after the zero point correction.

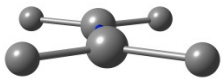

F

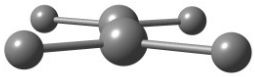

Minima, optimized at MP2(full)/aug-cc-pVTZ level . The binding energy is -529 cm^{-1} (with the counterpoise correction) at this level of theory. The interaction energy is -287 cm^{-1} after the zero point correction.

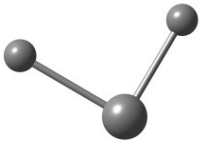

G

Transition state, optimized at MP2(full)/aug-cc-pVTZ level . The binding energy is -414 cm^{-1}(with the counterpoise correction) at this level of theory. The interaction energy is -217 cm^{-1} after the zero point correction.

H

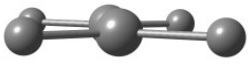

Structure H, Saddle point of order 2, optimized at MP2(full)/aug-cc-pVTZ level . The binding energy is -420 cm^{-1} (without counterpoise correction) at this level of theory.

Table III.A.6. The frequencies of the intra-molecular modes of C_2H_4•••H_2S calculated at MP2(full)/aug-cc-pVTZ level on the counterpoise corrected surface is listed below.

Vibrational frequencies (cm^{-1})
813, 949, 986, 1040, 1230,1246, 1385, 1484, 1687,
2757, 2793, 3177, 3209, 3249, 3282

Table III.A.7. S-H frequency shifts (in cm^{-1}) for C_2H_4•••H_2S calculated at MP2 (full) level on the counterpoise corrected surface using different basis sets:

	6-31G*	6-311++G**	6-311++G(3df,2p)	6-311++G(3df,pd)	aug-cc-pVDZ	aug-cc-pVTZ
Symmetric stretch	-6	-9	-21	-21	-21	-28
Asymmetric stretch	-4	-7	-8	-9	-9	-7

Table III.A.8. S-H frequency shifts (in cm^{-1}) for C_2H_4•••H_2S calculated at MP2 (full) level on the counterpoise uncorrected surface using different basis sets:

	6-31G*	6-311++G**	6-311++G(3df,2p)	6-311++G(3df,pd)	6-311++G(3df,3pd)	aug-cc-pVDZ	aug-cc-pVTZ
Symmetric stretch	-10	-12	-30	-25	-24	-29	-34
Asymmetric stretch	-9	-10	-11	-11	-9	-11	-11

Table III.A.9. Vibrational frequencies (in cm^{-1}) of structures A-G at MP2 (full) level. The frequencies for the structure A has been calculated using 6-311++G (3df,pd) basis set. The frequencies of the rest of the structures have been calculated using aug-cc-pVTZ basis set.

Structure A	Structure B	Structure C	Structure D	Structure E	Structure F	Structure G	Structure H
-33	57	-154	-159	-152	15	-129	-144
33	70	-3	-101	-81	56	13	-25
58	97	28	21	14	62	57	45
73	166	63	25	34	92	73	71
115	183	71	70	68	106	73	77
256	260	180	166	160	160	182	179
832	845	815	818	811	817	816	815
965	987	947	935	946	950	949	949
991	1017	981	983	980	982	979	981
1077	1074	1067	1064	1064	1053	1065	1067
1228	1219	1205	1202	1208	1213	1209	1206
1247	1252	1246	1246	1243	1247	1247	1246
1383	1372	1384	1384	1384	1386	1384	1384
1479	1496	1485	1483	1484	1485	1484	1485
1682	1666	1687	1687	1687	1687	1686	1688
2781	2769	2786	2785	2789	2782	2786	2786
2816	2786	2798	2795	2800	2800	2799	2799
3167	3117	3174	3173	3175	3176	3174	3173
3183	3147	3205	3206	3207	3207	3206	3205
3262	3182	3249	3249	3248	3248	3248	3247
3287	3213	3280	3280	3280	3279	3280	3278

Table III.A.10. Intermolecular harmonic vibrational frequencies of C_2H_4•••D_2S complex calculated at MP2(full)/aug-cc-pVTZ level of theory

Intermolecular motions	Vibrational frequencies (cm^{-1})
Rotation of D_2S about hydrogen bond couples with the rotation of ethylene about its 'c' principal axis	29
Rotation of D_2S about its C_2 symmetric axis coupled with the rotation of ethylene about its 'b' principal axis	49
Rotation of D_2S about its 'c' principal axis coupled with the rotation of ethylene about its C-C bond axis.	74
Intermolecular stretching	88
Rotation of D_2S about its 'c' principal axis coupled with the rotation of ethylene about its 'a' principal axis	133
Sweeping of the bonded deuterium of D_2S over the π cloud of ethylene coupled with the rotation of ethylene about its 'b' principal axis.	200

Table III.A.11. Intermolecular harmonic vibrational frequencies of C_2D_4•••H_2S complex calculated at MP2(full)/aug-cc-pVTZ level of theory

Intermolecular motions	Vibrational frequencies (cm^{-1})
Rotation of H_2S about hydrogen bond coupled with the rotation of C_2D_4 about its 'c' principal axis	37
Rotation of H_2S about its C_2 symmetric axis coupled with the rotation of C_2D_4 about its 'b' principal axis	44
Rotation of H_2S about its 'c' principal axis coupled with the rotation of C_2D_4 about its C-C bond axis.	57
Intermolecular stretching	86
Rotation of H_2S about its 'c' principal axis coupled with the rotation of C_2D_4 about its 'a' principal axis	172
sweeping of the bonded deuterium of H_2S over the π cloud of C_2D_4 coupled with the rotation of C_2D_4 about its 'b' principal axis.	279

Table III.A.12. Intermolecular harmonic vibrational frequencies of C_2D_4•••D_2S complex calculated at MP2(full)/aug-cc-pVTZ level of theory.

Intermolecular motions	Vibrational frequencies (cm^{-1})
Rotation of D_2S about hydrogen bond coupled with the rotation of C_2D_4 about its 'c' principal axis	28
Rotation of D_2S about its C_2 symmetric axis coupled with the rotation of C_2D_4 about its 'b' principal axis	43
Rotation of D_2S about its 'c' principal axis coupled with the rotation of C_2D_4 about its C-C bond axis.	55
Intermolecular stretching	84
Rotation of D_2S about its 'c' principal axis coupled with the rotation of C_2D_4 about its 'a' principal axis	126
Sweeping of the bonded deuterium of D_2S over the π cloud of C_2D_4 coupled with the rotation of C_2D_4 about its 'b' principal axis.	199

Figure III.A.2. AIM calculation of Structure F shows bond critical points and the ring critical points connecting the hydrogens of ethylene to the sulphur. The electron density(ρ) at BCP(1) = 0.006 au. The electron density at BCP(2) =0.006 au. The Laplacian of the electron density at BCP(1) is 0.020 au. The Laplacian of the electron density at BCP(2) is 0.020 au for both the critical points and these are well within the range for Propelier's criterion of hydrogen bonding.

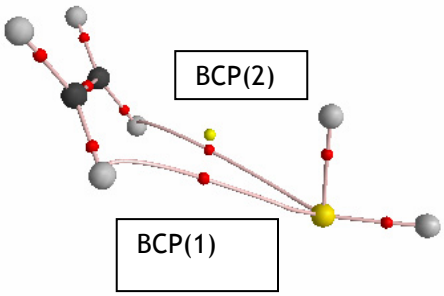

Chapter IV

Rotational Spectra and Structure of phenylacetylene···H_2O

IV.A. Introduction

Since the invention of modern Balle-Flygare spectrometer, microwave spectroscopy has revolutionised the study of numerous van der Waals complexes. The isolated condition provided by the molecular beam is a unique way to testify the advancement of the modern day *ab initio* theory. The ultimate goal of such studies is to develop an understanding of the interaction potentials of atoms and molecules interacting with each other and to relate it to more complex condensed phase where the three-body and many-body interactions begin to play their role.

Interaction of a water molecule with an aromatic ring is of interest as it could act as a model for the study of hydrophobic interaction. Several 1:1 complexes of water and aromatic ring have been characterised by microwave spectroscopy e.g benzene•••water[1-2], phenol•••water[3-4], aniline•••water[5], benzonitrile•••water[6-8]. With benzene, water acts as a hydrogen bond donor. In phenol•••water, water acts as a hydrogen bond acceptor. With aniline, water forms O-H•••N hydrogen bond whereas in benzonitrile•••water, water is lying almost in the plane of phenyl ring forming C-H•••O and O-H•••N hydrogen bonds. Thus even with this limited set of examples, one can have a glimpse of the variety of structures, when the substituent in the phenyl ring is changed. Further, a question of fundamental importance is that can we predict the orientation of the monomers with respect to each other beforehand when there are multiple sites capable of accepting or donating electrons present in the molecule? In this regard, Legon and Millen had derived a set of empirical rules to predict the geometry of hydrogen bonded systems B•••HX, where B has either π electrons or a non-bonding pair or both.[9] These rules are derived from a large set of experimental data obtained from microwave spectroscopic studies and are based on the electrostatic interaction between the two interacting partners. The basic principle is that the hydrogen atom will seek the most electron rich region of B and this electron rich region is either along the axis of the lone pair or along the π bonding electron pair. The first part of the rule says that if B has lone pair, then the axis of the HX molecule always coincides with that of the lone pair. The second part of the rule says that if B has π bonding pair, then the axis of the HX molecule intersects the internuclear axis of the atoms forming the π bond and is perpendicular to the plane of symmetry of the

π bond. The third part of the rule predicts the lone pair to be the nucleophilic site when both π and lone pair are present in the molecule. Though, there are examples in the literature where the co-existence of both the isomers have been reported,[10] most often, the global minimum structure has been found to be the one as predicted by the rule.

In this regard, phenylacetylene is an interesting system having multiple sites which can participate in hydrogen-bond formation e.g phenyl ring π cloud and acetylenic π cloud as H-bond acceptors and the acetylenic acidic proton as H-bond donor. Experimental data on this kind of system can provide valuable insight to extend our understanding of the geometry and energetics of the weakly bound clusters. Apart from this, phenylacetylene has been found to be crucial intermediate in the formation of polycyclic aromatic hydrocarbons (PAH).[11] The chemistry of PAH affects both the atmospheric and the interstellar medium. The combustion processes are a source of the PAH and these contribute to the global warming. In the interstellar medium, PAH-like species constitutes 10% of the cosmic carbon budget. These are the suspected carriers of the UIR (unidentified infrared bands) and DIB (diffuse interstellar bands). Despite of these importances of the PAH, the formation route of its very first building block i.e. phenylacetylene is unknown. Under the low temperature condition of the interstellar medium, phenylacetylene and its complexes could be found and the microwave spectroscopic data on these systems may prove valuable to identify these complexes.

Considering the structural variety shown by these complexes, we could imagine three possible structures shown by phenylacetylene•••water (C_6H_5CCH•••H_2O) system:1) Water acting as a donor by forming a hydrogen bond with the π cloud of phenyl ring (Structure I) 2) the acetylene chromophore of phenylacetylene acting as a hydrogen bond donor to water (C-H•••O)(Structure II) 3) water acting as both hydrogen bond donor and acceptor thus forming O-H•••π (π electron density of acetylene chromophore) and C-H•••O (phenyl C-H bond acting as a donor to the oxygen of water) bonds. (Structure III). These geometries are shown in Figure IV.1. IR-UV double resonance study[12] of C_6H_5CCH•••H_2O indicated the third structure to be the probable one. This study identified two bands in the O-H stretch region. One corresponds to the bonded O-H stretch and the other corresponds to the free O-H stretch. Moreover, the Fermi resonance in the acetylenic stretch region disappeared in the complex which indicated that the

acetylenic π cloud is involved in the complexation. Recently a theoretical study has been reported where high level *ab initio* calculations at CCSD(T)/aug-cc-pVDZ level indicated that Structure III is energetically most favoured structure.[13] The binding energies are -6.5 kJ/mol, -6.2 kJ/mol and -7.1 kJ/mol for Structure I, Structure II and Structure III respectively which supports the IR-UV experiments. However the structural assignments from these studies are indirect and are not definitive. Hence it was decided to carry out the microwave spectroscopic studies of $C_6H_5CCH•••H_2O$ complex for the definitive assignment of the gas-phase structure of this complex. The *ab initio* derived rotational constants have been obtained from the authors of reference 12 in a personal communication and are reported in Table IV.1. From Table IV.1, one can immediately recognize that the rotational constants for these structures are significantly different to be assigned unambiguously by means of rotational spectroscopy.

Figure IV.1. The three possible geometries of $C_6H_5CCH•••H_2O$ complex

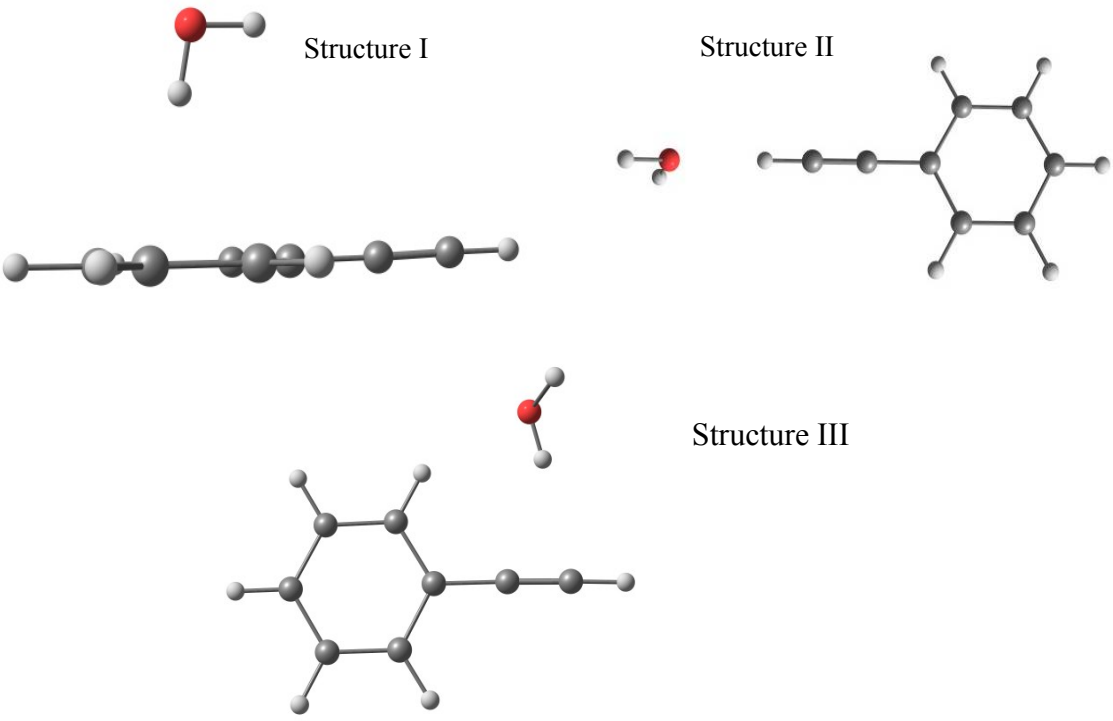

Table IV. 1. Ab initio derived rotational constants (obtained from the authors of reference 12) for the three geometries of C_6H_5CCH•••H_2O at MP2/aug-cc-pVDZ level. These constants are significantly different to characterise the geometries without any ambiguity by means of Fourier Transform Microwave Spectroscopy.

Rotational constants	Structure I	Structure II	Structure III
A (MHz)	2083	5518	2678
B (MHz)	1132	506	998
C (MHz)	995	464	729

IV.B. Experimental details

All the spectra were collected with the PNFTMW spectrometer described in Chapter II. Helium was used as the carrier gas. The reason for choosing helium as the carrier gas is explained in the next section. Helium was bubbled at a flow rate of 20 SCCM through phenylacetylene and at a flow rate of 1 SCCM through water and both the samples were mixed with a bath of Helium (200 SCCM) at a four-way junction and the mixture was carried to the nozzle. The mixture was expanded from a back pressure of 0.8-0.85 bar. The pulse dependence experiments revealed that a microwave pulse of 1.0 μs duration could produce the highest signal intensity for the *a*-dipole transitions. A pulse of 0.5 μs was optimum for the *b*-dipole transitions. Phenylacetylene (98%) and Phenylacetylene-D (C_6H_5CCD, 99 atom% D) were obtained from Aldrich and were used without any further purification. Isotopically enriched samples were used for $H_2{}^{18}O$ (97 atom% ^{18}O, Isotech). The spectrum for C_6H_5CCH•••HOD was obtained by mixing H_2O and D_2O (99.96 atom% D, Aldrich) in 50:50 proportion.

IV. C. Search and assignments

The initial prediction for the complex was based on the *ab initio* rotational constants reported in Table IV.1 The search region was chosen in such a way that all the possible structures of the complex would have some of their transitions in that region. Argon was chosen as the carrier gas for the initial search of $C_6H_5CCH•••H_2O$ complex. The carrier gas (argon) was flown at a rate of 150 SCCM. Argon was needed to flow through phenylacetylene and water in order to carry them to the nozzle. Argon was flown at a rate of 15 SCCM and 5 SCCM through phenylacetylene and water respectively. The mixture was expanded at a backing pressure of 0.5 bar. A microwave pulse of 0.5 μs duration was used to polarize the sample. Around 1500-2000 gas pulses were averaged. A total of 20 FIDs were collected for each gas pulse. A total of 256 points were sampled during the data acquisition. The scanning was started at 9200.4 MHz. A downward search was performed upto 7178.0 MHz and many transitions were observed. However, most of the transitions which were found, turned out to be from Ar•••phenylacetylene complex. These transitions were new and were not reported earlier.[14] The newly found transitions for Ar•••phenylacetylene are listed in the appendix at the end of this chapter. Only one weak line was found at 8143.0807 MHz, which was not a part of this series. Presence of only one line in this region was quite surprising considering the length of the search. As a result of this unsuccessful search in argon, the conditions were needed to be rechecked. The dependence of the signal at 8143.0807 MHz was tested and it was found to depend on both phenylacetylene and water. In fact, this line was very close to the predicted $4_{04}\rightarrow5_{05}$ transition of the Structure III. The predicted transition was at 8126.0 MHz. This weak line was tested using helium as the carrier gas. Under these conditions, the signal intensity improved considerably and in fact, this line was observed as a doublet with one more transition at 8142.2742 MHz. Further experiments were carried out under these conditions using helium as the carrier gas. The reason for this sensitivity enhancement could be the inability of helium to form complexes with phenylacetylene which increases the relative concentration of phenylacetylene monomer in the cavity so that it can form complex with H_2O. Assuming the above mentioned line as the $4_{04}\rightarrow5_{05}$ transition, the search was done for $5_{05}\rightarrow6_{06}$ transition. The search was started at 9758.0 MHz and one more doublet was located at 9597.8176 MHz and 9598.8931 MHz, ~1.45

GHz above the other transition. This difference is very close to the differences between the $K_a = 0$ *a*-dipole transitions as was predicted using the *ab initio* rotational constants for the Structure III. Thus, the observed transitions were very close to the prediction for the Structure III. Rest of the transitions could be located relatively easily. All of the transitions were observed as a doublet. Figure IV.2 shows the doublets corresponding to the $4_{04} \rightarrow 5_{05}$ transition. The transitions were fitted using Watson's A reduction Hamiltonian.[15] Both the series were fitted independently. After having the assignments for the *a*-dipole transitions, search was performed for the *b*-dipole transitions and could be observed easily. The *b*-dipole transitions were stronger than the *a*-dipole transitions. The *b*-dipole transitions were also observed as doublets. The optimum pulse for the *a*-dipole transitions was 1.0 μs whereas for the *b*-dipole transition, it was 0.5 μs. The list of the transitions and the fitted parameters for the parent isotopologue are shown in Table IV.2 and Table IV.7. respectively. As the rigid rotational constants predicted by the *ab initio* was close to the experimentally observed geometry, the spectra for all the isotopologues were predicted and located based on this geometry. All the transitions for the isotopologues are listed in Table IV.3 –Table IV.6. All the isotopologues, except C_6H_5CCH•••HOD, show doubling of the transition frequencies. The fitted parameters for the isotopologues are listed in Table IV.8. No hyperfine structure could be resolved for C_6H_5CCH•••HOD and C_6H_5CCH•••D_2O. The search for the ^{13}C isotopologues were not attempted as the signal intensity for the parent isotopologue was not high enough to see them in natural abundance.

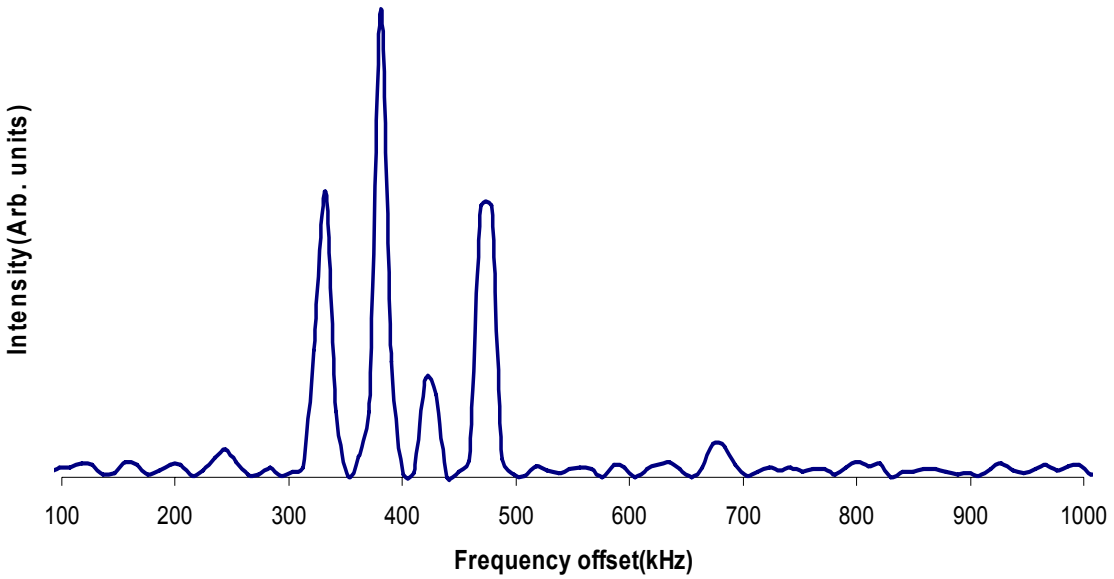

Figure IV.2. The $4_{04}\rightarrow 5_{05}$ transitions of C_6H_5CCH•••H_2O. Search using Helium showed doubling of the transition frequencies. Each of the transitions is split further due to the Doppler effect. The intensity of one transition is almost one-third of the other one. The signals were averaged for 1000 gas pulses. Thirteen FIDs were collected for each gas pulse. A total of 512 points were sampled for each FID.

Table IV.2. Experimentally observed rotational transitions and their assignments for C_6H_5CCH•••H_2O complex

Transitions[a]	Strong /MHz	Residue(kHz)	Weak/MHz	Residue(kHz)
4_{14}-5_{15}	-	-	7313.3681	-0.3
3_{12}-4_{13}	7377.2239	-0.8	7377.1167	-1.5
3_{03}-4_{14}	7469.9099	-3.1	-	-
4_{14}-5_{15}	7871.0364	-0.2	7870.0680	0.2
4_{04}-5_{05}	8143.0807	1.0	8142.2742	0.8
4_{23}-5_{24}	8575.9471	5.3	8575.4126	1.2
4_{04}-5_{15}	8699.4556	2.5	8698.9750	2.2
1_{10}-2_{21}	8747.9047	-2.8	8750.8803	-0.1
5_{15}-6_{06}	9041.4890	-1.8	9041.1213	1.2
1_{11}-2_{20}	9042.5188	-1.1	9044.6475	0.2
4_{22}-5_{23}	9072.0932	0.3	9071.8680	-0.6
4_{13}-5_{14}	9153.4035	-0.1	9153.2243	0.8
5_{15}-6_{16}	9391.9782	-2.6	9390.7862	1.1
6_{25}-7_{16}	9574.4927	1.4	9572.3070	-0.1
5_{05}-6_{06}	9598.8931	-0.3	9597.8176	-1.9
5_{05}-6_{16}	9948.3535	-0.8	9947.4832	-1.3
2_{11}-3_{22}	10211.3150	5.9	10214.0197	-0.2
5_{24}-6_{25}	10239.0055	-2.9	-	-
5_{33}-6_{34}	10477.6610	-0.0	-	-
6_{16}-7_{07}	10687.3803	0.2	10685.8271	1.6
5_{14}-6_{15}	10874.3312	-0.2	10874.0427	1.0
6_{16}-7_{17}	10895.7674	1.6	10894.3327	-0.4
5_{23}-6_{24}	11004.1483	-1.8	-	-
6_{06}-7_{07}	11036.8388	-2.2	11035.9982	-5.6
6_{06}-7_{17}	11245.2288	2.1	11243.9982	0.1
6_{25}-7_{26}	11875.5196	-0.5	11874.6923	-0.7
7_{17}-8_{08}	12266.3368	1.9	12264.5854	-1.5
7_{17}-8_{18}	12385.8729	-1.3	-	-
7_{07}-8_{08}	-	-	12473.0986	4.0

[a] *Transitions are listed as $J''_{Ka''Kc''}$-$J'_{Ka'Kc'}$*

Table IV.3. Experimentally observed rotational transitions and their assignments for C_6H_5CCH•••D_2O complex

Transitions[a]	Strong/(MHz)	Residue(kHz)	Weak/(MHz)	Residue(kHz)
2_{02}-3_{03}	4879.8129	-1.9	4879.8129	0.4
3_{13}-4_{14}	6103.4511	-3.7	6103.4997	2.1
3_{03}-4_{04}	6402.7017	7.3	-	-
4_{14}-5_{05}	6989.9181	2.5	6990.0177	-3.8
3_{03}-4_{14}	7275.0634	2.5	7274.9904	-4.2
4_{14}-5_{15}	7592.6171	-0.1	7592.6758	2.0
4_{04}-5_{05}	7862.2781	-4.0	7862.3142	2.6
4_{04}-5_{15}	8464.9861	2.4	-	-
5_{15}-6_{06}	8673.9217	-5.0	8674.0249	-4.1
4_{13}-5_{14}	8779.0901	-1.2	8779.0213	-0.8
5_{15}-6_{16}	9064.2232	-1.2	9064.2950	-1.3
5_{05}-6_{06}	9276.6291	0.8	9276.6831	1.7
5_{05}-6_{16}	9666.9220	-4.0	9666.9474	-1.3
5_{24}-6_{25}	9843.5036	6.3	-	-
2_{11}-3_{22}	9997.9802	-0.2	9997.9608	0.0
6_{16}-7_{07}	10279.9605	0.9	10280.0727	5.9
5_{14}-6_{15}	10442.6530	-4.4	10442.5923	4.5
5_{23}-6_{24}	10517.8896	0.9	10517.8104	-0.5
6_{16}-7_{17}	10520.0474	-0.1	10520.1344	-1.4
6_{06}-7_{07}	10670.2610	3.7	10670.3336	-0.5
6_{25}-7_{26}	10910.3453	0.1	10910.4061	2.9
7_{17}-8_{08}	11423.8391	-2.9	-	-
7_{17}-8_{18}	11820.8681	3.1	11820.9801	-2.6
6_{15}-7_{16}	11962.9115	-1.5	11963.0191	0.7
7_{07}-8_{08}	12045.4611	0.9	12045.4026	-2.3
7_{07}-8_{18}	12060.9550	2.0	12061.0535	1.8
6_{06}-7_{17}	12202.9978	-3.1	12203.0850	-2.4

[a]*Transitions are listed as $J''_{Ka''Kc''}$-$J'_{Ka'Kc'}$*

Table IV.4. Experimentally observed rotational transitions and their assignments for C_6H_5CCH•••HOD complex

Transitions[a]	Frequency(MHz)	Residue(kHz)
1_{01}-2_{02}	3376.0999	-3.1
2_{02}-3_{03}	4998.5991	0.9
3_{13}-4_{04}	5383.1567	3.6
2_{02}-3_{13}	6167.9561	-7.3
3_{13}-4_{14}	6244.0877	2.8
3_{03}-4_{04}	6552.5189	0.5
4_{14}-5_{05}	7178.5777	-1.7
3_{12}-4_{13}	7259.4733	-3.6
4_{14}-5_{15}	7765.4392	0.9
4_{04}-5_{05}	8039.5094	-1.8
4_{04}-5_{15}	8626.3761	6.0
1_{10}-2_{21}	8740.6683	-2.7
5_{15}-6_{06}	8893.5292	-5.5
4_{22}-5_{23}	8914.9734	-3.8
4_{13}-5_{14}	9011.2874	0.3
5_{15}-6_{16}	9268.0845	4.4
5_{05}-6_{06}	9480.4020	8.5
5_{05}-6_{16}	9854.9380	-1.0
5_{24}-6_{25}	10088.5637	-3.2
2_{11}-3_{22}	10185.6857	-4.8
6_{16}-7_{07}	10527.0795	-0.0
5_{14}-6_{15}	10712.0944	-1.6
6_{16}-7_{17}	10754.0969	-0.6
5_{23}-6_{24}	10813.6711	1.1
6_{06}-7_{07}	10901.6439	0.9
2_{12}-3_{21}	11088.2486	10.0
6_{06}-7_{17}	11128.6413	-1.7
3_{12}-4_{23}	11499.2399	-2.7
7_{17}-8_{08}	12094.3226	-3.1
6_{15}-7_{16}	12346.2835	4.6

[a]*Transitions are listed as $J''_{Ka''Kc''}$-$J'_{Ka'Kc'}$*

Table IV.5. Experimentally observed rotational transitions and their assignments for C_6H_5CCD•••H_2O complex

Transitions[a]	Strong/MHz	Residue(kHz)	Weak/MHz	Residue(kHz)
3_{13}-4_{14}	6197.1539	-0.6	-	-
3_{03}-4_{04}	6500.7486	1.9	6500.1811	-4.2
4_{14}-5_{05}	7173.1047	-0.8	7171.8512	1.5
5_{24}-6_{15}	7188.8364	-0.0	-	-
3_{03}-4_{14}	7296.2949	0.6	-	-
4_{14}-5_{15}	7704.5633	0.8	7703.6020	-2.6
4_{04}-5_{05}	7968.6556	2.5	7967.8513	-0.2
4_{04}-5_{15}	8500.1102	0.0	8499.6057	-0.8
5_{15}-6_{06}	8860.7195	2.3	8859.3511	0.1
4_{13}-5_{14}	8965.9070	-2.9	8965.7311	0.2
5_{15}-6_{16}	9192.6244	-0.6	9191.4411	-0.0
5_{05}-6_{06}	9392.1737	-0.5	9391.1077	1.8
5_{05}-6_{16}	9724.0808	-1.2	9723.1923	-3.8
6_{16}-7_{07}	10467.0288	0.1	10465.4972	-4.9
5_{14}-6_{15}	10649.2319	2.0	10648.9449	2.3
6_{06}-7_{07}	10798.9321	-4.4	10797.5874	-4.8
6_{06}-7_{17}	10995.7069	-1.6	10994.4706	0.5
7_{17}-8_{08}	12009.3631	-1.9	12007.6409	1.3
7_{07}-8_{08}	12206.1385	1.4	12204.5192	1.8
7_{07}-8_{18}	12318.3659	3.5	12316.8098	7.9

[a] *Transitions are listed as $J''_{Ka''Kc''}$-$J'_{Ka'Kc'}$*

Table IV.6. Experimentally observed rotational transitions and their assignments for C_6H_5CCH•••$H_2{}^{18}O$ complex

Transitions[a]	Frequency	Residue	Frequency	Residue
4_{14}-5_{15}	-	-	7587.6948	-0.4
5_{15}-6_{06}	-	-	8688.1026	1.0
4_{13}-5_{14}	8805.1067	2.3	8805.3708	0.1
5_{15}-6_{16}	9054.7981	-2.4	9055.9917	4.0
5_{05}-6_{06}	-	-	9264.0632	-1.4
5_{05}-6_{16}	9631.0682	-3.9	-	-
6_{16}-7_{07}	-	-	10284.8832	-2.2
	10467.1563	-1.6	-	-
6_{06}-7_{17}	-	-	10652.7705	0.3
6_{06}-7_{07}	10874.6966	5.1	10875.9179	-0.9

[a] *Transitions are listed as $J''_{Ka''Kc''}$-$J'_{Ka'Kc'}$*

Table IV.7. Fitted rotational constants and the distortion constants for C_6H_5CCH•••H_2O complex. The inertial defect Δ is defined as $\Delta = I_c - I_a - I_b$

Parameters	Strong	Weak
A	2672.092(3)	2673.135(3)
B	996.3581(8)	996.3929(9)
C	731.7055(4)	731.5733(4)
Δ_J (kHz)	0.366(6)	0.392(8)
Δ_{JK} (kHz)	-0.58(2)	-0.69(2)
Δ_k (kHz)	5.1(6)	6.9(5)
δ_J (kHz)	0.077(3)	0.091(4)
δ_k (kHz)	1.1(1)	1.5(1)
Δ (amu Å^2)	-5.67	-5.46
SD(kHz)	2.2	1.7
# [a]	27	24

[a] *Total number of fitted transitions*

Table IV.8. Fitted rotational constants and the distortion constants for the isotopologues. The inertial defect Δ is defined as $\Delta = I_c - I_a - I_b$

Parameters	$C_6H_5CCH\cdots D_2O$		$C_6H_5CCD\cdots H_2O$		$C_6H_5CCH\cdots H_2{}^{18}O$ [a]		$C_6H_5CCH\cdots HOD$
	Strong	Weak	Strong	Weak	-	-	
A (MHz)	2625.266(7)	2625.044(6)	2602.00(2)	2602.99(3)	2616.32(1)	2615.382(3)	2672.744(4)
B (MHz)	951.432(2)	951.414(2)	976.61(2)	976.645(4)	956.6621(6)	956.6468(4)	979.0377(1)
C(MHz)	707.623(8)	707.636(8)	716.020(8)	715.891(1)	705.8523(6)	705.9508(1)	722.5126(7)
Δ_J (kHz)	0.39(1)	0.40(1)	0.9(1)	0.9	0.366	0.392	0.38(1)
Δ_{JK} (kHz)	0.17(1)	-0.6(1)	-4.4(4)	-4.4	-0.58	-0.69	-0.7(1)
Δ_k (kHz)	4.4(1)	4.8(1)	-130(4)	130	5.1	6.9	5.4(8)
δ_J (kHz)	0.056(5)	0.070(6)	0.34(5)	0.34	0.077	0.091	0.092(5)
δ_K (kHz)	2.7(1)	1.1(2)	6(3)	6	1.1	1.5	1.5(2)
Δ(amu Å^2)	-9.49	-9.53	-5.89	-5.67	-5.65	-5.63	-5.81
SD(kHz)	3.1	2.6	1.9	3.1	2.2	1.8	3.9
#[b]	27	23	20	17	5	8	30

[a] *Intensities of the rotational transitions observed were not clear enough to distinguish the stronger and weaker state* [b] *Total number of fitted transitions*

IV.D. Structure of $C_6H_5CCH•••H_2O$ complex

A comparison of Table IV.1 and Table IV.7 immediately shows that the experimentally obtained rotational constants are very close to that of Structure III and supports the conclusions drawn on the structure of $C_6H_5CCH•••H_2O$ by Patwari and co-workers. The experimentally observed geometry has been re-optimized at MP2/aug-cc-pVDZ level starting from a C_{2v} symmetric structure of phenylacetylene monomer and the frequencies have been recalculated. The re-calculated structure at MP2/aug-cc-pVDZ level has the *A* rotational constant even closer to the experiment. The complex has also been optimized at MP2 level using 6-311++G** and aug-cc-pVTZ besis sets. All these calculations have been performed by the G03 suite of programme.[16] The equilibrium rotational constants calculated for the $C_6H_5CCH•••H_2O$ complex calculated using different basis sets is listed in Table IV.9. The rotational constants determined from the experiments unequivocally confirm the structure to be the one where the H_2O is in the plane of phenylacetylene monomer forming O-H•••π and C-H•••O hydrogen bonds.

Table IV.9. The equilibrium rotational constants and the equilibrium inertial defects for $C_6H_5CCH•••H_2O$ complex at MP2 level using different basis sets. The last column lists the experimentally obtained constants for the stronger series. The aug-cc-pVDZ constants are in excellent agreement to the experimental ones.

Parameters	6-311++G**	aug-cc-pVDZ	aug-cc-pVTZ	Experiment
A (MHz)	2664.3392	2672.7410	2741.0248	2672.092(3)
B (MHz)	1010.8831	998.8403	1007.6348	996.3581(8)
C (MHz)	734.7249	729.3653	743.1090	731.7055(4)
Δ (amu Å^2)	-1.8	-2.2	-5.8	-5.7

From Table IV.7. and Table IV.8, it is clear that the experimental inertial defects for all the isotopologues are significantly small and do not change much with the substitutions, which obviously indicates that the structure is effectively planar with all the heavy atoms lying in the same plane. The inertial defects do not change at all by the ^{18}O substitution which clearly tells that the oxygen atom is lying in the *ab* inertial plane of the complex.

However, the location of the two hydrogen atoms of H_2O may not be very precise especially the non-bonded hydrogen which may shuttle in and out of the plane without facing any appreciable barrier. The change in the inertial defect between the planar and non-planar structure, which differs just in the position of the non-bonded hydrogen atom, is quite small. Thus, the inertial defect for the *ab initio* geometry optimized at MP2(full)/aug-ccpVDZ level is -2.47 amuÅ^2, whereas a planar structure where the hydrogen atom is in the plane gives a value of 0.00 amuÅ^2. This difference can easily be outweighed by the vibrational effects especially where an atom as light as hydrogen is involved. However, from Table IV.8., it is to be noted that substitution of the bonded hydrogen of H_2O moiety produces little change in the inertial defect whereas the substitution of the other hydrogen which is away from the acetylene group increases the inertial defect by almost two times. This can lead one to think that, in the vibrationally averaged structure, the other hydrogen which is away from the acetylene moiety is off the *ab* inertial plane. However, the *ab initio* optimized rigid non-planar geometry (where the non-bonded hydrogen is located outside the plane) optimized at MP2/aug-cc-pVDZ level shows a change of only 0.4 amuÅ^2 while going from $C_6H_5CCH•••H_2O$/ $C_6H_5CCH•••HOD$ to $C_6H_5CCH•••D_2O$. Thus, the rigid structure does not reflect these changes in the inertial defects. The ground state rotational constants in the harmonic approximation have been calculated at MP2 level using 6-311++G** basis set and the aug-cc-pVDZ basis set for $C_6H_5CCH•••H_2O$, $C_6H_5CCH•••HOD$ and $C_6H_5CCH•••D_2O$ and are listed in Table IV.10. The experimentally observed changes in the inertial defects for these isotopes are reproduced satisfactorily by the calculated effective rotational constants within the harmonic approximation. The inertial defect gets almost doubled when one goes from $C_6H_5CCH•••H_2O$ / $C_6H_5CCH•••HOD$ to $C_6H_5CCH•••D_2O$ as shown by these calculated vibrationally averaged rotational constants. The agreement is in fact excellent at both level of theory. Hence, this increase in inertial defect in case of $C_6H_5CCH•••D_2O$ is because of the presence of an out of plane vibration which samples different geometry in case of the H_2O/HOD and D_2O complexes. This motion is best described as flipping of the hydrogen below and above the heavy atom structure. A closer look at the vibrational frequencies of the complex calculated at MP2/aug-cc-pVDZ level shows one mode where the motion is like the flipping of this non-bonded hydrogen

of H_2O. The vibrational frequency is 120 cm^{-1}. It is not easy to conclude about the planarity or non-planarity of the other hydrogen in the equilibrium structure as the barrier for this motion can be sufficiently low to sample all the available dihedral angles as it is discussed later.

A direct structural analysis of the complex is possible by the Kraitchman Substitution analysis of the experimental rotational constants of the parent complex and the singly substituted isotopologues. The labelling of the atoms in the C_6H_5CCH•••H_2O complex along with the approximate location of the principal axes is shown in Figure IV.3. The small vale of inertial defect suggests the complex to be nearly planar and it was assumed to be so during the analysis. Hence, the *c* co-ordinates of all the atoms have been assumed to be zero. The distances of the substituted atoms from the center of mass can be determined by using the following sets of equations:

$$|a| = \sqrt{\left[\frac{\Delta I_b}{\mu}\left(1+\frac{\Delta I_a}{(I_a - I_b)}\right)\right]} \quad (1)$$

$$|b| = \sqrt{\left[\frac{\Delta I_c}{\mu}\left(1+\frac{\Delta I_b}{(I_b - I_c)}\right)\right]} \quad (2)$$

The substitution co-ordinates for all the atoms are shown in Table IV.11. The limitation of the substitution analysis is apparent from the imaginary *b* co-ordinate for the eleventh hydrogen atom. This atom is very close to the *a* principal axis of the complex, as can be seen in Figure IV.3., which results in this imaginary co-ordinate.

Table IV.10 Effective ground state rotational constants and the inertial defects calculated within the harmonic approximation at MP2 level using different basis sets.

Parameters/Basis set	$C_8H_6\cdots H_2O$	$C_8H_6\cdots HOD$	$C_8H_6\cdots D_2O$	$C_8H_6\cdots H_2{}^{18}O$	$C_6H_5CCD\cdots H_2O$
A (MHz) /6-311++G**	2664.3390	2660.2312	2616.7368	-	-
B (MHz)/6-311++G**	1010.8846	992.7268	964.4386	-	-
C (MHz)/6-311++G**	734.7236	724.7770	707.5089	-	-
Δ(amu Å^2)/6-311++G**	-1.77	-1.76	-2.84		
A (MHz) /aug-cc-pVDZ	2672.7409	2668.3402	2622.8509	2614.5156	2603.8157
B (MHz) /aug-cc-pVDZ	998.8413	981.6689	955.6103	959.8943	978.0893
C (MHz)/aug-cc-pVDZ	729.3644	719.8491	703.9310	704.2225	713.1774
Δ(amu Å^2)/aug-cc-pVDZ	-2.14	-2.15	-3.60	-2.15	-2.16

Figure IV.3. Labeling of the atoms used in the structural analysis for C_6H_5CCH•••H_2O complex. The approximate location of the principal axes is shown in the figure. The c principal axis is perpendicular to the plane of the paper.

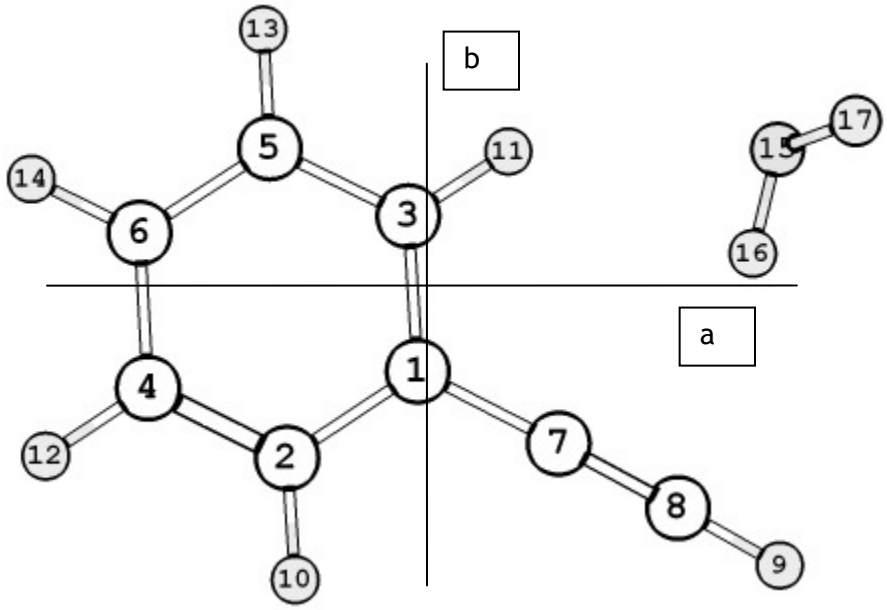

Table IV.11. Kraitchman substitution co-ordinates (r_s) for the substituted atoms of C_6H_5CCH•••H_2O complex. The co-ordinates are in given in Å.

	|a|	|b|	|c|
O_{15}	3.24	1.49	0.0
H_{16}	3.00	0.23i	0.0
H_{17}	3.85	1.89	0.0
H_9	3.18	2.30	0.0

The five independent set of rotational constants for the five isotopes can be used to derive an approximate position of water with respect to the phenylacetylene monomer. The internal co-ordinates were fitted directly to the moments of inertia to obtain a r_0 structure for C_6H_5CCH•••H_2O complex. The non-linear least square fitting routine STRFIT[17] was used for this purpose. A few numbers of constraints were used during the fitting. The first assumption is that the monomer geometries are unchanged due to the complexation. The r_0 geometry of phenylacetylene monomer[18] and H_2O[19] were used in the fitting.

Keeping these constraints, the parameters which were fitted are r($O_{15}C_7$), ∠$O_{15}C_7C_8$, D($O_{15}C_7C_8C_3$), A($H_{16}O_{15}C_7$) and D($H_{16}O_{15}C_7C_3$). Keeping the dihedral angle D($H_{17}O_{15}H_{16}C_3$) fixed at the *ab initio* optimized value of 117.1° (as the MP2/aug-cc-pVDZ rotational constants are very close to the experiments, this value was taken from the aug-cc-pVDZ optimized geometry) produced a very high standard deviation of 134 amuÅ^2. Keeping this dihedral angle in the range of 90°-100° produced the minimum standard deviation. Further, the standard deviation didn't vary much over this range of angle. The minimum standard deviation was obtained by keeping the dihedral angle D($H_{12}O_{10}H_{11}C_4$) at 99°. The fitted parameters and their deviations are shown in Table IV.12 for this fitting. It is clear from Table IV.12. that the structural parameters relating to the lighter H atoms show a higher deviation than the ones which involve only the heavy atoms. A better standard deviation needs more heavy atom substitutions which is beyond the scope of this investigation.

Table IV.12.Fitted structural parameters for C_6H_5CCH•••H_2O complex. The errors in the fitted value are shown in the parentheses.

Parameters	Fitted value
r($O_{15}C_7$) (Å)	3.423(4)
∠$O_{15}C_7C_8$ (degree)	80.4(1)
D($O_{15}C_7C_8C_3$) (degree)	-11.1(6)
A($H_{16}O_{15}C_7$) (degree)	25(3)
D($H_{16}O_{15}C_7C_3$) (degree)	226(12)

Table IV.13 shows some of the derived internal parameters of the C_6H_5CCH•••H_2O complex from the fitting. These parameters were not fitted directly but these are dependent on the fitted parameters in Table IV.12. The parameters listed in Table IV.13 characterise the hydrogen bonds formed between phenylacetylene and H_2O.

Table IV.13: Derived H-bond structural parameters for C_6H_5CCH•••H_2O complex

π (acetylene)•••H (Å)	2.477
H_{11}•••O_{15} (Å)	2.544
∠O_{15}-H_{16}•••π (degree)	154.9
∠$C_3H_{11}O_{15}$ (degree)	145.6
D($H_{16}O_{15}H_{11}C_3$) (degree)	45.8

Table IV.14. The cartesian co-ordinates (Å) of the C_6H_5CCH•••H_2O complex in the abc principal axes system of the complex derived from the fitting of the r_0 structure to the experimentally derived moments of inertia of all the isotopologues.

Atoms	*a*	*b*	c
C_1	0.091	-0.516	0.045
C_2	1.261	1.253	0.120
C_3	0.136	0.136	0.136
C_4	2.490	0.594	0.156
C_5	1.368	1.368	1.368
C_6	2.546	0.027	2.547
C_7	-1.184	-1.195	0.082
C_8	-2.248	-1.763	0.113
H_9	-3.179	-2.259	0.140
H_{10}	1.215	2.325	0.219
H_{11}	-0.773	1.433	0.302
H_{12}	3.401	1.163	0.284
H_{13}	1.409	2.600	0.238
H_{14}	3.499	0.055	3.499
O_{15}	-3.278	1.502	-0.144
H_{16}	-2.990	0.642	0.186
H_{17}	-3.666	1.318	-1.008

Table IV.15. The equilibrium cartesian co-ordinates (Å) of C_6H_5CCH•••H_2O complex in the abc principal axes system calculated at MP2/aug-cc-pVDZ level

Atoms	*a*	*b*	*c*
C_1	0.055	0.502	-0.015
C_2	1.235	1.281	0.054
C_3	0.142	-0.910	-0.071
C_4	2.490	0.650	0.066
C_5	1.404	-1.527	-0.060
C_6	2.579	-0.754	0.008
C_7	-1.227	1.160	-0.033
C_8	-2.317	1.748	-0.054
H_9	-3.253	2.276	-0.084
H_{10}	1.158	2.371	0.097
H_{11}	-0.774	-1.505	-0.121
H_{12}	3.399	1.256	0.119
H_{13}	1.470	-2.618	-0.105
H_{14}	3.558	-1.241	0.016
O_{15}	-3.205	-1.508	0.025
H_{16}	-2.976	-0.565	0.043
H_{17}	-3.652	-1.655	0.870

Table IV.14 shows the r_0 cartesian co-ordinates of the complex and these are in reasonable agreement with the substitution co-ordinates derived by the Kraitchman substitution analysis. Table IV.15 shows the equilibrium co-ordinates for the C_6H_5CCH•••H_2O complex calculated at MP2/aug-cc-pVDZ level. The substitution co-ordinates, r_0 co-ordinates and the equilibrium co-ordinates calculated by *ab initio* indicate that the co-ordinates for the oxygen atom and the H atoms numbered nine and sixteen (Figure IV.3) (terminal H atom of the acetylenic group of the phenylacetylene) are quite close for each of these structures whereas the co-ordinates for the non-bonded hydrogen (H atom numbered 17 in Figure IV.11) atom of water moiety differ a lot. This is not surprising considering the large amplitude motions which may affect this hydrogen which is discussed in the next section.

From Table IV.13, it is apparent that the distance of the ortho hydrogen of phenyl ring to the H_2O oxygen is 2.544 Å, which is less than the sum of van der Waals radii of H and O. This distance, in fact, is in close agreement to the predicted value, which has been calculated based on the radii suggested by Arunan and co-workers for H and different

acceptor atoms involved in strong, medium and weak H-bonding interaction.[20-21] The distance of the ortho hydrogen to the oxygen can be calculated as R_H(C-H) + R_H(O) = (1.07 + 1.40) Å = 2.47 Å . This value is quite close to the tabulated value in Table IV.13. Hence, there is a strong evidence of a secondary interaction present in the complex. This conclusion is further justified when one looks at the hydrogen bond angles. In literature, this kind of deviation from linearity has been found to be caused by the presence of a secondary interaction.[22] The ∠O-H•••π hydrogen bond angles made by various hydrogen bond donors to the acetylene π cloud is quoted in Table IV.16. Thus, all of them are linear whereas the ∠O-H•••π in C_6H_5CCH•••H_2O is far from linearity as can be seen from Table IV.13. It is further interesting to note that these fitting derived bond distance of the oxygen atom to the ortho hydrogen of the phenyl ring in C_6H_5CCH•••H_2O is 2.48 Å, which is very close to that of benzonitrile•••H_2O.[8] Moreover, the angle of the oxygen atom to the ortho C-H group is also very similar in both the complexes. This angle is close to 144° for both these complexes. It is noted that the distance of the hydrogen from the π center of acetylene group in C_6H_5CCH•••H_2O is also in close agreement to the calculated distance based on the H-bond radii. The calculated distance is R_H(O-H) + R_H(C^c) = 0.89 + 1.55 = 2.44 Å which is close to derived value listed in Table IV.13.

Table IV.16. B-H•••X angles in degrees for B-H•••HCCH complexes

B (donor atom)	A
F	180°[23]
Cl	180°[24]
Br	180° [25]
O	179°[26]

IV.E. AIM calculations

AIM[27] calculations were performed to locate the bond critical points in the $C_6H_5CCH•••H_2O$ complex. The bond critical points, bond paths and the ring critical points are shown in Figure IV.4. Two bond-critical points have been located. The BCP1 is connecting the water O-H to the mid point of the acetylenic π clound whereas the BCP2 is connecting the ortho C-H group to the water oxygen. Apart from the phenyl ring critical point, one more ring critical point has been located which signifies a ring closure due to the formation of O-H•••π and C-H•••O bonds. The electron densities (ρ) and the Laplacian ($\nabla^2\rho$) at the BCP1 and the BCP2 are shown in Table IV.17. These values are well within the range as was suggested by Koch and Popelier.[28] The ρ value at BCP should lie within the range [0.002, 0.035] au and the Laplacian of the electron density at BCP should lie within the range [0.024, 0.139] au as was suggested in reference 28.

Figure IV.4. The bond critical points and the ring critical points of $C_6H_5CCH•••H_2O$ complex located by AIM theoretical calculations.

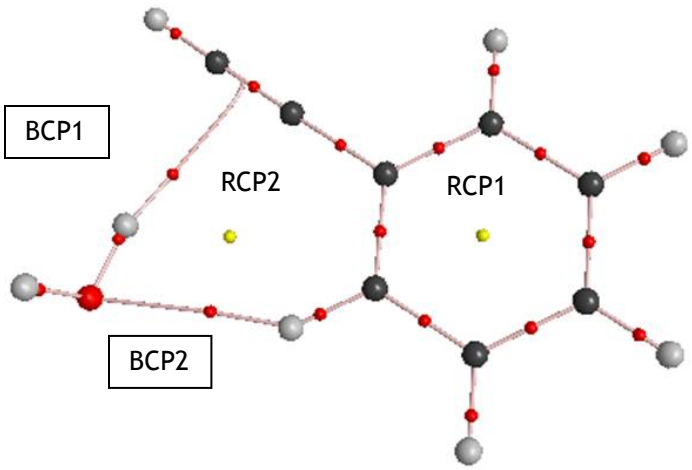

Table IV.17. Electron densities (ρ) and Laplacian of the electron densities ($\nabla^2\rho$) at BCP1 and BCP2 calculated by AIM theory.

Interaction	ρ (BCP)	L(ρ)
O-H•••π	0.013	0.036
C-H•••O	0.011	0.032

Thus, the results from the AIM theoretical calculations support the presence of a secondary C-H•••O interaction. Hence, we conclude that this deviation in the ∠O-H•••π bond angle from linearity in case of the C_6H_5CCH•••H_2O complex has been caused by the presence of the additional C-H•••O interaction. Moreover, the ρ value at BCP1 and BCP2 indicates that O-H•••π and C-H•••O are almost equally strong.

IV.F. Internal rotation of the H_2O moiety

All the isotopologues except the C_6H_5CCH•••HOD show a doubling of the transition frequencies which is because of the large amplitude motion of the H_2O moiety. The water subunit can undergo three kinds of internal motions in the complex (as shown in Figure IV.5):1. an internal rotation of the non-bonded hydrogen (the rotation about the α co-ordinate) as was observed in case of C_6H_6•••H_2O[1-2] 2. flipping of the non-bonded hydrogen of the water moiety in and out of the plane (inversion kind of motion) 3. the interchange of the equivalent hydrogens of H_2O about its C_2 axis (rotation about the angle θ). It is to be noted that none of these motions changes the *a* and *b*-dipole in the complex. Hence, it is expected that any of these motions would give rise to a semi- rigid rotor spectrum for the *a*-dipole and the *b*-dipole transitions, which can be fitted without the inclusion of any additional tunnelling splitting term in the Hamiltonain. In fact, as mentioned, both the series could be fitted independently. Hence, we cannot measure the tunnelling splitting directly from the spectra. The quenching of the observed splitting in case of C_6H_5CCH•••HOD complex confirms that this splitting arises because of the internal rotation of the H_2O about its C_2 symmetry axis. The rotational constant

differences for the isotopologues are reported in Table IV.18. From Table IV.18., it is evident that as we go from C_6H_5CCH•••H_2O to C_6H_5CCH•••D_2O, the magnitude of the splitting decreases by one order of magnitude. This tells us that the internal rotation of H_2O in C_6H_5CCH•••H_2O is a hindered in nature. This is expected as this motion involves the breaking of both the hydrogen bonds. On the other hand, the splitting shows little variation with the substitution of the hydrogen on the phenyl ring or with the oxygen atom substitution.

Figure IV.5. The co-ordinates describing the internal rotation of H_2O moiety in C_6H_5CCH•••H_2O complex.

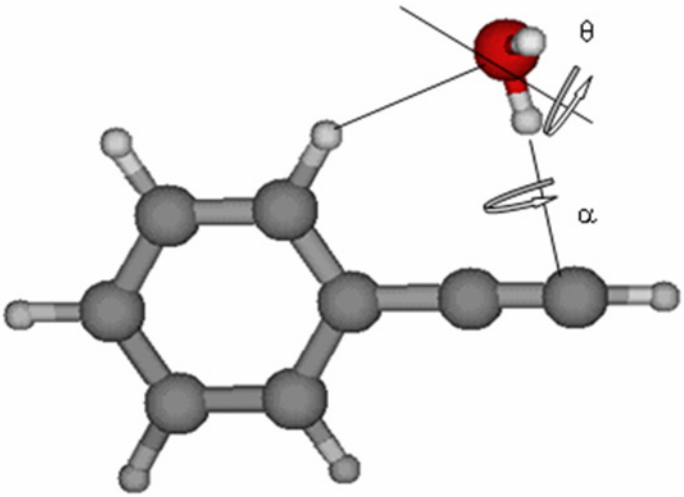

Table IV.18: Experimentally derived differences in the rotational constants for both the stronger and the weaker series for C_6H_5CCH•••H_2O and its isotopologues.

	C_8H_6-H_2O	C_8H_6-$H_2{}^{18}O$	C_8H_5D-H_2O	C_8H_6-D_2O
$\|\Delta A\|$ (MHz)	1.043	0.938	0.99	0.222
$\|\Delta B\|$ (MHz)	0.348	0.0153	0.035	0.018
$\|\Delta C\|$ (MHz)	0.1322	0.099	0.129	0.013

A potential energy curve has been calculated for the rotation of H_2O about the C_2 symmetry axis at MP2/aug-cc-pVDZ level and is shown in Figure IV.6. The potential energy barrier is 1186 cm^{-1} at this level of theory, which is significantly high to cause a hindered potential for this rotation. From the frequency calculations, one mode has been identified at 415 cm^{-1} (ZPE = 208 cm^{-1}) corresponding to the rotation of H_2O about its C_2 symmetry axis. Thus, the barrier height is almost six times higher than the ZPE along this co-ordinate. This is not surprising as a rotation of the H_2O moiety in C_6H_5CCH•••H_2O would lead to the breaking of both the hydrogen-bonds.

Figure IV.6. Potential energy curve for the rotation of the H_2O about the θ coordinate.

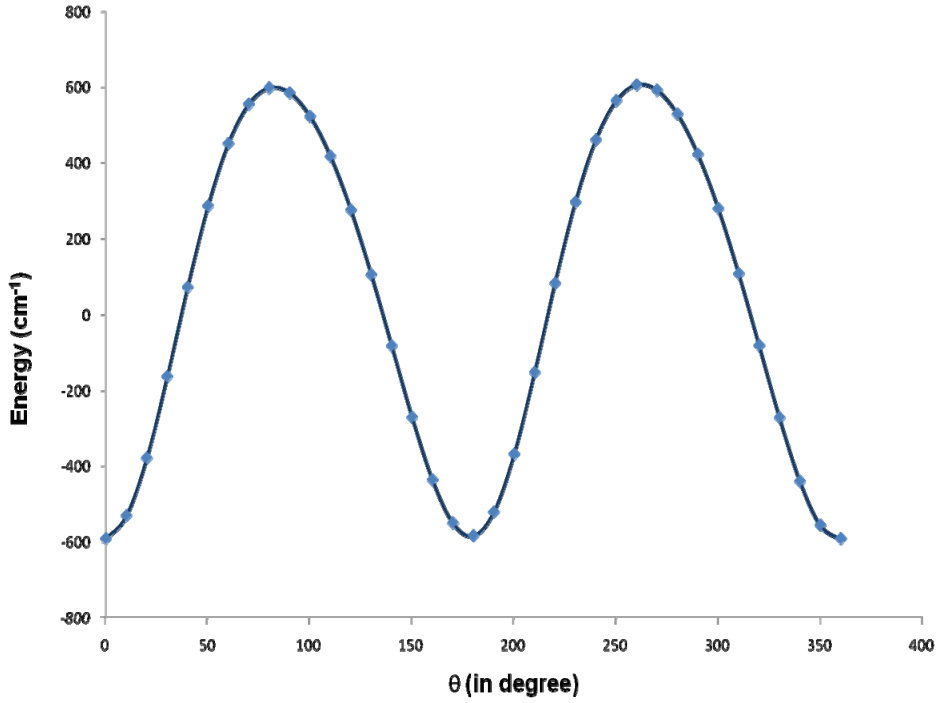

Potential energy curves have also been calculated for the complete rotation of H_2O about the α co-ordinate. The curve is shown in Figure IV.7. This motion faces two barriers; one is for a configuration where the non-bonded hydrogen is in the *ab* inertial plane of the complex but away from the phenylacetylene moiety and the other is the non-bonded hydrogen is in the plane but facing the phenylacetylene moiety. The barrier for the

former configuration is 70 cm^{-1}, whereas the barrier faced by the later configuration is 315 cm^{-1}. In the later configuration the ring hydrogen and the non-bonded hydrogen both come very close to each other and because of that the barrier increases. This indicated that a flipping inversion motion of the non-bonded hydrogen is more likely than a complete rotation of the hydrogen by 360°. However, experimentally we do not have any direct evidence for this motion, though we have some indirect evidence from the inertial defects. This motion, if present, would reverse the *c*-dipole moment of the complex and the splitting in the *c*-dipole transitions can differ by several MHz depending on the effective barrier height. It may be noted that the rigid *ab initio* geometry prediction for the dipole moment of the complex at MP2/aug-cc-pVDZ level gives $|\mu_a|$=0.7154 Debye, $|\mu_b|$= 0.9484 Debye and $|\mu_c|$= 1.3515 Debye. This shows that the *c*-dipole transition is the strongest. However, we do not have assignments for the *c*-dipole transitions for this complex. This could be because that the *c*-dipole moment is averaged out because of a complete rotation of the non-bonded hydrogen about the hydrogen bond. The other reason could be that the inversion motion of the non-bonded hydrogen produce very large splitting and as a result, the transitions can fall beyond the searched range.

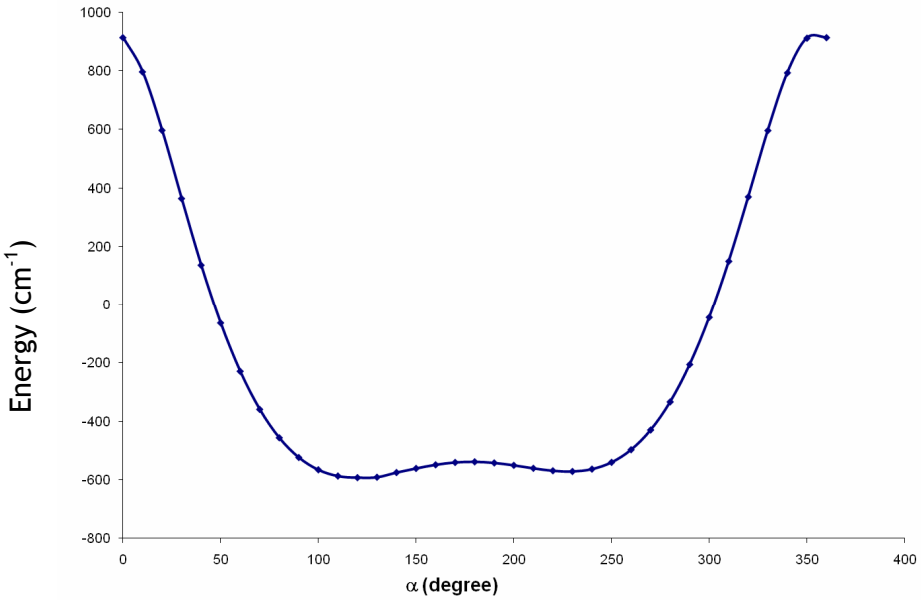

Figure IV.7. Potential energy curve for the rotation of the H_2O about the α-co-ordinate.

Considering the structural similarity with the benzonitrile•••H_2O[6-8]complex, let us compare the splitting pattern of these complexes. The splitting in the observed rotational constants for benzonitrile•••H_2O is less than what has been observed for C_6H_5CCH•••H_2O complex. The change in the rotational constants of the two states for benzonitrile•••H_2O are $|\Delta A|$ = 0.14 MHz, $|\Delta B|$ = 0.023 MHz and $|\Delta C|$ = 0.004 MHz. However, this is in contrast to the higher value of barrier height calculated here for C_6H_5CCH•••H_2O complex. On the other hand, the barrier for the rotation of H_2O about the C_2 symmetric axis in benzonitrile•••H_2O is significantly less than the calculated barrier height for C_6H_5CCH•••H_2O complex. A barrier height of ~284 cm^{-1} has been reported for benzonitrile•••H_2O complex.[8] This discrepancy in the barrier height may arise as the rotation of H_2O about the C_2 axis in C_6H_5CCH•••H_2O is not a one-dimensional problem and the reduced mass involved in the motion causing the splitting may be higher. The motion may involve the relation of other structural parameters which may change the barrier height. In benzonitrile•••H_2O, a previous study by Dreizler and co-workers yielded a barrier of 467 cm^{-1} for this C_2 rotation of H_2O.[29] Their model did not take the structural relaxations into account. However a flexible model calculation by taking into consideration of the relaxation of N-O distance and the C-N-O angle yielded a barrier height of 287 cm^{-1}. Thus, the relaxation of the structural parameters may be needed to achieve a reasonable barrier height for these strongly hydrogen-bonded systems.

IV.G. Conclusions

Rotational spectra of five isotopologues of C_6H_5CCH•••H_2O complex have been measured and assigned. The spectra revealed a nearly planar structure where the H_2O is donating its hydrogen to acetylenic π cloud forming O-H•••π bond whereas the ortho C-H group is involved in a secondary interaction with the H_2O oxygen. The rotational constants are in close agreement to the *ab initio* derived rotational constants and unequivocally confirm the planar structure. The experimentally derived distance of the hydrogen atom of H_2O from the center of the acetylenic π cloud is ~2.5 Å whereas the distance of the H_2O oxygen from the ortho hydrogen of the phenyl ring is also ~2.5 Å,

which is within the limit of a C-H•••O interaction. The presence of this secondary interaction causes a large deviation of the O-H•••π angle from linearity. The rotational spectrum exhibits a splitting of the transitions due to the interchange of the two equivalent hydrogens of the H_2O subunit which is more likely due to the rotation of H_2O about its C_2 symmetry axis. The decrease of the splitting in C_6H_5CCH•••D_2O by one order of magnitude indicates that the motion faces an appreciable barrier due to the breaking of O-H•••π and C-H•••O hydrogen bonds.

IV.H. References

1. S. Suzuki, P. G. Green, R. E. Bumgarner, S. Dasgupta, W. A. Goddard III, G. A. Blake, *Science*, **1992**, 257, 942.
2. H. S. Gutowski, T. Emilsson, E. Arunan, *J. Chem. Phys.* **1993**, 99, 4883.
3. M. Gerhards, M. Schmitt, K. Kleinermanns, W. Stahl, *J. Chem. Phys.* **1996**, 104, 967.
4. S. Melandri, A. Maris, P. G. Favero, W. Caminati, *Chem. Phys.* **2002**, 283, 185.
5. U. Spoerel, W. Stahl, *J. Mol. Spetrosc.* **1998**, 190, 278.
6. V. Storm, D. Consalvo, H. Dreizler, *Z. Naturforsch. A*, **1997**, 52, 293.
7. R. M. Helm, H-P Vogel, H. J Nuesser, V. Storm, D. Consalvo, H. Dreizler, *Z. Naturforsch*, **1997**, 52, 655.
8. S. Melandri, D. Consalvo, W. Caminati, P. G. Favero, *J. Chem. Phys.* **1999**, 111, 3874.
9. A. C. Legon, D. J. Millen, *Chem. Soc. Rev.* **1987,** 16, 467.
10. J. Wu, J. Zhang, Z. Wang, W. Cao, *J. Chem. Phys.* **2007**, 127, 175102.
11. R. L. Kaiser, *Angew. Chem. Int. Ed.* **2007**, 46, 6866.
12. P. C. Singh, B. Bandyopadhyay, G. Naresh patwari, *J. Phys. Chem. A* **2008**, 112, 3360.
13. R. Sedlack, P. Hobza, G. N. Patwari, *J. Phys. Chem. A*. **2009**, 113, 6220.
14. H. Dreizler, B. Hertke, H. D. Rudolph, *J. Mol. Struct.* **2006**, 825, 1.
15. J. K. G. Watson, in *Vibrational Spectra and Structure,* Ed. J. R. Durig (Elsevier, Amsterdam, **1977**, 6, 1. We thank G. T. Fraser for providing us with the programme ASYM82 by A. G. Maki which was used in the fitting. Ankit Jain added a feature

that enables the programme to remove one line from the fitting at a time and compare the rms deviation with the full fitting. The feature aids in identifying a wrong assignment.

16. M.J Frisch, G. W. Trucks, H. B Schlegel, G. E. Scuseria, M. A.Robb, J. R.Cheeseman, J. A. Montgomery Jr., T. Vreven, K. N. Kudin, J. C. Burant, J. M. Millam, S. S. Iyengar, J. Tomasi, V. Barone, B. Mennucci, M. Cossi, G. Scalmani, N. Rega, G. A Petersson, H. Nakatsuji, M. Hada, M. Ehara, K. Toyota, R. Fukuda, J. Hasegawa, M. Ishida, T. Nakajima, Y. Honda, O. Kitao, H. Nakai, M. Klene, X. Li, J. E. Knox, H. P. Hratchian, J. B.Cross, C. Adamo, J. Jaramillo, R. Gomperts, R. E. Stratmann, O. Yazyev, A. J. Austin, R. Cammi, C. Pomelli, J. W. Ochterski, P. Y. Ayala, K. Morokuma, G. A. Voth, P. Salvador, J. J. Dannenberg, V. G. Zakrzewski, S. Dapprich, A. D. Daniels, M. C. Strain, O. Farkas, D. K. Malick, A. D. Rabuck, K. Raghavachari, J. B. Foresman, J. V. Ortiz, Q. Cui, A. G. Baboul, S. Clifford, J. Cioslowski, B. B. Stefanov, G. Liu, A. Liashenko, P. Piskorz, I. Komaromi, R. L. Martin, D. J. Fox, T. M. Keith, A. Al-Laham, C. Y. Peng, A. Nanayakkara, M. Challacombe, P. M. W. Gill, B. Johnson, W. Chen, M. W. Wong, C. Gonzalez, J. A. Pople, *Gaussian 03*, Revision C-02; Gaussian, Inc. Wallingford CT, **2004.**
17. Z. Kisiel, *J. Mol. Spectrosc.* **2003**, 218, 58.
18. H. Dreizler, H. D. Rudolph, B. Hertke, *J. Mol. Strutct.* **2004**, 698, 1.
19. F. C. deLucia, P. Helminger, R. L. Cook, W. Gordy, *Phys. Rev. A.* **1972**, 5, 487.
20. P. K. Mandal , E. Arunan, *J. Chem. Phys*. **2001**, 114, 3880.
21. B. Raghavendra, P. K. Mandal, E. Arunan, *Phys. Chem. Chem. Phys*. **2006,** 8, 5276.
22. A. C. Legon, *Angew. Chem. Int. Ed.* **1999**, 28, 2686.
23. A.C. Legon, P. D. Aldrich, W. H. Flygare, *J. Chem. Phys.* **1981**, 75, 625.
24. W. G. Read, W. H. Flygare, *J. Chem. Phys.,* **1982**, 76**,** 2238.
25. S. A. C. McDowell, *Phys. Chem. Chem. Phys.,* **2001**, 3, 2754.
26. F. H. Allen, J. A. K. Howard, V. J. Hoy, G. R. Desiraju, D. S. Reddy, Chick C. Wilson, *J. Am. Chem. Soc.,* 1**996**, 118, 4081.
27. R. W. F. Bader, Atoms in Molecules: A Quantum Theory, Clarendon Press: Oxford, 1990.
28. U. Koch, P. L. A. Popelier, *J. Phys. Chem.* **1995,** 99, 9747.

29. V. Storm, H. Dreizler, D. Consalvo, *Chem. Phys.* **1998**, 239, 109.

Appendix

Table IV.A. 1. Newly observed transitions of Ar•••C_6H_5CCH complex during the search for C_6H_5CCH•••H_2O complex

Transitions	Frequencies/MHz
2_{11}-3_{22}	6150.7655
3_{13}-4_{04}	6159.1832
3_{13}-4_{14}	7144.3570
3_{31}-4_{32}	7150.5070
3_{12}-4_{13}	7446.5318
3_{21}-4_{22}	7582.1946
4_{32}-5_{23}	8001.6611
4_{23}-5_{14}	8288.3467
4_{13}-5_{14}	8584.3707
4_{13}-5_{24}	8696.6241
3_{21}-4_{32}	8959.1046

Table IV.A.2. Structural parameters of experimentally observed structure of C_6H_5CCH•••H_2O complex calculated at MP2/aug-cc-pVTZ level of theory

Parameters	Values	Parameters	Values	Parameters	Values
R(1,2)	1.403	R (4, 12)	1.082	R (15, 16)	0.966
R (1,3)	1.403	R (2, 10)	1.082	R (15, 17)	0.962
R (3,5)	1.392	R (1, 7)	1.428	A (2, 1, 3)	119.8
R (2,4)	1.391	R (3, 11)	1.082	A (2, 1, 7)	119.6
R (5,6)	1.394	R (5, 13)	1.082	A (3, 1, 7)	120.6
R (4,6)	1.395	R (7, 8)	1.220	A (1, 2, 4)	120.0
R (6, 14)	1.082	R (8, 9)	1.063	A (1, 2, 10)	119.3

Table IV.A.2. continued..

Parameters	Values	Parameters	Values	Parameters	Values
A(4, 2, 10)	120.7	A(5, 6, 14)	120.1	D(3, 1, 2, 4)	0.1
A(1, 3, 5)	119.7	A(1, 7, 16)	108.2	D(3,1,2,10)	180.0
A(1, 3, 11)	119.5	A(9, 8, 16)	121.0	D(7,1,2,4)	-179.7
A(5, 3, 11)	120.9	A(3, 11, 15)	143.1	D(7,1,2,10)	0.2
A(2, 4, 6)	120.2	A(11, 15, 16)	73.9	D(2,1,3,5)	-0.1
A(2, 4, 12)	119.7	A(11, 15, 17)	120.0	D(2,1,3,11)	179.5
A(6, 4, 12)	120.1	A(16, 15, 17)	104.3	D(7,1,3,5)	179.7
A(3, 5, 6)	120.5	A(7, 16, 15)	150.8	D(7,1,3,11)	-0.7
A(6, 5, 13)	120.0	A(7, 8, 9)	179.0	D(2,1,7,16)	-167.1
A(4, 6,5)	119.8	A(1, 7, 8)	179.1	D(3,1,7,16)	13.2
A(4, 6,14)	120.1	A(8, 16, 15)	172.3	D(1,2,4,6)	-0.0
D(1,2,4,12)	180.0	D(10,2,4,6)	-179.9	D(10,2,4,12)	0.1
D(1,3,5,6)	0.0	D(1,3,5,13)	-180.0	D(11,3,5,6)	-179.6
D(11,3,5,13)	0.5	D(1,3,11,15)	-22.6	D(5,3,11,15)	157.0
D(2,4,6,5)	-0.0	D(2,4,6,14)	180.0	D(12,4,6,5)	180.0
D(12,4,6,14)	-0.0	D(3,5,6,4)	0.0	D(3,5,6,14)	-180.0
D(13,5,6,4)	-180.0	D(13,5,6,14)	0.0	D(1,7,16,15)	-15.0
D(9,8,15,11)	169.6	D(9,8,15,17)	-73.5	D(3,11,15,16)	20.3
D(3,11,15,17)	-77.2	D(11,15,16,7)	2.4	D(17,15,16,7)	120.1

Figure IV.A.3. Numbering of atoms for C_6H_5CCH•••H_2O which has been used to designate the structural parameters in Table IV.A.1.

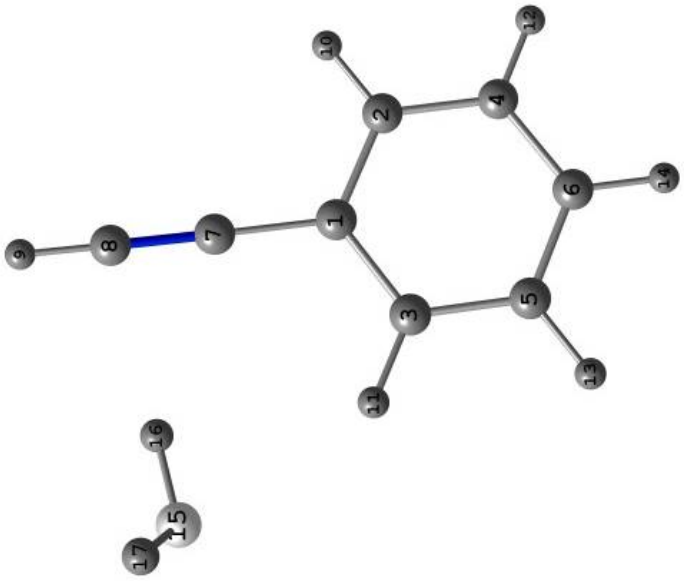

Table IV.A.4. Calculated distortion constants for C_6H_5CCH•••H_2O complex under the harmonic approximation at MP2/aug-cc-pVDZ level of theory.

	C_8H_6···H_2O	C_8H_6···HOD	C_8H_6···D_2O	C_6H_5D···H_2O	C_8H_6···$H_2{}^{18}O$ -
Δ_J (kHz)	0.208	0.198	0.185	0.191	0.209
Δ_{JK}(kHz)	-0.411	-0.324	-0.239	-0.390	-0.347
Δ_k (kHz)	0.335	3.328	3.245	3.333	3.364
δ_J (kHz)	0.065	0.062	0.055	0.062	0.066
δ_K (kHz)	0.445	0.446	0.436	0.410	0.466

Table IV.A.5. Vibrational frequencies for C_6H_5CCH•••H_2O complex calculated under the harmonic approximation at MP2/aug-cc-pVDZ level of theory.

Frequencies (cm^{-1})
30, 75, 112, 120, 130, 159, 208, 317, 399, 415, 460, 471, 497, 548, 614, 621, 643, 743, 761, 848, 906, 934, 965, 996, 1041, 1093, 1166, 1193, 1213, 1317, 1429, 1479, 1493, 1602, 1627, 1631, 2095, 3202, 3212, 3219, 3227, 3232, 3474, 3745, 3900

Chapter V

Rotational Spectra and Structure of phenylacetylene···H_2S

V.A. Introduction

Microwave spectroscopic studies of the complexes involving the first row and second row hydrides with aromatic ring are of interest as it provides the basis to understand the nature of the physical forces that dominate their interaction energy. How different/similar is the structure and dynamics when we compare the interactions of the first row and second row hydrides with the π cloud? With ethylene, HF,[1] HCl,[2,3] H_2O,[4,5] H_2S[6] all of them form π-bonded structure. Same is the case with benzene. C_6H_6•••H_2O,[7,8] C_6H_6•••H_2S,[9] C_6H_6•••HCl[10] and C_6H_6•••HF[12] all of them have π hydrogen bonded geometry. However, the nature of binding exhibited by the first and second row hydrides can change significantly when the substituent on the benzene ring changes and there are multiple possibilities. The global minimum for fluorobenzene•••H_2O[13,14] has a cyclic structure having O-H•••F and C-H•••O interaction whereas the fluorobenzene•••HCl[15] has π hydrogen bond. Theoretical and experimental studies of furan with the first row and the second row hydrides have been reported in literature. These studies in fact pose challenge to the Legon-Millen rules.[16] The third among these rules proposed by Legon and Millen says that if there is π-pair and a non-bonding pair, the hydrogen bond donor always goes to the non-bonding pair. However, recent infrared studies of furan with HCl detected both the σ bonded (bonded to the oxygen lone pair) and the π bonded (bonded to the furan π electron density) complexes in a molecular beam under the same condition.[17] One recent theoretical study of the complexes of furan with the first and second row hydrides has proposed that in case of the first row hydrides, the σ type complex is more stable than the π type complex, whereas in case of the second row hydrides, the π-type complexes are more stable than the σ type complexes.[18] A multifunctional molecule like phenylacetylene would be more challenging in this aspect to provide a definitive guideline for the prediction of the most stable structure of its complexes with the first row and the second row hydrides. Thus, a large set of experimental data are essential in this regard. We have already seen that phenylacetylene forms a planar complex with H_2O where the water molecule is donating one of its hydrogen to the acetylenic π cloud and the ortho hydrogen of the phenyl ring is involved in a secondary interaction with the oxygen atom of H_2O.[19] Interestingly, recent studies[20] show that the complexes of

phenylacetylene with NH_3, CH_3NH_2, CH_3OH exhibit structural diversity when the hydrogen bond donor is changed. Keeping this in mind, we wanted to explore the geometry of phenylacetylene•••H_2S (C_6H_5CCH•••H_2S) complex. Like H_2O complex of phenylacetylene in chapter IV, hydrogen sulphide could interact with phenylacetylene in three different ways: 1. H_2S can act as a donor to the π cloud of the phenyl group similar to what was observed in case of benzene•••H_2S complex. 2. The acetylenic C-H group of phenylacetylene can donate its hydrogen to the S atom forming a C-H•••S hydrogen bond. 3. H_2S can donate one of its hydrogen to the actylenic π cloud forming S-H•••π bond while the phenyl ring donates its ortho hydrogen to sulphur atom making a C-H•••S hydrogen bond and thus, forming a structure very similar to the corresponding water complex. Microwave spectroscopic studies on the C_6H_5CCH•••H_2S complex and its isotopologues are reported in this chapter along with the *ab initio* and AIM theoretical studies on the possible geometries of C_6H_5CCH•••H_2S complex.

V.B. Experimental

The spectrum was collected using the PNFTMW Spectrometer described in Chapter II. Helium was used as the carrier gas. The carrier gas was bubbled at a flow rate of 20 SCCM through the sample of phenylacetylene placed in a container at ambient condition. The flow rate of H_2S was ~ 1 SCCM. The samples were mixed with a bath of Helium (200 SCCM) at a four-way junction and the mixture was carried to the nozzle. The mixture was expanded using a stagnation pressure of 0.8-0.9 bar through the nozzle. Initially, a microwave pulse of 1.0 μs was used for the search. However, after having few transitions located, the conditions were re-optimized and a microwave pulse of 0.5 μs produced the best result. The signals seen for C_6H_5CCH•••H_2S were stronger than those of C_6H_5CCH•••H_2O. The optimum pulse for C_6H_5CCH•••H_2O *a*-dipole transitions was 1.0 μs whereas the *b* -dipole transitions needed 0.5 μs. The component dependence of the signals was tested and no transition could be observed in absence of either phenylacetylene or H_2S. The rest of the spectrum was obtained under these optimized conditions. Phenylacetylene (98%) and Phenylacetylene-D (C_6H_5CCD, 99 atom% D) were obtained from Aldrich and was used without any further purification. D_2S was

produced by passing ~ 1 SCCM of H_2S through the sample of D_2O (99.96 atom% D, Aldrich). HDS was produced by passing H_2S through a 50:50 mixture of H_2O and D_2O. The signals for $C_6H_5CCH\bullet\bullet\bullet H_2{}^{34}S$ were observed in natural abundance.

V.C. Rotational spectra

The search for the parent complex was guided by the *ab initio* calculations which are discussed in detail in the later sections. The calculations revealed that a geometry where H_2S is sitting on top of the phenylacetylene plane is the most stable one. The principal axes system for the global minimum obtained at MP2/aug-cc-pVDZ level is shown in Figure V.1. Both *a* and *b*-dipole transitions are expected to be present. The *ab initio* derived dipole moments at MP2/aug-cc-pVDZ level of the complex are $|\mu_a|$ = 1.5379 D, $|\mu_b|$ = -0.8290 D and $|\mu_c|$ = 0.0017 D. Search was started for $4_{14}\rightarrow5_{15}$, $4_{14}\rightarrow5_{05}$, $4_{04}\rightarrow5_{15}$ and $4_{04}\rightarrow5_{05}$ quartet at ~8250.0 MHz. The transitions $4_{14}\rightarrow5_{15}$, $4_{14}\rightarrow5_{05}$, $4_{04}\rightarrow5_{15}$ and $4_{04}\rightarrow5_{05}$ are closely spaced and their frequency increases in this order. As the prediction showed, the difference between the two $K_a = 0$ (*a* and *b*-dipole transitions) transitions is 9 kHz whereas the two $K_a = 1$ lines ('*a*' and '*b*' dipole) are also separated by 9 kHz. The difference between the $4_{14}\rightarrow5_{05}$ and $4_{04}\rightarrow5_{15}$ transitions is 110 kHz. These differences are found to decrease as we go to the higher J and at a certain J they appear at a single frequency. As we go to lower J, these transitions become widely separated from each other gradually. These transitions are referred as $K_a = 0/1$ quartet in the text. The pattern was similar in case of $4_{13}\rightarrow5_{24}$, $4_{13}\rightarrow5_{14}$, $4_{23}\rightarrow5_{24}$ and $4_{23}\rightarrow5_{14}$ transitions and they are referred as $K_a = 1/2$ quartet. The K_a=2/3 quartet also showed the same behaviour. The assignment of the transitions was facilitated by the fact that all these predicted $K_a = 0/1$, $K_a = 1/2$, $K_a = 2/3$ quartet transitions of successive J are separated by ~1.56 GHz from their corresponding lines at higher J. The difference is a constant number as one approaches the higher J. As we go to the lower J, the spacing between the individual transitions of the $K_a = 0/1$, $K_a = 1/2$, $K_a = 2/3$ quartet increases and hence, they cannot be located as easily as the higher J transitions. Thus search for $4_{14}\rightarrow5_{15}$, $4_{14}\rightarrow5_{05}$, $4_{04}\rightarrow5_{15}$ and $4_{04}\rightarrow5_{15}$ transitions yielded several transitions dependent on phenylacetylene and H_2S. Several other transitions could be located at around ~1.4 GHz above these lines. The corresponding transitions could be located for subsequent higher J also. However,

the higher J transitions could not be fitted as K_a=0/1 quartet. Eventually, they could be fitted as K_a=2/3 transitions. Both *a* and *b*-dipole transitions could be assigned. Moreover, the application of Ritz combination principle also aided a lot in the assignment. Thus, the sum of two appropriately chosen *a* -dipole transitions are equal to the sum of two correspondingly chosen *b*-dipole transition e.g. the frequencies of $4_{04}\rightarrow5_{05}$ and $4_{14}\rightarrow5_{15}$ transitions is equal to the sum of the frequencies of $4_{04}\rightarrow5_{15}$ and $4_{14}\rightarrow5_{05}$ transitions. Identification of such Ritz quartet aided a lot in the assignment.

Each of the observed transitions was split into two sets arising from some internal rotation of H_2S discussed later. These two sets were fitted into two independent series using Watson's A reduction semi-rigid rotor Hamiltonian. It was an interesting aspect of the spectrum that as we go towards higher J, the tunnelling splitting increases whereas the K_a = 0/1 quartet, K_a = 1/2 quartet and K_a= 2/3 quartet splitting decreases. The $6_{25}\rightarrow7_{34}$, $6_{34}\rightarrow7_{25}$ transitions for $C_6H_5CCH\bullet\bullet\bullet H_2S$ are shown in Figure V.2. List of the transitions and their assignments for the parent isotopologues are shown in Table V.1. It is to be noted that the residues for some of the transitions e.g the $5_{24}\rightarrow6_{15}$ and $5_{14}\rightarrow6_{25}$ transitions in Table V.1 are more than the experimental uncertainties. This is caused due to the overlapping of the transitions. Unlike the case of $C_6H_5CCH\bullet\bullet\bullet H_2O$, the first searched transition was quite far from the prediction. The assigned spectrum had the $4_{04}\rightarrow5_{15}$, $4_{04}\rightarrow5_{05}$, $4_{14}\rightarrow5_{15}$,$4_{14}\rightarrow5_{05}$ quartet ~496 MHz below the predicted line. This difference was used as a guide to predict the spectra of the isotopologues from the *ab initio* predicted geometry. The transitions for the $C_6H_5CCH\bullet\bullet\bullet H_2{}^{34}S$ could be located immediately in this way. However for $C_6H_5CCH\bullet\bullet\bullet HDS$ and $C_6H_5CCH\bullet\bullet\bullet D_2S$ isotopologues, locating the initial transition involved a search of 30-40 MHz. The fitted transitions for all other isotopes along with their residues are listed in Table V.2-Table V.4. The spectrum for the $C_6H_5CCD\bullet\bullet\bullet H_2S$ isotopologue was observed as a doublet whereas the spectra for $C_6H_5CCH\bullet\bullet\bullet HDS$, $C_6H_5CCH\bullet\bullet\bullet D_2S$ didn't show any splitting in the spectra. The weaker series could not be seen for $C_6H_5CCH\bullet\bullet\bullet H_2{}^{34}S$ isotopologues as the intensities of the signals were really low to be seen in natural abundance. No hyperfine transition could be resolved for $C_6H_5CCH\bullet\bullet\bullet HDS$ and $C_6H_5CCH\bullet\bullet\bullet D_2S$. The fitted parameters for all the isotopes are shown in Table V.5.

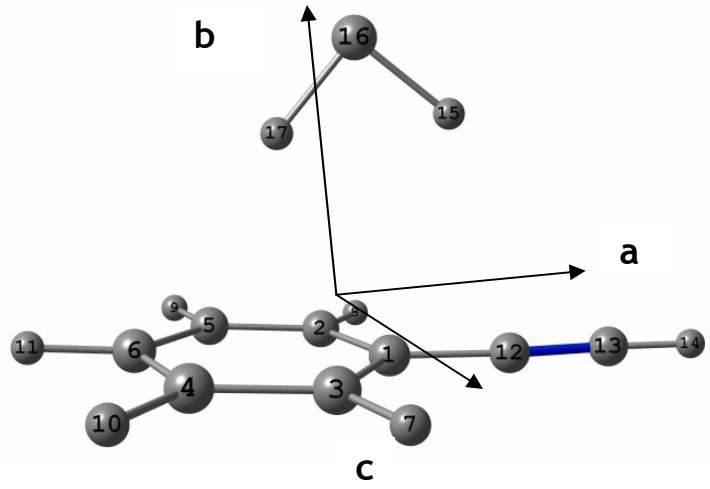

Figure V.1: The principal axes system for the global minimum of $C_6H_5CCH\bullet\bullet\bullet H_2S$ complex at MP2/aug-cc-pVDZ level. The numbering of the atoms is shown in the figure.

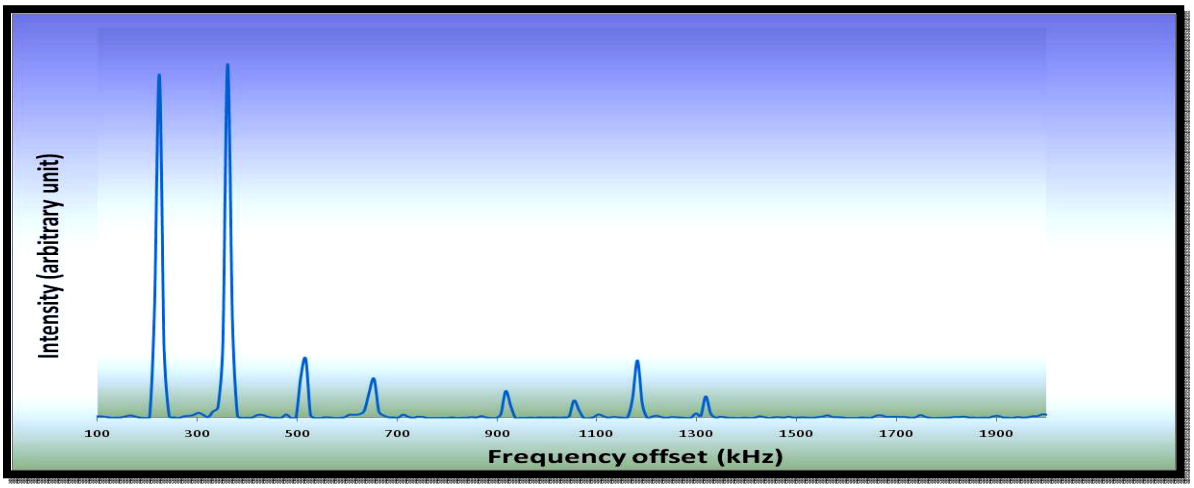

Figure V.2: The $6_{24}\rightarrow 7_{35}$ and $6_{35}\rightarrow 7_{24}$ transitions of $C_6H_5CCH\bullet\bullet\bullet H_2S$ complex. The signal was averaged for 5000 shots. A total of thirteen FIDS were collected for a single gas pulse. For each FID, 512 pints were digitized at a sampling speed of 5 MHz

Table V.1. Assigned transitions and their residues for C_6H_5CCH•••H_2S complex. Wherever the residues are larger than the experimental uncertainties, it has been caused by the overlapping of the transitions.

Transitions[a]	Strong /MHz	Residue(kHz)	Weak/MHz	Residue(kHz)
1_{11}-2_{12}	3330.6570	-2.5	3330.3838	-14.1
1_{01}-2_{02}	3394.2861	-5.7	3394.2861	16.8
1_{01}-2_{12}	3403.0740	5.9	3403.0740	-34.3
1_{10}-2_{11}	4134.4356	3.2	4133.9944	7.1
2_{12}-3_{13}	4826.0996	-3.0	4825.8517	-10.0
2_{02}-3_{03}	4834.2325	0.4	4834.0623	13.3
2_{02}-3_{13}	4834.8812	2.3	4834.7182	17.5
3_{03}-4_{14}	6294.6155	-36.0	6294.3036	-39.4
3_{03}-4_{04}	6294.6155	1.1	6294.3036	-2.1
3_{13}-4_{14}	6294.0008	-3.9	6293.6881	-3.3
3_{13}-4_{04}	6294.0008	33.2	6293.6881	34.0
3_{22}-4_{13}	7146.0437	-0.9	7145.6726	-8.3
3_{22}-4_{23}	7150.5410	-0.1	7150.2385	6.2
3_{12}-4_{13}	7189.1079	-1.3	7189.1419	-0.8
3_{12}-4_{23}	7193.6091	3.4	7193.7070	13.0
4_{14}-5_{05}	7758.5565	2.6	7758.1466	2.0
4_{14}-5_{15}	7758.5565	0.9	7758.1466	0.3
4_{04}-5_{05}	7758.5907	-0.3	7758.1806	-1.1
4_{04}-5_{15}	7758.5907	-2.1	7758.1806	-2.9
4_{23}-5_{14}	8629.9980	-2.9	8629.7196	-8.7
4_{23}-5_{24}	8630.3302	-4.3	8630.0615	-3.9
4_{13}-5_{14}	8634.4986	-0.7	8634.2870	7.3
4_{13}-5_{24}	8634.8289	-2.1	8634.6278	11.0
5_{15}-6_{06}	9222.8401	11.1	9222.3321	2.6
5_{15}-6_{16}	9222.8401	11.8	9222.3321	2.6
5_{05}-6_{06}	9222.8401	2.9	9222.3321	0.9
5_{05}-6_{16}	9222.8401	2.9	9222.3321	0.9
5_{24}-6_{15}	10095.8254	19.4	10095.4734	15.7
5_{24}-6_{25}	10095.8254	0.1	10095.4737	-3.7
5_{14}-6_{15}	10096.1380	-1.5	10095.7960	0.8
5_{14}-6_{25}	10096.1380	-20.8	10095.7960	-18.5
6_{16}-7_{07}	10687.0715	0.2	10686.4657	0.9
6_{16}-7_{17}	10687.0715	0.2	10686.4657	0.9
6_{06}-7_{07}	10687.0715	0.1	10686.4657	1.0
6_{06}-7_{17}	10687.0715	0.1	10686.4657	1.0
5_{23}-6_{24}	-	-	10980.3515	37.8
5_{23}-6_{34}	-	-	10981.9682	-37.3
6_{25}-7_{16}	11559.8396	-0.7	11559.3903	-3.9
6_{25}-7_{26}	11559.8396	-1.6	11559.3903	-4.7

[a] *Transitions are listed as $J''_{Ka''Kc''}$-$J'_{Ka'Kc'}$*

Table V.1. (*continued)*

Transitions	Strong /MHz	Residue(kHz)	Weak/MHz	Residue(kHz)
6_{15}-7_{16}	11559.8593	-0.3	11559.4102	-3.3
6_{15}-7_{26}	11559.8593	-11.8	11559.4102	-4.2
7_{17}-8_{08}	12151.2572	-2.0	12150.5539	0.9
7_{17}-8_{18}	12151.2572	-2.0	12150.5539	0.9
7_{07}-8_{08}	12151.2572	-2.0	12150.5539	0.9
7_{07}-8_{18}	12151.2572	-2.0	12150.5539	0.9
7_{26}-8_{17}	13023.7752	-0.1	13023.2284	-1.0
7_{26}-8_{27}	13023.7752	-0.1	13023.2284	-1.1
7_{16}-8_{27}	13023.7752	-1.0	13023.2284	-1.9
7_{16}-8_{17}	13023.7752	-1.0	13023.2284	-1.9
8_{18}-9_{19}	13615.3910	-1.2	13614.5864	0.9
8_{18}-9_{19}	13615.3910	-1.2	13614.5864	0.9
8_{08}-9_{09}	13615.3910	-1.2	13614.5864	0.9
8_{08}-9_{19}	13615.3910	-1.2	13614.5864	0.9
7_{35}-8_{26}	13896.5838	8.1	13896.3068	-9.9
7_{35}-8_{36}	13896.5838	2.0	13896.3068	-3.8
7_{25}-8_{26}	13896.6909	-0.5	13896.1932	-5.9
7_{25}-8_{36}	13896.6909	-6.6	13896.1932	0.2
8_{27}-9_{18}	14487.6882	3.2	14487.0388	0.1
8_{27}-9_{28}	14487.6882	3.2	14487.0388	0.1
8_{17}-9_{18}	14487.6882	3.1	14487.0388	0.1
8_{17}-9_{28}	14487.6882	3.1	14487.0388	0.1
9_{19}-10_{010}	15079.4650	2.6	15078.5561	1.9
9_{19}-10_{110}	15079.4650	2.6	15078.5561	1.9
9_{09}-10_{010}	15079.4650	2.6	15078.5561	1.9
9_{09}-10_{110}	15079.4650	2.6	15078.5561	1.9
8_{36}-9_{27}	15359.8840	-4.9	15359.4152	12.6
8_{36}-9_{37}	15359.8840	-5.2	15359.4152	12.4
8_{26}-9_{27}	15359.9028	7.7	15359.4152	6.6
8_{26}-9_{37}	15359.9028	7.4	15359.4152	6.3
9_{28}-10_{19}	15951.5486	-4.9	15950.8013	2.4
9_{28}-10_{29}	15951.5486	-5.2	15950.8013	2.4
9_{18}-10_{19}	15951.5486	7.7	15950.8013	2.4
9_{18}-10_{29}	15951.5486	7.5	15950.8013	2.4
10_{110}-11_{011}	16543.4613	-1.1	16542.4487	-2.9
10_{110}-11_{111}	16543.4613	-1.1	16542.4487	-2.9
10_{010}-11_{011}	16543.4613	-1.1	16542.4487	-2.9
10_{010}-11_{111}	16543.4613	-1.1	16542.4487	-2.9
9_{37}-10_{28}	-	-	16822.6772	2.2

Table V.1 (*continued*)

Transitions	Strong /MHz	Residue(kHz)	Weak/MHz	Residue(kHz)
9_{37}-10_{38}			16822.6772	2.2
9_{27}-10_{28}			16822.6772	2.4
9_{27}-10_{38}			16822.6772	2.4
10_{29}-11_{110}	17415.3425	-1.2	17414.4931	0.9
10_{29}-11_{210}	17415.3425	-1.2	17414.4931	0.9
10_{19}-11_{110}	17415.3425	-1.2	17414.4931	0.9
10_{19}-11_{210}	17415.3425	-1.2	17414.4931	0.9
10_{38}-11_{29}	18286.6487	-1.8	18285.9485	-5.6
10_{38}-11_{39}	18286.6487	-1.8	18285.9485	-5.6
10_{28}-11_{29}	18286.6487	-1.8	18285.9485	-5.6
10_{28}-11_{39}	18286.6487	-1.8	18285.9485	-5.6

Table V. 2: Assigned transitions and the residues for C_6H_5CCD•••H_2S complex. Wherever the residues are larger than the experimental uncertainties, it has been caused by the overlapping of the transitions.

Transitions[a]	Strong /MHz	Residue(kHz)	Weak/MHz	Residue(kHz)
3_{13}-4_{04}	6132.9536	0.2	6132.5457	-3.5
3_{13}-4_{14}	6132.9536	-1.5	6132.5457	-5.7
3_{03}-4_{04}	6132.9536	-3.4	6132.6118	-2.2
3_{03}-4_{14}	6132.9536	-5.1	6132.6118	-4.3
3_{12}-4_{13}	7000.2284	-3.2	-	-
3_{12}-4_{23}	7000.6363	0.6	7000.6119	-1.2
4_{14}-5_{05}	7558.1959	2.5	7557.7416	0.2
4_{14}-5_{15}	7558.1959	2.4	7557.7416	0.1
4_{04}-5_{05}	7558.1959	0.8	7557.7416	-2.0
4_{04}-5_{15}	7558.1959	0.7	7557.7416	-2.0
4_{23}-5_{14}	8420.8239	-3.6	8420.5017	-4.5
4_{23}-5_{24}	8420.8480	5.1	8420.5261	1.1
4_{13}-5_{14}	8421.2264	-5.1	8420.9558	5.7
4_{13}-5_{24}	8421.2461	-0.9	8420.9802	11.3
5_{15}-6_{06}	8983.4333	1.6	8982.8768	2.3
5_{15}-6_{16}	8983.4333	1.6	8982.8768	2.3
5_{05}-6_{06}	8983.4333	1.2	8982.8768	2.2
5_{05}-6_{16}	8983.4333	1.2	8982.8768	2.2

[a] *Transitions are listed as $J''_{Ka''Kc''}$-$J'_{Ka'Kc'}$*

Table V.2 (*continued*)

Transitions	Strong /MHz	Residue(kHz)	Weak/MHz	Residue(kHz)
5_{24}-6_{15}	9846.0275	-2.8	9845.6173	-3.6
5_{24}-6_{25}	9846.0275	-3.3	9845.6173	-4.3
5_{14}-6_{15}	9846.0466	0.9	9845.6369	-2.7
5_{14}-6_{25}	9846.0466	0.4	9845.6369	-3.5
6_{16}-7_{07}	10408.6348	4.4	10407.9706	2.8
6_{16}-7_{17}	10408.6348	4.4	10407.9706	2.8
6_{06}-7_{17}	10408.6348	4.4	10407.9706	2.8
6_{06}-7_{07}	10408.6348	4.4	10407.9706	2.8
5_{33}-6_{24}	10708.0656	0.7	10707.7491	0.7
5_{33}-6_{34}	10708.1484	6.7	10707.8421	3.4
5_{23}-6_{24}	10709.6656	-6.6	-	-
5_{33}-6_{24}	10709.7632	14.3	-	-
6_{25}-7_{16}	11271.0518	-1.8	11270.5394	0.6
6_{25}-7_{26}	11271.0518	-1.8	11270.5394	0.6
6_{15}-7_{16}	11271.0518	-2.4	11270.5394	-0.2
6_{15}-7_{26}	11271.0518	-2.1	11270.5394	-0.2
7_{17}-8_{08}	11833.7820	-0.6	11833.0156	1.1
7_{17}-8_{18}	11833.7820	-0.6	11833.0156	1.1
7_{07}-8_{08}	11833.7820	-0.6	11833.0156	1.1
7_{07}-8_{18}	11833.7820	-0.6	11833.0156	1.1
6_{24}-7_{25}	12133.3465	5.3		-
6_{24}-7_{35}	12133.3465	2.1		-
7_{26}-8_{17}	12696.0340	-1.9	12695.4163	2.1
7_{26}-8_{27}	12696.0340	-1.9	12695.4163	2.1
7_{16}-8_{17}	12696.0340	-1.9	12695.4163	2.1
7_{16}-8_{27}	12696.0340	-1.9	12695.4163	2.1
8_{18}-9_{09}	13258.8829	1.3	13258.0098	1.9
8_{18}-9_{19}	13258.8829	1.3	13258.0098	1.9
8_{08}-9_{09}	13258.8829	1.3	13258.0098	1.9
8_{08}-9_{19}	13258.8829	1.3	13258.0098	1.9
7_{35}-8_{26}	13557.8903	-0.9	13557.4193	1.4
7_{35}-8_{36}	13557.8903	-1.0	13557.4193	1.2
7_{25}-8_{26}	13557.8903	-4.0	13557.4193	-2.8
7_{25}-8_{36}	13557.8903	-4.1	13557.4193	-3.0
8_{27}-9_{18}	14120.9665	0.4	14120.2340	-3.2
8_{27}-9_{28}	14120.9665	0.4	14120.2340	-3.2
8_{17}-9_{18}	14120.9665	0.4	14120.2340	-3.2
8_{17}-9_{28}	14120.9665	0.4	14120.2340	-3.2

Table V.2. (*continued*)

Transitions	Strong /MHz	Residue(kHz)	Weak/MHz	Residue(kHz)
9_{19}-10_{010}	14683.9173	-3.6	14682.9381	-3.4
9_{19}-10_{110}	14683.9173	-3.6	14682.9381	-3.4
9_{09}-10_{010}	14683.9173	-3.6	14682.9381	-3.4
9_{09}-10_{110}	14683.9173	-3.6	14682.9381	-3.4
9_{28}-10_{19}	15545.8325	-1.1	15544.9931	-4.1
9_{28}-10_{29}	15545.8325	-1.1	15544.9931	-4.1
9_{18}-10_{19}	15545.8325	-1.1	15544.9931	-4.1
9_{18}-10_{29}	15545.8325	-1.1	15544.9931	-4.1
8_{26}-9_{37}	-	-	14981.9130	0.4
8_{26}-9_{27}	-	-	14981.9130	0.4
8_{36}-9_{27}	-	-	14981.9130	0.6
10_{29}-11_{110}	16970.6336	3.5	16969.6903	4.4
10_{29}-11_{210}	16970.6336	3.5	16969.6903	4.4
10_{19}-11_{110}	16970.6336	3.5	16969.6903	4.4
10_{19}-11_{210}	16970.6336	3.5	16969.6903	4.4

Table V.3. Assigned transitions and their residues for C_8H_6•••HDS and C_8H_6•••D_2S complex. Wherever the residues are larger than the experimental uncertainties, it has been caused by the overlapping of the transitions.

Transitions[a]	C_8H_6-HDS/MHz	Residue(kHz)	C_8H_6-D_2S/MHz	Residue(kHz)
3_{13}-4_{14}	6263.5945	-3.3	6240.6051	1.2
3_{03}-4_{04}	6265.9610	-7.5	6242.8564	-4.1
3_{22}-4_{23}	7096.8414	4.1		
3_{12}-4_{13}	7181.9152			
4_{14}-5_{05}	7721.7415	24.8		
4_{14}-5_{15}	7721.7415	0.2	7693.2040	1.5
4_{04}-5_{05}	7721.9853	11.4	7693.4285	-0.6
4_{04}-5_{15}	7721.9853	-23.5		
4_{23}-5_{24}	8586.7664	-2.9	8556.4779	1.1
4_{13}-5_{14}	8602.4610	-4.3	8571.4366	-2.9
5_{15}-6_{06}	9178.9895	1.1	9144.9460	1.8
5_{15}-6_{16}	9178.9895	-1.0	9144.9460	-0.1
5_{05}-6_{06}	9179.0154	2.4	9144.9710	4.4
5_{05}-6_{16}	9179.0154	0.3	9144.9710	2.5
4_{32}-5_{33}	9363.3094	0.5	9333.5629	0.2

[a] *Transitions are listed as $J''_{Ka''Kc''}$-$J'_{Ka'Kc'}$*

Table V.3 (*continued*)

Transitions[a]	C_8H_6-HDS/MHz	Residue(kHz)	C_8H_6-D_2S/MHz	Residue(kHz)
4_{22}-5_{23}			9542.7290	2.6
5_{24}-6_{25}	10049.1701	-2.7	10013.1371	-2.9
5_{14}-6_{15}	10051.2775	-0.9	10015.1044	-1.5
6_{16}-7_{07}	10636.1307	1.9	10596.5849	0.2
6_{16}-7_{17}	10636.1307	1.7	10596.5849	0.0
6_{06}-7_{07}	10636.1307	-0.3	10596.5849	-1.7
6_{06}-7_{17}	10636.1307	-0.4	10596.5849	-1.8
			10918.7636	-2.1
6_{25}-7_{26}	11506.5363	4.0	11464.9734	3.4
6_{15}-7_{16}			11465.1848	-4.1
5_{32}-6_{33}			11937.6056	-0.3
7_{17}-8_{08}	12093.2228	0.1	12048.1803	0.3
7_{17}-8_{18}	12093.2228	0.1	12048.1803	0.3
7_{07}-8_{08}	12093.2228	-0.1	12048.1803	0.2
7_{07}-8_{18}	12093.2228	-0.1	12048.1803	0.2
6_{34}-7_{35}	12375.8242	-3.6	12332.4554	-0.4
6_{24}-7_{25}	12385.8202	-0.9	12341.8041	3.6
7_{26}-8_{27}			12916.2533	-0.9
7_{16}-8_{17}			12916.2780	1.8
8_{18}-9_{09}	13550.2681	1.2	13499.7265	-0.0
8_{18}-9_{19}	13550.2681	1.2	13499.7265	-0.0
8_{08}-9_{09}	13550.2681	1.2	13499.7265	-0.0
8_{08}-9_{19}	13550.2681	1.2	13499.7265	-0.0
7_{35}-8_{36}	13834.4193	-0.4	13785.3921	-7.7
7_{25}-8_{26}	13835.8118	4.5	13786.6718	5.4
8_{27}-9_{28}	14420.0432	0.6		
8_{17}-9_{18}	14420.0432	-1.8	14367.5100	1.0
9_{19}-10_{010}	15007.2519	-1.1	14951.2144	-1.5
9_{19}-10_{110}	15007.2519	-1.1	14951.2144	-1.5
9_{09}-10_{010}	15007.2519	-1.1	14951.2144	-1.5
9_{09}-10_{110}	15007.2519	-1.1	14951.2144	-1.5
10_{110}-11_{011}			16402.6414	0.9
10_{110}-11_{111}			16402.6414	0.9
10_{010}-11_{011}			16402.6414	0.9
10_{010}-11_{111}			16402.6414	0.9

Table V. 4. Assigned transitions and their assignments for $C_6H_5CCH\bullet\bullet\bullet H_2{}^{34}S$ complex. Wherever the residues are larger than the experimental uncertainties, it has been caused by the overlapping of the transitions.

Transitions[a]	Frequencies (MHz)	Residue(kHz)
3_{03}-4_{14}	6158.2051	-5.6
4_{14}-5_{05}	7588.0484	-3.5
4_{14}-5_{15}	7588.0484	-18.7
5_{15}-6_{06}	9019.2999	0.5
5_{15}-6_{16}	9019.2999	-0.5
5_{05}-6_{06}	9019.3195	5.0
6_{05}-6_{16}	9019.3195	3.9
6_{16}-7_{07}	10450.4388	-3.0
6_{16}-7_{17}	10450.4388	-3.0
6_{06}-7_{07}	10450.4388	-4.0
6_{06}-7_{17}	10450.4388	-4.1
7_{17}-8_{08}	11881.5351	-2.6
7_{17}-8_{18}	11881.5351	-2.6
7_{07}-8_{08}	11881.5351	-2.7
7_{07}-8_{18}	11881.5351	-2.7
8_{18}-9_{09}	13312.5842	2.9
8_{18}-9_{19}	13312.5842	2.9
8_{08}-9_{09}	13312.5842	2.9
8_{08}-9_{19}	13312.5842	2.9

[a] *Transitions are listed as $J''_{Ka''Kc''}$-$J'_{Ka'Kc'}$*

TableV.5: Fitted parameters for $C_6H_5CCH\bullet\bullet\bullet H_2S$ complex and their isotopologues.

	C_8H_6-H_2S		C_8H_6-D_2S	C_8H_6-HDS	C_6H_5D-H_2S		C_8H_6-$H_2{}^{34}S$
	Strong	Weak			Strong	Weak	
A (MHz)	1206.551(7)	1206.732(7)	1219.193(4)	1224..093(7)	1159.94(2)	1160.18(2)	1203.4(1)
B (MHz)	1134.152(6)	1134.056(6)	1108.204(4)	1111.107(7)	1129.11(1)	1128.93(2)	1097.6(1)
C(MHz)	732.192(6)	732.141(8)	725.914(3)	728.6674(5)	716.020(8)	712.6391(7)	715.6518(7)
Δ_J (kHz)	1.6(5)	4.2(4)	3.1(1)	3.7(2)	3(1)	-2(1)	1.6[c]
Δ_{Jk} (kHz)	23(1)	17(1)	1.9(2)	5.4(6)	-4(3)	0.6(4)	23[c]
Δ_k (kHz)	-27.0(3)	-32(1)	7.6(4)	12.3(7)	11(1)	20(1)	-27.0[c]
δ_J (kHz)	0.7(2)	2.0(2)	1.41(5)	1.72(9)	1.6(6)	-0.9(7)	0.7[c]
δ_K (kHz)	13.1(2)	14.4(3)	3.41(9)	2.8(2)	2.1(4)	-0.6(4)	13.1[c]
$P_{cc}{}^a$	87.12	87.08	87.18	87.07	87.08	87.05	87.11
SD(kHz)	6.8	10.6	2.3	5.9	3.2	3.2	7.5
#[b]	83	91	46	41	71	66	21

a. The planar moment of inertia defined as $P_{cc} = \frac{1}{2}(-I_c + I_a + I_b)$ *b. The number of fitted transitions c. These parameters were fixed at a value obtained from the fitting of the stronger series of the parent complex.*

V.D. Structure from the rotational spectra

The fitted rotational constants are consistent with a structure where the H_2S subunit is located over the phenylacetylene plane. A direct comparison of the experimentally derived structure with all the *ab initio* optimized geometries clearly discards all other geometries which is shown later. Let us now turn towards the experimental results. The '*A*' rotational constant of the parent isotopologues is affected the least on substitution of ^{32}S by ^{34}S. From Table V.5, The change in the *A* rotational constant is only 3 MHz, whereas the changes in *B* and *C* rotational constants are 37 MHz and 17 MHz respectively. Thus, the S atom is close to the *a* principal axis of the complex. A comparison of the rotational constants of the complex with the monomer rotational constants can provide important information about the orientation of the two monomers with respect to each other. Dreizler and co-workers[21] have determined very accurate values for the rotational constants of phenylacetylene monomer from a large set of isotopic data. The rotational constants of the phenylacetylene monomer are *A* = 5680.32 (0.06) MHz, *B* = 1529.7409 (2) MHz and *C* = 1204.9562 (2) MHz whereas the constants for C_6H_5CCD monomer are *A* = 5680.51 (6) MHz, *B* = 1450.2356 (3) MHz and *C* = 1155.0722 (2) MHz. A comparison of the rotational constants of $C_6H_5CCH{\bullet\bullet\bullet}H_2S$ and $C_6H_5CCD{\bullet\bullet\bullet}H_2S$ complexes with the monomer rotational constants reveal that the *A* rotational constant of these complexes are very close the *C* rotational constant of C_6H_5CCH and C_6H_5CCD respectively. Hence, H_2S is located very close to the *c* principal axis of the phenylacetylene monomer which is perpendicular to the phenylacetylene plane. Further, the planar moment of inertia P_{bb} for the phanylacetylene momomer is 88.9 amuÅ^2. This value is very close to the P_{cc} values for the parent complex and the isotopologues as reported in Table V.5. This indicates that H_2S is lying in the *ac* inertial plane (symmetry plane) of the monomer, which is the *ab* inertial plane for the complex. Thus, the complex has effective C_s symmetry in the ground vibrational state.

From Figure V.1, it can be realised that the predicted geometry from the calculation has the S atom closer to the *b* principal axis of the complex. However the discussion on the previous paragraph clearly indicates that S atom is located closer to the *a* principal axis of the complex. The predicted values of the rotational constants for the

$H_2{}^{32}S$ and $H_2{}^{34}S$ isotopologues from the ab initio geometry are A = 1279 MHz, B = 1176 MHz, C = 782 MHz and A = 1228 MHz, B = 1175 MHz *and* C = 765 MHz respectively. These values clearly show that S atom is closer to the *b* principal axis of the *ab initio* geometry. Thus, there is a switching of the *a* and *b* principal axes between the *ab initio* structure and the experimentally observed structure which is explained later in this chapter.

The distance of the substituted atom from the center of mass of the complex can be found from the following Kraitchman relations:

$$|a| = \sqrt{\left[\frac{\Delta P_a}{\mu}\left(1+\frac{\Delta P_b}{(I_a - I_b)}\right)\left(1+\frac{\Delta P_c}{(I_a - I_c)}\right)\right]} \qquad (1)$$

$$|c| = \sqrt{\left[\frac{\Delta P_c}{\mu}\left(1+\frac{\Delta P_a}{(I_c - I_a)}\right)\left(1+\frac{\Delta P_b}{(I_c - I_b)}\right)\right]} \qquad (2)$$

$$|b| = \sqrt{\left[\frac{\Delta P_b}{\mu}\left(1+\frac{\Delta P_c}{(I_b - I_c)}\right)\left(1+\frac{\Delta P_a}{(I_b - I_a)}\right)\right]} \qquad (3)$$

The substitution co-ordinates for the S atom and the terminal H atom of the acetylenic group of the phenylacetylene monomer are shown in Table V.6. The *ab initio* values for these co-ordinates are also shown in Table V.6 for comparison. The co-ordinates of the sulphur atom were derived from the rotational constants of $C_6H_5CCH{\bullet\bullet\bullet}H_2S$ and $C_6H_5CCH{\bullet\bullet\bullet}H_2{}^{34}S$ complexes whereas the co-ordinates for the terminal hydrogen atom of the acetylenic group of phenylacetylene were derived from the rotational constants of $C_6H_5CCH{\bullet\bullet\bullet}H_2S/C_6H_5CCD{\bullet\bullet\bullet}H_2S$ complexes. From the comparison of the substitution co-ordinates and the *ab initio* co-ordinates of the S atom and the H14 atom, it is clear that the *a* and *b* axes system have interchanged. The substitution co-ordinates for the two hydrogen atoms of H_2S can also be derived from the rotational constants of $C_6H_5CCH{\bullet\bullet\bullet}H_2S/C_6H_5CCH{\bullet\bullet\bullet}HDS/C_6H_5CCH{\bullet\bullet\bullet}D_2S$ isotopologues. However, the positions of these hydrogen atoms are far from being unambiguous. The substitution analysis based on the rotational constants of $C_6H_5CCH{\bullet\bullet\bullet}H_2S$/ $C_6H_5CCH{\bullet\bullet\bullet}HDS$ complexes produce unreasonable values for the position of the hydrogen atoms. The

substitution co-ordinates give |*a*| to be 3.39 Å whereas the |*b*| and the |*c*| co-ordinates of this hydrogen turn out to be imaginary. The substitution analysis based on the rotational constants of $C_6H_5CCH•••HDS/C_6H_5CCH•••D_2S$ complexes produced the |*a*|, |*b*| and |*c*| co-ordinates of the other hydrogen to be 1.02 Å, 1.26 Å and 0.34 Å respectively. Though, we know only the absolute numbers from this analysis, any combinations of signs of these co-ordinates would not produce a reasonable S-H bond length as we expect for H_2S.

Table V.6: The experimentally derived Kraitchman substitution co-ordinates for the sulphur atom and the terminal hydrogen atom of the phenylacetylene monomer are reported along with the ab initio (MP2/aug-cc-pVDZ) derived cartesian co-ordinates for these atoms in the parentheses.

Atoms	|*a*| (Å)	|*b*| (Å)	|*c*| (Å)
S	2.69 (0.413)	0.93 (2.624)	0.21 (-0.004)
H14	0.87 (4.146)	4.11 (-1.402)	i (0.0)

Also, the substitution co-ordinates for the H_2S hydrogens values are very far from the *ab initio* derived co-ordinates for these atoms. The *ab initio* (geometry optimized at MP2/aug-cc-pVDZ level) derived *a*, *b* and *c* co-ordinate for H15 and H17 are 1.391 Å, 1.691 Å, 0.000 Å and -0.550 Å, 1.674 Å , 0.001 Å respectively. This discrepancy in the position of the two hydrogens of H_2S may be caused by the large amplitude motions which hinder the determination of the vibrationally averaged positions of these two hydrogens. The only conclusion we can draw is that the H_2S hydrogens are lying more or less in the *ab* inertial plane (symmetry plane) of the complex. The c.m.-c.m. (distance between the center of mass of both the monomers in the complex) separation can be calculated following the assumption that both the hydrogens of H_2S are symmetrically bound to the phenylacetylene monomer. Further, we assume that the whole H_2S sub-unit is lying in the *ab* inertial plane of phenylacetylene. This lets us use the parallel axis theorem which gives the following sets of equations:

$$I_b(complex) = I_a(phac) + I_a(H_2S) + \mu R^2 \qquad (4)$$

$$I_c(complex) = I_b(phac) + I_c(H_2S) + \mu R^2 \qquad (5)$$

Here, μ is the reduced mass of the complex and R is the c.m.-c.m. separation. R has been calculated to be 3.73 Å and 3.75 Å from equations 4 and 5. In the *ab initio* optimized geometry, the distance of the S atom from the center of mass of the phenylacetylene monomer is 3.57 Å. As mentioned previously, the S approaches the ring along a direction which is very close to the *c* principal axis of the phenylacetylene monomer. This certainly indicates that S is away from the phenylacetylene ring center and is shifted towards the acetylenic group. This is analogous to the structure of C_6H_5CCH•••Ar[22,23] and benzonitrile•••Ar[24] where the noble gas atom is away from the center of the π cloud towards the substituent. In case of C_6H_5CCH•••Ar complex, the argom atom is shifted by 0.280 Å from the center of the phenyl ring whereas in case of benzonitrile•••Ar, the shift is 0.247 Å. These results can provide important clues about the nature of interaction. e.g. for the complex fluorobenzene•••Ar, Ar atom is shifted towards the F atom by 0.297 Å from the ring center whereas the experimental shift of the Cl atom in flourobenzene•••HCl is 0.162 Å towards the para C atom of the ring. The reason was attributed to the fact that in case of fluorobenzene•••Ar, the dispersion interactions dominate whereas in case of flurobenzene•••HCl, the interaction is mainly electrostatic in nature.[10] However, the exact location of the sulphur atom along the '*b*' co-ordinate could not be determined in case of C_6H_5CCH•••H_2S. The distance between the S atom and H14 can be found out from the determined substitution co-ordinates if we know the sign of the numbers. The *ab initio* optimized geometry was used as a guidance to know the signs keeping the switching of the *a* and *b* principal axis in mind. From the substitution co-ordinates, the distance of the S atom from H14 comes to be 4.79 Å. This distance is much smaller than the *ab initio* optimized distance of 5.490 Å. This may be an indication that the experimentally observed geometry of the complex has the S atom shifted from the phenylacetylene center of mass towards the acetylene group. The present sets of experimental data do not allow locating the S atom above the ring with more precision.

The rotational constants for C_6H_5CCH•••H_2S, C_6H_5CCH•••HDS and C_6H_5CCH•••D_2S complexes, reported in Table V.5, show an interesting trend. The *A* rotational constants of C_6H_5CCH•••HDS and C_6H_5CCH•••D_2S complexes are higher

than that of the $C_6H_5CCH•••H_2S$ complex. A rigid geometry predicts a decrease of 9 MHz and 18 MHz in the *A* rotational constant for the HDS and D_2S isotopologues compared to the parent isotopologues respectively. Experimentally, the *B* and *C* rotational constants show the usual trend of decrease as we go from H_2S to HDS to D_2S isotopologue. Moreover, if we compare the HDS and D_2S isotopologues in Table V.5, all the rotational constants show a decrease, though only by 5 MHz in *A* and 3 MHz for both *B* and *C*. The decrease in the *B* and *C* rotational constants is 23 MHz and 3 MHz while going from H_2S to HDS isotopologues. The increase in the *A* rotational constant of the deuterated isotopologue compared to the parent ones could be the result of different dynamically averaged structure for the HDS and D_2S isotopmers compared to the H_2S isotopologue. A similar kind of increase in the rotational constants have been observed for anisole•••H_2O [25]complex. It was attributed to the different conformational preference for the anisole•••H_2O and anisole•••D_2O. For $C_6H_5CCH•••H_2S$, this increase in the A rotational constant may result from a sliding motion of H_2S over the π cloud of the ring. The deuteration will increase the total mass and hence would sample small range of distances. This kind of sliding motion is present in Ar•••C_6H_5CCH complex which hindered the determination of the accurate location of argon over the ring. However, if the translation of H_2S is the candidate, we should have observed a similar effect for $C_6H_5CCH•••H_2{}^{34}S$ as well. But that is not the case here as is evident from the rotational constants of $C_6H_5CCH•••H_2{}^{34}S$. The *A* rotational constant for $C_6H_5CCH•••H_2{}^{34}S$ shows a decrease of 3 MHz compared to the parent isotopologues which is further an indication that this change in *b* co-ordinate is not the result of the translation of H_2S over the phenylacetylene π cloud. The likely motion is the rotation of H_2S about its own *c* principal axis. The averaged *b* co-ordinate (in the principal axes system of the complex) of the two hydrogens can shrink on deuteration which may produce this increase in the *A* rotational constant. This is further possible that the hydrogen atoms of H_2S are closer to *a* axis than any other axis (as the S atom is closer to the *a* principal axis of the complex which is experimentally verified). Thus the increase in mass is overweighed by the decrease in the effective distance as the atoms are closer to the axis. If it is a translation of the H_2S over the π cloud, the change in the rotational

constant would show a similar trend while going from the $H_2{}^{32}S$ to the $H_2{}^{34}S$ isotopologue.

V.E. Splitting in the spectra

As was mentioned, the parent isotopologue and $C_6H_5CCD\bullet\bullet\bullet H_2S$ complex show the doubling of the lines in the spectra. However, the D_2S and HDS complexes do not show any splitting in the spectra. The absence of the splitting in case of $C_6H_5CCH\bullet\bullet\bullet HDS$ isotopologue indicates that the doubling is caused by the interchange of equivalent hydrogens of H_2S. Further, the quenching of the motion in case of $C_6H_5CCH\bullet\bullet\bullet D_2S$ isotopologue indicates that the motion is a hindered one. Interchange of the equivalent hydrogens of H_2S would happen if the H_2S moiety rotates about its C_2 symmetric axis. No other motion i.e. the rotation of H_2S about its own *a* or *c* principal axis will lead to the interchange of the equivalent hydrogens of H_2S. The barrier for the rotation of H_2S about its C_2 symmetry axis has been calculated and is reported in the next section.

V.F. *Ab initio* calculations

Three different geometries of $C_6H_5CCH\bullet\bullet\bullet H_2S$ complex were optimized at MP2/aug-cc-pVDZ level using the Gaussian 03 suite of programme.[26] The monomer geometries were optimized at the same level of theory and the structural parameters from these calculations are supplied as the input during the geometry optimization of the complex. The frequencies were calculated to ensure that the optimized geometries were true minima. The vibrational frequencies of the complex are listed in the appendix at the end of this chapter. All these structures turned out to be true minima. The binding energies were calculated using supermolecular approach[27] and they were corrected for the BSSE using counterpoise method.[28] Zero point energy corrections on the binding energies were done for all these complexes. The optimized geometries of $C_6H_5CCH\bullet\bullet\bullet H_2S$ are shown in Figure V.3. Optimization was performed by starting from an initial geometry by placing H_2S on the top of the acetylenic π cloud. However the optimization led to the Structure B. The binding energies are reported in Table V.7. *Ab initio* calculations show the Structure B (H_2S is on the top of the phenyl ring) to be the global minimum as can be

seen from Table V.7. The energy differences with other geometries are significantly high. The geometry where the acetylenic C-H group is donating its hydrogen to the S atom is lying 600 cm^{-1} (~1.7 kcal/mol) above the experimentally observed geometry whereas the cyclic structure as was observed in $C_6H_5CCH•••H_2O$ complex is lying 311 cm^{-1} (0.9 kcal/mol) above this. The rotational constants for all the geometries are listed in Table V.8 and are compared with the experimentally derived ones (for the stronger series). From the Table V.8, it is clear that Structure B is the experimentally observed structure. However, the experimentally derived constants are smaller than the *ab initio* derived values. The difference is 40-50 MHz which means that the vibrationally averaged geometry is different from the one obtained by *ab initio* methods but of course the determined constants indicate the Structure B with no ambiguity. The optimized structural parameters obtained for all the geometries at MP2/aug-cc-pVDZ level of theory are listed in the appendix at the end of this chapter.

Figure V.3. The optimized geometries of $C_6H_5CCH•••H_2S$ at MP2/aug-cc-pVDZ level

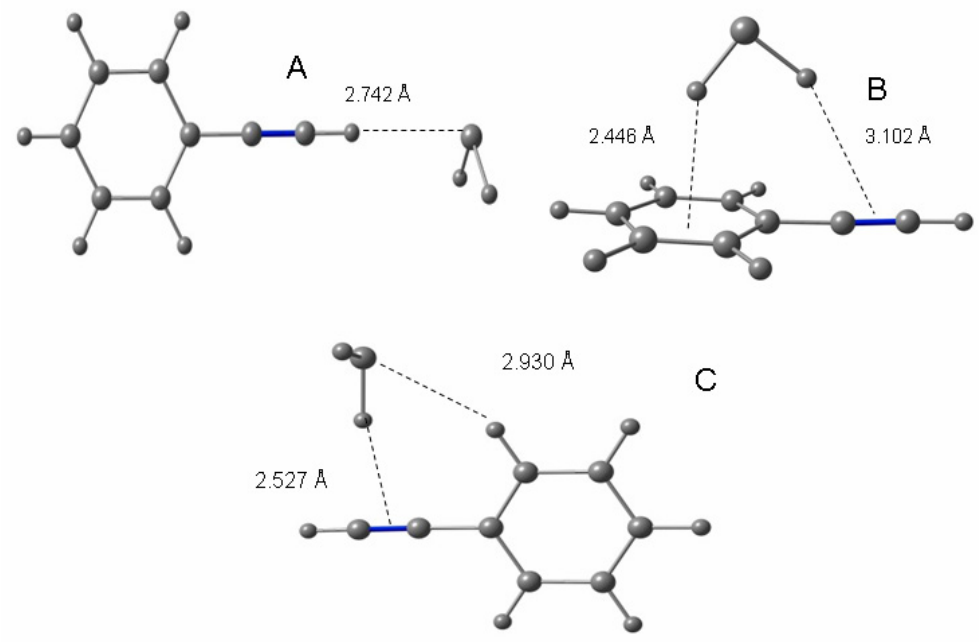

Table V.7. Binding energies (in cm^{-1}) of different geometries of $C_6H_5CCH•••H_2S$ complex calculated at MP2/aug-cc-pVDZ level of theory. The binding energies have been corrected for BSSE and ZPE.

	Binding energy (cm^{-1})
Structure A	-157
Structure B	-857
Structure C	-546

Table V.8: Rotational constants of different geometries of $C_6H_5CCH•••H_2S$ complex calculated at MP2/aug-cc-pVDZ level of theory.

Rotational constants	Structure A	Structure B	Structure C	Experiment[a]
A (MHz)	5374	1279	2209	1206.551(7)
B (MHz)	313	1176	652	1134.152(6)
C (MHz)	296	782	506	732.192(6)

[a]*Rotational constants for the stronger series is listed.*

It has been mentioned previously that experimentally, S atom is closer to the '*a*' principal axis of the complex whereas in the *ab initio* global minimum 'B', the S atom is closer to the *b* principal axis. To understand this, some tests were done by varying the location of one monomer with respect to the other. It is shown that a variation of the perpendicular distance of the H_2S unit from the phenylacetylene center of mass by 0.1 Å can produce this switching of the '*a*' and '*b*' principal axis system. Both phenylacetylene and H_2S were fixed at their optimized geometry at the same level of theory. The H_2S hydrogens were placed symmetrically (both the hydrogens facing the phenylacetylene) on

top of the phenylacetylene ring and the distance of H_2S from the center of mass of phenylacetylene were varied in steps of 0.2 Å. The minimum of the interaction energy was found in a configuration where S is located at 3.7 Å from the center of mass of the phenylacetylene monomer. The principal axes system for this geometry is shown in the structure labelled as II in Figure V.4. The distance between the center of mass of phenylacetylene to the S is 3.6 Å for I in Figure V.4, whereas it is 3.8 Å for III in Figure V.4. It is very clear from Figure that the '*a*' and '*b*' principal axis shows a switching when the distance of the S from the center of mass of phenylacetylene is increased. Thus, S is located close to the '*b*' principal axis in I whereas it is located very close to the '*a*' principal axis in II.

Figure V.4. Switching of the 'a' and 'b' principal axes of C_6H_5CCH•••H_2S complex caused by the increase of the distance of H_2S from the phenylacetylene center of mass is shown in the figure. Here X, Y and Z are equivalent to the 'a', 'b' and 'c' principal axes system.

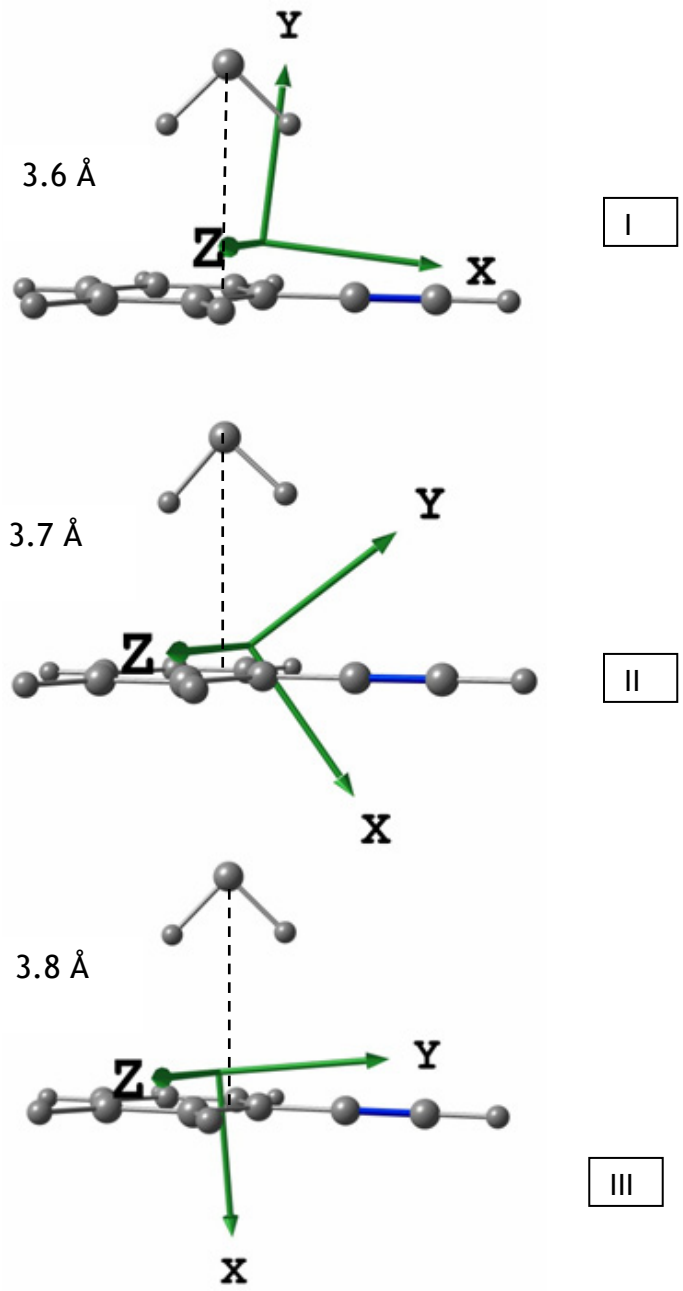

The potential energy scans at MP2/aug-cc-pVDZ level were done for the sliding motion of H_2S over the phenylacetylene ring to find out the flatness of the potential energy curve along this co-ordinate. Keeping this perpendicular distance fixed, H_2S was moved over the ring. The co-ordinate is defined as $\Delta R_{\parallel}$, the parallel displacement of the S atom from the center of mass of the phenylacetylene monomer. $\Delta R_{\parallel} = 0$ when the S atom is right on top of the phenylacetylene center of mass. A '+' ve value of $\Delta R_{\parallel}$ indicates the displacement of the H_2S from the center of mass of the phenylacetylene towards the acetylene group whereas a '-'ve value for $\Delta R_{\parallel}$ indicates that the S atom is shifted from the phenylacetylene center of mass towards the phenyl ring center. The generated potential energy curve is shown in Figure V.5. The minimum of the energy is located at a position where the S is shifted by 0.4 Å from the center of mass of the phenylacetylene monomer towards the acetylene group. From the frequency calculation at MP2/aug-cc-pVDZ level, the zero point energy corresponding to this vibration is 15 cm^{-1}. This magnitude of zero point energy would mean that H_2S would slide a distance of ~+0.8 Å over the phenylacetylene ring. Thus, H_2S is likely to be shifted from the phenylacetylene center of mass towards the acetylene group which may be the reason that the distance of the S from H14 is less as was deduced by the experiment.

The barrier for the rotation of H_2S about its C_2 symmetry axis was calculated staring from the optimized geometry of the $C_6H_5CCH\bullet\bullet\bullet H_2S$ complex. The generated potential energy curve is shown in Figure V.6. The calculated barrier for this motion is 403 cm^{-1}. The normal mode frequency which corresponds to this mode has been identified from the *ab initio* calculations at MP2/aug-cc-pVDZ level. The zero point energy along this mode is 63 cm^{-1} which is almost seven times less than the barrier height for this rotation. This indicates that the motion is a hindered one and supports the quenching of the splitting in case of $C_6H_5CCH\bullet\bullet\bullet D_2S$ complex. The barrier for the rotation of H_2S about its C_2 symmetry axis is much higher than what has been observed for $C_6H_6\bullet\bullet\bullet H_2S$ complex. For $C_6H_6\bullet\bullet\bullet H_2S$, the barrier for this rotation is ~ 3.5 cm^{-1}. This is because in $C_6H_5CCH\bullet\bullet\bullet H_2S$, the H_2S hydrogens are closer to C1 and the rotation of the H_2S hydrogens take the hydrogens away from the π electron backbone which is not the case with $C_6H_6\bullet\bullet\bullet H_2S$ complex.

Does this displacement of the H_2S towards the acetylenic group indicate an interaction of the H_2S hydrogen with the acetylenic π cloud? An optimization of the π bonded geometry of HCCH•••H_2S at the same level of theory shows that the distance of the bonded hydrogen from the acetylene π bond is 2.574 Å which is much smaller than the distance of H_2S hydrogen from the acetylenic π cloud in the optimized geometry of C_6H_5CCH•••H_2S complex. The distance of the hydrogen closer to the acetylenic π cloud is 3.102 Å from the center of the triple bond. However, a bending of the acetylene group towards the H_2S has been observed in the *ab initio* optimized geometry. Thus, in the complex, the dihedral angles $D(C_1C_2C_5C_6)$ = -0.2° (0° in the monomer), $D(C_{12}C_1C_2C_5)$ = -177.2° (180° in the monomer) and the angle $A(C_{12}C_1C_6)$ = 177.7° (180° in the monomer). A similar kind of bending from the planarity was observed in case of the *ab initio* calculations of C_6H_5CCH•••Ar[23] complex as well. However, the accuracy of the experiments does not allow this observation to be verified. Thus, the assumption that the monomer geometries are unchanged due to the complexation is valid within the accuracy limit of the experiment.

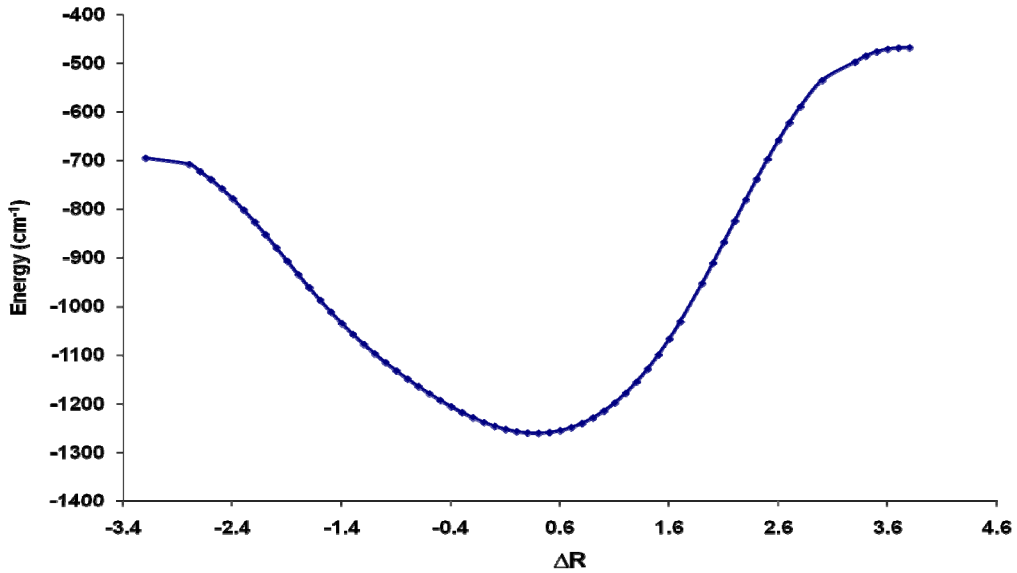

Figure V.5: The potential energy curve for the sliding motion of H_2S over the phenylacetylene plane.

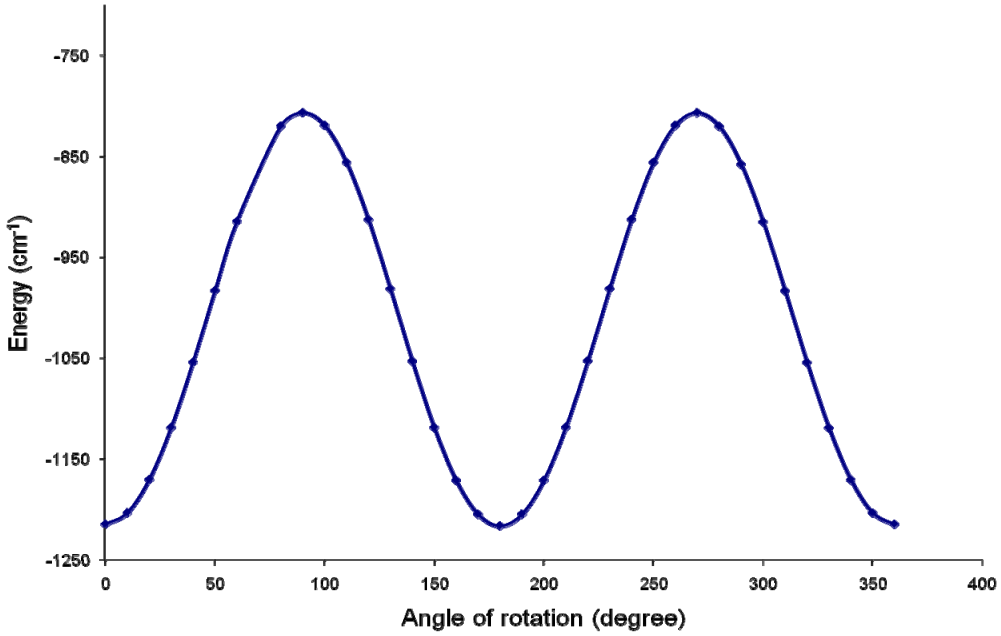

Figure V.6: The potential energy curve for the rotation of H_2S about its C_2 symmetric axis in $C_6H_5CCH•••H_2S$ complex

The H_2S monomer frequencies are compared to the frequencies of intramolecular H_2S modes in the complex calculated at MP2/aug-cc-pVDZ theory and are shown in Table V.9.

Table V.9. Frequencies of the symmetric and asymmetric stretches of H_2S monomer in different optimized geometries of $C_6H_5CCH•••H_2S$ complex. The frequencies of H_2S monomer are also listed in the table.

Modes	H_2S	Structure A	Structure B	Structure C
Symmetric stretch	2764 cm^{-1}	2749 cm^{-1}	2733 cm^{-1}	2724 cm^{-1}
Asymmetric stretch	2790 cm^{-1}	2774 cm^{-1}	2755 cm^{-1}	2767 cm^{-1}

From Table V.9, all the optimized geometries show red shifts of the S-H stretch frequencies. The structure A also shows red shift even if H_2S acts as a 'hydrogen-bond' acceptor in the complex. In Structure A, the shift is ~-15 cm^{-1} for the symmetric stretch and ~-16 cm^{-1} for the asymmetric stretch, considerably smaller than the other hydrogen-

bonded geometries. The π-bonded (phenyl π cloud, Structure B) geometry shows a shift of ~-33 cm^{-1} and ~ -35 cm^{-1} for the symmetric and asymmetric stretch respectively. The cyclic structure shows a red shift of ~40 cm^{-1} and ~23 cm^{-1} respectively for the symmetric and symmetric stretches. Thus, the theoretical calculations indicate a considerable red shift of the S-H stretches (harmonic frequencies) for the π-hydrogen bonded complex of $C_6H_5CCH•••H_2S$. For a comparison, the frequency shift for the $C_2H_4•••H_2S$ complex calculated at MP2(full)/aug-cc-pVDZ level is -29 cm^{-1} and -11 cm^{-1} for the symmetric and asymmetric stretches respectively (though the experimentally observed shift is much smaller as was described in chapter III), whereas the frequency shift for $HCCH•••H_2S$ (π bonded complex) calculated at the same level of theory i.e. MP2/aug-cc-pVDZ level of theory is -24 cm^{-1} and -19 cm^{-1} for the symmetric and the asymmetric stretch respectively.

V.G. *AIM* calculations

Atoms in molecules[29] theoretical calculations have been done for all the optimized geometries of $C_6H_5CCH•••H_2S$. All the wave functions have been calculated at MP2/aug-cc-pVDZ level of theory. The calculated critical points for these geometries are shown in Figure V.7. In case of Structure A, a bond critical point along the bond path connecting the S atom to the acetylenic C-H group has been located and it corresponds to the C-H•••S interaction. For Structure B, a bond critical point has been located along the bond path which connects the H atom of H_2S to the phenyl ring carbon bearing the substituent. The calculations do not show any other bond critical point connecting this hydrogen to any other carbon of the phenyl ring. However, one more ring critical point apart from the one corresponding to the phenyl ring (Structure B in Figure V.7) has been located. This indicates that this H atom interacts with at least one of the other carbon atoms of the phenyl ring so that a ring structure is formed, which gives rise to the ring critical point. Surprisingly, no bond critical point connecting the other hydrogen (closer to the acetylenic π bond in Structure B) to any atom of phenylacetylene monomer could be located for this geometry at this level of calculation. Thus, the AIM calculations do not indicate any interaction of the H atom and the acetylene π cloud of the

phenylacetylene monomer in Structure B. The Structure C is characterised by the presence of the S-H•••π and C-H•••S interaction. The electron density (ρ) at the bond critical points and the Laplacians of the electron density at the critical point are listed in Table V.10. In general, the stronger the 'hydrogen bond', more is the electron density at the critical point corresponding to that hydrogen bond. A look at the Table V.10 makes one realise that there is not much difference in terms of the electron densities at HBCP (hydrogen bond critical point) for these three optimized geometries. The electron densities (ρ) and the Laplacian of the electron densities (ρ) are well within the range for hydrogen bonds as suggested by Popelier for all the complexes.[30]. Based on the analysis of C-H•••O interaction, Koch and Popelier suggested that the ρ value at BCP should lie within the range [0.002, 0.035] au and the Laplacian of the electron density at BCP should lie within the range [0.024, 0.139] au for 'hydrogen bonds'.

Figure V.7. The bond critical points, ring critical points, cage critical points and the bond paths located for the three optimized geometries of C_6H_5CCH•••H_2S at MP2/aug-cc-pVDZ level of theory.

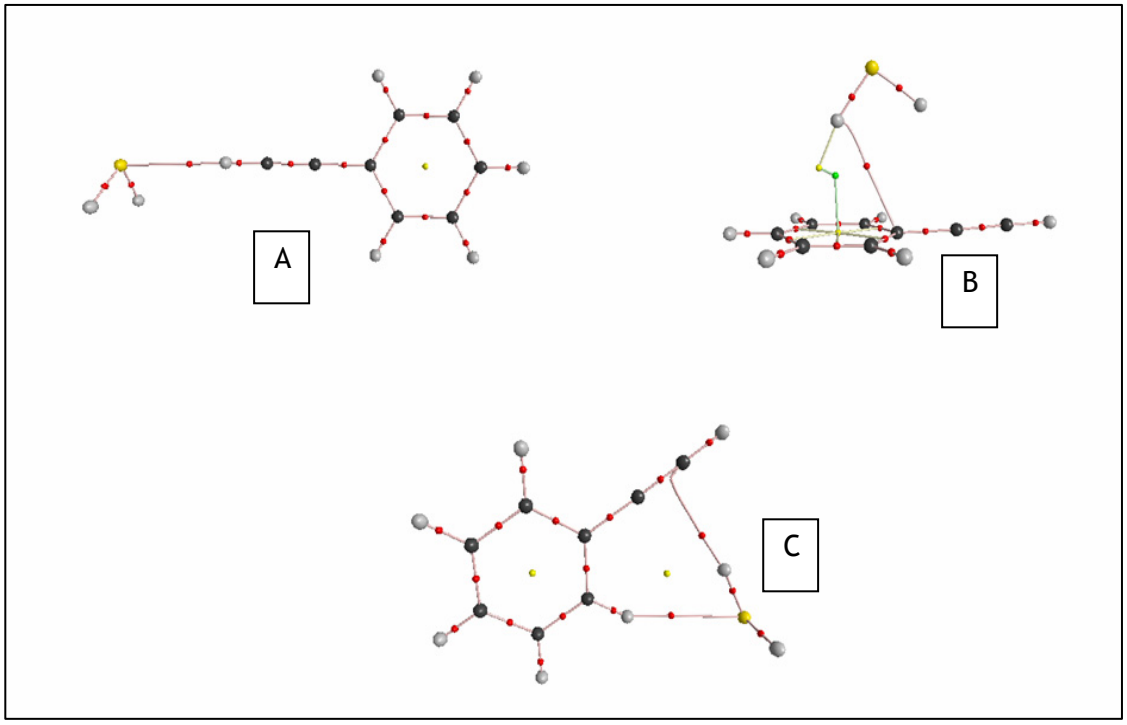

Table V.10. The electron density (ρ) and the Laplacian of the electron density ($\nabla^2(\rho)$) of Structure A, Structure B and Structure C calculated by AIM theoretical calculations.

	ρ (a.u)	∇^2 (ρ)
Structure A (C-H···S)	0.010	0.025
Structure B (S-H···C)	0.008	0.025
Structure C, S-H···π	0.012	0.027
Structure C, C-H···S	0.008	0.020

V.H. Discussion

From the above studies, it is clear that $C_6H_5CCH•••H_2S$ possesses a geometry where H_2S is located over the π cloud of phenylacetylene. This geometry is similar to what was observed for fluorobenzene•••HCl, though here H_2S is shifted towards the acetylenic group. On the contrary, the complex $C_6H_5CCH•••H_2O$ has a cyclic structure where H_2O donates its hydrogen to the acetylenic π cloud forming a O-H•••π bond and the ortho C-H group of phenyl ring forms a C-H•••O bond with H_2O. The geometry for $C_6H_5CCH•••H_2O$ is similar to what was observed for fluorobenzene•••H_2O. The structure of $C_6H_5CCH•••H_2S$ complex can be compared to those of $C_6H_5CCH•••CH_3OH$ and $C_6H_5CCH•••CH_3NH_2$ complexes.[20] $C_6H_5CCH•••CH_3OH$ forms a π bonded structure where CH_3OH donates the O-H hydrogen to the phenyl π cloud. In case of $C_6H_5CCH•••CH_3NH_2$, the N-H group donates its hydrogen to the π cloud of phenyl ring whereas in $C_6H_5CCH•••NH_3$, the terminal C-H bond of the acetylene group donates its hydrogen to NH_3 forming a C-H•••N hydrogen bond. In reference no. 20, the authors have called it as 'methyl group -induced hydrogen bond switching'. The SAPT-DFT interaction energy decomposition analysis done by these authors show that the electrostatics play a major role in stabilizing the observed complexes of H_2O and NH_3 whereas for CH_3OH and CH_3NH_2, the major component of the interaction energy is the dispersion energy. The reason for the increased contribution of the dispersion has been attributed to the increased polarisability of the O-H and N-H group in CH_3OH and CH_3NH_2 due to the electron donating ability of the methyl group.

Thus comparing these results, it is not hard to understand the preference of H_2S to go to the top of the phenylacetylene plane whereas H_2O prefers to be in the plane. The increased polarisability of H_2S must be the reason which leads to increased dispersion energy component. This in fact goes in line with the notion that that the complexes of second row hydrides are mainly dominated by the dispersion whereas in case of first row hydrides, the main component of the interaction energy is electrostatic.[31] Further, in case of the H_2S complex, it seem that the secondary C-H•••S interaction is not stabilizing enough to hold the cyclic structure and hence, the π bonded structure is the most favourable in terms of energetics.

V.I. Conclusions

Rotational spectra of $C_6H_5CCH•••H_2S$ and its isotopologues $C_6H_5CCH•••D_2S$, $C_6H_5CCH•••HDS$, $C_6H_5CCH•••H_2{}^{34}S$, $C_6H_5CCD•••H_2S$ have been obtained. The spectra confirm a structure where H_2S is located over the phenylacetylene plane. The observed structure is the global minimum found by the *ab initio* calculations at MP2/aug-cc-pVDZ level. The c.m-c.m (c.m of H_2S to c.m. of phenylacetylene) distance has been determined to be ~3.74 Å. From the spectra it is clear that H_2S is shifted from the phenyl ring center towards the acetylenic group. The spectra of $C_6H_5CCH•••H_2S$ and $C_6H_5CCH•••H_2{}^{34}S$ indicate that the S is very close to the phenylacetylene *c* principal axis. The spectra for the parent and $C_6H_5CCH•••H_2S$ show a doubling whereas those for the $C_6H_5CCH•••HDS$ and $C_6H_5CCH•••D_2S$ show no doubling of the transitions. This splitting is caused by the rotation of H_2S about its C_2 symmetry axis in the complex. The barrier for this rotation is 403 cm^{-1} as has been indicated by the calculation at MP2/aug-cc-pVDZ level of theory. The *ab initio* calculation also indicates that the potential energy curve for the sliding motion of H_2S over the phenylacetylene ring is quite flat and this motion samples an appreciably large distance of 0.8 Å. The ab initio calculation considering a symmetric structure indicates that the minimum in the interaction energy occurs when H_2S is located at a distance of 0.4 Å from the phenylacetylene center of mass towards the acetylenic group.

V.J. References

1. J. A. Shea, W. H. Flygare, *J. Chem. Phys.* **1982**, 76, 4857.
2. P. D. Aldrich, A. C. Legon, W. H. Flygare, *J. Chem. Phys*. **1981**, 75, 2126.
3. S. G. Kukolich, P. D. Aldrich, W. G. Read, E. J. Campbell, *J. Chem. Phys*. **1983**, 79, 1105.
4. K. I. Peterson, W. Klemperer, *J. Chem. Phys.* **1986***,* 85, 725.
5. A. M. Andrews, R. L. Kuczkowski, *J. Chem. Phys.* **1993***,* 98,791
6. Chapter III in this thesis
7. S. Suzuki, P. G. Green, R. E. Bumgarner, S. Dasgupta, W. A. Goddard III, G. A. Blake, *Science*, **1992**, 257, 942.
8. H. S. Gutowsky, T. Emilsson, E. Arunan *J. Chem. Phys.* **1993**, 99, 4883.
9. E. Arunan, T. Emilsson, H. S. Gutowsky, G. T. Fraser, G de Oliveria, C. E Dykstra, *J. Chem. Phys.* **2002**, 117, 9766.
10. W. G. Read, E. J. Campbell, G. Henderson, *J. Chem. Phys.* **1983**,78, 3501.
11. W. G. Read, E. J. Campbell, G. Henderson, W. H. Flygare, *J. Am. Chem. Soc.* **1981**,103, 7670.
12. F. A. Baiocchi, J. H. Williams, W. Klemperer, *J. Phys. Chem.* **1983**, 87, 2079.
13. Jäger and co-workers, *International Symposium on Molecular Spectroscopy*, Columbus, Ohio, **2002.**
14. P. Tarakeshwar, K. S. Kim, B. J. Brutschy, *J. Chem. Phys*. **1999**, 110, 8501.
15. M. E. Sanz, S. Antolínez, J. S. Alonso, J. C. López, R. L. Kuczkowski, S. A. Peebles, R. A. Peebles, F. C. Boman, E. Kraka, D. Cremer, *J. Chem. Phys.* **2003***,* 118, 9278.
16. A. C. Legon, D. J. Millen, *Chem. Soc. Rev.* **1987**, 16, 467.
17. P. Asselin, B. Madebéle, P. Soulard, P. Reinhardt, M. E. Alikhani, *J. Chem. Phys.* **2008**, 128, 244301.
18. J. Wu, J. Zhang, Z. Wang, W. Cao, *J. Chem. Phys.* **2007**, 127, 175102.
19. Chapter IV of this thesis
20. R. Sedlak, P. Hobza, G. N. Patwri, *J. Phys. Chem. A*. **2009**, 113, 6220.
21. H. Dreizler, H. D. Rudolph, B. Hertke, *J. Mol. Struct.* **2004**, 698, 1.

22. K. Siglow, H. J. Neusser, *Chem. Phys. Lett*. **2001**, 343, 475.
23. H. Dreizler, B. Hertke, H. D. Rudolph, *J. Mol. Struct.* **2006**, 825, 1.
24. U. Dahmen, W. Stahl, H. Dreizler, *Ber. Bunsenges. Phys. Chem.* **1994,** 98, 970.
25. B. M. Giuliano, W. Caminati, *Angew. Chem. Int. Ed.* **2005**, 44, 603.
26. M. J Frisch, G. W. Trucks, H. B Schlegel, G. E. Scuseria, M. A.Robb, J. R.Cheeseman, J. A. Montgomery Jr., T. Vreven, K. N. Kudin, J. C. Burant, J. M. Millam, S. S. Iyengar, J. Tomasi, V. Barone, B. Mennucci, M. Cossi, G. Scalmani, N. Rega, G. A Petersson, H. Nakatsuji, M. Hada, M. Ehara, K. Toyota, R. Fukuda, J. Hasegawa, M. Ishida, T. Nakajima, Y. Honda, O. Kitao, H. Nakai, M. Klene, X. Li, J. E. Knox, H. P. Hratchian, J. B.Cross, C. Adamo, J. Jaramillo, R. Gomperts, R. E. Stratmann, O. Yazyev, A. J. Austin, R. Cammi, C. Pomelli, J. W. Ochterski, P. Y. Ayala, K. Morokuma, G. A. Voth, P. Salvador, J. J. Dannenberg, V. G. Zakrzewski, S. Dapprich, A. D. Daniels, M. C. Strain, O. Farkas, D. K. Malick, A. D. Rabuck, K. Raghavachari, J. B. Foresman, J. V. Ortiz, Q. Cui, A. G. Baboul, S. Clifford, J. Cioslowski, B. B. Stefanov, G. Liu, A. Liashenko, P. Piskorz, I. Komaromi, R. L. Martin, D. J. Fox, T. M. Keith, A. Al-Laham, C. Y. Peng, A. Nanayakkara, M. Challacombe, P. M. W. Gill, B. Johnson, W. Chen, M. W. Wong, C. Gonzalez, J. A. Pople, *Gaussian 03*, Revision C-02; Gaussian, Inc. Wallingford CT, **2004.**
27. F. B. van Duijneveltd, J. G. C. M. van Duijneveltd-van de Rijdt, J. H. van Lenthe, *Chem. Rev*. **1994**, 94, 1873.
28. S. F. Boys, F. Bernardi, *Mol. Phys.* **1970**, 19, 553.
29. R. W. F. Bader, *Atoms in Molecules: A Quantum Theory,* Clarendon Press: Oxford, **1990.**
30. U. Koch, P. L. A. Popelier, *J. Phys. Chem.* **1995,** 99, 9747.
31. F-M Tao, W. Klemperer, *J. Chem. Phys*. **1995**, 103, 950.

Appendix

Table V.A.1 Structural parameters for the H_2S monomer optimized at MP2/aug-cc-pVDZ level of theory. The distances are reported in Å and the angles are reported in degrees.

Parameters	Values
S-H	1.350
∠H-S-H	92.4°

Table V.A.2. Structural parameters for the phenylacetylene monomer optimized at MP2/aug-cc-pVDZ level of theory. The distances are reported in Å and the angles are reported in degrees.

Parameters	Values	Parameters	Values	Parameters	Values
R(1,2)	1.416Å	A(5,2,8)	120.7	D(3,1,2,5)	0.0
R(1,12)	1.439	A(1,3,4)	120.0	D(3,1,2,8)	180.0
R(2,5)	1.404	A(1,3.7)	119.3	D(12,1,2,5)	180.0
R(2,8)	1.094	A(4,3,7)	120.7	D(12,1,2,8)	0.0
R(4,6)	1.408	A(3,4,6)	120.3	D(2,1,3,4)	0.0
R(4,10)	1.094	A(3,4,10)	119.6	D(2,1,3,7)	180.0
R(6,11)	1.094	A(6,4,10)	120.0	D(12,1,3,4)	180.0
R(12,13)	1.237	A(2,5,6)	120.3	D(12,1,3,7)	0.0
R(13,14)	1.074	A(2,5,9)	119.6	D(3,1,2,5)	0.0
A(2,1,3)	119.5	A(6,5,9)	120.0	D(3,1,2,8)	180.0
A(2,1,12)	120.3	A(4,6,5)	119.7	D(12,1,2,5)	180.0
A(1,2,5)	120.0	A(4,6,11)	120.1	D(12,1,2,8)	0.0
A(1,2,8)	119.3	A(5,6,11)	120.1	D(2,1,3,4)	0.0

Table V.A.2. continued

Parameters	Values
D(1,2,5,6)	0.0
D(1,2,5,9)	180.0
D(8,2,5,6)	180.0
D(8,2,5,9)	0.0
D(1,3,4,6)	0.0
D(1,3,4,10)	180.0
D(7,3,4,6)	180.0
D(7,3,4,10)	0.0
D(3,4,6,5)	0.0
D(3,4,6,11)	180.0
D(10,4,6,5)	180.0
D(10,4,6,11)	0.0
D(2,5,6,4)	0.0
D(2,5,6,11)	180.0
D(9,5,6,4)	180.0
D(9,5,6,11)	0.0

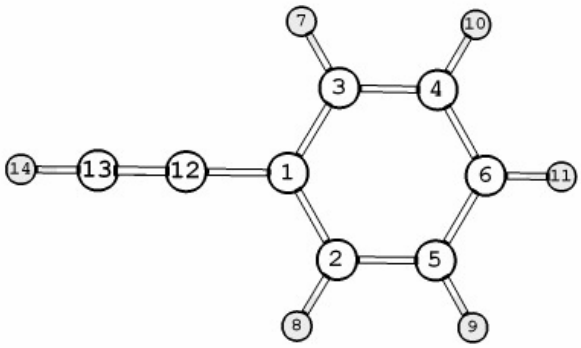

Table V. A. 3. *Ab initio* derived structural parameters for the global minimum of the phenylacetylene-H_2S complex at MP2/aug-cc-pVDZ level of theory. The distances are in Å s and the angles and dihedrals are in degrees.

Structure B		Structure C		Structure A	
Parameter	Values	Parameter	Values	Parameter	Values
R(1,2)	1.409	R(2,1)	1.408	R(1,2)	1.408
R(2,3)	1.405	R(3,2)	1.404	R(2,3)	1.405
R(3,4)	1.416	R(4,3)	1.416	R(3,4)	1.416
R(4,5)	1.416	R(5,4)	1.417	R(5,4)	1.416
R(5,6)	1.404	R(6,5)	1.405	R(6,5)	1.405
R(4,7)	1.439	R(7,4)	1.441	R(7,4)	1.439
R(7,8)	1.237	R(8,7)	1.238	R(8,7)	1.238
R(4,9)	3.601	R(9,8)	3.896	R(9,8)	3.819
R(3,10)	1.094	R(10,3)	1.094	R(10,8)	1.078
R(5,11)	1.094	R(11,5)	1.094	R(11,3)	1.094
R(6,12)	1.094	R(12,6)	1.094	R(12,5)	1.094
R(2,13)	1.094	R(13,2)	1.094	R(13,2)	1.094
R(1,14)	1.094	R(1,14)	1.094	R(14,6)	1.094
R(8,15)	1.074	R(8,15)	1.075	R(15,1)	1.094
R(9,16)	1.351	R(9,16)	1.353	R(16,9)	1.350
R(9,17)	1.353	R(9,17)	1.350	R(17,9)	1.350
A(3,2,1)	120.3	A(3,2,1)	120.3	A(3,2,1)	120.3
A(4,3,2)	119.9	A(4,3,2)	119.9	A(4,3,2)	120.1
A(5,4,3)	119.7	A(5,4,3)	119.8	A(5,4,3)	119.4
A(6,5,4)	119.9	A(6,5,4)	119.7	A(6,5,4)	120.1
A(7,4,5)	120.1	A(7,4,5)	120.5	A(7,4,3)	120.3
A(8,7,4)	177.6	A(8,7,4)	178.9	A(8,7,4)	179.9
A(9,4,5)	85.6	A(9,8,7)	82.1	A(9,8,7)	1.408

Table V. A. 3. continued

Structure B		Structure C		Structure A	
Parameters	Values	Parameters	Values	Parameters	Values
A(10,3,4)	119.3	A(10,3,4)	119.3	A(10,8,9)	1.4
A(11,5,4)	119.3	A(11,5,4)	119.6	A(10,3,4)	119.2
A(12,6,5)	119.7	A(12,6,5)	119.5	A(11,5,4)	119.2
A(13,2,3)	119.7	A(13,2,3)	119.6	A(12,2,3)	119.6
A(14,1,2)	120.1	A(14,1,2)	120.1	A(13,6,5)	119.6
A(15,8,7)	178.3	A(15,8,7)	179.6	A(14,1,2)	120.1
A(16,9,4)	46.2	A(16,9,8)	5.28	A(15,9,8)	94.8
A(17,9,4)	45.5	A(17,9,8)	97.3	A(16,9,8)	94.5
D(4,3,2,1)	0.2	D(4,3,2,1)	-0.0	D(4,3,2,1)	0.0
D(5,4,3,2)	-0.9	D(5,4,3,2)	-0.1	D(5,4,3,2)	0.0
D(6,5,4,3)	0.9	D(6,5,4,3)	0.1	D(6,5,4,3)	-0.0
D(7,4,5,6)	-177.2	D(7,4,5,6)	-179.8	D(7,4,3,2)	180.0
D(8,7,4,5)	87.7	D(8,7,4,5)	168.5	D(8,7,4,3)	-57.3
D(9,4,5,6)	-81.0	D(9,8,74)	-173.8	D(9,8,7,4)	-123.9
D(10,3,4,5)	-179.8	D(10,3,4,5)	180.0	D(10,8,9,7)	178.8
D(11,5,4,3)	179.8	D(11,5,4,3)	180.0	D(11,3,4,5)	-180.0
D(12,6,5,4)	179.2	D(12,6,5,4)	179.8	D(12,5,4,3)	180.0
D(13,2,3,4)	-179.2	D(13,2,3,4)	180.0	D(13,2,3,4)	-180.0
D(14,1,2,3)	-179.5	D(14,1,2,3)	-179.9	D(14,6,5,4)	180.0
D(15,8,7,4)	-178.5	D(15,8,7,4)	-27.8	D(15,1,2,3)	180.0
D(16,9,4,5)	-120.0	D(16,9,8,7)	-58.6	D(16,9,8,7)	-45.2
D(17,9,4,5)	60.4	D(17,9,8,7)	-85.8	D(17,9,8,7)	47.7

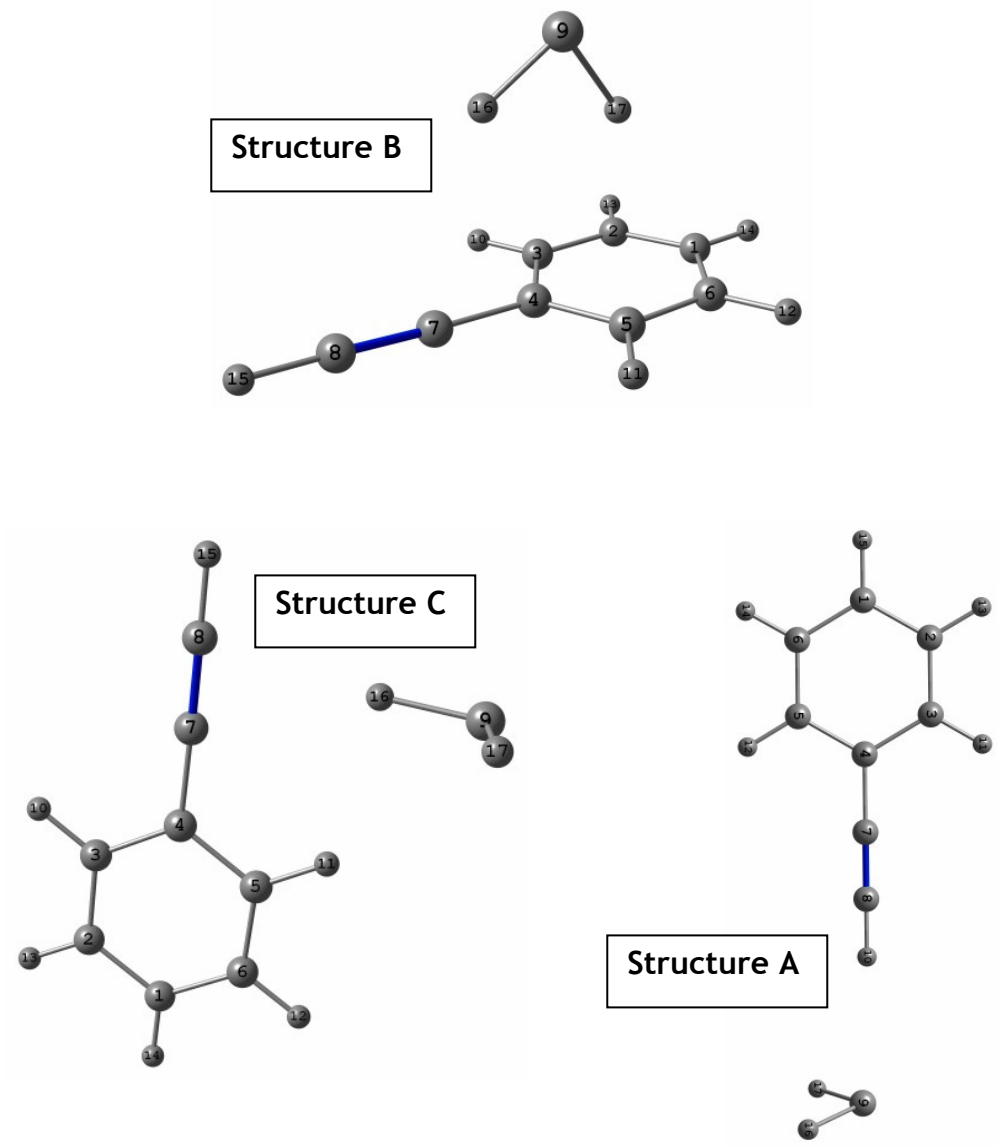

Figure V. A. 1. Numbering of the atoms in Structure A, Structure B and Structure C used in Table V.A. 2 and V. A. 3. These are shown for reference.

Table V. A. 4. Vibrational frequencies of the three minima named Structure A, Structure B and Structure C calculated at MP2/aug-cc-pvDZ level of theory.

Structure B	Structure C	Structure A
Frequencies (cm^{-1})	Frequencies (cm^{-1})	Frequencies (cm^{-1})
29	19	7
57	53	24
88	77	28
126	84	67
141	101	125
145	126	128
168	151	169
173	295	172
323	315	331
395	398	397
460	460	462
496	474	500
498	493	514
561	549	615
610	608	638
614	616	687
652	644	733
747	742	741
762	761	763
841	846	838
899	901	889
953	934	931
954	958	941
996	996	996

Table V. A. 4. continued

Structure B	Structure C	Structure A
Frequencies (cm^{-1})	Frequencies (cm^{-1})	Frequencies (cm^{-1})
1038	1040	1039
1087	1091	1086
1166	1166	1165
1183	1189	1183
1185	1193	1193
1216	1213	1215
1306	1312	1305
1431	1428	1427
1482	1478	1478
1489	1492	1491
1600	1602	1602
1629	1630	1631
2102	2097	2097
2733	2724	2749
2755	2767	2774
3204	3203	3201
3212	3211	3209
3220	3219	3218
3227	3226	3225
3234	3232	3232
3479	3474	3429

Chapter VI

The Hydrogen Bond: a Molecular Beam Microwave Spectroscopist's view

(This work has appeared as a perspective article in Phys. Chem. Chem. Phys., 11, 2009, 8974)

VI.A. Introduction

There has been a continuous debate about what a hydrogen bond is and how it is different from the more general 'van der Waals interaction', though both are nearly a century old concepts. Considering the importance of this debate, IUPAC has recently formed a task group to come up with a modern definition of hydrogen bonding.[1] Nevertheless, the importance of "hydrogen bonding" is well-recognized in chemistry and biology.[2-7] It is known for long that H_2O and H_2S from the same group have remarkably different properties under ambient conditions. Due to this, it was traditionally thought that H_2O forms hydrogen bonds and H_2S does not.[7] However, the modern view is that both molecules have very different 'hydrogen bonding' capabilities.[2-6] In any case, this difference is often rationalized due to the less electronegativity of sulphur compared to that of oxygen which makes the former a poor hydrogen bond donor/acceptor.[8] Thus, under ambient temperature and pressure H_2O is a liquid and H_2S is a gas. The crystal structures of H_2O and H_2S also exhibit remarkable differences. In ice, each of the H_2O molecules is coordinated to four others in a tetrahedral arrangement. On the other hand, under ambient pressure H_2S has been found to crystallize (freezing point -60° C) in a close-packed fashion where each hydrogen sulphide molecule is in contact with twelve equidistant neighbors.[7] This disorder in the crystal structure of H_2S is attributed to the isotropic nature of the interaction among the neighbours, which are essentially spherical. Does it mean that H_2S can never participate in 'hydrogen bond' formation?

Our knowledge of 'hydrogen bonding' has been evolving over the last century and we now know that a wide and versatile range of chemical entities are capable of forming hydrogen bonds. Thus, in a hydrogen bond, which is typically denoted by X-H•••Y, X and Y were initially observed to be only the most electronegative elements, N, O or F.[7] However, Pimentel and McClellan in their authoritative book on *The Hydrogen bond* chose not to put any restriction on X or Y.[2] According to them, if there is evidence that an H atom is simultaneously bonded to X and Y then there is hydrogen bond. Their conviction proved right and there have been numerous examples of hydrogen bonding beyond what was initially believed and X could be any element with an electronegativity larger than that of H, including S.[5] Moreover Y could be a lone pair, π pair, unpaired electron, sigma bonding electrons, hydride ions etc. and the list is expanding.[9-12] It has

been shown recently that the carbon atom of methane can act as a hydrogen-bond acceptor.[13]

In the literature, there are well accepted criteria which are widely used to characterize hydrogen bonds.[2-7] These criteria, though helpful in many cases, are not without ambiguities. First and foremost was the belief that hydrogen bonding was purely electrostatic.[7,14] Now it is well recognized that 'the electrostatic picture' is incomplete.[15,16] Compton scattering[17] and NMR[18] experiments in the last decade have given unambiguous evidence for a partial covalent nature in hydrogen bonding. The next most important criterion was the red shift of the X-H stretching frequency on hydrogen bond formation.[2] It is a well established signature of 'hydrogen-bond' formation that holds true in most cases. However, recently, it has been observed that there are 'hydrogen bonds' which cause a blue shift in the X-H stretching frequencies.[19] Moreover, Joseph and Jemmis have shown that it is possible to have systems with no shift of the X-H stretch frequencies upon hydrogen-bond formation.[20] Another popular and stringent criterion has been that the distance between the X and Y atoms should be less than the sum of their van der Waals' radii.[21] It has been relaxed to some extent now and the distance between H and Y atoms is compared to the sum of their van der Waals radii. The stringent criterion has been strongly criticized by many as too limiting most of the times[3-5,22-26] and the relaxed criterion is criticized as too generous on individual cases such as 1,2-diols.[26] Recently, a hydrogen bond radius has been proposed as an alternative to van der Waals radius for the atoms typically found to be involved in hydrogen bonding.[22-25] However, one aspect about hydrogen bonding that is widely accepted is the directionality, i.e. X-H•••Y is found to be linear in most cases. Though, secondary interactions in a system could force X-H•••Y away from linearity,[27] it is the directionality in hydrogen bonding resulting in an anisotropic intermolecular potential that contrasts it from the more general 'van der Waals forces' expected to be isotropic. There have been suggestions about energy cutoffs for hydrogen bonds and these are at best suggestive and subjective and at worst arbitrary.

Recently, Koch and Popelier have proposed a set of eight criteria to detect and characterize hydrogen bonds.[28] These criteria are based on Bader's Atoms In Molecules (AIM) theory.[29] According to Bader himself, presence of a bond critical point connecting

the H from the donor group XH to the acceptor Y is sufficient to conclude about the presence of a hydrogen bond. In the original contribution of Koch and Popelier, these criteria were used to predict if C-H•••O contacts in some van der Waals complexes and anti-AIDS drug AZT could be classified as 'hydrogen bonded' based on detailed analysis of the charge density. These have gained popularity owing to the platform it provides to differentiate 'hydrogen bonding' from other closed shell interactions through the characterization of the properties of the bond critical point found between hydrogen and the acceptor atom. It should be remembered that these criteria are based on the analysis of rigid equilibrium geometry. While the application of these criteria for crystal structures is less ambiguous, it is not clear if the conclusions reached through this analysis will hold good when one considers the non-rigid/dynamic structure of the weakly bound van der Waals complexes.

Let us now turn our attention to H_2S again. Dynamics indeed decide the fate of H_2S and there are evidences in the literature that the structural behavior of H_2S changes on further cooling and compression.[30-32] The structure becomes gradually ordered with the signature of hydrogen bond formation. As pointed out by Nelmes, Hamel and co-workers, it is interesting to note that H_2S is the only hydride which shows this behavior on compression.[31] Further, they concluded that H_2S can be a good model system where we can tune the hydrogen bond strength from "absent or very weak to structurally significant". On the other hand, gas phase studies like scattering and spectroscopic studies in supersonic beam are complementary to these studies in the condensed phase. These studies provide a direct or indirect estimate of the strength of the 'hydrogen bonding' interaction in smaller dimers and trimers in isolated condition. A recent scattering experiment of Aquilanti et al. on the complexes of rare gas with H_2O and H_2S showed that for H_2O complexes, there is a progressive shift in the 'glory' pattern towards higher velocities as one moves from He to Xe. The Authors concluded that this was an indication of the increase in binding strength more than what would be predicted by a van der Waals' model, which according to them, is based on polarizabilities of the interacting partners.[33] This was attributed to an onset of hydrogen bonding (O-H•••Rg) and it was further supported by the *ab initio* calculations. Unlike these complexes of H_2O with rare gas atoms, in case of the Rg•••H_2S complexes, the increase in binding strength could be

explained by the polarizabilities of H_2S and those of rare gas atoms and the effect due to the permanent dipole moment of H_2S.[34] Thus, it was concluded that the nature of interaction becomes spherical with "no measurable anisotropic effect" when the binding partner changes from H_2O to H_2S. It was concluded further that there was no signature of hydrogen bonding in case of H_2S complexes with rare gas atoms. It should be pointed out here that an interaction involving permanent electric dipole moment of H_2S can not lead to an isotropic potential. The difference between the Rg•••H_2O and Rg•••H_2S interaction has its origin elsewhere and that is the main focus of this work

The situation may also be different when one considers a stronger acceptor rather than the rare gas atoms. Thus, there are examples of the 'hydrogen bonded' geometry of H_2S complexes characterized by microwave experiments in the supersonic beam e.g. C_6H_6•••H_2S[35] and C_2H_4•••H_2S.[36] The ground state structures obtained from the experiments showed that these H_2S complexes are 'hydrogen bonded' similar to their H_2O counterparts.[37,38] Moreover, the H_2S dimer has an equilibrium geometry which is hydrogen bonded[39] similar to that of H_2O dimer[40]. These observations do not change the fact that H_2O is a liquid and H_2S is a gas at ambient conditions. In a supersonic molecular beam, there is an extensive cooling of the translational, rotational and vibrational degrees of freedom. This facilitates the formation of these complexes which are weakly bound. However, even at these conditions large amplitude motions of the H_2S/H_2O within these complexes lead to observable splitting in the microwave spectrum of all these complexes. Are these interactions, then, different from the Rg-H_2O/H_2S interactions? As it has been shown in this thesis and elsewhere,[13,29] the equilibrium structures of Ar•••H_2O, Ar•••H_2S, C_2H_4•••H_2O and C_2H_4•••H_2S would all be hydrogen bonded according to the AIM theoretical criteria given for C-H•••O contacts by Koch and Popelier.[28]

What happens when one considers the dynamical structure i.e. the effect of the large amplitude motions in these complexes? In a supersonic expansion, the zero-point energy is the main contributor to the dynamics of the system. Hence, the question asked is what criterion one should look for, to call a system 'hydrogen-bonded', while considering the zero-point energy averaged structure. The important point to be reemphasized here is that the 'zero point dynamics' can not be restricted even at zero

Kelvin. The proposed answer is that the potential barriers of different motions which take the bonded hydrogen away from the acceptor moiety should be significantly above the zero-point energy along that co-ordinate. It should be emphasized here that this barrier is not related to the dissociation energy of the complex under consideration. These large amplitude motions have periodic potentials along vibrational coordinates that do not lead to dissociation. This can be made clear by looking at the schematic drawn in Figure VI.1. Typically, both X-H•••Y and Y•••X-H could be below the dissociation limit corresponding to XH + Y along the stretching co-ordinate. If it is not bound in this stretching co-ordinate, the complex does not exist. Even when the complex is bound along the stretching co-ordinate, the large amplitude motion of the HY unit within the complex can take the hydrogen away from the acceptor moiety in a vibrationally averaged structure. In such a situation, the structure clearly will not be hydrogen bonded. This large amplitude motion of X•••HY is described as bending or internal rotation or free rotation depending on the barrier.

Here in this part of the thesis, we analyze the effect of zero-point energy on the equilibrium structures of four complexes e.g. Ar_2•••H_2O, Ar_2•••H_2S, C_2H_4•••H_2O and C_2H_4•••H_2S to test their characterization as 'hydrogen bonded' complexes. These are chosen as typical examples where the presence of a hydrogen bond is a matter of debate. The potential energy barriers for the rotation of H_2O and H_2S about their principal axes are calculated for all the complexes. The barriers were calculated using *ab initio* theory and were compared to the zero point energies along these co-ordinates. A comparison like this is useful to have an estimate of the relative strength of the interaction and it can provide important insight when one asks "is the 'hydrogen bonding', if it exists at all, strong enough to be experimentally detected and measured?"

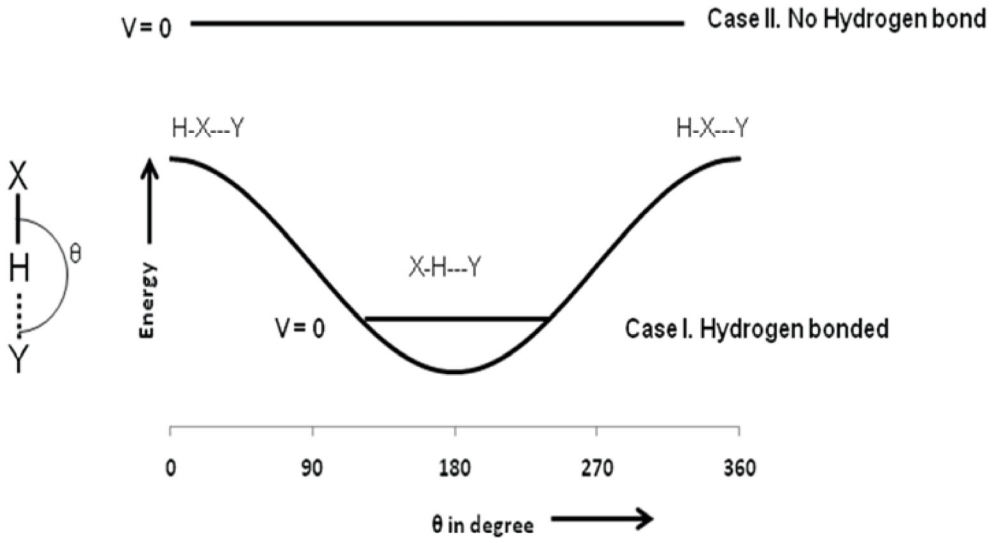

Figure VI.1. Schematics showing the effect of zero-point motion on the equilibrium structure of a hydrogen-bonded complex. Case I. If the barrier for the large amplitude motion is high enough compared to the zero-point energy, the dynamically averaged structure will be able to hold the 'hydrogen-bonded' configuration. Case II. When the zero-point energy along the co-ordinate is lying far above the barrier, the 'zero-point' motion becomes a 'nearly free rotation' and 'dynamic' structure will not execute any orientational preference characteristic of a 'hydrogen bond'.

VI.B. Computational methodology

All the four complexes were fully optimized at MP2(full)/aug-cc-pVTZ level of theory using Gaussian 03 suite of programme.[41] Harmonic frequency calculations were done at the same level of theory to determine the zero-point energy along the intermolecular modes. Further, the absence of any imaginary frequency ensured that the optimized geometries were true minima. However, these intermolecular frequencies are expected to be anharmonic. To check how the anharmonicity affects the frequencies of these modes, we have performed both harmonic and anharmonic frequency calculations for C_2H_4•••H_2S complex at a lower level of theory i.e. MP2(full)/aug-cc-pVDZ level. The differences in the frequency values from the harmonic and anharmonic calculations have been found to be in the range of 2-40 cm^{-1}. These numbers indicate that the conclusions drawn in this chapter are not going to alter as we would see later. The AIM theoretical

calculations have been performed using AIM 2000 software for the optimized geometries at this level of theory [42]

Having the fully optimized geometries for all the complexes, it was decided to explore the anisotropic nature of the potential energy hyper surfaces by varying the H_2O/H_2S orientation in the complexes. For the one dimensional potential energy surface calculations for different orientations of H_2O/H_2S, we chose more symmetric structures (C_{2v} for Ar_2•••H_2O/Ar_2•••H_2S and C_s for C_2H_4•••H_2O/C_2H_4•••H_2S) as the starting points so that the number of parameters which are to be taken care of during the scans get reduced. Both hydrogen atoms are placed symmetrically between two Ar atoms for Ar_2•••H_2O/Ar_2•••H_2S. For C_2H_4•••H_2O and C_2H_4•••H_2S, the starting geometry was chosen such that the O-H•••π and S-H•••π angles were 180°. These constraints on the symmetry of the starting geometry were convenient and were also reasonable as they still represent the main features of the experimentally observed structure. The rotational spectroscopic studies on Ar_2•••H_2O and Ar_2•••H_2S indicated a vibrationally averaged ground state structure having C_{2v} symmetry. [43-45] The positions of the hydrogen atoms could not be determined form the spectra as it was affected by the large amplitude motion. However, the change in the rotational constants (change in the '*B*' rotational constant of Ar_2•••H_2O and change in the '*A*' rotational constant in case of Ar_2•••H_2S) upon isotopic substitution indicated that both the hydrogen atoms are almost at the same distance from the center of mass. For C_2H_4•••H_2O and C_2H_4•••H_2S, the analysis of the experimental data showed that both H_2O and H_2S are situated on top of the π cloud of ethylene and only one of the hydrogen is pointing towards the π cloud.[38,36] Further, for C_2H_4•••H_2O, it was also concluded that in the vibrationally averaged geometry, the plane of H_2O molecule is bisecting the C=C bond of C_2H_4.[46] Furthermore, It should be pointed out that the barrier heights are not expected to be changed drastically by the assumption of the reference geometry being symmetric in case of Ar_2•••H_2X systems as the difference of energy in the symmetric and the asymmetric structure is only marginal. Thus, in case of Ar_2•••H_2O, this difference is only 30 cm^{-1} whereas in case of Ar_2•••H_2S, this difference is 44 cm^{-1}. For all the four complexes single point scans have been performed by fixing the monomer geometry as was obtained from the monomer

optimization at the same level of theory. Counterpoise corrections were done at each point to correct for the basis set superposition error (BSSE).[47] The principal axes of H_2O and H_2S are shown in Figure VI.2. The structural parameters which were varied during the calculations are shown in Figure VI.3. For Ar_2•••H_2O/Ar_2•••H_2S, R is defined as the distance of O/S to the mid-point of Ar•••Ar bond. The Ar-Ar distance was fixed at the value obtained from the optimized geometry of the corresponding complexes. The rotation of H_2O/H_2S about its '*c*' principal axis is described by the variation of angle θ. Similarly, the variation in ϕ and τ describe the rotation of H_2O/H_2S about it's '*a*' and '*b*' (C_2 symmetry axis) axes. Initially, for Ar_2•••H_2O, R was varied from 2.5 Å to 4.0 Å in steps of 0.1 Å whereas for Ar_2•••H_2S, it was varied from

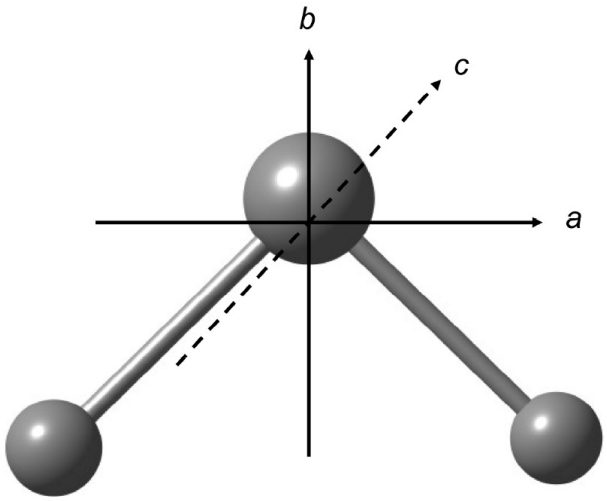

Figure VI.2. Principal axes system of H_2O and H_2S

3.1 Å to 3.8 Å with the same step size keeping all other parameters to be fixed. The minimum of the interaction energy was found to be at 3.4 Å for Ar_2•••H_2O and for Ar_2•••H_2S, it was found to be at 3.8 Å. For C_2H_4•••H_2O and C_2H_4•••H_2S, R is defined as the distance of the oxygen/sulphur from the center of π bond in ethylene. For these complexes, the minima of the interaction energy along R lie at 3.4 Å and 4.0 Å respectively for C_2H_4•••H_2O and C_2H_4•••H_2S. At this fixed value of R, each of θ, ϕ and

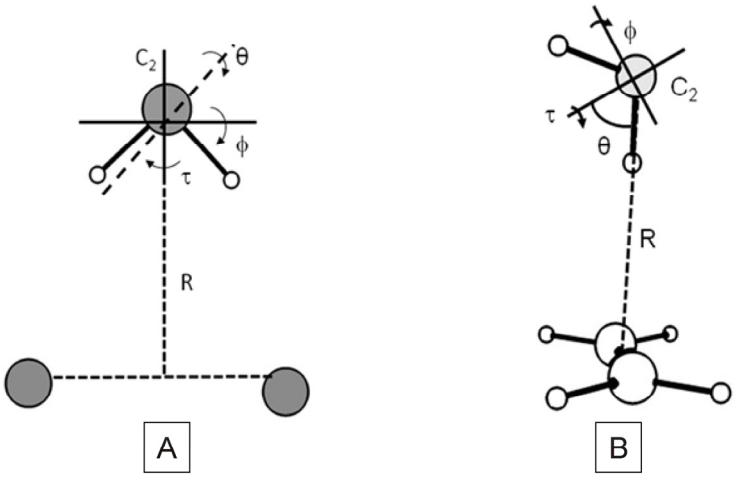

Figure VI.3. Structural parameters of the complexes which were varied to generate the potential energy surfaces. A. For Ar_2•••H_2O/Ar_2•••H_2S, the starting reference geometry was a doubly hydrogen bonded C_{2v} symmetric structure. B. For C_2H_4•••H_2O/C_2H_4•••H_2S, the reference geometry was a singly hydrogen bonded one having C_s symmetry. The rotation of H_2O and H_2S along ϕ, τ and θ co-ordinate define the rotation of H_2O/H_2S along its own a, b and c principal axes.

τ were varied in steps of 10° to generate the one-dimensional potential curves. The barrier heights along different co-ordinates are reported by taking the lowest point as the reference point along that curve. All the curves, except the rotation of H_2O/H_2S about its '*c*' principal axis in C_2H_4•••H_2O/H_2S, are symmetric about 180° which is obvious considering the symmetry of the reference systems.

VI.C. Results and Discussions

VI.C.1. Optimized geometries and the AIM parameters

Figure VI.4 shows the optimized geometries of Ar_2•••H_2O and Ar_2•••H_2S complexes at MP2 (full)/aug-cc-pVTZ level of theory. For Ar_2•••H_2O, these two minima were obtained by imposing the C_s symmetry constraints. Unstrained geometry optimization

also converged to C_s symmetry for both the structures of Ar_2•••H_2O. For Ar_2•••H_2S, both of the converged minima had C_1 symmetry as shown in Figure VI.4. For both the complexes, Structure I is more stable than Structure II. The energy differences between the minima are 23 cm^{-1} and 25 cm^{-1} respectively for Ar_2•••H_2O and Ar_2•••H_2S. BSSE correction increases this difference to 27 cm^{-1} in case of Ar_2•••H_2O and to 34 cm^{-1} for Ar_2•••H_2S. Single point calculations at CCSD(T)/aug-cc-pVDZ level were performed for the Structures I and II , in case of both Ar_2•••H_2O and Ar_2•••H_2S followed by the counterpoise correction. These calculations show the difference to be only 8 cm^{-1} for Ar_2•••H_2O, Structure I is still being the lower energy structure. The energy difference is 12 cm^{-1} for the two optimized configurations of Ar_2•••H_2S at CCSD(T)/aug-cc-pVDZ level and the ordering of the energy is the same as the MP2 level. Thus, the differences of the energy between the Structure I and Structure II at CCSD(T) and MP2 level are close enough and hence, the level of calculation employed here is adequate for the purpose. Fully optimized geometries of C_2H_4•••H_2O and C_2H_4•••H_2S are shown in Figure VI.5. These geometries correspond to O/S-H•••π interactions. Both the geometries have C_1 symmetry. For C_2H_4•••H_2O, the ∠O-H•••π is ~169°. For the optimized geometry of C_2H_4•••H_2S complex, the S-H•••π bond is more linear, the angle being ~178°. The intermolecular frequencies calculated for these optimized geometries were used to have the estimate of the zero point energy along a particular co-ordinate. Bond critical points and the bond paths between the hydrogen of H_2O/H_2S and the Ar/C atoms could be located using AIM theoretical calculations. For both C_2H_4•••H_2O and C_2H_4•••H_2S, the bond critical points have been found connecting the hydrogen to the ethylene carbon instead of the center of C=C bond. The electron density and the Laplacian of the electron density at the BCP for the hydrogen-bonds are given in Table I. It can be seen that for all the complexes, both the parameters are well within the range suggested for 'C-H•••O hydrogen-bonds' by Koch and Popelier.[28] Raghavendra and Arunan have recently shown that Ar•••H_2O and Ar•••H_2S complexes

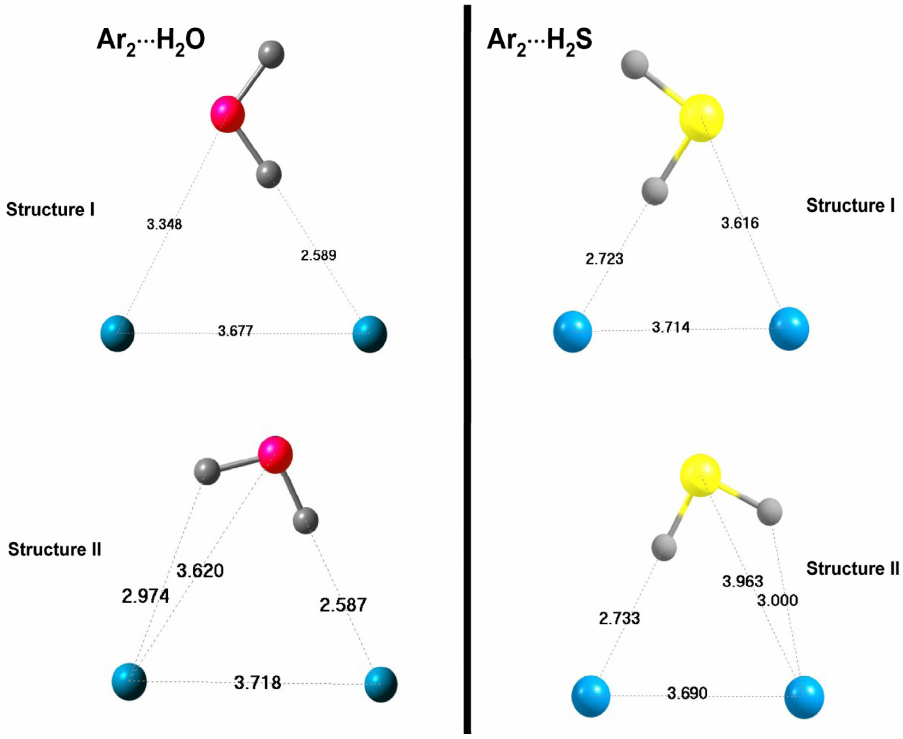

Figure VI.4. Fully optimized geometries of Ar_2•••H_2O and Ar_2•••H_2S complexes at MP2(full)/aug-cc-pVTZ level of theory. Distances between the atoms are shown in Å.

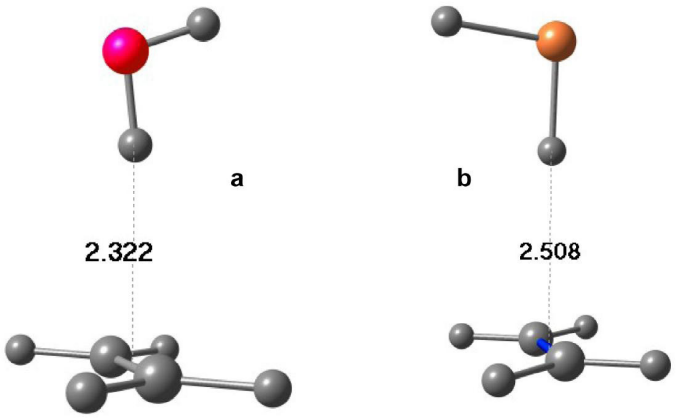

Figure VI.5. Fully optimized geometries of a) C_2H_4•••H_2O and b) C_2H_4•••H_2S complexes at MP2(full)/aug-cc-pVTZ level. Selected bond distances (Å) are shown in the figures.

*Table VI.1. Electron density at Hydrogen Bond Critical Point (HBCP), ρ, and Laplacian (L) of the electron density at HBCP calculated by AIM. **

Complex	ρ (au)	L (au)
$Ar_2\cdots H_2O$	0.008	0.032
$Ar_2\cdots H_2S$	0.007	0.026
$C_2H_4\cdots H_2O$	0.021	0.031
$C_2H_4\cdots H_2S$	0.017	0.023

**All these values are well within the range of hydrogen-bonds as suggested by Koch and Popelier for C-H•••O contacts. The ρ value at BCP should lie within the range [0.002, 0.035] au and the Laplacian of the electron density at BCP should lie within the range [0.024, 0.139] au.*[28]

obey most of the criteria given by Koch and Popelier for C-H•••O contacts to be classified as hydrogen bonded, including the necessary and sufficient condition.[13] These are conclusions based on the static equilibrium structures. We now turn our attention to the dynamic structures.

VI.C.2. Features of the one dimensional potentials

VI.C.2.a. Ar_2•••H_2O and Ar_2•••H_2S

Figure VI.6 shows the potential energy curves for the variation of angle θ (rotation about *c* axis of H_2X) in Ar_2•••H_2O and Ar_2•••H_2S. The nature of the curve is very shallow. The minimum on the curve corresponds to 30° for Ar_2•••H_2O and 40° for Ar_2•••H_2S respectively. This corresponds to the geometry where both the hydrogen atoms are pointing toward the Ar•••Ar moiety in an unsymmetrical fashion. This rotation has to pass over an energy barrier of 46 cm^{-1} for Ar_2•••H_2O and 64 cm^{-1} for Ar_2•••H_2S corresponding to a geometry where O/S is pointing towards the Ar•••Ar bond (θ = 180°).

Another maximum was observed with a smaller barrier, for both Ar_2•••H_2O and Ar_2•••H_2S, when both the hydrogen atoms are placed symmetrically between two argon atoms (the reference geometry for Ar_2•••H_2X systems). This barrier is very small being 5 cm^{-1} for Ar_2•••H_2O and 7 cm^{-1} for Ar_2•••H_2S. At θ =70°, one hump was observed for Ar_2•••H_2O corresponding to a geometry where one of the hydrogen is interacting with one of the argon atoms and the other hydrogen atom is away from the Ar•••Ar moiety. Similar characteristic was observed for Ar_2•••H_2S at θ =90° . A fully relaxed optimization of this geometry indeed converged to Structure I, which is more stable than the one where both the hydrogen atoms are facing the Ar•••Ar moiety, though the difference is very small.

Figure VI.6. Potential energy curves for the rotation of H_2O and H_2S about its 'c' principal axis in Ar_2•••H_2O and Ar_2•••H_2S complexes.

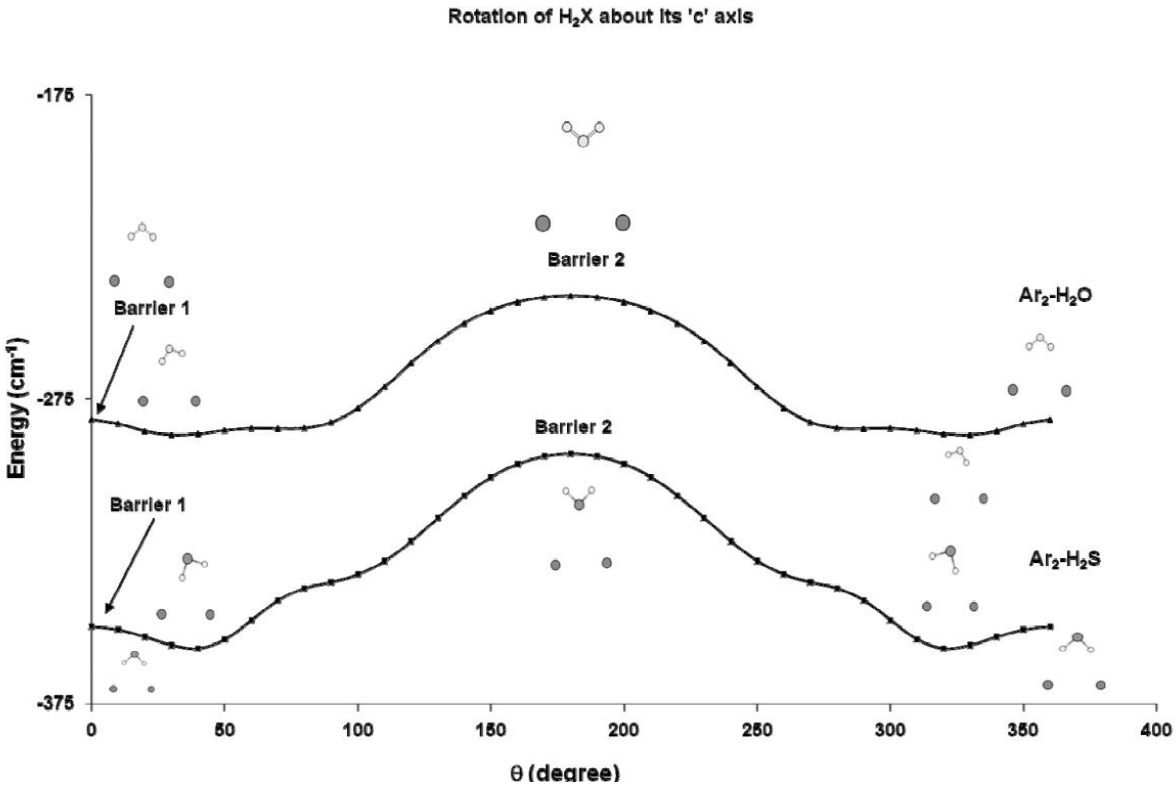

Variation of energy along the τ co-ordinate (rotation about the *b* axis of H_2X) is shown in Figure VI.7. For Ar_2•••H_2O, the lowest point along this co-ordinate lies at 0°

and 180° where both the hydrogen atoms are pointing towards the Ar•••Ar bond and all the five atoms are in the same plane. An energy barrier of 38 cm^{-1} separates these minima. This barrier corresponds to τ = 90° , where the H_2O molecular plane is perpendicular to the Ar···Ar bond. Looking at Figure VI.7, it is immediately obvious that Ar_2•••H_2S is much floppier along this co-ordinate compared to Ar_2•••H_2O. Given an extremely floppy nature of the potential, it is not possible to locate the minima for Ar_2•••H_2S along this co-ordinate. However, it's noted that for Ar_2•••H_2S, the geometry where all the atoms are in the same plane (τ = 0°, 180°) does not correspond to the lowest point along this co-ordinate, rather the

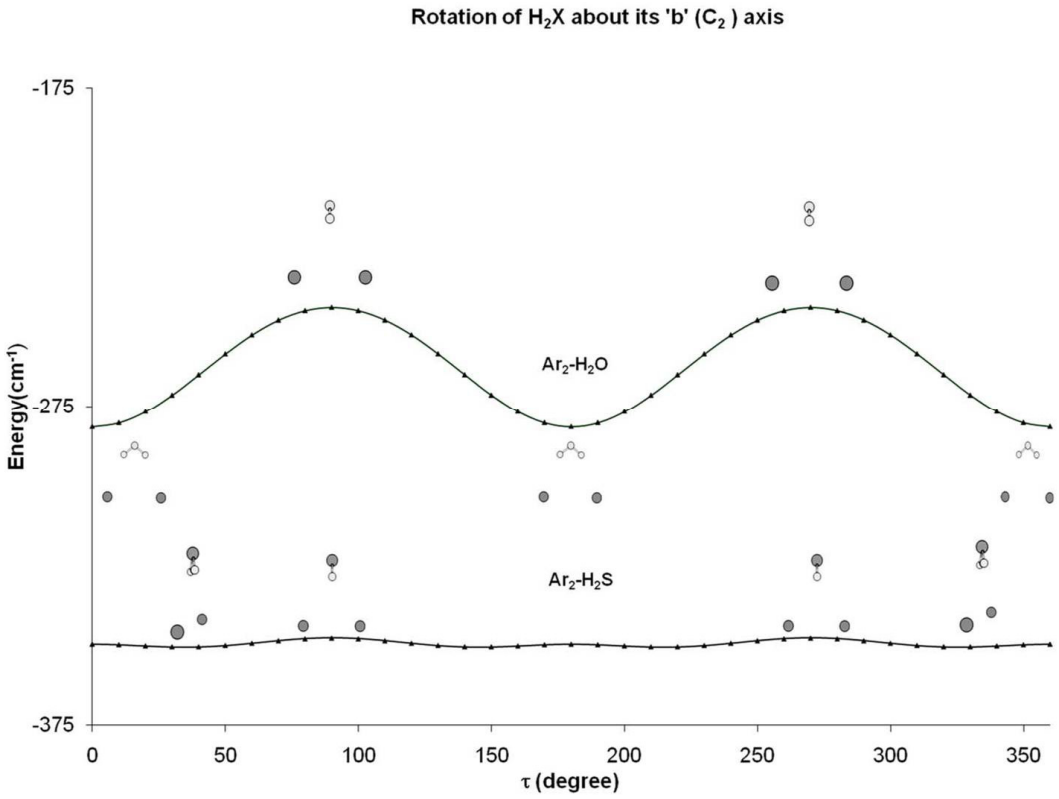

Figure VI.7.Variation of potential energy for the rotation of H_2O/H_2S about its C_2 symmetry ('b' principal axis) axis in Ar_2•••H_2O and Ar_2•••H_2S complexes.

lowest point lies at ~35° , just 1 cm^{-1} below the τ = 0° geometry. For Ar_2•••H_2S, the energy barrier for this rotation corresponds to τ =90° and the barrier is only 3 cm^{-1}.

Variation of potential energy along the ϕ co-ordinate (rotation about *a* axis) is shown in Figure VI.8. The lowest energy point on the curve corresponds to the geometry

where all the atoms are in the same plane and both the hydrogen atoms are pointing towards the Ar•••Ar moiety (ϕ = 0°). One local minimum could be located for both Ar_2•••H_2O and Ar_2•••H_2S, respectively at 40 cm^{-1} and 57 cm^{-1} above the lowest energy configuration along this co-ordinate. This local minimum corresponds to O-down or S-down configuration. The maximum on the curve lies at 90° and 270° for Ar_2•••H_2O and 110° and 250° for Ar_2•••H_2S.

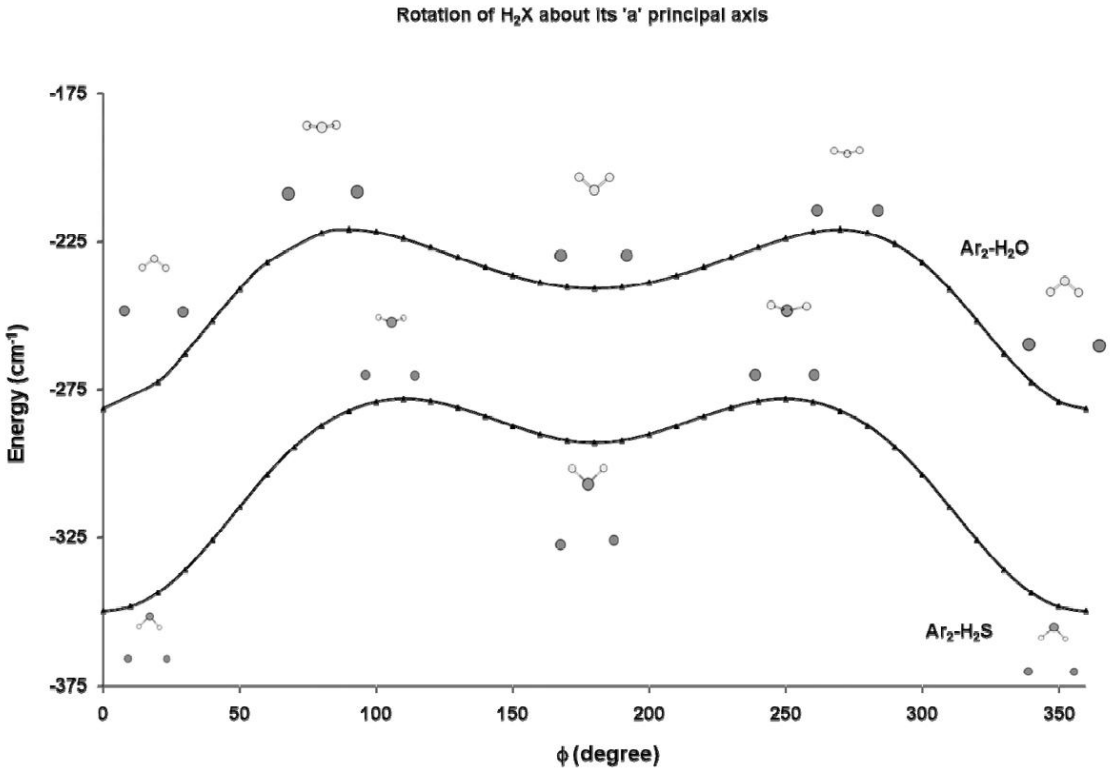

Figure VI.8: Variation of potential energy for the rotation of H_2O/H_2S about its 'a' axis in Ar_2•••H_2O and Ar_2•••H_2S complex.

VI.C.2.b C_2H_4•••H_2O and C_2H_4•••H_2S

Figure VI.9 shows the variation of energy along the θ co-ordinate (rotation about *c* axis of H_2X) for C_2H_4•••H_2O and C_2H_4•••H_2S. For both C_2H_4•••H_2O and C_2H_4•••H_2S, the least energy configuration along this co-ordinate is the one where one of the hydrogen is

pointing towards the π system. Rotation of H_2O and H_2S along this co-ordinate faces two barrier – one is for a configuration where both the hydrogen atoms are pointing towards the π system (θ = 60° for C_2H_4•••H_2O, θ = 50° for C_2H_4···H_2S) and the other is for O/S down configuration (θ = 240° for C_2H_4•••H_2O, θ = 230° for C_2H_4•••H_2S). The former causes a destabilization of 426 cm^{-1} for C_2H_4•••H_2O and 153 cm^{-1} for C_2H_4•••H_2S. For C_2H_4•••H_2O,

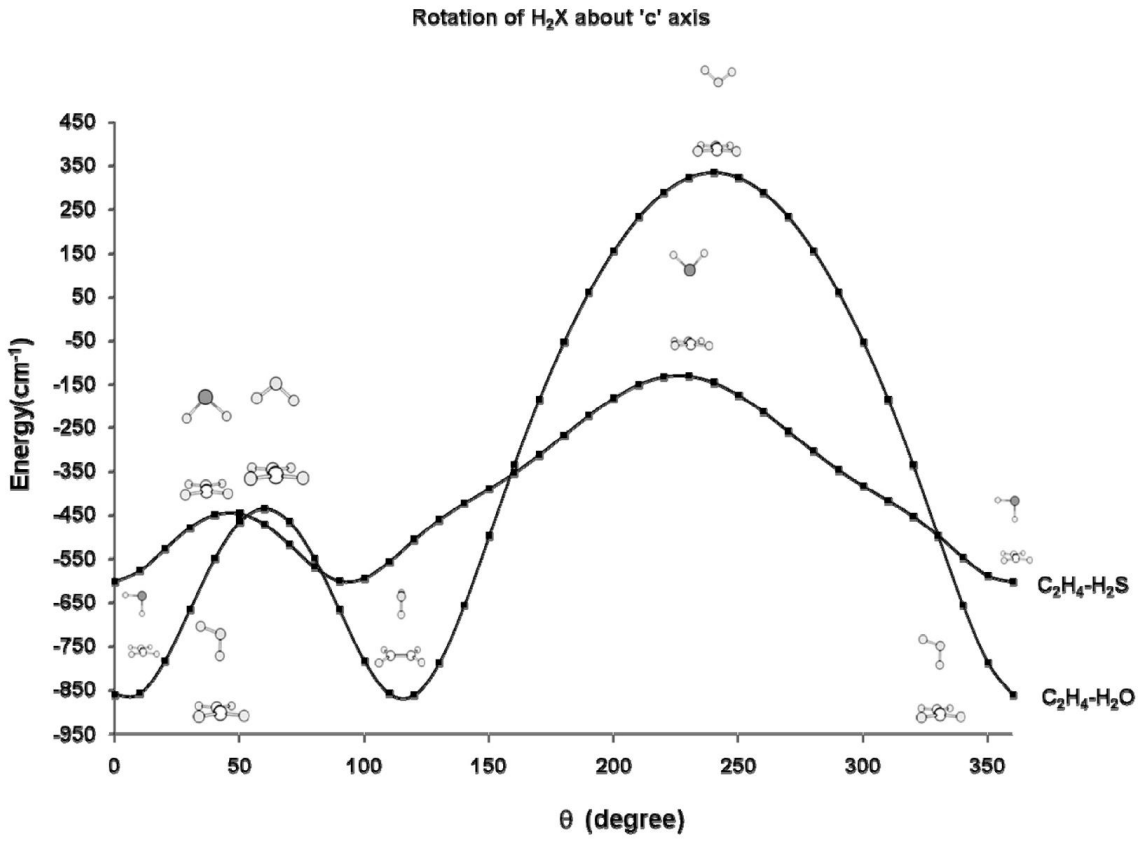

Figure VI.9: Potential energy variation for the rotation of H_2O/H_2S about 'c' principal axis in C_2H_4•••H_2O and C_2H_4•••H_2S.

the later configuration faces a huge barrier of 1195 cm^{-1} and for C_2H_4•••H_2S complex this barrier is 467 cm^{-1}.

As shown in Figure VI.10, the rotation of H_2O about its '*b*' principal axis (C_2 symmetry axis) passes through a barrier of 878 cm^{-1} corresponding to a structure of C_s

symmetry where the O-lone pair is pointing towards the π-cloud of ethylene (τ = 90°). For C_2H_4•••H_2S, this barrier is 436 cm^{-1}. The minima along this co-ordinate lies again at the configuration where only one of the hydrogen is pointing towards the π-system of ethylene (τ = 0°) for both H_2O and H_2S complex.

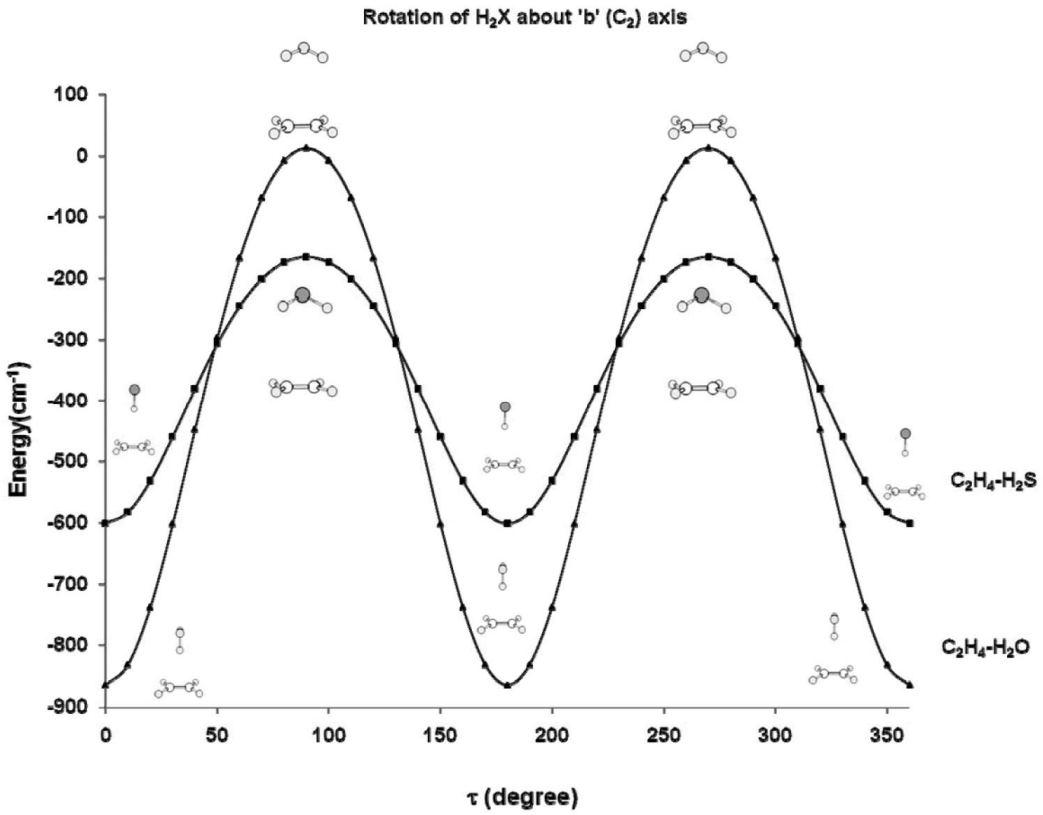

Figure VI.10. Potential energy variation for the rotation of H_2O/H_2S about 'b' principal axis in C_2H_4•••H_2O and C_2H_4•••H_2S.

Figure VI.11 shows the variation of energy along the ϕ co-ordinates (rotation about *a* axis of H_2X) for all the complexes. Along this co-ordinate, the minimum of the energy lies at 'singly hydrogen-bonded' (ϕ = 0°) structure for both C_2H_4•••H_2O and C_2H_4•••H_2S complexes. For C_2H_4•••H_2O, the region near the maxima shows a plateau

like structure. Also, the barrier along this path corresponds to the structure where the oxygen lone pair is facing the π system of C_2H_4 and the barrier is 903 cm^{-1}. For C_2H_4•••H_2S, this geometry where sulphur lone pair is pointing towards the π system (ϕ = 180°, C_{2v}), appears to be a local minima on this one-dimensional surface. The maximum of the energy lies at ϕ = 100° and 260° and corresponds to a barrier of 447 cm^{-1} for C_2H_4•••H_2S.

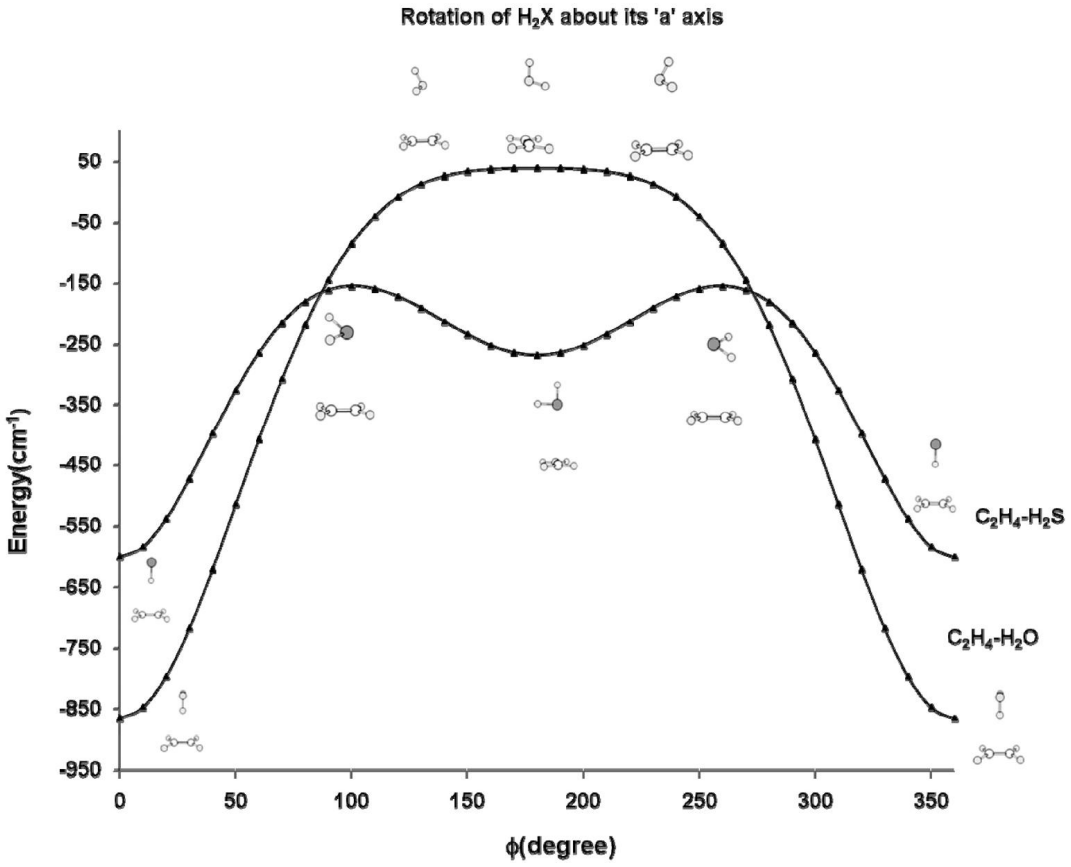

Figure VI.11. Potential energy variation for the rotation of H_2O/H_2S about its a principal axis in C_2H_4•••H_2O and C_2H_4•••H_2S.

VI.C.3. Nature of the inter-molecular vibrations

The zero point energies of the motions which are of interest are listed along with the barrier heights in Tables VI.2-VI.5 for Ar_2•••H_2O, Ar_2•••H_2S, C_2H_4•••H_2O and

C_2H_4•••H_2S respectively. The normal mode vibration corresponding to all these frequencies are dominated by internal rotation of H_2O/H_2S monomer within the complex. The normal mode vibrations which relate to the rotation of H_2O or H_2S monomer about its '*c*' principal axis could be readily identified in all the complexes. For C_2H_4•••H_2O and C_2H_4•••H_2S, this motion is partly coupled to the movement of ethylene hydrogen atoms as well, but the contributions of H_2O/H_2S hydrogen atoms are more significant. The zero point energies which relate to the rotation of H_2O/H_2S around its '*b*' principal axis are also listed in the Tables. In case of Ar_2•••H_2O and Ar_2•••H_2S, the normal mode vibration which corresponds to this motion is such that the displacement of the hydrogen, which is away from the center of Ar•••Ar bond is more than the other hydrogen as was seen both in Structure I and Structure II. As we go from Ar_2•••H_2O to Ar_2•••H_2S, the differences in the magnitude of the displacements of two hydrogen atoms decrease. This difference is 1:10 for both the structures of Ar_2•••H_2O. This ratio is 1:3 and 1:4 respectively for Structure I and Structure II of Ar_2•••H_2S. For the normal mode vibration which relate to the rotation of H_2O/H_2S around its '*a*' principal axis, the trend is reverse in all the complexes i.e. the hydrogen which is closer to the Ar•••Ar center moves faster than the other, the ratio of the displacements of two hydrogen atoms being the same as the rotation around '*b*'. For C_2H_4•••H_2O and C_2H_4•••H_2S, these motions are localized on one of the hydrogen atom of H_2O or H_2S. Rotation of H_2O/H_2S about its '*a*' axis in these complexes is more like a free rotation of the non-bonded hydrogen about the hydrogen bond and the rotation about the '*b*' axis is more like a dangling of the bonded hydrogen over the π system of ethylene.

VI.D. Zero-point energies and barrier heights

From the Tables VI.2-VI.5, we can see that for Ar_2•••H_2O/Ar_2•••H_2S system, all the zero-point energies are above or comparable to the barrier heights. For both the optimized geometries of Ar_2•••H_2O and Ar_2•••H_2S, the zero-point energy for the rotation of H_2O/H_2S about the '*a*' principal axis is either above or comparable to the barrier heights as can be seen from Table VI.2 and Table VI.3. The situation is also similar for

the rotation of H_2O/H_2S about its '*c*' axis. For the rotation of H_2O/H_2S about its '*b*' principal axis in case of Structure I, the zero-point energy is three times the barrier height for Ar_2•••H_2O and twenty five times that of Ar_2•••H_2S. For the structure II, in case of Ar_2••• H_2O, the zero point energy for this motion (rotation about '*b*') is comparable to the barrier height whereas for Ar_2•••H_2S the zero point energy is almost ten times higher. Thus, the rotation of H_2O/H_2S about the C_2 symmetric axis appears to be a freer in nature compared to the other two motions which take the two hydrogen atoms away from the Ar•••Ar system. This certainly suggests some orientational preferences, but all these wash away when we consider the zero point energy along the other torsional modes. The zero point energy being above the barrier heights for all these modes clearly suggests that these vibrational motions access all possible configurations, be it the oxygen/sulphur oriented towards Ar•••Ar or the hydrogen atoms towards the Ar•••Ar moiety . Hence, we conclude that Ar_2•••H_2O and Ar_2•••H_2S complexes are 'non-hydrogen-bonded' complexes, based on these results.

Let us turn our attention towards C_2H_4 systems now. The differences in barrier, as we go from H_2O to H_2S systems, are pronounced when the acceptor molecule is ethylene. The hydrogen-bonding capabilities of Ar•••Ar system is poor enough to outweigh the relative strength of H_2O as hydrogen bond donor compared to H_2S. However, the stronger acceptor i.e. the ethylene π-cloud can distinguish between a strong hydrogen bond donor and a weaker one confirming that H_2S is far poor hydrogen-bond donor than H_2O. For the rotation of H_2O/H_2S about its '*a*' principal axis which takes both the hydrogen atoms away from the π cloud of ethylene, the barrier is one hundred twenty nine times the zero-point energy along this co-ordinate for H_2O whereas for the H_2S complex it is twenty four times. In C_2H_4•••H_2O, for the rotation of H_2O about its *c*

Table VI.2. Zero point energies (ZPE) and barrier heights for different motions of $Ar_2\cdots H_2O$ complex

Nature of vibration	ZPE (cm^{-1}) Structure I	ZPE(cm^{-1}) Structure II	Barrier 1 (cm^{-1})	Barrier 2 (cm^{-1})
Rotation of H_2O about 'a'	55	125	60	-
Rotation of H_2O about 'c'	68	51	46	5
Rotation of H_2O about 'b'	126	41	38	

Table VI.3. Zero point energies (ZPE) and barrier heights for different motions of $Ar_2\cdots H_2S$ complex

Nature of vibration	ZPE(cm^{-1}) Structure I	ZPE(cm-1) Structure II	Barrier1 (cm^{-1})	Barrier2 (cm^{-1})
Rotation of H_2S about 'a'	45	72	72	-
Rotation of H_2S about 'c'	56	43	64	7
Rotation of H_2S about 'b'	74	32	3	-

axis i.e. along the θ co-ordinate, the barrier energy for bringing the oxygen towards the π cloud of ethylene is nine times that of the zero-point energy. The energy barrier pertaining to a configuration where both the hydrogen atoms are pointing towards the π cloud of ethylene is less but appreciable and it is thrice the zero-point energy along that co-ordinate. Along this co-ordinate, for $C_2H_4\bullet\bullet\bullet H_2S$, the energy required to bring the sulphur towards the π cloud of ethylene is five times the zero-point energy. The energy

***T**able VI.4. Zero point energies (ZPE) and barrier heights for different motions of $C_2H_4\cdots H_2O$ complex*

Nature of vibration	ZPE(cm^{-1})	Barrier 1(cm^{-1})	Barrier 2(cm^{-1})
Rotation of H_2O about 'a'	7	903	-
Rotation of H_2O about 'c'	128	1195	426
Rotation of H_2O about 'b'	175	878	-

barrier to attain a configuration where both the hydrogen atoms of H_2S are pointing towards ethylene π is twice the zero point energy along this co-ordinate (Barrier 2). The barrier for rotation of H_2O/H_2S about its '*b*' axis (τ co-ordinate) is five times the zero-point energy along this co-ordinate for the C_2H_4•••H_2O complex and three times of that for the C_2H_4•••H_2S complex. Thus, for both the H_2O and H_2S complexes of ethylene, the 'hydrogen bonded' geometry is more preferred compared to the oxygen/sulphur-bonded geometry. All the motions which bring the oxygen/sulphur towards the π-cloud face an appreciable barrier to be overcome by the zero point energy. Thus both C_2H_4•••H_2O and C_2H_4•••H_2S are 'hydrogen bonded'. However the anisotropy of the potential energy surface is much more pronounced for C_2H_4•••H_2O compared to C_2H_4•••H_2S, which makes the former 'strong' hydrogen bonded system and the later a 'weak' hydrogen bonded system.

Table VI.5. Zero point energies (ZPE) and barrier heights for different motions of $C_2H_4\cdots H_2S$ complex

Nature of vibration	ZPE(cm^{-1})	Barrier 1 (cm^{-1})	Barrier 2(cm^{-1})
Rotation of H_2S about 'a'	19	447	-
Rotation of H_2S about 'c'	88	465	153
Rotation of H_2S about 'b'	140	436	-

VI.E. Discussion

The results presented above indicate that even when the equilibrium geometry is 'hydrogen bonded', the zero point dynamics can break the hydrogen bond leading to no specific orientational preference favoring a hydrogen bond. This result makes one wonder if systems like Ar•••HF satisfies this criterion to be called 'hydrogen –bonded'. Bader has identified both Ar•••HF and Ne•••HF to be a hydrogen-bonded complex.[29] Both Ar•••HF and Ne•••HF have bond critical points between Ar/Ne and hydrogen and there is a bond path which connects the hydrogen to the rare gas atom. The topological properties of the bond critical point do follow most of the criteria as was suggested by Koch and Popelier for C-H•••O contacts[28], including the necessary and sufficient criteria of hydrogen bonding.[13] A thorough study including both experimental and theoretical results on the potential energy surface for Ar•••HF has been reported earlier[48]. The barrier for the bending coordinate is about 120 cm^{-1} and the first excited state of this mode is at 52 cm^{-1}, both from the ground level. Hence, in addition to the zero point level, we have the first excited state below the barrier for Ar•••HF and it can be classified as 'hydrogen bonded'. However, for Ne•••HF, it was shown by Nesbitt and co-workers that the lowest bound state lies 4-6 cm^{-1} above the saddle point and clearly it is not hydrogen bonded.[49] These authors further point out that the internal rotation of HF is virtually free in He•••HF and the orientation of HF becomes more directed as we move towards Ar•••HF. Thus, the inherent characteristic of hydrogen-bonding i.e. 'directionality' becomes more pronounced as we move from He to Ar in case of the HF complexes with

the rare gases. Thus it is of no surprise that the scattering studies for rare gas•••H_2O reveal the 'birth of a hydrogen bond' when the binding partner changes from He to Xe. The reason is that the motions which take the bonded hydrogen away from the acceptor moiety become gradually hindered as we move from He to Xe. However, in the case of Rg•••H_2S complexes, this must not be the case as experimental evidence for the anisotropy is not found.

It is important at this juncture to point out that the absolute numbers of the barrier heights and zero point energies reported here could vary with the level of calculations. These numbers may reduce, if we perform a relaxed scan of the potential energy surface. As for example, in Ar_2•••H_2O, for rotation of H_2O around its 'c' axis, if we optimize the stationary points, the difference between the lowest and the highest point on the curve decreases to 31 cm^{-1} from 46 cm^{-1}. However, it is clear that a variation of this magnitude would not alter the trends or conclusions observed here. Moreover, the main purpose of this work is not to establish any benchmark, rather to testify a concept which can serve as a guideline for a system to be classified as 'hydrogen-bonded'.

We realize that the procedure described above to characterize a system as hydrogen bonded is too elaborate and some general guidelines could be useful. The torsional frequencies for all these complexes are typically of the order of 50 - 300 cm^{-1}. Hence, the zero point energies are going to be at the most 200 cm^{-1} and most often less. It is suggested that for a system to be classified as hydrogen bonded, the barrier along a torsional coordinate that breaks the hydrogen bond be sufficiently above the zero point energy so that there is at least one bound level. Looking at the typical numbers given above, a barrier of 350 cm^{-1} (1 kcal mol^{-1}) could ensure that an anisotropic orientation could favour a hydrogen bonded geometry. One could reach this conclusion by optimizing only the minimum and saddle point along the torsional coordinate. It should be emphasized again that this barrier is for the large amplitude motion and not related to the binding energy of the complex as a whole.

Clearly, this conclusion could be extended to any temperature and any medium. In a crystal, if the thermal energy along a coordinate that can break the hydrogen bond is larger than the barrier along that coordinate, this orientation will not be stabilized. When the temperature reduces significantly and the pressure increases, this motion becomes

restricted leading to the observation of hydrogen bonded geometry. Thus, though H_2S remains a gas at room temperature and has 12 neighbours when it freezes at -60º C, at lower temperatures and high pressures, it has a crystal structure exhibiting hydrogen bonding. It is interesting to find that Loveday et al. in their work on crystalline H_2S have observed that formation of a hydrogen bond involves 'a change as simple as suppressing free rotation about a single axis.[31]

There have been several attempts to decompose the binding energy of a 'hydrogen bond' to probe which of the physical forces dominate in hydrogen bonding.[50-53] As pointed out earlier, initially it was expected to be a 'simple electrostatic interaction'. However, it became apparent soon that forces due to electrostatic interaction, induction, dispersion and exchange repulsion all contribute to different extents in various hydrogen bonds and there is evidence for partial covalency as well. It has been pointed out that dispersion plays a dominant role in 'hydrogen bonded' geometries of second row hydrides compared to the first row hydrides,[4] though dispersion is usually considered as 'van der Waals forces'. While these studies are useful in identifying the forces involved in different hydrogen bonding environments, it is clear that there is no single physical force that can be identified as hydrogen bonding force. Irrespective of the forces that dominate, hydrogen bonding is directional. This directionality can manifest itself to experimental and theoretical observations, if the barriers to vibrational motions that break the hydrogen bond are significantly above the thermal energy available along these coordinates. For some systems, such as Ar_2•••H_2S, the barrier is below the zero point energy and clearly this complex is not hydrogen bonded even at zero Kelvin.

Finally, the definition given by Pimentel and McClellan appears to be the most appropriate for a hydrogen bond. According to them, "A hydrogen bond is said to exist when: 1) there is evidence of a bond and 2) there is evidence that this bond specifically involves a hydrogen atom already bonded to another atom". We suggest that one of the evidence for the presence of the hydrogen bond be that at least the zero point energy along any torsional degree of freedom that can break a hydrogen bond be significantly below the barrier energy along that coordinate. Unlike the other evidences proposed in the literature, we submit that the evidence proposed here is absolute.

VI.F. Conclusions

To conclude, the analysis of the potential energy barriers for different motions of H_2O/H_2S in Ar_2•••H_2O/Ar_2•••H_2S and C_2H_4•••H_2O/C_2H_4•••H_2S complexes have been done and are compared to the zero-point energy for the respective motion. It is found that for Ar_2•••H_2O/Ar_2•••H_2S, the barriers for different motions of H_2O/H_2S are comparable or even lower than the zero point energy along these co-ordinates whereas for C_2H_4•••H_2O/C_2H_4•••H_2S, the barriers are lying well above the zero point energy along the co-ordinates. These results indicate that though, the equilibrium structures of Ar_2•••H_2O and Ar_2•••H_2S exhibit a 'hydrogen bonded' geometry, the geometry cannot even be stabilized at zero Kelvin. This is evidenced by the large amplitude motions of H_2O and H_2S in the microwave spectral studies where the dynamical structure of H_2O and H_2S were almost spherical in the complexes. On the other hand, both C_2H_4•••H_2O and C_2H_4•••H_2S are 'hydrogen bonded' according to the present analysis. Though the magnitude of the anisotropy in C_2H_4•••H_2S is less compared to that of the H_2O complex, C_2H_4•••H_2S emerges to be 'hydrogen bonded' in the present analysis and the interaction is strong enough to be detected at the low temperature of the supersonic expansion. This is indeed the case as has been evidenced by the microwave studies. Such an analysis and verification is essential to shed light on the possible existence/non-existence of a specific hydrogen-bonding interaction. It is not enough to conclude about the existence of hydrogen bonding between a donor and an acceptor from the rigid *ab initio* geometry optimization and AIM theoretical calculations. It is to be stressed that the anisotropy of the hydrogen-bonding interaction should be strong enough to 'hold' the 'hydrogen bond' at least at the 'zero point level', otherwise it is better to think of it as 'non-existent'. At a given temperature, the thermal energy along a coordinate that can break the hydrogen bond should be below the barrier along that coordinate.

VI.G. References

1. E. Arunan, *Chemistry International*, **2007**, 29, 16. See also the website: http://ipc.iisc.ernet.in/iupac/ for more details.
2. G.C. Pimentel, A.L.McClellan, *The Hydrogen Bond,* W. H. Freeman and Co, San Fransisco, **1960.**
3. G. A.Jeffrey, W. Saenger, *Hydrogen Bonding in Biological Structures,* Springer Verlag, Berlin, **1991.**
4. S. Scheiner, *Hydrogen Bonding: A theoretical perspective,* Oxford University Press, Oxford, **1997.**
5. G. R Desiraju, T.Steiner, *The Weak Hydrogen Bond: In Structural Chemistry and Biology,* Oxford University Press, Oxford, **1999.**
6. S. J. Grabowski (Ed.), *Hydrogen Bonding: New Insights*, Springer, Dordrecht, The Netherlands, **2006.**
7. L.Pauling, *The Nature of the Chemical Bond,* Cornell University Press, Ithaca, New York, **1960.**
8. P. G. Sennikov, *J. Phys. Chem.* **1994**, 98, 4973.
9. I. Alkorta, I. Roza, J. Ekguero, *Chem. Soc. Rev.* **1998**, 27, 163.
10. J. J.Sczymczak, S. J. Grabowski,. S. Roszak, J. Leszczynski, *Chem. Phys Lett.* **2004**, 393, 81.
11. T. F. Koetzle, O. Eisenstein, A. L. Rheingold, R. H. Crabtree, *Angew. Chem., Int. Ed. Engl.* **1995**, 34, 2507.
12. B. Raghavendra, E. Arunan, *J. Phys. Chem.* **2007,** 111, 9699.
13. B. Raghavendra, E. Arunan, *Chem. Phys. Lett.* **2008**, 467, 37.
14. A. D. Buckhingham, P. Fowler, *Can. J. Chem.* **1985**, 63, 2018.
15. B. F. King, F. Weinhold, *J. Chem. Phys.* **1995**, 103, 333.
16. C. A. Coulson, *Research*, **1957**, 10, 149.
17. E. D. Isaacs, A. Shukla, P. M. Platzman, D. R. Hamann, B. Barbiellini, C. A. Tulk, *Phys. Rev. Lett.* **1999**, 82, 600.
18. A. J. Dingley , S. Grzesiek, *J. Am. Chem. Soc.* **1998**, 120, 8293.
19. P. Hobza, Z. Havla, *Chem. Rev.* **2000**, 100, 4253.
20. J. Joseph, E. D. Jemmis, *J. Am. Chem. Soc.* **2007**, 129, 4620.

21. I. J. Bruno, J. C. Cole, P. R. Edgington, M. K. Kessler, C. F. Macrae, P. McCabe, J. Pearson, R. Taylor, *Acta. Crystallogr. Sect. B*, **2002**, B58, 389. Available at the website: http://www.ccdc.cam.ac.uk/support/documentation/#mercury.
22. P. K. Mandal , E. Arunan, *J. Chem. Phys*. **2001**, 114, 3880.
23. E. Arunan, A. P. Tiwari, P. K. Mandal ,P. C. Mathias, *Curr. Sci*. **2002**, 82, 533.
24. B. Lakshmi, A. G. Samuelson, K. V. J. Jose, S. R. Gadre, E. Arunan, *New J. Chem*. **2005**, 29, 371.
25. B. Raghavendra, P. K. Mandal ,E. Arunan, *Phys. Chem. Chem. Phys*. **2006,** 8, 5276.
26. R. A. Klein, *Chem. Phys. Lett.* **2006**, 425, 128.
27. A. C. Legon, *Angew. Chem. Int. Ed.* **1999**, 38, 2686.
28. U. Koch, P. L. A. Popelier, *J. Phys. Chem.***1995,** 99, 9747.
29. R. W. F. Bader, *Atoms in Molecules: A Quantum Theory,* Clarendon Press: Oxford, **1990**.
30. R. Rousseau, M. Boero, M. Bernasconi, M. Parrinello, K. Terakura *Phys. Rev. Lett*. **1999**, 83, 2218.
31. J. S. Loveday, R. J. Nelmes, S. Klotz, J. M. Besson, G. Hamel, *Phys. Rev. Lett.* **2000**, 85, 1024.
32. T. Ikeda, *Phys. Rev. B.* **2001**, 64, 104103.
33. V. Aquilanti, E. Cornicchi, M. M. Teixidor, N. Saendig, F. Pirani, D. Cappelletti, *Angew. Chem. Int. Ed.* **2005**, 44, 2356.
34. A. F. A Vilela, P. R. P Barreto, R. Gargano, F. Pirani, V. Aquilanti, *J. Chem. Phys.* **2006,** 125, 133111.
35. E. Arunan, T. Emilsson, H. S. Gutowsky, G. T. Fraser, G. de Oliveria, C. E. Dykstra, *J. Chem. Phys.* **2002**, 117, 9766.
36. M. Goswami, P. K. Mandal, D. J. Ramdass, E Arunan, *Chem. Phys. Lett.* **2004,** 393, 22.
37. H. S. Gutowsky, T. Emilsson , E. Arunan, *J. Chem. Phys.* **1993**, 99, 4883.
38. P. I. Peterson , W. Klemperer, *J. Chem.Phys*. **1986**, 85, 725.
39. F. J Lovas, P. K. Mandal, E. Arunan, *unpublsihed results*.
40. G. T. Fraser, *Int. Rev. Phys. Chem.* **1991**, 10, 189.

41. M.J Frisch, G. W. Trucks, H. B Schlegel, G. E. Scuseria, M. A.Robb, J. R.Cheeseman, J. A. Montgomery Jr., T. Vreven, K. N. Kudin, J. C. Burant, J. M. Millam, S. S. Iyengar, J. Tomasi, V. Barone, B. Mennucci, M. Cossi, G. Scalmani, N. Rega, G. A Petersson, H. Nakatsuji, M. Hada, M. Ehara, K. Toyota, R. Fukuda, J. Hasegawa, M. Ishida, T. Nakajima, Y. Honda, O. Kitao, H. Nakai, M. Klene, X. Li, J. E. Knox, H. P. Hratchian, J. B.Cross, C. Adamo, J. Jaramillo, R. Gomperts, R. E. Stratmann, O. Yazyev, A. J. Austin, R. Cammi, C. Pomelli, J. W. Ochterski, P. Y. Ayala, K. Morokuma, G. A. Voth, P. Salvador, J. J. Dannenberg, V. G. Zakrzewski, S. Dapprich, A. D. Daniels, M. C. Strain, O. Farkas, D. K. Malick, A. D. Rabuck, K. Raghavachari, J. B. Foresman, J. V. Ortiz, Q. Cui, A. G. Baboul, S. Clifford, J. Cioslowski, B. B. Stefanov, G. Liu, A. Liashenko, P. Piskorz, I. Komaromi, R. L. Martin, D. J. Fox, T. M. Keith, A. Al-Laham, C. Y. Peng, A. Nanayakkara, M. Challacombe, P. M. W. Gill, B. Johnson, W. Chen, M. W. Wong, C. Gonzalez, J. A. Pople, *Gaussian03*, Revision C-02; Gaussian, Inc. Wallingford CT, **2004**.
42. F. Biegler-Konig, J. Schonbohm, R. Derdau, D. Bayles, and R. F. W. Bader, *AIM 2000 version 1*, Bielefeld, Germany, **2000.**
43. E. Arunan, T. Emilsson, H. S. Gutowsky, *J. Am. Chem. Soc.* **1994,** 116*,* 8418
44. E. Arunan, C. E Dykstra, T. Emilsson, H. S. Gutowsky, *J. Chem. Phys.* **1996,** 105**,** 8495.
45. P. K. Mandal, D. J. Ramdass, E. Arunan, *Phys. Chem. Chem. Phys.* **2005**, 7, 2740.
46. A. M. Andrews, R.L. Kuczkowski *J. Chem. Phys.* **1993**, 98*,* 791.
47. S. B. Boys, F. Bernardi *Mol. Phys.* **1970,** 19*,* 553.
48. J. M. Hutson, *J. Chem. Phys*. **1992**, 96**,** 6752.
49. C. M. Lovejoy, D. J. Nesbitt, J. Chem. Phys., **1991**, 94**,** 208.
50. H. Umeyama, K. Morokuma, *J. Am. Chem. Soc.* **1977**, 99, 1316.
51. E. D. Glendening, *J. Phys. Chem. A*. **2005**, 109, 11936.
52. I. Rozas, I. Alkorta, J. Elguero, *Struct. Chem.* **2008**, 19, 923.
53. R. Z. Khaliullin, E. A. Cobar, R. C. Lochan, A. T. Bell, M. Head-Gordon, *J. Phys. Chem. A* **2007**, 111, 8753.

List of publications

1. "Rotational Spectra and structure of the floppy C_2H_4-H_2S complex: bridging hydrogen-bonding and van der Waals interaction", **M. Goswami**, P.K. Mandal, D. J. Ramdass and E. Arunan, *Chemical Physics Letters*, 393, **2004**, 22.

2. "Rotational spectra of weakly bound complexes containing H_2O/H_2S: Hydrogen bonding vs van der Waals interaction", E. Arunan, P.K. Mandal, **Mausumi Goswami** and B. Raghavendra, *Proceedings of Indian National Science Academy*, 71 A, **2005,** 377.

3. "Pulsed nozzle Fourier transform microwave spectroscopic and *ab initio* investigations on the weakly bound Ar-$(H_2S)_2$ trimer", Pankaj K. Mandal, **Mausumi Goswami** and E. Arunan, *Journal of Indian Institute of Science*, 85, **2006**, 5276.

4. "The Hydrogen Bond: A Molecular Beam Microwave Spectroscopist's view with a Universal Appeal" **Mausumi Goswami** and E. Arunan, *Phys. Chem. Chem. Phys*. 11, **2009,** 8974.

5. "Rotational spectra of C_2H_4-H_2S complex and its isotopomers: nature of large amplitude motion in C_2H_4-H_2S complex", **Mausumi Goswami** and E. Arunan **(manuscript under preparation)**.

6. "Rotational Spectra and structure of phenylacetylene-H_2O complex", **Mausumi Goswami** and E. Arunan **(manuscript under preparation)**

7. "Rotational Spectra and structure of phenylacetylene-H_2S complex", **Mausumi Goswami** and E. Arunan **(manuscript under preparation)**